UNIVERSITY OF NAPLES FEDERICO II

FACULTY OF MATHS, PHYSICS AND NATURAL SCIENCES

PHD IN Chemical Sciences
XXVI CYCLE

Chemical Structure of cell-wall components isolated from pathogen bacteria

Flaviana Di Lorenzo

TUTOR

Prof. Rosa Lanzetta

SUPERVISOR

Prof. Piero Pucci

Summary

Aim of the present PhD thesis is the extraction, purification and structural elucidation of lipopolysaccharides (LPS), or endotoxins, isolated from human pathogen bacteria. LPSs are amphiphilic macromolecules that compose about 75% of the outer membrane of Gram-negative bacteria that are indispensable for their growth and survival. LPSs have a structural role since increase the strength of bacterial cell envelope and mediate the contacts with the external environment. The general structure of LPSs is characterised by three distinct portions: the **lipid A**, composed of the typical glucosamine disaccharide backbone variously acylated, the **core oligosaccharide**, distinguishable in a inner core and a outer core, and the **O-chain** polysaccharide built up of oligosaccharide repeating units. This latter moiety can be absent and in that case LPSs are named lipooligosaccharides (LOS). Furthermore, LPS elicits host immune response through the TLR4 and MD-2 receptorial complex expressed on macrophages and neutrophils. Recognition between LPS and its physiological receptor is crucial since excessive exposure (or excessive host responses) to LPS can lead to an uncontrolled inflammation process in infected patients, as in case of individuals affected by Cystic Fibrosis (CF), in which premature death occurs after a permanent chronic inflammation state.

The basic genetic defect predisposes CF patients to recurrent pulmonary infections that are the major cause of morbidity and mortality in CF. Characteristic CF pathogens include *Pseudomonas aeruginosa*, bacteria belonging to the *Burkholderia cepacia* complex (BCC) and the newly identified genus *Pandoraea*. Since LPS is involved in the elicitation of host immune response in a structure-dependent mode, the investigation of the LPS structure is mandatory to understand the virulence of the abovementioned microorganisms and the effect on the host.

The endotoxins analysed in the present PhD work are extracted from opportunistic Cystic Fibrosis pathogens.

The first part of the project has been focused on the structural characterisation of endotoxins from *Burkholderia dolosa*, *Pandoraea pulmonicola* and a chronic strain of *Pseudomonas aeruginosa*. Moreover, the biological activity of the LOS isolated from *B. dolosa* and *P. aeruginosa* has been also assessed.
Chemical and biological properties of the LOS from *Burkholderia dolosa* IST4208, an isolate recovered from a CF patient in a Portuguese CF Center, were analysed. The infected CF patient was chronically colonised for 5.5 years with *B. dolosa* until death, following severe pulmonary deterioration. The structural determination was attained by a combination of chemical, spectrometrical and spectroscopal methods and brought to a novel structure; the LOS was also tested for its immunostimulatory activity on human HEK 293 cells expressing TLR4, MD-2 and CD-14, showing a strong pro-inflammatory activity. These findings allow to speculate that the novel and heterogeneous structure of the core oligosaccharide portion plays a key function in the molecular mechanism of the interaction with the TLR4/MD-2 receptorial complex, thus demonstrating a notable role in the pathogenicity of *B. dolosa*.
Pandoraea pulmonicola is a newly identified CF pathogen that showed to possess a potent pro-inflammatory activity. Since the O-chain moiety constitutes the antigenic determinant of the LPS, making this latter highly immunogenic, is crucial to know the primary structure of this polysaccharide moiety. Thus, it was determined for the first time the O-chain structure of the LPS isolated from *Pandoraea pulmonicola* strain LMG 18108, a clinical isolate from a US CF patient. *Pandoraea pulmonicola* revealed to possess a LPS composed of a novel polysaccharide, whose structure consisted of a trisaccharide repeating unit bearing a very

unusual acyl substituent, a five-membered ring acyl residue, the 3-hydroxy-2,3-dimethyl-5-oxoprolyl group.

Pseudomonas aeruginosa, considered the key pathogen in CF, causes severe acute and chronic infections at the basis of the decline of lung functions leading patients to death. The establishment of a chronic infection implies that bacteria have to adapt themselves to the CF environment and this is possible due to their intrinsic plasticity. Indeed, many publications have reported that *P. aeruginosa* can undergo several phenotypic and genotypic changes, most of which regard the LPS molecule. Despite these studies, very little is known about the molecular mechanism of the adaptation process and about other changes that can occur in the LPS structure of this CF pathogen. In this scenario, the present work reports the elucidation of the structure and the biological activity of the LOS isolated from the CF chronic strain *P. aeruginosa* RP73. The complete structural analysis was achieved by chemical analyses, NMR spectroscopy and MALDI MS spectrometry experiments, while the assessment of the biological activity was attained testing the *in vivo* pro-inflammatory capacity of the isolated LOS molecule. *P. aeruginosa* RP73 LOS showed to possess a singular structure since it is composed of the typical core moiety found in other CF *P. aeruginosa* strains but also of an under-acylated lipid A found in a non-cystic fibrosis strain. As a consequence, the isolated LOS showed to possess a very low inflammatory power that could be explained as a bacterial attempt to escape from the host immune system.

Furthermore, it was analysed the structural changes that occur in the LPS structure of *Burkholderia cenocepacia* during the process of chronic colonisation in CF patients, by studying the LPS extracted from four strains isolated at different stages of colonisation. This work demonstrated that, during the colonisation process of the body districts, *B. cenocepacia* loses the O-chain

moiety of its LPS molecule leading to a less immunogenic non-typable strains.

A second part of this PhD thesis was dedicated to the biological aspects of the relationship between the LPS structure and its function. Indeed, it was studied the biological role of amino-arabinoses of *Burkholderia cenocepacia* LPS. This bacterium is well known to possess high antibiotic resistance and capability to cause severe inflammation. This resistance is commonly attributed to often unknown characteristics of the bacterial outer membrane. The work here reported that this high resistance is due to the presence of 4-amino-4-deoxy-L-arabinose (L-Ara4N); moreover, the L-Ara4N modification of LPS showed to provide a molecular signature required for LPS export and proper assembly at the outer membrane of *B. cenocepacia*. These conclusions were achieved by isolating and characterising the LPS of three *B. cenocepacia* suppressor mutants that remained viable despite their inability to either synthesize L-Ara4N or transfer it to the LPS. In this context, it is also reported the fine genetic and molecular biology experiments executed to assess the importance of these sugar residues on the LPS macromolecule.

An extensive part of the present thesis has been also dedicated to the study of the molecular mechanisms of interaction between *B. cenocepacia* LPS and TLR4/MD-2 receptorial complex. The typical paradigm of LPS recognition has the *E. coli* hexa-acylated lipid A species as the typical ligand of the TLR4/MD2 complex whereas underacylated LPSs are less or not sensed by the complex. Here it has been showed that *Burkholderia cenocepacia* lipid A triggers the innate immune response by binding to the same receptor system although it only possesses a penta-acylated or even more underacylated lipid A. By using site-directed mutagenesis and modeling experiments on *Burkholderia cenocepacia*, overall results led to propose that the increased length of the acyl chains and the

presence of amino-arabinoses in the *Burkholderia* LPS is the key feature allowing the lipid A moieties to i) fulfill the binding pocket of MD-2 and ii) to be exposed to induce TLR4 dimerization. This suggested that *B. cenocepacia* lipid A possesses a new model of TLR4/MD2 activation and opens new trails of discussion that can explain the yet unexplained activation of innate immunity by different hypoacylated bacterial LPSs.

Finally, a small section of the current thesis has been focused on the structure characterisation of LPSs composing the outer membrane of extremophilic Gram-negative bacteria, focusing attention on thermophilic bacteria. Bacteria adapted to heat have developed peculiar structure for their cell wall components. Since the outer membrane of Gram-negative bacteria is constituted mainly by LPSs, then it is reasonable to assume that structural changes could also be present in these macromolecules isolated from thermophilic bacteria. Moreover, it was previously demonstrated that lipid A from non-pathogenic bacteria are non toxic and, in some cases, can antagonize many effects of pathogenic LPSs. Thus, it is of great interest to determine their LPS structure and to test the biological activity on human cells. In this context, the characterisation of the endotoxin isolated from the thermophilic bacterium *Thermomonsas hydrothermalis* was determined. A LOS was found with an unique structure composed of a hexa-saccharide skeleton in which a galacturonic acid was linked to the core oligosaccharide via phosphodiester linkage. Moreover, also lipid A turned out to have a peculiar backbone structure characterised by the presence of galacturonic acids linked to the phosphate groups. These features render the overall structure of *T. hydrothermalis* LOS highly negatively charged. Interaction between LOS-negative charges and cations contribute to the rigidity of the outer membrane, resulting in bacterial high resistance to external stresses, emphasizing the important role of LPS in high resistance of extremophiles to extreme environments.

The biological activity assessment showed, moreover, that *T. hydrothermalis* LOS has a low immunopotential and an antagonistic activity versus the high immunogenic hexa-acylated *E. coli* LPS at low doses.

Part of this PhD thesis was adapted from the following articles co-written by the author of the present thesis:

Di Lorenzo F., Silipo A., Costello A., Sturiale L., Garozzo D., Callaghan M., Lanzetta R., Parrilli M., McClean S., Molinaro A., Structural Study of the lipopolysaccharide O-Antigen produced by the emerging cystic fibrosis pathogen *Pandoraea pulmonicola*. **2012**, *Eur. J. Org. Chem*., 2243-2249.

Hamad M.A., Di Lorenzo F., Molinaro A., Valvano M.A., Aminoarabinose is essential for lipopolysaccharide export and intrinsic antimicrobial peptide resistance in *Burkholderia cenocepacia*. **2012**, *Mol. Microbiol*., 85(5), 962-74.

Di Lorenzo F., Sturiale L., Palmigiano A., Fazio L. L., Paciello Ida, Coutinho C. P., Sá-Correia I., Bernardini M. L., Lanzetta R, Garozzo D., Silipo A. and Molinaro A. Chemistry and biology of the potent endotoxin from a *Burkholderia dolosa* clinical isolate from a cystic fibrosis patient. **2013**, *ChemBioChem*., 14, 1105-1115.

Di Lorenzo F., Silipo A., Bianconi I., Lorè N.I., Scamporrino A., Sturiale L., Garozzo D., Lanzetta R., Parrilli M., Bragonzi A., Molinaro A., **2014**, *Molecular Immunology*, accepted.

Other papers not related to this thesis are:

Loutet S.A., Di Lorenzo F., Clarke C., Molinaro A., Valvano M.A., Transcriptional responses of *Burkholderia cenocepacia* to polymyxin B in isogenic strains with diverse polymyxin B resistance phenotypes. **2011**, *BMC Genomics*, 12, 472.

De Soyza A., Di Lorenzo F., Silipo A., Lanzetta R., Molinaro A. Lipopolysaccharide structure and biological activity from the cystic fibrosis pathogens *Burkholderia cepacia* complex. **2012**, *Carbohydrate Chemistry*, RSC Publishing, 38, 13-39.

Silipo A., Di Lorenzo F., Fazio L.L., Paciello Ida, Sturiale L., Palmigiano A., Parrilli M., Grant W.D., Garozzo D., Lanzetta R., Bernardini M.L., Molinaro A. Structure and immunological activity of the lipopolysaccharide isolated from the species *Alkalimonas delamerensis* ". **2013**, *Eur. J. Org. Chem.*, 2653-2665.

The author of the present PhD thesis acknowledges: Dr. Silipo A., Prof. Molinaro A., Prof. Lanzetta R., Prof. Parrilli M., Prof. De Castro C., Prof. Bernardini M.L., Dr. Bianconi I., Dr. Bragonzi A., Dr. Callaghan M., Dr. Clarke C., Dr. Costello A., Dr. Coutinho C.P., Prof. da Costa M.S., Prof. De Soyza A., Dr. Fazio L.L., Dr. Garozzo Domenico, Prof. Grant W.D., Dr. Hamad M.A., Prof. Jerala R., Dr. Kubik Ł., Dr. Lorè N.I., Dr. Loutet S.A., Dr. Martin-Santamaria S., Dr. McClean S., Dr. Paciello I., Dr. Palmigiano A., Prof. Sá Correira I., Dr. Sturiale L. and Prof. Valvano M.A. for the scientific support.

Abbreviations

Ac	Acid ceramidase
AP	Antimicrobial peptide
APC	Antigen presenting cell
Ara4N	4-amino-4-deoxy-L-arabinose
ASL	Airway surface liquid
Asm	Acid sphingomyelinase
BALF	Bronchoalveolar lavage fluid
BCC	*Burkholderia cepacia* complex
BCLA	*Burkholderia cenocepacia* lipid A
BC-LOS	*Burkholderia cenocepacia* lipooligosaccharide
BCR	B cell receptor
BLP	Braun's lipoprotein or Bacterial lipoprotein
BMDM	Bone marrow derived macrophage
CF	Cystic fibrosis
CFTR	Cystic fibrosis transmembrane conductance regulator
COSY	Correlation Spectroscopy
DAMP	Damage associated molecular pattern
DHB	Dihydroxybenzoic acid
DMEM	Dulbecco's modified eagle medium
DMSO	Dimethyl sulphosside
DQF COSY	Double-quantum filtered COSY
EDTA	Ethylenediaminetetraacetic acid
ELISA	Enzyme-linked immunosorbent assay
ENaC	Epithelia Na^+ channel
ESI	Electrospray Ionization
FA	Fatty acid
FBS	Fetal bovine serum
GC-MS	Gas chromatography-Mass spectrometry
HDP	Host defence peptide
HEK	Human embryonic kidney
HMBC	Heteronuclear multiple-bond correlation

HSP	Heat shock protein
HSQC	Heteronuclear single-quantum correlation
IL	Interleukine
IRF	Interferon regulator factor
LA	Lipid A
LAMUT	*B. cenocepacia* mutant lipid A
LBP	Lipopolysaccharide binding protein
LOS	Lipooligosaccharide
LPS	Lipopolysaccharide
LRR	Leucine rich repeat
MALDI	Matrix assisted laser desorption
MD	Molecular Dynamics
MD-2	Myeloid differentiation factor -2
m-DAP	meso-diaminopimelic acid
MGA	Methyl glycoside per-acetylated
MHC	Major histocompatibility complex
MIC	Minimal inhibitory concentration
MILST	Multilocus sequence typing
MPO	Myeloperoxidase
MSD	Membrane spanning domain
MUT-LOS	*B. cenocepacia* mutant lipooligosaccharide
NBD	Nucleotide binding domain
NF-κB	Nuclear factor-κB
NMR	Nuclear magnetic resonance
NOESY	Nuclear Overhauser effect spectroscopy
OS	Oligosaccharide
PAMP	Pathogen associated molecular pattern
PBS	Phosphate buffered saline
PCR	Polymerase chain reaction
PCP	Phenol/Chloroform/Petroleum ethere
PMN	Polymorphonuclear neutrophilic leukocyte
PRR	Pattern recognition receptor
RLU	Renilla luciferase unit

ROESY	Rotating frame Overhauser effect spectroscopy
SIRS	Systemic inflammation response syndrome
TCR	T cell receptor
TFA	Trifluoracetic acid
TIR	Toll/IL-1 receptor
TLR	Toll like receptor
TOCSY	Total correlation spectroscopy
t-ROESY	TransverseROESY
TSA	Trypticase soy agar
TSB	Trypticase soy broth
THAP	2,4,6-trihydroxyacetophenone

Index

SECTION I : Introduction

Chapter 1: Gram-negative bacteria 2
1.1 The Prokaryotic cell 3
1.2 Bacterial cell envelope 5
1.3 Lipopolysaccharides (LPSs) 7
1.3.1 *The Lipid A moiety: structure and activity* 10
1.3.2 *The core oligosaccharide: structure and activity* 15
1.3.3 *The O-polysaccharide moiety: structure and activity* 17
1.4 LPS and Elicitation of Host Immune response 17
1.4.1 *Innate immunity and Adaptive Immunity* 17
1.4.2 *LPS and Innate Immunity* 22
1.5 Gram-negative infections in Cystic Fibrosis 25
1.5.1 *Cystic Fibrosis: an overview* 25
1.5.2 *Cystic Fibrosis as a complex microbial pathology* 29
References 34
Chapter 2: Structural Characterisation of Lipopolysaccharides and Lipooligosaccharides 41
2.1 Extraction and Purification of LPS and LOS 42
2.2. Structural determination of the saccharide moities 43
2.2.1 *Chemical analyses of the saccharide moities* 45
2.2.2 *NMR Spectroscopy Analysis of the saccharide moieties* 48
2.2.3 *Mass Spectrometry Analysis of the saccharide moieties* 51
2.3 Structural determination of the lipid A moiety 52
2.3.1 *Chemical analyses of the lipid A moiety* 53
2.3.2 *Mass Spectrometry Analysis of the Lipid A moiety* 53
References 55

SECTION II : Chemistry and Immunity of Endotoxins isolated from Cystic Fibrosis Pathogens

Chapter 3: Structural and biological activity elucidation of the potent endotoxin isolated from *Burkholderia dolosa* 58
Premise 59
3.1 Isolation and SDS-PAGE analysis of *B. dolosa* LOS 60
3.2 Chemical analyses of LOS from *B. dolosa* 60
3.3 Structural characterization of LOS oligosaccharide moiety by NMR spectroscopy 61
3.4 Structural characterisation by MALDI mass spectrometry of the intact LOS and lipid A 68
3.5 Assessment of the Biological Activity of *B. dolosa* LOS 72
3.6 Discussion 75
References 80

Chapter 4: Structural Characterisation of the LPS O-antigen moiety isolated from *Pandoraea pulmonicola* 82
Premise 83
4.1 Purification and Chemical Analyses of the LPS 84
4.2 NMR analysis of the LPS O-chain from *P. pulmonicola* 84
4.3 Discussion 92
References 94
Chapter 5: Structural and Biological Study of the LOS isolated from the chronic strain *Pseudomonas aeruginosa* RP73 96
Premise 97
5.1 Isolation and Compositional Analysis of LOS from *P. aeruginosa* RP73 .. 98
5.2 Structural Characterisation of OS Product by NMR spectroscopy 99
5.3 Structural Characterisation by MALDI Mass Spectrometry of the Lipid A moiety 107
5.4 *In vivo* pro-inflammatory effect of the LOS from *P. aeruginosa* RP73 110
5.5 Discussion 111
References 114
Chapter 6: Structural Determination ofendotoxins from clinical isolates of *Burkholderia cenocepacia* retrieved atdifferent stages of colonisation 117
Premise 118
6.1 Isolation and Chemical Analyses of LPSs isolated from *B. cenocepacia* strains IST439, IST4113 IST4129, IST4134 120
6.2. Structural Determination of oligo-/polysaccharide moieties of LOSs/LPS from strains *B. cenocepacia* strains IST439, IST4113 IST4129, IST4134 by NMR spectroscopy 121
6.3 MALDI-MS Analysis on intact LOSs/LPS from strains *B. cenocepacia* strains IST439, IST4113 IST4129, IST4134 126
6.4 Discussion 130
References 132
Chapter 7: Assessment of the biological role of amino-arabinose residues on *Burkholderia cenocepacia* LPS structure 134
Premise 135
7.1 Isolation of suppressor *B. cenocepacia* strains 136
7.2 Isolation and SDS-PAGE analysis of LPS from suppressor *B. cenocepacia* strains 137
7.3 Structural analyses of LPS isolated from suppressor *B. cenocepacia* strains 140
7.4 Assessment of the role of amino-arabinoses on *B. cenocepacia* LPS structure 144
7.5 Trasmission electron microscopy analysis on *B. cenocepacia* suppressor mutant cells 145
7.6 Discussion 145
References 149

SECTION III : Molecular mechanism of TLR4/MD-2/LPS interaction
Chapter 8: Activation of TLR4/MD-2 by LPS from *Burkholderia cenocepacia* 152
8.1 TLR4/MD-2/LPS interaction: state-of-art ... 153
8.2 Assessment of the agonist activity of *B. cenocepacia* lipid A on TLR4/MD-2 complex ... 157
8.3 Identification of amino acid residues of MD-2 involved in the interaction with LPS ... 160
8.3.1 *The hydrophobic pocket* ... 160
8.3.2 *The surface charged residues* ... 162
8.3.3 *Conclusions on biological assays results* ... 165
8.4 Molecular modelling of docking of BC-LOS to the MD-2 and TLR4 activation ... 166
8.4.1 *Model for the binding of LAMUT and BCLA* ... 167
8.4.2 *3D model for the human TLR4/MD-2 dimer in complex with B. cenocepacia LPS* ... 172
8.4.3 *Conclusions on molecular modeling experiments* ... 173
8.5 Discussion ... 175
References ... 179

SECTION IV : Study of LPS isolated from Extremophilic bacteria
Chapter 9: Elucidation of the Structure and Biological Activity of Endotoxins isolated from the thermophilic bacteria *Thermomonas hydrothermalis* ... 183
9.1 Extremophiles: an overview ... 184
9.2 Thermophiles ... 187
Premise ... 189
9.3 Extraction, Purification and Compositional Analyses of LOS from *Thermomonas hydrothermalis* ... 191
9.4 Isolation and structural characterisation of core oligosaccharide by NMR spectroscopy ... 192
9.5 Structural analyses of lipid A and core oligosaccharide by MALDI mass spectrometry ... 200
9.6 Biological activity of isolated *T. hydrothermalis* LOS ... 204
9.7 Discussion ... 207
References ... 212

SECTION V : Experimental Section
Chapter 10: Bacterial Growth and LPS Structural Analysis ... 216
10.1 Growth of *Burkholderia dolosa* cells for LOS extraction ... 217
10.2 Isolation of *Pseudomonas aeruginosa* strain RP73 ... 217
10.3 Bacterial growth conditions for *Burkholderia cenocepacia* ΔarnBC and ΔarnT-arnBC⁻ strains ... 218
10.4 Growth of *Thermomonas hydrothermalis* cells strains ... 218
10.5 Chemical Analyses ... 219
10.6 Isolation of oligosaccharide (OS) from *B. dolosa*, *B. cenocepacia* IST

and K56-2 strains 220
10.7. Isolation of polysaccharide portion from *Padoraea pulmonicola* 220
10.8 Isolation of oligosaccharide moiety from *Pseudomonas aeruginosa* RP73 and *Thermomonas hydrothermalis* 220
10.9 Isolation lipid As from all bacterial strains analysed 221
10.10 NMR Analyses 221
10.11 MALDI TOF mass spectrometry analysis 222
10.12 HEK293 hTLR4/CD14/MD-2 cell culture, transfection, and stimulation of *B. dolosa* 223
10.13. Bone marrow-derived macrophages (BMDMs) culture and stimulation assay with *B. dolosa* LOS 224
10.14 Mice treatment in *P. aeruginosa* LOS analysis 225
10.15 HEK293 cell activation assay-luciferase reporter assay on *B. cenocepacia* LPS 226
10.16 HEK293 hTLR4/CD14/MD-2 cell culture, transfection, and stimulation in *T. hydrothermalis* analysis 226
10.17 BMDMs culture and stimulation assays in *T. hydrothermalis* analysis 227
10.18 Molecular modeling on *B. cenocepacia* LOS and lipid A 227
10.18.1 *Docking studies of LAMUT-and BCLA on MD-2* 227
10.18.2 *Docking studies of BC-LOS core on TLR4* 228
10.18.3 *Building of the full complex of human MD-2/TLR4 with BC-LOS* 229
10.19 Genetic manipulation on *B. cenocepacia* K56-2 229
10.19.1 *Construction of an unmarked L-Ara4N conditional* 230
10.19.2 *Construction of a suppressor strain that is viable in the absence of L-Ara4N synthesis* 230
10.19.3 *Construction of a suppressor strain that can synthesize L-Ara4N but lacks arnT* 231
10.19.4 *Single copy gene replacement of lpt genes into Prha-arn* 232
10.19.5 *Site direct mutagenesis and replacement of wild-type lptG with* $lptG_{D31H}$ 233
10.19.6 *Antimicrobial peptide sensitivity testing and MIC determination* 234
10.19.7 *Transmission electron microscopy* 234
References 235

CONCLUSION 237

A Giulia.....

SECTION I

Introduction

Chapter 1

Gram-negative bacteria

1.1 The Prokaryotic cell

The three-domain system, which classifies organisms on Earth into three distinct kingdoms – *Archea*, *Bacteria* and *Eukarya* – was designed by the American microbiologist Carl Woese in the 1990. Otherwise, an alternative biological classification system currently used is known as "the six-kingdoms system of life" and include *Archaebacteria*, *Eubacteria*, *Protista* (comprising one-celled organisms), *Fungi*, *Plantae* and *Animalia* (Figure 1). While *Archaebacteria* and *Eubacteria* constitute the *Archaea* and *Bacteria* domains respectively (both representing the **Prokarya** kingdom), *Protista*, *Fungi*, *Plantae* and *Animalia* together form the **Eukarya** kingdom of life (Figure 1.1).

Most prokaryotic cells have diameters in the range of 1-10 μm, much smaller than most eukaryotic cells (typically 10-100 μm). Despite their small size and structural simplicity, prokaryotes have an immense impact on our world; indeed it is enough to mention all the known and yet unknown bacterial species that cause serious illnesses in humans, animals and plants. On the other hand, of enormous importance are also beneficial bacteria as well as all the decomposers prokaryotes that live in soil, at the bottom of lakes, rivers and oceans, where they return chemical elements to the environment in the form of inorganic compounds, that can be used by plants, which in turn feed animals. Therefore, it is understandable that if decomposers prokaryotes were to disappear, the chemical cycle that sustains life on Earth would halt, and all forms of eukaryotic life would also die; in contrast, prokaryotic life would undoubtedly persists in absence of eukaryotes, as it once did for billions of years.

Prokaryotes have a cellular organization different from that of eukaryotes; whereas these latter have a membrane-enclosed nucleus and numerous membrane-enclosed organelles, prokaryotic

cells lack these structural features. Typically, *Archea* domain includes all the extremophiles prokaryotic organisms that live and thrive in inhospitable, from a human viewpoint, environments such as alkaline and acidic waters, boiling hot springs, high pressure waters, ultra saline brines, without excluding a combination of aforesaid chemical and physical extremes which is typical of polyestremophilic microbes (Mesbah and Wiegel, 2008).

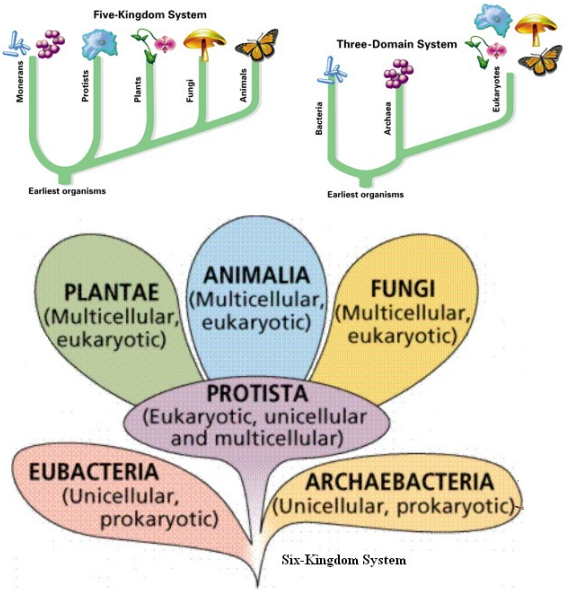

Figure 1.1 The dogmas of the organisms classification.

Bacteria comprise a wide group of microorganisms characterised by a bewildering assortment of size, shapes and arrangements reflecting the diverse environments in which they grow and reproduce (Pommerville, 2010). Despite the high structural variability, *Bacteria* can be divided on the basis of their basic cell morphologies: a bacterial cell with a rod shape is called “bacillus” whereas spherical and curved cells are called “cocci” and “spirilli”

respectively (Raven and Johnson, 2001). Some rod-shaped and spherical bacteria form colonies adhering end-to-end after their cellular division forming chains, whereas spirilla bacteria generally do not form associations with other cells. However, early systems for classifying bacteria relied on differential stains such as the colorimetric assay developed by the Danish physician Hans Gram, in use to date, that allows the distinction of bacteria in Gram-positive and Gram-negative on the basis of the different response to the test. The differences between Gram-positive and Gram-negative bacteria are related to diversities in the structure and chemical composition of their cell wall: Gram-positive bacteria have the thicker cell envelope, nearly uniformly dense layers, and stain the purple color of the crystal-violet typically used in the Gram stain, whereas Gram-negative bacteria contain just a single or two layers and lose the purple-coloured dye (Staley *et al*., 2007).

1.2 Bacterial cell envelope

The complex system of layers that surrounds bacterial cells are referred collectively as the cell envelope. It consists of a cytoplasmic membrane (or plasma membrane), cell wall, and for some bacteria, capsule and glycocalyx from inner to outer surface. Both Gram-positive and Gram-negative bacteria present the cytoplamatic membrane, namely a phospholipid bilayer surrounding the cytoplasm representing a physical semi-permeable barrier that regulates the transport of nutrients and metabolic products in and out the cell. This membrane is, in turn, enclosed by the cell wall, an important structure that maintains the cellular shape and protects the cell from swelling and rupturing (Raven and Johnson, 2001). The bacterial cell wall differs markedly from archaeal and eukaryotic cells walls in containing **peptidoglycan** (or *murein*) which is a network of saccharide molecules connected by polypeptide cross-links. In detail, it is composed of β-(1→4)-linked

disaccharide chains, alternating *N*-acetylglucosamine and *N*-acetylmuramic acid residues in turn cross linked by short peptide stems composed of alternating L- and D-amino acids (Figure 1.2). It is possible to classify peptidoglycan on the basis of the third amino acid residue of the stem peptide; indeed, in Gram-negative bacteria this residue is the unusual meso-diaminopimelic acid (m-DAP) while in Gram-positive bacteria is commonly a lysine (Figure 1.2).

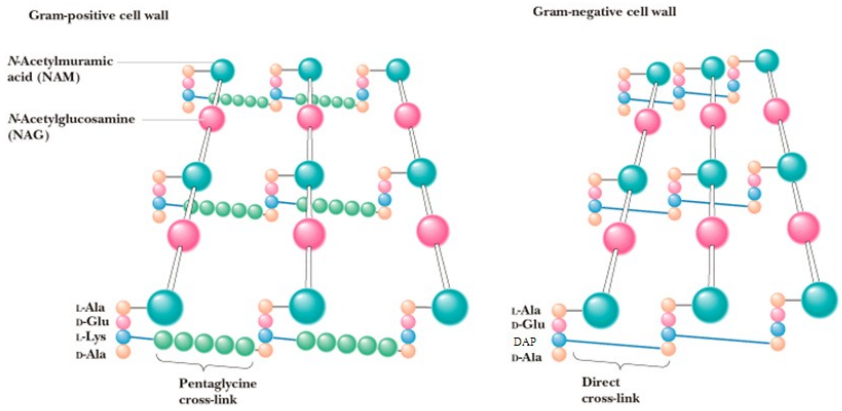

Figure 1.2 Peptidoglycan structure in Gram-positive (left) and in Gram-negative (right) bacteria.

Furthermore, in Gram-negative bacteria the external portion of the cell is composed by 95% of rigid peptidoglycan cell wall that may be one of the reason why they retain the crystal-violet of Gram stain (Figure 1.3); on the contrary, in Gram-negative cells there is a thin layer of peptidoglycan, almost 5-10% of the cell wall, surrounded by an additional asymmetric phospolipid bilayer, termed outer membrane (OM) (Figure 1.3). This external membrane is a unique feature of Gram-negative bacteria and represents the first barrier that protects bacterial cell from

environmental stress factors, thus it is essential for bacterial survival. The outer membrane is separated by a gel-like compartment, termed periplasm, from the cytoplasmatic membrane and shows to have a structure similar to that of the plasma membrane, from which nonetheless differs for important physical and chemical properties. The inner portion of the OM is mainly composed of phospholipids, while the external leaflet is occupied for the 75% by glycolipids known as lipopolysaccharides (LPS) (Alexander and Rietschel, 2001). Furthermore, the outer membrane is also constituted by a large number of proteins, among which there is the Braun's lipoprotein (BLP or murein lipoprotein), that acts as a bridge between the outer membrane and the peptidoglycan.

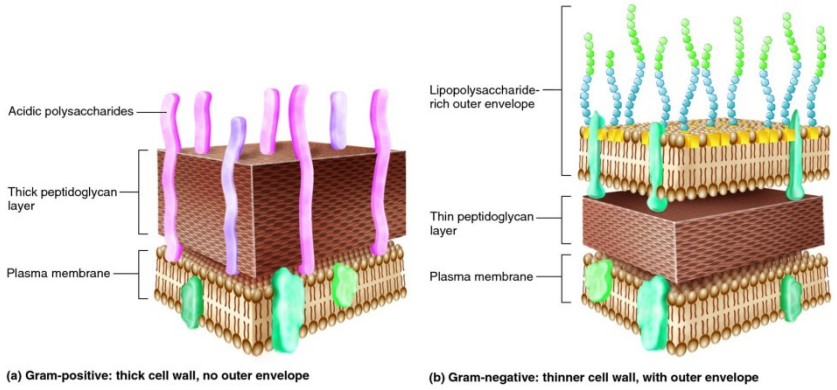

Figure 1.3 Cell-wall structure of Gram-positive (left) and Gram-negative bacteria (right).

1.3 Lipopolysaccharides (LPSs)

Lipopolysaccharides are heat-stable amphiphilic molecules indispensable for viability and survival of Gram-negative bacteria, as they heavily contribute to the structural integrity of the OM and to the protection of the bacterial cell envelope (Holst *et al.*, 1996).

Being intercalated into the outer membrane, they form hydrophobic interactions with the phospholipid bilayer composing the inner layer, giving rise to the typical asymmetry of Gram-negative bacteria OM (Holst *et al*., 1996). The highly ordered structure and low fluidity of the LPS monolayer, stabilised by electrostatic interactions of divalent cations (as Ca^{2+} and Mg^{2+}) with negatively charged groups present on LPS molecules, is responsible for the increase of permeability to hydrophobic compounds and to higher molecular weight hydrophilic compounds but also for the bacteria resistance to external stress factors. Indeed, most of the common used antibiotics directed against Gram-negative bacteria, such as polymyxin B, are able to destabilise abovementioned ionic interactions leading to the disruption of membrane integrity (Cardoso *et al*., 2007). In addition, since they are exposed toward the external environment, LPS molecules participate in crucial mechanisms of host-bacterium interactions like colonisation, virulence in the case of pathogen and opportunistic bacteria, adhesion and symbiosis (Silipo *et al*., 2010). Among all these activities, LPS has been shown to be the most potent immunostimulant molecule playing a key role in the pathogenesis of Gram-negative infections triggering the immune system in a wide range of eukariotic organisms ranging from insects to humans (Alexander and Rietschel, 2001). LPSs belonging to different bacterial species possess different structures, but also LPS of an individual bacterial strain is not a single molecule, possessing a specific chemical structure, but rather a blend of various molecules characterised by an intrinsic size and structural heterogeneity (Raetz, 1990; Raetz and Whitfield, 2002). Furthermore, bacteria of the same species producing diverse LPS molecules under different growth conditions were also found. Despite the high structural heterogeneity, all LPSs broadly comply with a common basic architecture composed of well-conserved domains in which three distinct regions encoded by different gene clusters, can be

distinguished (Figure 1.4). Indeed, they consist of a polysaccharide (also known as O-antigen, O-side chain or O-specific polysaccharide) characterised by a highly variable structure which constitutes the chemical basis for the serological classification of bacterial strains, that is covalently linked to an oligosaccharide part (core), in turn, linked to a glycolipid portion (lipid A) that is the most conserved region of the entire macromolecule. even among different species belonging to the same genus (Holst *et al*., 1996).

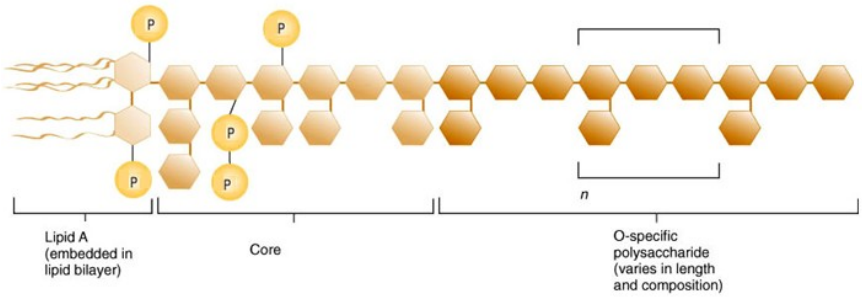

Figure 1.4 Schematised structure of Gram-negative LPSs.

The lipid A moiety is embedded in the outer leaflet of the OM whereas the sugar chain is oriented outwards (Raetz and Whitfield, 2002). The O-polysaccharide chain is not ubiquitous, as it can be absent or partly truncated in some Gram-negative strains. Bacterial colonies can be catalogued by gross colony morphology as *rough* or *smooth* on the basis of the occurrence of the O-side chain, being absent in the former and present in the latter (Lüderitz *et al*., 1966). The terminology currently used to designate the different LPS types, namely with or without the O polysaccharide portion, is S-LPS or R-LPS (or lipooligosaccharide, LOS), respectively (Raetz and Whitfield, 2002).

1.3.1 The Lipid A moiety: structure and activity

Lipid A represents the hydrophobic and endotoxic principle of the LPS molecule since it acts as a potent stimulator of the host innate immune system (see paragraph 1.4.2). It possesses a high conservative structure consisting of a β-(1→6)-linked D-glucosamine disaccharide backbone substituted with a number of amide- and ester-linked 3-hydroxy fatty acids at the positions 2 and 3 (Figure 1.5), respectively. The acyl groups that are directly linked to the sugar backbone are defined primary and some are further acylated at the hydroxy groups by secondary acyl chains. Furthermore, the sugar backbone is generally α-phosphorylated at position O-1 of the reducing glucosamine (Glc*p*N I) and at position O-4' of the non-reducing glucosamine (Glc*p*N II) (Figure 1.5) (Zahringer *et al*., 1999). The first lipid A characterised were from *Escherichia coli* (Figure 1.5) and *Salmonella enterica* LPSs in 1983. *E. coli* LPS lipid A is built up of the following sugar backbone [P→4-β-D-Glc*p*N-(1→6)-α-D-Glc*p*N-1→P] acylated at position 2 and 3 of both Glc*p*Ns by four C14:0 (3-OH) (Figure 1.5). The primary fatty acids located on the Glc*p*NII were both esterified at their hydroxy group by two secondary acyl chains: the C14:0 (3-OH) was esterified by a C12:0 while the C14:0 (3-OH) by a C14:0 (Figure 1.5).

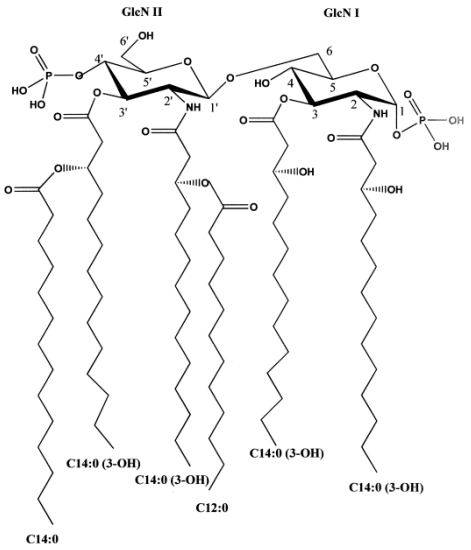

Figure 1.5 Lipid A from *Escherichia coli*.

Despite their general architecture, lipid As also present a microheterogeneity due to the presence of subtle chemical differences depending on a wide number of factors including bacterial adaptation, incomplete biosynthesis, changing of environment, presence of external stimuli and chemical modifications resulting from the procedures used for lipid A extraction from bacterial cells. Microheterogeneity has been observed in the acylation (number, type and distribution of acyl chains) and phosphorylation patterns, and, less commonly, also in the disaccharide backbone as in the case of bacterial species as *Aquifex pyrophilus* (Hellerqvist *et al*., 1971), *Brucella abortus* (Hellerqvist *et al*., 1969), whose GlcN residues may be replaced with 2,3-diamino-2,3-dideoxy-D-glucopyranose (GlcN3N) residues. Moreover, phosphate groups can be substituted by further phosphate groups, producing a pyrophosphate, but also by other polar substituents such as 4-amino-4-deoxy-L-arabinopyranose

(amino-arabinose, Ara4N) and 2-amino-ethanol group (EtN), or by acid residues such as galacturonic acid (GalA); phosphate groups can be absent, as in the case of *Bdellovibrio bacteriovorus* lipid A, characterised by the replacement of phosphate groups with two mannose residues generating a totally neutral lipid A. Concerning the acylation pattern, fatty acids can be attached to the disaccharide backbone either symmetrically (3+3, e.g. *Neisseria meningitides*) or asymmetrically (4+2, e.g. *Escherichia coli*). Finally, lipid A fatty acids present less frequently further structural features such as methyl branch, different functional and hydroxyl groups, length of the chains up to 28 carbon atoms, odd numbered carbon chains and unsaturation (Figure 1.6). Environmental- or growth conditions-dependent changes in lipid A structure have been found in several bacterial species; as example, lipid A from *E. coli* can undergo structural changes as the addition of palmitate residues in presence of antimicrobial peptides and low concentration of Mg^{2+}. It is worth to note that some bacterial species, such as the cystic fibrosis opportunistic pathogens *Burkholderia*, were found to constitutively synthesize a lipid A substituted by L-Ara4N residues, that are, in physiological conditions, positively charged elements whose presence on LPS molecule reduces the net charge surface of the outer membrane, thus increasing bacterial resistance against cationic antimicrobial compounds as polymyxin B or cationic antimicrobial peptides (CAMP) (Hamad et al., 2012) (see chapter 7). Moreover, a very frequent substitution mainly involving bacteria that live in extreme habitats (termed extremophiles), is that of galacturonic acid residues that can be attached either on the Kdo moiety or on the lipid A glucosamine-backbone (see chapter 9). Even the most subtle variation in chemical structure of lipid A can affect the LPS molecule bioactivity, since this latter is strictly structure-related; indeed, the lipid A intrinsic conformation is responsible for its agonistic and antagonistic activity on innate immune system (Brandenburg *et al*., 1993; Rietschel *et al*., 1994;

Seydel *et al*., 2000; Fukuoka *et al*., 2001; Oikawa *et al*., 2004) (see details in Section III).

A plethora of studies aimed to the elucidation of the LPS structure-activity relationship have highlighted that the hexa-acylated bisphosphorylated lipid A with an asymmetric 4:2 fatty acid distribution, found in the majority of enterobacteria, as the aforesaid *E. coli* lipid A, is considered to have the highest immunostimulatory capacity in mammals cells. In contrast, the hypoacylated synthetic precursor of *E. coli* lipid A, the tetra-acylated lipid IV_A, showed to have weak agonistic effects for some species of mammals and is well known to possess a strong antagonistic activity on human cells (Golenbock *et al*., 1991). These different biological effects are correlated to two interconnected structural parameters:

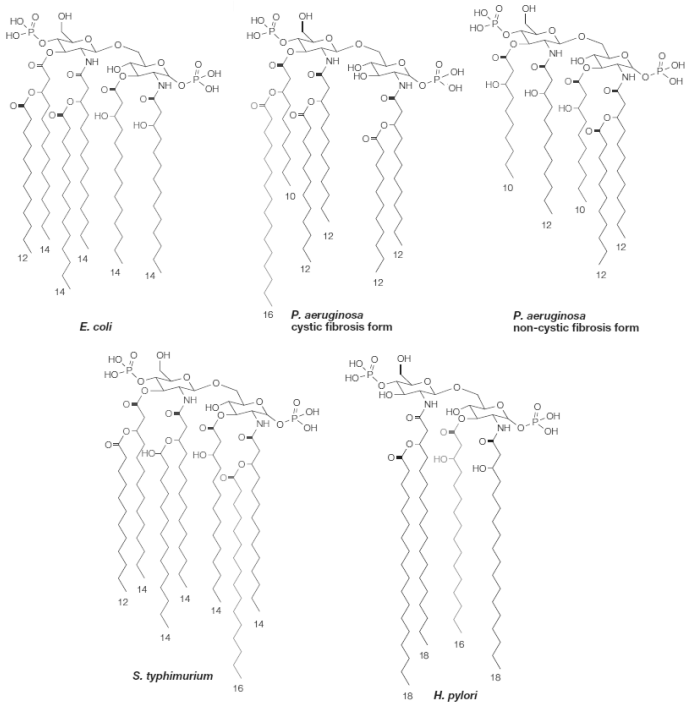

Figure 1.6 Lipid A chemical structures showing their diversity in Gram-negative bacteria.

the molecular shape of the lipid A and the tilt angle between the diglucosamine backbone and fatty acid chains that is the inclination of lipid A hydrophilic moiety respect to the hydrophobic portion (Netea *et al*., 2002). In details, the molecular shape possessed by lipid A influences its ability to be recognised by host immune system receptors, indeed it has been shown that at 37°C, in aqueous solution and in physiological conditions, the most agonistic lipid A has a truncated cone form that drives to a hexagonal supra-structure, while lipid As presenting an antagonistic activity assume a cylindrical shape leading to a lamellar structure (Netea *et al*., 2002). Regarding the tilt angle, it has been found that the most active form has a conical structure with a tilt angle >50°, while the antagonist structures present smaller values of tilt angles (Seydel *et al*., 2000): species with a tilt angle <25°, such as lipid IV_A and the penta-acylated and symmetrically (3+3) hexaacylated lipid As, act as antagonists; species with an angle between 25-50°, as monophosphorylated lipid A, have a low bioactivity (Figure 1.7) (Seydel *et al*., 2000).

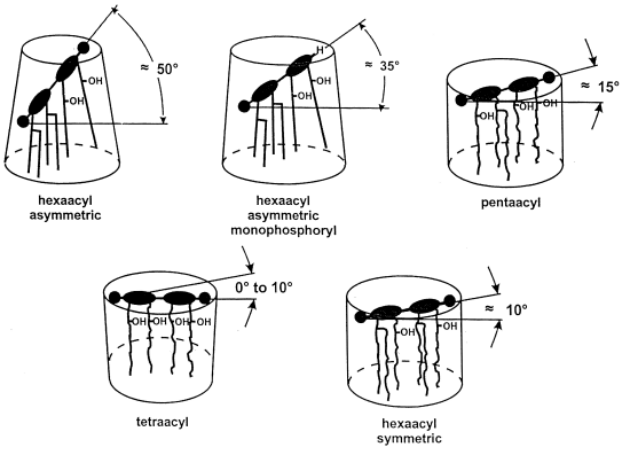

Figure 1.7 Tilte angle of lipid A depends from the acylation pattern.

These physical parameters are reflected in the different binding-mode of the LPS molecule to its physiological receptor, the TLR4/MD-2 complex, since they regulate the lipid A affinity to the MD-2 hydrophobic binding pocket that is pivotal for the innate immune receptor activation.

1.3.2 The core oligosaccharide moiety: structure and activity

Core oligosaccharide is a complex component of the LPS molecule since it can be characterised by up to fifteen monosaccharides which can be organised giving either a linear or a branched structure (Holst, 1999). In the core LPS portion two different regions can be distinguished on the basis of the monosaccharide composition termed: *inner core* and *outer core* (Holst, 1999). The inner core region is directly linked to the lipid A, is well conserved and consists of uncommon sugar residues such as heptoses (L-*glycero*-D-manno-heptose and, less commonly, D-*glycero*-D-*manno*-heptose) (De Soyza *et al*., 2008) and Kdo (3-deoxy-D-*manno* octulosonic acid) (Figure 1.8); this latter is considered a diagnostic marker for all Gram-negative bacteria that connects the core oligosaccharide to the lipid A backbone with an α-configured ketosidic linkage in almost every LPS investigated to date.

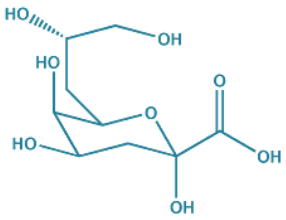

Figure 1.8 Structure of the Kdo residue.

The only two exceptions in which Kdo is not the first residue of the inner core regards *Acinetobacter* (Vinogradov *et al*., 1997) and *Shewanella* (Vinogradov *et al*. 2003): in the former Kdo is replaced by its C-3 hydroxy-derivative, the D-*glycero*-D-*talo*-oct-2-ulosonic acid (Ko), whereas in the latter it is replaced by its C-8 amino-derivative, the 8-amino-8-deoxy-*manno*-oct-2-ul-osonic acid (Kdo8N). The L-*glycero*-D-*manno*-heptose residues are often decorated with charged substituents like phosphate, pyrophosphate, Ara4N or uronic acids, as found in bacteria belonging to *Pseudomonas* genus and in many other species. Particularly, Ara4N residue is always present as terminal non-reducing monosaccharide of the trisaccharide Ara4N-(1→8)-α-Ko-(2→4)-α-Kdo in *Burkholderia* LPS (see chapters 3, 6-8). It is speculated that all the substituents bearing a positively charged free amino group, as Ara4N residues, might play a role in pathogenesis since they reduce the negatively charged surface on the outer membrane rendering it positively charged or in an isoelectric state that, in turn, confers resistance to antibiotic compounds and antimicrobial peptides (Raetz and Whitfield, 2001; Hamad *et al*., 2012) (see chapter 7). The outer core region is the most exposed portion, often branched, and is characterised by a higher structural variability than the inner core region. It is typically characterised by common hexoses such as glucose, galactose, *N*-acetyl glucosamine and *N*-acetyl galactosamine and it may also contain residues as 6-deoxy-L-mannose (L-Rha) and *N*-acetyl-2,6-dideoxy-D-glucosamine (D-QuiNAc). It is possible to find peculiarities also in this region although less commonly; as example, in *Shewanella* LPS a new kind of glycosidic linkage has been found that involves an open chain acetal linkage of a glucosamine residue that is present as a non cyclic carbonyl form (Vinogradov *et al*., 2003).

1.3.3 The O-polysaccharide moiety: structure and activity

The O-chain polysaccharide is the most variable portion of the LPS also within bacteria belonging to the same genus; it consists of up to 50 identical repeating oligosaccharide units composed of two to eight different glycosil residues (heteroglycans) or, in some bacteria as *L. pneumophila*, of identical sugars (homoglycans). A single bacterium produces LPSs with O-chains characterised by a wide range of lengths as a result of incomplete synthesis of the polysaccharide chain (Raetz and Whitfield, 2001); this different degree of polymerization is responsible for the "ladder-like" pattern, showed by SDS-PAGE (Kittelberger and Hilbink, 1993) typical of a *smooth* LPS. The high structural variability of the O-polysaccharide is ascribable to the large number of sugar residues (in both pyranose and furanose rings, anomeric and absolute configurations) that can build up the repeating units as well as to the glycosidic sequence and to the presence of non-carbohydrate substituents such as phosphate, amino acids, sulphate, acetyl or formamide groups, often present in a non-stoichiometric fashion (Adinolfi *et al*., 1996). The function of these substituents is frequently unknown although it can be speculated that bacteria can modify their LPSs to mask themselves to the host immune system.

1.4 LPS and Elicitation of Host Immune Response

1.4.1 Innate Immunity and Adaptive Immunity

From the moment of birth and throughout our lifetime, humans are continuously exposed to a multitude of potential pathogen bacteria, through inhalation, direct contact and ingestion. The ability to avoid most of these infections depends on the adaptive immune system which remembers the previous encounters with specific pathogens and destroys them when they attack again

(Alberts *et al*., 2007). Adaptive immune responses, however, are slow to develop on the first exposure to a new pathogen, since it is required the activation and expansion of specific cells that take approximately 7 days prior to give an effective response. For this reason, the first days of exposure to a new pathogen see the intervention of the innate immune system (Alberts *et al*., 2007). Indeed, innate immune system is the first line of defense against invading organisms while the adaptive immune system acts as a second line of defense and also affords protection against re-exposure to the same pathogen; moreover the innate immune responses are not specific to a particular pathogen in the way that the adaptive immune responses are.

The strategy of recognition typical of the innate immune system relies on the detection of constitutive and conserved microbial molecular targets, that are common to many pathogens but are absent in the host; these latter are known as PAMPs or (Pathogen Associated Molecular Patterns) and are recognised by specific receptors, the PRRs (Pattern Recognition Receptors) present on the surface of some phagocytic cells that rapidly destroy them. It is worth to note that in Vertebrates, the skin and other epithelial surfaces, including those lining the lung and gut, provide a physical barrier between the inside of the body and the outside world, thus can be considered part of the innate immune system (Alberts *et al*., 2007). The microorganisms that pass this first barrier are recognised by the sentinels of innate immunity which are phagocytes, or white blood cells, or leukocytes, that are distinguishable in: neutrophils, polymorphonuclear neutrophilic leukocytes (PMN), macrophages and monocytes (Figure 1.9).

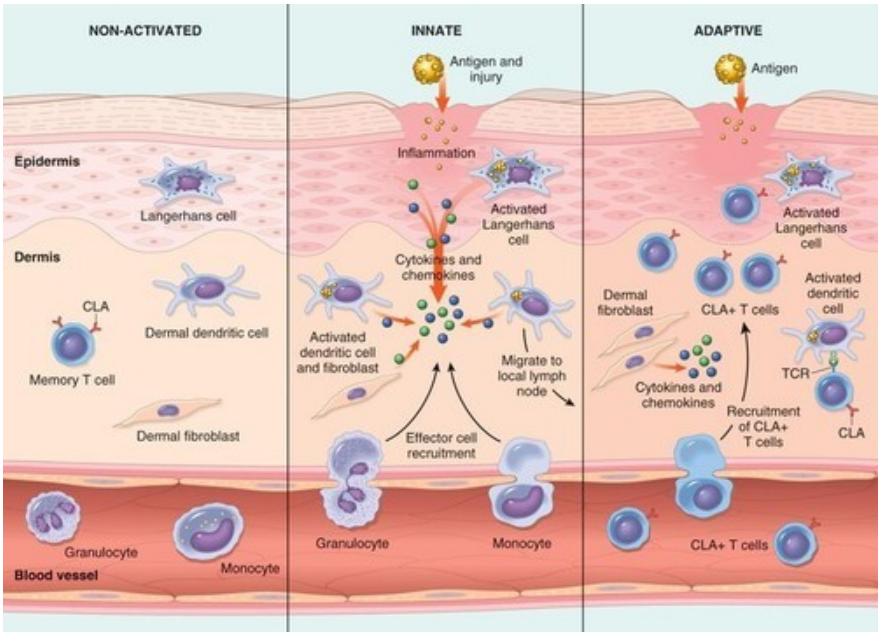

Figure 1.9 Overview of the innate and adaptive immune responses.

Macrophages and neutrophils show a variety of cell surface receptors, which make them able to recognise different types of microorganisms; the attack of a ligand to these receptors induces actin-polymerization that allows the plasma membrane of phagocytes to surround the pathogens and to incorporate them forming a phagosome which becomes acidified (Figure 1.10). In addition to being phagocytic, macrophages and neutrophils have granules, called lysosomes, that contain lysozyme and hydrolases; the phagosome fuses with one or more lysosomes to generate a phagolysosome in which the lysosomal contents are released to degrade bacterial cell wall (Figure 1.10). After degradation, phagolysosomes exhibit the antigenic determinants on their cell surface with the consequent triggering of the mechanism of specific immune response (Janeway *et al*., 2001).

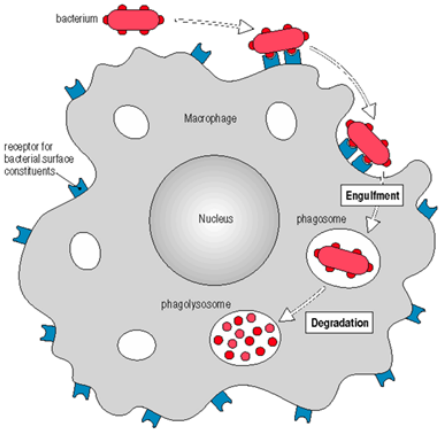

Figure 1.10 Phagocytosis mechanism as starting point of the innate immunity.

Compared to the innate immunity, specific immunity (or acquired or adaptive immunity) represents a more sophisticated system of defense. A peculiarity of this second line of defense is the ability to discriminate between exogenous antigens and autologous antigens (Janeway *et al*., 2001). Therefore acquired immunity strengthens the role of the innate immune response, amplifying, focusing and directing this response against foreign agents. It is possible to schematically distinguish two types of specific immunity: *humoral immunity* and *cell-mediated immunity* (Figure 1.11). The main components of acquired immunity are two other types of white blood cells that are called lymphocytes, which are divided into B lymphocytes (expression of humoral immunity and developed in the bone marrow) and T lymphocytes (expression of cell-mediated immunity and developed in the thymus). The acquired immune response consists in a first step of antigen-processing by macrophages and dendritic cells (termed "antigen presenting cells" or APC) and a second step of presentation to T and B lymphocytes which ensure the recognition by specific receptors (TCR and BCR, T and B cell receptors) expressed on their cell membrane. The

binding of the antigen to these receptors determines the activation, proliferation and differentiation into effector cells by a process of clonal selection. In details, in the *humoral* immune response, activated B cells (or plasma cells) secrete antibodies (or immunoglobulins) that circulate in the bloodstream and permeate other body fluids, where they bind specifically to the foreign antigen that stimulated their production, causing its destruction (Figure 1.11). In *cell-mediated* immune response, some T cells, termed cytotoxic, attack the leukocytes which present the antigenic determinants complexed to proteins of the major histocompatibility complex of class I (MHC I), and destroy them (Figure 1.11).

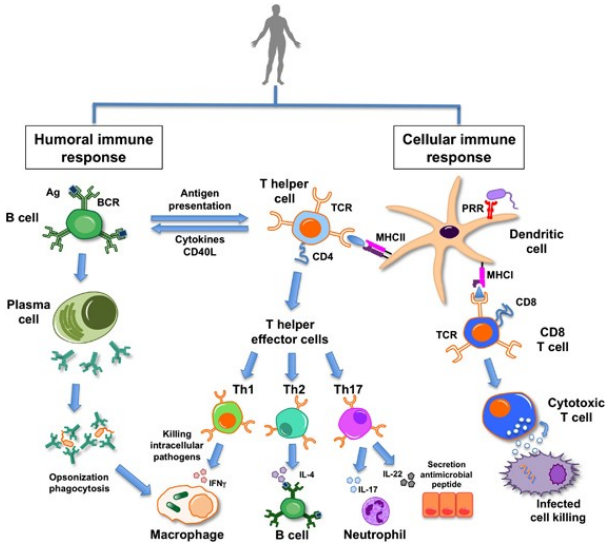

Figure 1.11 The humoral and cell-mediated immune responses.

Other T cells, the helper T immature cells, recognise the complex formed between the antigen and MHC class II proteins, and produce cytokines, known as macrophage colony-stimulating factor and gamma interferon, which promote the activity of macrophages. Moreover, the helper T cells secrete interleukin-2, which stimulates

the proliferation of abovementioned cytotoxic T cells (Alberts *et al*., 2007). Following expulsion of the antigen, the immune response gradually comes to an end. Some cells, produced during clonal expansion, undergo a phase of differentiation into memory cells, which are capable, in case of a possible new encounter with the same antigen, to respond more quickly and with higher efficiency (Alberts *et al*., 2007).

1.4.2 LPS and Innate Immunity

As described in the above paragraph 1.4.1, innate immune response is activated after recognition of bacterial conservative molecular targets termed PAMPs, by specific innate immune receptors, termed PRRs (Janeway, 1989). PAMPs have three common features that make them ideal targets for innate immune recognition:

1. are produced only by microbes and not by host
2. are invariant between microorganisms of a given class
3. are essential for microbial survival (Medzhitov, 2001)

In case of Gram-negative bacteria, lipopolysaccharides respond to all aforesaid three features, being recognised as PAMPs by a component of a family of PRRs known as Toll-Like Receptors (TLRs). Upon recognition of the real endotoxic principle of LPS, the lipid A moiety, the host innate immune system is immediately activated. The core oligosaccharide or, in *smooth* bacterial colonies, the O-chain, are the antigenic determinants recognised by the adaptative immunity. TLRs comprise a family of ten transmembrane receptors in humans, which are characterised by an extracellular leucine-rich repeat (LRR) domain and an intracellular Toll/IL-1 receptor (TIR) domain (Hashimoto *et al*., 1988; Medzhitov *et al*., 1997). Among all TLRs, TLR4 is the receptor designated to recognise the LPS macromolecule, but its detection

requires several accessory molecules. The first host protein involved in LPS recognition is a serum protein, the LBP (LPS-binding protein) that forms a high affinity complex with LPS lipid A released from bacterial lysis or replication, or still bound to the outer membrane of the intact microbial cell (Pålsson-McDermott and O'Neill, 2004). The N-terminal domain of LBP is responsible for the LPS lipid A binding while the C-terminal domain is specific for the further recognition by CD14 (Figure 1.12). This latter can be found in two forms, soluble (secreted into serum) and membrane bound (as glycophosphoinositol-linked protein on the surface of macrophages) (Haziot *et al*., 1996), and has a crucial role in the enhancement of host response to endotoxins since it facilitates the recognition of LPS by the final receptor complex TLR4/MD-2. It was demonstrated that CD14-deficient mice have a profound defect in responsiveness to LPS, thus showing the pivotal role of CD14 in LPS-recognition process (Haziot *et al*., 1996). Once CD14 binds to the LPS, it has been shown that CD14 can chaperone LPS from LBP to TLR4 at the cell surface. This latter is linked, through its extracellular domain, to a small glycoprotein, MD-2 (myeloid differentiation factor 2), which turns out to be absolutely necessary for the proper functioning of TLR4 receptor; indeed, the same MD-2 protein is able, by itself, to recognise lipid A with a good affinity, and also to discriminate different lipid A types. Therefore, TLR4 might be considered as a "pseudo-receptor", since, in the absence of MD-2, does not recognise its ligand. The TLR4/MD-2 complex has been shown to bind LPS with higher affinity than soluble MD-2 (Akashi *et al*., 2003). However, the binding affinity of MD-2 or the MD-2/LPS complex for TLR4 is the same (Visintin *et al*., 2005).

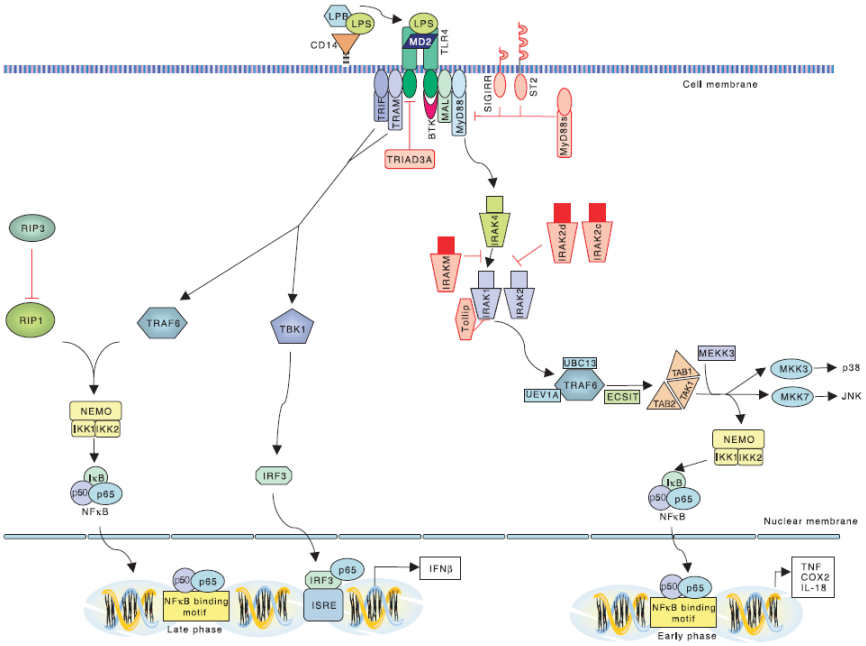

Figure 1.12 Schematised model of LPS signaling.

TLR4 with the MD-2 protein forms an heterodimer that recognizes a common structural motif in different LPS molecules (see details in Section III). The binding of LPS to TLR4/MD-2 receptorial complex can activate two different immune response pathways (Figure 1.12) (Park *et al.*, 2009). In the first case, it results in activation of the transcription factor NF-κB, which regulates the expression of genes encoding for inflammatory cytokines; whereas the second pathway results in activation of MAP-kinases which regulate the transcription of genes involved in increasing the stability of particular regions of the mRNA. In both cases, the final result is the amplification of the transduction signal with the consequent massive production of inflammatory proteins thus eliciting the inflammatory process (Figure 1.12) (Park *et al.*, 2009). If the inflammatory response is amplified and uncontrolled, due to

the high toxicity of the LPS from the infecting pathogen, there may occur a fulminating septic shock syndrome.

1.5 Gram-negative infections in Cystic Fibrosis

1.5.1 Cystic Fibrosis: an overview

Cystic Fibrosis (CF) is the most common lethal single gene disorder in Europe. The CF condition arises due to an autosomal recessive gene defect with an incidence of approximately 1/2000 live births in the Western hemisphere. The basic genetic defect in CF reflects mutations in a gene, located on the long arm of chromosome 7, encoding for an epithelial chloride channel, named Cystic Fibrosis Transmembrane Regulator (CFTR) (Figure 1.13), a protein of 1480 residues (De Soyza *et al*., 2012). Over 1000 mutations are described to date, but the most common disorder is the ΔF508, present in one or both alleles in approximately 90% of CF patients (Riordan, 2008), that leads to a single amino acid mutation generating a failure in CFTR folding and maturation. CFTR is a cyclic AMP-regulated chloride channel expressed on the apical membrane of the epithelial cells in the airways, pancreas, intestine, testis and exocrine glands, as well in some non-epithelial cell types (Lukacs and Verkman, 2011). It is constituted by two membrane-spanning domains (MSD1 and MSD2), two nucleotide-binding domains (NBD1 and NBD2) that participate in ATP binding and hydrolysis, and a regulatory domain (R) whose phosphorylation regulates channel gating (Lukacs and Verkman, 2011). CFTR maintains the ion and fluid homeostasis since it is the unique ABC protein that functions as ion channel.

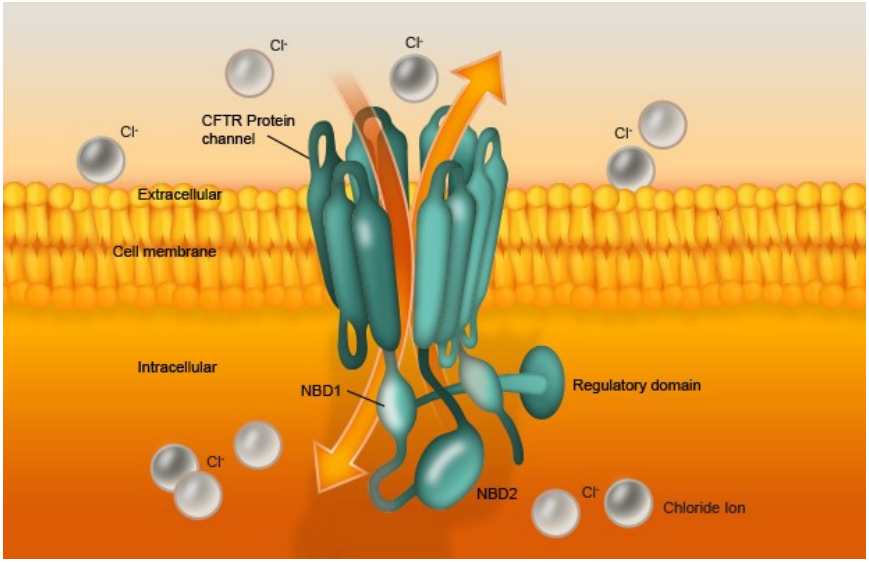

Figure 1.13 The CFTR trans-membrane protein.

Mutations in CFTR protein cause the CF phenotype characterised by multiple organ system collapse including liver, gastrointestinal, reproductive and pulmonary involvement, leading to death. However, a wide variability in the clinical expression is found among patients. Up to 20% of affected infants are born with intestinal obstruction and present inspissated meconium (meconium ileus). Other patients are diagnosed with various modes of presentation from birth to adulthood and with considerable variability in the severity and rate of disease progression. Even within the same CFTR genotype, there is evidence that other genes, as well as environmental factors, make important contributions to the pulmonary phenotype. Moreover, inactive CFTR causes an immune-deficiency against pathogens thus producing chronic bacterial lung infections which are a hallmark of the condition with episodic worsening “exacerbations” leading to multiple courses of

antibiotics, hospitalisation and precipitous terminal decline (De Soyza *et al*., 2012).

In healthy conditions a mucus layer permeates epithelium surface allowing an efficient ciliar beat and providing for an optimal lubrificant activity. The normal hydration of epithelia is due to their capability to absorb and secrete salts with water moving osmotically in response to salts gradient. In this scenario, CFTR represents the Cl^- channel, while the epithelia Na^+ channel (ENaC) and the Na^+/K^+-ATPase regulate Na^+ transport in and out the membrane (Figure 1.14). Mucus clearance is guaranteed by CFTR that acts either as Cl^- channel or as an inhibitor of the ENaC; indeed, when airway surface liquid (ASL) reduces, the channel ENaC is inhibited while CFTR starts to secrete Cl^- anions with the consequent water osmotic passage across the membrane that reconstitutes the normal ASL hydration (Figure 1.14). In a CF tissue, abnormal CFTR allows little to no Cl^- ion movement and an unregulated Na^+ adsorption, resulting in a severe dehydration that causes a collapse of mucus layer on periciliary liquid layer (Figure 1.14). Retention of sticky secretions further promotes bacteria persistence and prevents mucociliary clearance of virulence factors (Figure 1.14). These processes collectively promote further airway damage and inflammation leading to the vicious cycle paradigm.

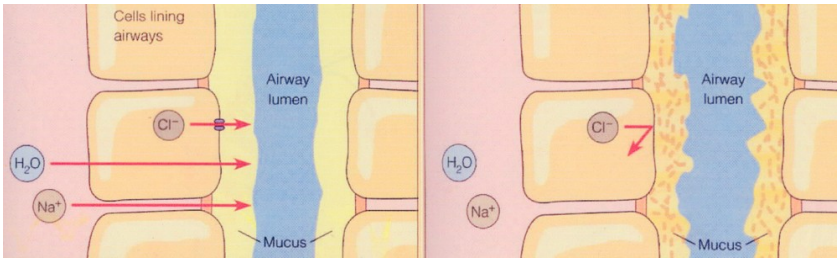

Figure 1.14 Ions movement through epithelia of healthy (left) and cystic fibrosis individuals (right).

Recently, CFTR has been shown to be a negative regulator of a central pro-inflammatory controller Nuclear Factor kappa B (NF-κB) (Hunter, 2010). Hence, mutations in CFTR may be themselves pro-inflammatory. Cytokines of relevance in CF include interleukin 8 (IL-8), IL-1, IL-6, IL-17 and TNF-α (Salva *et al*., 1996; Raoust *et al*., 2009). These cytokines have a pro-inflammatory effect through vasodilatation, direct chemokinesis, neutrophil priming and angiogenesis. Recently, more novel pro inflammatory moieties that have been associated with inflammation in CF include endogenous damage associated molecular patterns (DAMPS) such as lipid metabolites as ceramide (Brodlie *et al*., 2011). Indeed, CF-dependent damage of lysosomes promotes ceramide accumulation. Biological membranes are mainly constituted by cholesterol, sphingomyelin and phospholipids. In lysosomes sphingomyelin is converted to ceramide through the acid sphingomyelinase (Asm); then ceramide is degraded in sphingosine by acid ceramidase (Ac). Lysosomes damages in respiratory cells induce an imbalance of both enzymatic activities that leads to a net accumulation of ceramide. As a consequence, the rate of cell death increases with an accumulation of DNA that facilitated pathogen infections (Döring and Gulbins, 2009). Moreover, ceramide accumulation also induces, as described above, a pro-inflammatory status since there is an increase synthesis and release of cytokines (Brodlie *et al*., 2011).

Despite elevated numbers of airway innate immune cells, there is clearly impaired immunity in CF phenotype. Data showed neutrophil dysfunction in CF, with evidence of neutrophil undergoing necrosis resulting in DNA release and increased mucous viscosity, compounding the problem of bacterial attachment (Callaghan and McClean, 2012). Another aspect of host immune defences that are compromised in CF regards the macrophage clearance of pathogens (Callaghan and McClean,

2012). Recent studies report that dysfunctional CFTR in macrophages impairs their bacteriocidal activity (Del Porto *et al*., 2011). Indeed, in normal conditions, after phagocytosis by lung macrophages, microbes enter the phagosome and lysosomes forming the phagolysosome (Figure 1.10) (see also paragraph 1.4.1). This mature organelle exhibits a low pH that destroys ingested bacteria. In case of defective CFTR-dependent acidification of lysosomal pH (Barasch *et al*., 1991), it has been observed a significant survival of the most common CF pathogen, *P. aeruginosa* (Di *et al*., 2006). Furthermore, many components of the *humoral* immune response are ineffective in cystic fibrosis such as host defence peptides (HDPs) which are impaired by dehydration of ASL (Boucher, 2007). Secretion of proteases in CF lung further compromises immune system functions, indeed it is possible to observe a predominance of neutrophil elastase that destroys a large number of anti-microbial proteins, degrades mucin (Henke et al., 2011) and increase IL-8 production from epithelial cells (Cosgrove *et al*., 2011). This latter is crucial since growth of many opportunistic bacterial species results enhanced in presence of IL-8.

1.5.2 Cystic Fibrosis as a complex microbial pathology

Characteristic opportunistic cystic fibrosis pathogens include *Haemophilus influenza*, *Staphylococcus aureus* (Liou *et al*., 2001), and *Pseudomonas aeruginosa* (Gomez and Prince, 2007). Important but less common bacterial pathogens include the *Burkholderia cepacia* complex (BCC) (Mahenthiralingam *et al*., 2005), non tuberculous *Mycobacteria*, *Acinetobacter* spp (Coenye *et al*., 2002), *Stenotrophomonas* spp (Brooke, 2012), *Achrombacter* spp (Emerson *et al*., 2010; Spicuzza *et al*., 2009) and *Pandorea* genus (Coenye *et al*., 2000). Though some of these can occasionally infect normal human lungs, aforesaid pathogens are predominantly opportunistic pathogens. A common clinical pattern

is a sequential replacement of pathogens over time from *Haemophilus* and S. *aureus* with *Pseudomonas* usually becoming the predominant pathogen by adulthood (Rosenfeld *et al*., 2001).

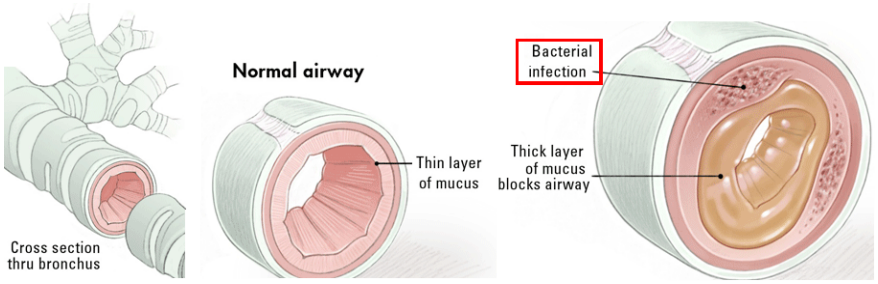

Figure 1.15. Cross section of bronchus showing mucus retention and bacterial infection (on the right)

Epidemiology of *P. aeruginosa* is characterised by an early stage of infection, that lasts about three months, followed by a chronic establishment of the inflammation that causes persistent respiratory symptoms and decline in pulmonary functions (Gibson *et al*., 2003; Ciganà *et al*., 2009). During the first period there is co-infection of different *P. aeruginosa* strains but then, with evolving of the inflammation, a single clone remains established. The establishment of a permanent relationship with the host chemically implies the adaptation of the bacterium to the CF airway which is possible due to its intrinsic genetic and phenotypic plasticity; indeed, it has previously been observed that *P. aeruginosa* isolates, early adapted to the lungs of CF patients, show peculiar genotypic and phenotypic characteristics which are not found in chronically infected individuals, implying that the chronic *P. aeruginosa* strain becomes completely different to the initially acquired strain (see chapther 5) (Di Lorenzo *et al*., 2014; Mena *et al*., 2008). Selective pressures on bacteria in persistent chronic CF infection are

plausible with exposure to repeated antibiotics, continual exposure to host defense molecules and changes in the local environment caused by worsening lung disease all likely forces (Eberl and Tummler, 2004). Certain features emerge in *Pseudomonas aeruginosa* strains from patients with advanced CF lung disease; indeed, antimicrobial resistance rates including pan-resistant strains are highly prevalent. Furthermore development of alginate and the "mucoid phenotype" and a hypermutator phenotype are also common during chronicity of infection (Waine *et al*., 2008). Biofilm forming capacity is common in strains isolated in cystic fibrosis, particularly those who have persistent infection for years (Hoiby *et al*., 2010). Biofilms are complex communities of bacteria with physical and functional aspects. They contribute to pathogenesis by increasing resistance to phagocytosis, but also by increasing antibiotic resistance (Hoiby *et al*., 2010; Bagge *et al*., 2000). The importance of multispecies biofilms is that supposedly low pathogenicity bacteria such as oral "commensal" can induce virulence factor upregulation in *Pseudomonas aeruginosa*. The effect of complex biofilm growth on cell surface virulence determinants is to date still an emerging field.

As for the second most dominant pathogen, *Burkholderia* is less prevalent than *Pseudomonas* but is responsible for the most feared infections. Previously, infections with "*Burkholderia cepacia*" were attributed to a single species. Indeed, such infections are caused by a variety of bacterial species, grouped into the *Burkholderia cepacia* complex (BCC) (Mahenthiralingam, 2000). Currently this complex comprises over 10 related species named *genomovars* which are phenotypically similar but genotypically different. The most prevalent clinical isolates from CF patients are *B. cenocepacia* strains (genomovar III) and *B. multivorans* strains (genomovar II) (De Soyza *et al*., 2004) and infection with the former is most often associated with patient-to-patient spread and

fatal invasive infection (the so-called "*cepacia syndrome*") (Govan and Deretic, 1996). Lung transplantation, whilst intensive and aggressive, is to date the only treatment that offers improved quantity and quality of life of CF patients with advanced lung disease. BCC's impact on the survival of CF patients following lung transplantation is viewed as so detrimental that infection with these organisms is considered a relative or absolute contraindication for transplantation (De Soyza and Corris, 2003). Post-transplant survival rates are 15% to 63% lower than those of CF patients not infected with BCC (Alezander *et al*., 2008), with death usually resulting from BCC sepsis in the early post-operative period. It is important to underline that there are great differences *in vitro* among different isolates from the same genetic lineage e.g. for the renowned *B. cenocepacia* epidemic strain ET-12 clonal strains J2315 and K56-2 strains behave differently when used *in vitro* and *in vivo* models (Mahenthiralingam *et al*., 2000). Hence this heterogeneity illustrates the importance of examining multiple clinical bacterial isolates and not generalising the results from studies of a single strain. Molecular differences among the BCC family has been suggested as the cause of their variable pathogenicity, and their LPS has been proposed as potentially important in this. Studies conducted soon after genomovar designation have assessed LPS chemotypes within the BCC (De Soyza *et al*., 2004). So far strains tested belonging to *B. cepacia* genomovar I and *B. multivorans* had *smooth* LPS. In contrast, isolates belonging to *B. cenocepacia*, expressed either *rough* or *smooth* LPS chemotype (Silipo *et al*., 2007). Importantly two clones of the *B. cenocepacia* ET-12 lineage differed with J2315 and K56-2 having a *rough* and a *smooth* chemotype respectively. Subsequent studies in clinical BCC strains assessing chemotype have demonstrated both *rough* and *smooth* LPS chemotypes are found. Other genomovars studied had predominantly *smooth* LPS though *B. multivorans* and *B. vietnamiensis* strains expressing

rough LPS were noted (Ieranò *et al.*, 2009). Moreover, it was demonstrated that BCC strains may differentially express LPS dependent on the local environment. This is clinically important as airway mucus may serve as a semi-solid growth media within CF lungs.

Nowadays, despite genetic bases of the pathology, a wide branch of research on CF is focused on the epidemiology, the pathogenicity and the treatment of CF pathogens infections. Thus, studies on virulence factors characterising CF pathogens are aimed to elucidate their chemical structure and biological activity, aid to identify new targets for therapies.

References

Adinolfi M., Corsaro M.M., De Castro C., Evidente A., Lanzetta R., Molinaro A., Lavermicocca P., Parrilli M., Analysis of the polysaccharide fraction of *Pseudomonas caryophylli*. **1996**, *Carb. Res*., 284, 119-133.

Akashi S., Saitoh S., Wakabayashi Y., Kikuchi T., Takamura N., Nagai Y., Kusumoto Y., Fukase K., Kusumoto S., Adachi Y., Kosugi A., Miyake K., Lipopolysaccharide interaction with cell surface Toll-like receptor 4-MD-2: higher affinity than that with MD-2 or CD14. **2003**, *J. Exp. Med.*, 198, 1035-1042.

Alberts B., Johnson A., Lewis J., Raff M., Roberts K., Walter P., Molecular Biology of the Cell, 4th edition (Ed.: Garland Science), New York, chapter 24, **2007**.

Alexander B.D., Petzold E.W., Reller L.B., Palmer S.M., Davis R.D., woods C.W., LiPuma J.J., Survival after lung transplantation of cystic fibrosis patients infected with *Burkholderia cepacia* complex. **2008**, *Am. J. Transplant,* 8, 1025-30.

Alexander C., Rietschel E.T., Bacterial lipopolysaccharides and innate immunity. **2001**, *J. Endotoxin Res.*, 7: 167-202.

Bagge N., Ciofu O., Skovgaard L.T., Hoiby N., Rapid development in vitro and in vivo of resistance to ceftazidime in biofilm-growing *Pseudomonas aeruginosa* due to chromosomal beta-lactamase. **2000**, *Apmis*, 108, 589-600.

Barasch J., Kiss B., Prince A., Saiman L., Gruenert D. , al-Awqati Q., Defective acidification of intracellular organelles in cystic fibrosis. **1991**, *Nature*, 352, 70–73.

Boucher R.C., Evidence for airway surface dehydration as the initiating event in CF airway disease. **2007**, *J. Intern. Med*., 261: 5-16.

Brandenburg K., Mayer H., Koch M.H., Weckesser J., Rietschel E.T., Seydel U., Influence of the supramolecular structure of free lipid A on its biological activity. **1993**, *Eur. J. Biochem*., 218: 555-563.

Brodlie M., McKean M.C., Johnson G.E., Gray J., Fisher A.J., Corris P.A., Lordan J.L., Ward C., Ceramide is increased in the lower airway epithelium of people with advanced cystic fibrosis lung disease. **2011**, *Am. J. Respir. Crit. Care Med.,* 182, 369-75.

Brooke S., *Stenotrophomonas maltophilia*: an emerging global opportunistic pathogen. **2012**, *Clin. Microbiol. Rev.,* 25, 2-41.

Callaghan M., McClean S., Bacterial host interactions in cystic fibrosis. **2012**, *Current Opinion in Microbiology*, 15:71–77.

Cardoso L.S., Araujo M.I., Góes A.M., Pacífico L.G., Oliveira R.R., Oliveira S.C., Polymyxin B as inhibitor of LPS contamination of *Schistosoma mansoni* recombinant proteins in human cytokine analysis. **2007**, *Microb. Cell Fact.*, 6, 1.

Ciganà C., Curcurù L., Leone M.R., Ieranò T., Lorè N.I., Bianconi I., Silipo A., Cozzolino F., Lanzetta R., Molinaro A., Bernardini M.L., Bragonzi A., *Pseudomonas aeruginosa* exploits lipid A and muropeptides modification as a strategy to lower innate immunity during cystic fibrosis lung infection. **2009**, *PLoS One*, 4(12), e8439.

Coenye T., Falsen E., Hoste B., Ohle M., Goris J., Govan J.R.W., Gillis M., Vandamme P., Description of *Pandoraea* gen. nov. with *Pandoraea apista* sp. nov., *Pandoraea pulmonicola* sp. nov., *Pandoraea pnomenusa* sp. nov., *Pandoraea sputorum* sp. nov. and *Pandoraea norimbergensis* comb. nov. **2000**, *International Journal of Systematic and Evolutionary Microbiology* , 50, 887–899.

Coenye T., Goris J.,. Spilker T, Vandamme P., LiPuma J.J., Characterization of unusual bacteria isolated from respiratory secretions of cystic fibrosis patients and description of *Inquilinus limosus* gen. nov., sp. nov. **2002**, *J. Clin. Microbiol.,* 40, 2062-9.

Cosgrove S., Chotirmall S.H., Greene C.M., McElvaney N.G., Pulmonary proteases in the cystic fibrosis lung induce interleukin 8 expression from bronchial epithelial cells via a heme/meprin/epidermal growth factor receptor/Toll-like receptor pathway. **2011**, *J. Biol. Chem.*, 286, 7692-7704.

Del Porto P., Cifani N., Guarnieri S., Di Domenico E.G., Mariggio M.A., Spadaro F., Guglietta S., Anile M., Venuta F., Quattrucci S., Ascenzioni F., Dysfunctional CFTR alters the bactericidal activity of human macrophages against *Pseudomonas aeruginosa*. **2011**, *PLoS ONE*, 6, e19970.

De Soyza A., Corris P.A., Lung transplantation and the *Burkholderia cepacia* complex. **2003**, *J. Heart Lung Transplant.,* 22, 954-8.

De Soyza A., Di Lorenzo F., Silipo A., Lanzetta R., Molinaro A., **2012**, *Carbohydrate Chemistry*, RSC Publishing, 38**,** 13-39.

De Soyza A., Ellis C.D., Khan C.M., Corris P.A., Demarco de Hormaeche R., *Burkholderia cenocepacia* lipopolysaccharide, lipid A, and proinflammatory activity. **2004**, *Am. J. Respir. Crit. Care Med*., 170, 70-7.

De Soyza A., Morris K., McDowell A., Doherty C., Archer L., Perry J., Govan J.R., Corris P.A., Gould K., Prevalence and clonality of *Burkholderia cepacia* complex genomovars in UK patients with cystic fibrosis referred for lung transplantation. **2004**, *Thorax*., 59, 526-8.

De Soyza A., Silipo A., Lanzetta R., Govan J.R., Molinaro A., Chemical and biological features of *Burkholderia cepacia* complex lipopolysaccharides. *Innate Immun.*, 2008, 14, 127-144.

Di A., Brown M.E., Deriy L.V., Li C., Szeto F.L., Chen Y., Huang P., Tong J., Naren A.P., Bindokas V., Palfrey H.C., Nelson D.J., CFTR regulates phagosome acidification in macrophages and alters bactericidal activity. **2006**, *Nat. Cell Biol*., 8(9), 933-44.

Di Lorenzo F., Silipo A., Bianconi I., Scamporrino A., Sturiale L., Garozzo D., Lanzetta R., Parrilli M., Bragonzi A., Molinaro A., Persistent cystic fibrosis isolate *Pseudomonas aeruginosa* strain RP73 exhibits an under-acylated LPS structure responsible of its low inflammatory activity. **2014**, *Molecular Immunology*, In press.

Doring G., Gulbins E., Cystic fibrosis and innate immunity: how chloride channel mutations provoke lung disease. **2009**, *Cellular Microbiology*, 11, 208-216.

Eberl L., Tummler B., *Pseudomonas aeruginosa* and *Burkholderia cepacia* in cystic fibrosis: genome evolution, interactions and adaptation. **2004**, *Int. J. Med. Microbiol.,* 294, 123-31.

Emerson J., McNamara S., Buccat A.M., Worrell K., Burns J.L., Changes in cystic fibrosis sputum microbiology in the United States between 1995 and 2008. **2010**. *Pediatr. Pulmonol.,* **45**, 363-70

Fukuoka S., Brandenburg K., Müller M., Lindner B., Koch M.H., Seydel U., Physico-chemical analysis of lipid A fractions of lipopolysaccharide from *Erwinia carotovora* in relation to bioactivity. **2001**, *Biochim. Biophys. Acta.*, 1510, 185-197.

Gibson R.L., Burns J.L., Ramsey B.W., Pathophysiology and management of pulmonary infections in cystic fibrosis. **2003**, *Am. J. Respir. Crit. Care Med*. 168, 918–951.

Golenbock D.T., Hampton R.Y., Qureshi N., Takayama K., Raetz C.R., Processing and secretion of tumor necrosis factor alpha in endotoxin-treated Mono Mac 6 cells are dependent on phorbol myristate acetate. **1991**, *J. Biol. Chem*., 266, 19490-19498

Gomez M.I, Prince A., Opportunistic infections in lung disease: *Pseudomonas* infections in cystic fibrosis. **2007**, *Curr. Opin. Pharmacol.,* **7**, 244-51.

Govan J.R., Deretic V., Microbial pathogenesis in cystic fibrosis: mucoid *Pseudomonas aeruginosa* and *Burkholderia cepacia*. **1996**, *Microbiological Reviews*, 60, 539-74.

Hamad M.A., Di Lorenzo F., Molinaro A., Valvano M.A., Aminoarabinose is essential for lipopolysaccharide export and intrinsic antimicrobial peptide resistance in *Burkholderia cenocepacia*. **2012**, *Molecular Microbiology*, 85, 5, 962–974.

Hashimoto C., Hudson K.L., Anderson K.V., The Toll gene of Drosophila, required for dorsal-ventral embryonic polarity, appears to encode a transmembrane protein. **1988**, *Cell*, 52, 269-279.

Haziot A., Ferreo E., Kontgen F., Hijiya N., Yamamoto S., Silver J., Stewart C.L., Goyert S.M., Resistance to endotoxin shock and reduced dissemination of gram-negative bacteria in CD14-deficient mice. **1996**, *Immunity*, 4, 407-414.

Hellerqvist C.G., Lindberg B., Samuelsson K., Lindberg A.A., Structural studies on the O-specific side-chains of the cell-wall lipopolysaccharide from *Salmonella parathyphi* A var. durazzo. **1971**, *Acta Chem. Scand.*, 25, 955-961.

Hellerqvist C.G., Lindberg B., Svensson S., Holme T., Lindberg A.A., Structural studies on the O-specific side chains of the cell wall lipopolysaccharides from *Salmonella typhi* and *S. enteritidis*. **1969**, *Carbohydr. Res.*, **9**, 237-241

Henke M.O., John G., Rheineck C., Chillappagari S., Naehrlich L., Rubin B.K., Serine proteases degrade airway mucins in cystic fibrosis. **2011**, *Infect. Immun.*, 79, 3438-3444.

Holst O. in *Endotoxin in Health and Disease* (Eds.: H. Brade, D. C. Morrsion, S. Opal, S. Vogel), DEKKER, New York, **1999**, 115 –154.

Holst O., Ulmer A.J., Brade H., Flad H.D., Rietschel E.T., Biochemistry and cell biology of bacterial endotoxins. *FEMS Immunol. Med. Microbial.,* **1996**,16, 83-104.

Hunter M.J., Treharne K.J., Winter A.K., Cassidy D.M., Land S., Mehta A., Expression of wild-type CFTR suppresses NF-kappaB-driven inflammatory signalling. **2010**, *PLoS One*, 5, e11598.

Ieranò T., Silipo A., Sturiale L., Garozzo D., Bryant C., Lanzetta R., Parrilli M., Aldridge C., Gould F.K., Corris P.A., Khan C.M., De Soyza A., Molinaro A., First structural characterization of *Burkholderia vietnamiensis* lipooligosaccharide from cystic fibrosis-associated lung transplantation strains. **2009**, *Glycobiology*, 19, 1214-23.

Janeway C.A. Jr., Approaching the asymptote? Evolution and revolution in immunology. **1989**, *Cold Spring Harb. Symp. Quant. Biol*., 54, 1-13.

Janeway C.A. Jr, Travers P., Walport M., Shlomchik M.J., Immunobiology 5th edition (Ed.: Garland Science), New York, **2001**.

Kittelberger R., Hilbink F., Sensitive silver-staining detection of bacterial lipopolysaccharides in polyacrylamide gels. **1993**, *J. Biochem. Biophys. Methods*, 26 (1), 81-86.

Liou T.G., Adler F.R., Fitzsimmons S.C., Cahill B.C., Hibbs J.R., Marshall B.C., Predictive 5-year survivorship model of cystic fibrosis. **2001**, *American Journal of Epidemiology,* 153, 345-52.

Lüderitz O., Galanos C., Risse H.J., Ruschmann E., Schlecht S., Schmidt G., Schulte-Holthausen H., Wheat R., Westphal O., Schlosshardt, Structural relationship of *Salmonella* O and R antigens. **1966**, *J. Ann. NY Acad. Sci.*, 133, 347-349.

Lukacs G.L., Verkman A.S., CFTR: folding, misfolding and correcting the ΔF508 conformational defect. **2011**, *Trends in Molecular Medicine*, 18(2), 81-91.

Mahenthiralingam E., Coenye T., Chung J.W., Speert D.P., Govan J.R., Taylor P., Vandamme P., Diagnostically and experimentally useful panel of strains from the *Burkholderia cepacia* complex. **2000**, *Journal of Clinical Microbiology,* 38, 910-3.

Mahenthiralingam E., Urban T.A., Goldberg J.B., The multifarious, multireplicon *Burkholderia cepacia* complex. **2005**, *Nat. Rev. Microbiol.,* 3, 144-56.

Medzhitov R., Toll-like receptors and innate immunity. *2001*, *Nature Reviews Immunology*, 1(2): 135-45.

Medzhitov R., Preston-Hurlburt P., Janeway C.A. Jr., A human homologue of the Drosophila Toll protein signals activation of adaptive immunity. **1997**, *Nature*, 388, 394-397.

Mena A., Smith E.E., Burns J.L., Speert D.P., Moskowitz S.M., Perez J.L., Oliver A., Genetic adaptation of *Pseudomonas aeruginosa* to the airways of cystic fibrosis patients is catalyzed by hypermutation. **2008**, *J. Bacteriol.*, 190(24): 7910–7917

Mesbah N.M., Wiegel J., Life at extreme limits: the anaerobic halophilic alkalithermophiles. **2008**, *Ann. NY Acad. Sci.*, 1125: 44-57.

Netea M.G., van Deuren M., Kullberg B.J., Cavaillon J.M., van der Meer J.W., Does the shape of lipid A determine the interaction of LPS with Toll-like receptors?. **2002**, *Trends Immunol*., 23: 135–139

Oikawa M., Shintaku T., Fukuda N., Sekljic H., Fukase Y., Yoshizaki H., Fukase K., Kusumoto S., NMR conformational analysis of biosynthetic precursor-type lipid A: monomolecular state and supramolecular assembly. **2004**, *Org. Biomol. Chem*., 2: 3557-3565.

Pålsson-McDermott E.M., O'Neill L.A., Signal transduction by the lipopolysaccharide receptor, Toll-like receptor-4. **2004**, *Immunology,* 113:153-162.

Park B.S., Song D.H., Kim H.M., Choi B.S., Lee H., Lee J.O., The structural basis of lipopolysaccharide recognition by the TLR4-MD-2 complex. **2009**, *Nature*, 458: 1191-5

Pommerville J.C., Alcamo's fundamentals of microbiology 9th Edition, Chapter 4. (Eds.: Jones & Bartlett Publishers), Burlington, MA, **2010**,

Raetz C.R., Biochemistry of endotoxins. **1990**, *Annu. Rev. Biochem.*, 59: 129–70

Raetz C.R., Whitfield C., Lipopolysaccharide endotoxins. **2002**, *Annu. Rev. Biochem.*, 71: 635–700

Raoust E., Balloy V., Garcia-Verdugo I., Touqui L., Ramphal R., Chignard. M., *Pseudomonas aeruginosa* LPS or flagellin are sufficient to activate TLR-dependent signaling in murine alveolar macrophages and airway epithelial cells. **2009**, *PLoS One*, 4, e7259.

Raven P.H., Johnson G.B., Biology 9th Edition, Chapter 34 (Ed.: McGraw Hill), **2011**.

Rietschel E.T., Kirikae T., Schade F.U., Mamat U., Schmidt G., Loppnow H., Ulmer A.J., Zähringer U., Seydel U., Di Padova F., Schreier M., Brade H., Bacterial endotoxin: molecular relationships of structure to activity and function. **1994**, *FASEB J.*, 8: 217-225.

Riordan, J.R., CFTR function and prospects for therapy. **2008**, *Annu. Rev. Biochem.*,77, 701–726

Rosenfeld M., Gibson R.L., McNamara S., Emerson J., Burns J.L., Castile R., Hiatt P., McCoy K., Wilson C.B., Inglis A., Smith A., Martin T.R., Ramsey B.W., Early pulmonary infection, inflammation, and clinical outcomes in infants with cystic fibrosis. **2001**, *Pediatr. Pulmonol.,* 32, 356-66.

Salva P.S., Doyle N.A., Graham L., Eigen H., Doerschuk C.M., TNF-alpha, IL-8, soluble ICAM-1, and neutrophils in sputum of cystic fibrosis patients. **1996**, *Pediatric Pulmonology*, 21, 11-9.

Seydel U., Oikawa M., Fukase K., Kusumoto S., Brandenburg K., Intrinsic conformation of lipid A is responsible for agonistic and antagonistic activity. **2000**, *Eur. J. Biochem.*, 267: 3032-3039.

Silipo A., De Castro C., Lanzetta R., Parrilli M., Molinaro M. Prokaryotic cell wall compounds structure and biochemistry (Eds. Konig, H., Herald, C., Varma, A.) Springer-Verlag, Berlin, Germany, 133–154, **2010**.

Silipo A., Molinaro A., Ieranò T., De Soyza A., Sturiale L., Garozzo D., Aldridge C., Corris P.A., Khan C.M., Lanzetta R., Parrilli M., The complete structure and pro-inflammatory activity of the lipooligosaccharide of the highly epidemic and virulent gram-negative bacterium *Burkholderia cenocepacia* ET-12 (strain J2315). **2007**, *Chemistry.*, 13, 3501-11.

Spicuzza L., Sciuto C., Vitaliti G., Di Dio G., Leonardi S., La Rosa M., Emerging pathogens in cystic fibrosis: ten years of follow-up in a cohort of patients. **2009**, *Eur. J. Clin. Microbiol. Infect. Dis.,* 28, 191-5.

Staley J.T., Gunsalus R.P., Lory S., Perry J.J., Microbial Life 2nd Edition, chapter 4, **2007**.

Vinogradov EV, Bock K, Petersen BO, Holst O, Brade H., The structure of the carbohydrate backbone of the lipopolysaccharide from *Acinetobacter* strain ATCC 17905. **1997**, *Eur. J. Biochem*., 243(1-2):122-7.

Vinogradov E., Korenevsky A., Beveridge T.J., The structure of the rough-type lipopolysaccharide from *Shewanella oneidensis* MR-1, containing 8-amino-8-deoxy-Kdo and an open-chain form of 2-acetamido-2-deoxy-D-galactose. **2003**, *Carbohydr Res.,* 338(19):1991-7.

Visintin A., Halmen K.A., Latz E., Monks B.G., Golenbock D.T., Pharmacological inhibition of endotoxin responses is achieved by targeting the TLR4 coreceptor MD-2. **2005**. *J. Immunol*., 175, 6465-6472.

Waine D.J., Honeybourne D., Smith E.G., Whitehouse J.L. , Dowson C.G., Association between hypermutator phenotype, clinical variables, mucoid phenotype, and antimicrobial resistance in *Pseudomonas aeruginosa*. **2008**, *J. Clin. Microbiol.,* 46, 3491-3

Zahringer U., Lindner B., Rietschel E.T. in Endotoxin in Health and Disease (Eds.: H. Brade, S. M. Opal, S. N. Vogel, D. C. Morrison), Marcel Dekker, New York, Basel, 93-114, **1999**.

Chapter 2

Structural Characterisation of Lipopolysaccharides and Lipooligosaccharide

2.1 Extraction and Purification of LPSs and LOSs

The first approach aimed to the structural elucidation of LPS/LOS is represented by their extraction from intact microbial cells. This is conventionally achieved through two complementary procedures, that lead to the selective isolation of R-LPS (LOS) and S-LPS exploiting their different amphiphilic character; indeed the latter has higher hydrophilicity, due to the presence of the polysaccharide moiety of the O-chain, whereas the former, which lacks such portion, has a greater hydrophobic character. Thus, these different physical-chemical properties allow to perform a selective extraction of the LOS and LPS, with a high degree of purity. Liophilised bacterial cells are firstly washed with acetone, water and ethylic to remove cell contaminants. After this initial step of purification, the procedure of extraction can take place. Typically, *rough*-type LPSs are extracted with a phenol-chloroform-petroleum ether procedure (PCP) (Galanos *et al*., 1969) while *smooth*-type LPSs are extracted with the hot phenol-water protocol (Westphal and Jann, 1965).

The PCP extraction consists in the treatment of dried bacterial cells with phenol/chloroform/light petroleum in proportions 5:8:2; LOS is precipitated from pure phenol adding drops of water. After this extraction, cells undergo a second treatment with 90% phenol/water 1:1 at 68°. The two phases are then extensively dialysed and liophilised. As previously mentioned, typically the presence of the long O-chain moiety increases the hydrophilic nature of endotoxins, thus LPS molecules are extracted in the water phase even though several factors, as the occurrence within the repeating unit of hydrophobic groups as well as charged monosaccharides or the length of the polysaccharide chains, may modulate LPS solubility in water. Thus, it can be detected either in the water or in the phenol extract.

After the extraction procedure, enzymatic treatments to remove proteins and nucleic acids are executed. The typical protocol consists in LPS/LOS purification with nucleases (DNAse and RNAse) and protease followed by dialysis in order to remove digested material. The screening for detection of LPS is realised by SDS polyacrylamide electrophoresis gel (SDS-PAGE) followed by silver nitrate staining which allows to define the typology of the extracted material and its purification degree (Kittelberger and Hilbink, 1993). The presence of LPS is testified by the observation of the typical "ladder-like" pattern of the electrophoretic migration, due to the presence of molecules differing in their structure for the number of repeating units composing the O-polysaccharide moiety. Conversely, LOS appears as a dark band that quickly migrates at the bottom of the gel, denoting the lower molecular weight of LOS lacking O-chain domain.

2.2 Structural determination of the saccharide moities

Structural investigation of LPS/LOS is a difficult task since their amphiphilic nature determines the tendency to form micelles with low solubility in both aqueous and apolar organic solvents. Several strategies have been developed to overcome this obstacle, including the usage of solvent mixtures and chemical modifications or degradation of the molecules to improve dissolution in simple solvent systems.

The common protocol consists in the analysis of the lipid portion and saccharide moiety separately by using several hydrolysis techniques, as aqueous 1% acetic acid or acetate buffer. The above mild conditions are sufficient to cleave selectively the acid-labile glycosidic linkage between the Kdo residue and the non-reducing glucosamine of the lipid A, thus releasing the oligo-/polysaccharide moiety in the water solution. This linkage is very labile due to:

I. the absence of a whichever electron withdrawing group at position adjacent to anomeric (C-3 in this case since anomeric is C-2) that favors the formation of the reaction intermediate oxonium carbocation;

II. the passage from chair to half-chair conformation during the formation of the oxonium ion fastened by the presence of non substituted carbons;

III. the presence of a hydroxyl group in axial configuration at C-5 that contributes to a steric energy release in the formation of the intermediate carbocation.

The insoluble lipid A moiety can then be recovered by centrifugation and several washes with distilled water, whereas the supernatant is constituted by O-antigen still linked to core region, but this does not complicate the structural investigation since, in terms of monosaccharide residues number, the contribute of the core fraction is negligible respect to the O-chain. A disadvantage of above described methodology, based on an acid treatment, is that it produces a Kdo reducing unit with a microheterogeneity of various conformations (α and β anomers of pyranose and furanose rings, condensed or anhydro forms) that can render the study of the oligosaccharide by NMR spectroscopy particularly difficult. Thus, typically, the procedure to determine the primary structure of the core oligosaccharide portion consider the de-lipidation of the lipid A by means of alkaline treatment in two steps: first, a mild hydrazinolysis in anhydrous conditions to remove ester-linked fatty acids; second, a strong alkaline hydrolysis is performed to obtain the cleavage of amide-linked acyl chains (Holst, 2000). The obtained fraction is represented by an homogenous phosphorylated oligosaccharide, comprehensive of the lipid A disaccharide backbone, that can be easily studied through chemical and

spectroscopical investigations. Obviously, base-labile substituents of glycidic or non-glycidic nature are lost during this procedure. Therefore, it is possible to use the acid approach as a complement to the alkaline degradation, in order to evaluate the occurrence of base-labile groups lost during the alkaline treatment (i.e. pyrophosphate groups).

The primary structure determination of the saccharide portions so far obtained currently exploits state-of-art NMR experiments and soft-ionisation mass spectrometry techniques, together with compositional and linkage chemical analyses that allow the determination of:

- the quali-quantitative composition of sugar residues
- the absolute configuration of each monosaccharide
- the cyclisation ring sizes
- the glycosilation points of each monosaccharide
- the anomeric configuration of the linkages
- the monosaccharide sequence
- the location of non-carbohydrates substituents

Additional information on the nature and the sequence of monosaccharides can be obtained from *ad hoc* selectively cleavages of the polysaccharide such as partial acid hydrolysis, acetolysis, Smith degradation, β-elimination and solvolysis.

2.2.1 Chemical analyses of the saccharide moities

Chemical analyses (Figure 2.1) are useful to obtain important preliminary information regarding primary structure of poly/oligosaccharides. The procedure that provides the usage of Gas-Chromatography coupled with Mass-Spectrometry (GC-MS), can only be realised after conversion of the monosaccharides into apolar and volatiles derivatives. There is a plethora of techniques that can be employed to identify the monosaccharide type as well

as the glycosilation positions, thus the appropriate choice of the derivatisation method can highlight specific features of the sugar residues within the native LPS/LOS structure. Typically, the qualitative analysis by GC-MS is achieved by treating the oligo-/polysaccharide with MeOH/HCl leading to solvolysis of the molecule and to the formation of the *O*-methyl glycoside for each monosaccharide. Subsequent acetylation with acetic anhydride in pyridine produces the per-acetylated *O*-methyl glycosides (MGA), that can be injected and analysed by GC-MS. Comparison of the retention times from the GC analysis and the fragmentation pattern from the MS spectra analysis with opportune standards allow to the identification of the monosaccharide residues. Quantification analysis can then be obtained by using an internal standard, that usually is per-acetylated inositol. Since the MGA protocol provides a solvolysis in acid conditions, several isomers for each monosaccharide may form (i.e. pyranose and furanose either α and β anomers) resulting in the occurrence of many peaks in the corresponding chromatogram. Although not severely influencing the identification of the monosaccharides, this can lead to their misquantification. Therefore, an alternative and complementary approach that can be used leads to the formation of acetylated alditol derivatives. In this case, after strong acid hydrolysis with Trifluoroacetic Acid (TFA), the carbonyl moiety of the free residues is reduced with $NaBH_4$, thus providing a single molecule for each monosaccharide. The alditols acetylated are then injected and analysed via gas-chromatographic techniques.

A further procedure of chemical analysis that delivers the distinction between enantiomers provides that the solvolysis is executed with an enantiomerically pure alcohol as 2-(+)-octanol or 2-(+)-buthanol, thus the absolute configuration of each monosaccharide residues can be determined (Leontein and Lönngren, 1978). Indeed, after acetylation and injection to GC-MS, the comparison of the retention time of the acetyl 2-(+)-octyl

glycosides with the one of a standard mixture of O-2-(±)-octyl-glycosides of standard monoses in D or L configuration allows the assignment of the monosaccharide configuration.

The determination of the ring size and of the glycosilation sites of the monosaccharides is a further information obtainable through GC-MS analysis. The procedure consists in an extensively methylation of the oligo/polysaccharide with CH_3I in strongly alkaline conditions. Then, the permethylated oligo-polysaccharide is hydrolysed in acid conditions and reduced with a marked hydride ($NaBD_4$). The alditols so obtained have free hydroxyl groups at the positions previously involved in glycosidic linkages and cyclisation, that can be acetylated. These partially methylated alditols acetylated can be analysed by GC-MS and the fragments observed in the MS spectra are diagnostic for specific substitution patterns of acetyl and methoxyl groups, since molecule cleavages preferably occur in correspondence of a methoxyl group, better sustaining the positive charge because of resonance effects. To obtain desired information it is necessary to consider that position of the acetyl groups in the fragments accounts for the attachment point or for the position of ciclysation of the pyranose or furanose cycle whereas the methyl groups correspond to free positions, not involved in linkages. The reduction of the carbonilic function with sodium borodeuteride discriminates the fragments originated from the reduced position (even masses) form those originated from the last position (odd masses) (Hakomori, 1964). Information obtained from these chemical analyses helps and confirms the interpretation of subsequent NMR and MS experiments.

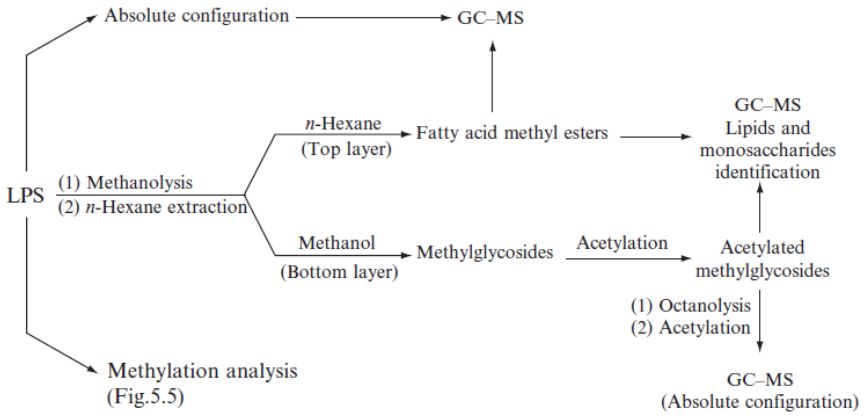

Figure 2.1 Convenient strategy for GC-MS analysis of LPS (LOS).

2.2.2 NMR Spectroscopy Analysis of the saccharide moieties

Nuclear Magnetic Resonance represents the most useful and decisive technique in the field of structural investigation of carbohydrates. This is due to the possibility of analysing molecules in solution in a native state, owing to the good solubility observed for oligo- and polysaccharides in aqueous solutions. During the structural study of saccharides, nuclei usually observed are ^{1}H, ^{13}C and ^{31}P, to detect phosphate groups and unusual phosphorous containing substituents.

Analysing a typical monodimensional ^{1}H-NMR spectrum for an oligo-/polysaccharide, it is possible to distinguish three different regions:

- The region between 5.5 and 4.6 ppm relative to the anomeric protons signals
- The region between 4.6 and 2.6 ppm where the ring proton signals are located
- The region between 2.5 and 1.0 ppm that is typical of the deoxy positions signals

Furthermore, from a ^{13}C NMR spectrum it is possible to obtain information about:

- 104-105 ppm : anomeric carbon atoms involved in a glycosidic linkage
- 80-60 ppm : oxymethylene or carbinolic carbon atoms
- 60-45 ppm : carbon atoms linked to nitrogen
- ~ 30 ppm : aliphatic methylene carbons of deoxy-sugar residues
- 20-17 ppm : methylene carbon atoms of 6-deoxy-sugar residues and of acetyl residues

The region relative to the ring protons signals is considerably narrow, and usually the identification of all chemical shifts is not made possible on the basis of the sole one dimensional NMR analysis. Thus, a combination of homo- and hetero-nuclear 2D-NMR experiments (such as DQF-COSY, TOCSY, NOESY, $^{1}H,^{13}P$-HSQC, $^{1}H,^{13}C$-HSQC, $^{1}H,^{13}C$-HMBC) are required in order to assign all the spin systems, to determine the location and the nature of non-carbohydrate substituents and to characterise the monosaccharide sequence. In detail, TOCSY and DQF-COSY spectra allow the correct identification and assignment of all ring protons, and on the basis of these data, the assignment for all ^{13}C resonances usually follows from the analysis of the $^{1}H,^{13}C$-HSQC spectrum; the *intra*-residue pattern of dipolar correlations in the 2D NOESY and ROESY spectra gives the proof for specific configurations; as example, NOE correlations between H-1/H-3 and H-5 are univocally diagnostic for a β-*gluco*-configuration, on the other hand a NOE connectivity between H-1 and only H-2 is indicative of a α-*gluco*-configuration. In general, protons orientations on the rings can be deduced from the $^{3}J_{H,H}$ coupling constant values that follow the Karplus law and assume high values (8 ÷ 10 Hz) in case of *trans*-diaxial orientation of vicinal protons and considerably lower values (< 4Hz) in case of equatorial/axial

orientation. These values can be attained from DFQ-COSY spectrum. Anomeric proton and carbon chemical shifts are the first hint for the anomeric configuration determination for each monomer, since usually α-configured proton signals appear at lower fields respect to corresponding β-anomers, whereas the opposite situation occurs for carbon chemical shifts. Anomeric configurations are then confirmed by the $^{3}J_{H1,H2}$ and by $^{1}J_{C1,H2}$ values. In detail, in monosaccharides with the H-2 axial (as glucose, galactose), a $^{3}J_{H1,H2}$ around 8 Hz is indicative of a β-orientation, whereas below 3 Hz of an α-configuration. Sugars with the H-2 equatorial (as mannose) show both $^{3}J_{H1,H2}$ below 3 Hz. Moreover a $^{1}J_{C1,H2}$ below 165 indicates a β-anomer, above 170 Hz a α-anomer. The downfield shift of ring proton signals (acylation shift) is useful to determine *O*- and *N*-acylation sites. *O*-phosphorylated protons undergo a similar down-field shift. In the $^{1}H,^{13}C$-HSQC spectrum, the down-field shift, or glycosilation shift, of carbon resonances (2 ÷ 10 ppm), allows to locate the positions of glycosidation and these may found confirmation in information previously obtained by means of chemical analyses. Information regarding the cyclisation ring is obtained by the observation in the $^{1}H,^{13}C$-HMBC spectrum of *intra*-residual long range correlations, i.e. H-1/C-5 and C-1/H-5 for pyranosidic rings or H-1/C-4 and C-1/H-4 for furanosidic rings. These latter are also identified by a low field displacement of all the ring resonances for the monosaccharide. Information concerning the sequence of the monosaccharides within the oligosaccharide (or the repeating unit of the polysaccharide) are then deduced from the observation of the *inter*-residual dipolar correlations in 2D NOESY and ROESY spectra (Figure 2.2) and from the existence of scalar long range correlations, in the $^{1}H,^{13}C$-HMBC spectrum, among the ^{1}H and ^{13}C nuclei involved in glycosidic linkages. Eventually, $^{1}H,^{31}P$-HSQC allows the localisation of the phoshorylation sites within the saccharide structure.

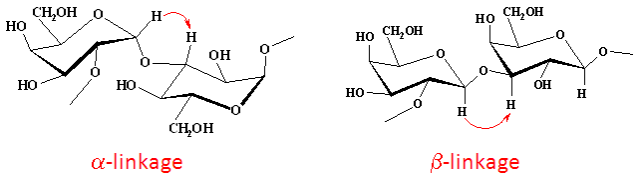

Figure 2.2 *Inter*-residue NOE correlations between disaccharides

2.2.3 Mass Spectrometry Analysis of the saccharide moieties

Mass spectrometry represents to date an essential and complementary technique in the structural characterisation of lipopolysaccharides and lipooligosaccharides especially with the development of soft ionisation techniques like MALDI (Matrix Assisted Laser Desorption Ionisation), ESI (ElectroSpray Ionisation), and the fragment analysis in MS/MS experiments. Apart from the ESI MS normally used in GC-MS analyses, mass spectrometric techniques allowing the definition of the molecular weight of the intact molecule are particularly useful, since they can provide additional information to the 1D and 2D NMR analyses that sometimes can be hard to construe. Usually, for carbohydrates, MALDI and ESI MS spectra are performed in negative ion mode, due to the presence of a great number of potentially ionising groups (hydroxyl or phosphate functions), nevertheless spectra in positive ion mode are also performed

MALDI-TOF analysis, in particular, gives an ideal profile of the sample by sketching all the molecules composing it, thus giving a picture of the eventual presence of different glycoforms differing for the presence of one or more glycidic or non-glycidic residues. This methodology consists in a soft ionisation of the sample that is suspended in a specific matrix that assists the analyte in ionisation phenomenon. The matrix has important roles among which the protection of the sample from the laser energy assuring a soft

ionisation with formation of single charged ions. Recently it has been pioneered the birth of new MALDI MS approaches through development of new methods of preparation and experimental study on the intact sample yielding a "picture" of the intact endotoxin, without any loss of structural information that can arise when the MS analysis is executed on derivatives of selective degradation necessary in the structural elucidation protocol (Sturiale *et al*., 2005). These procedures provide good spectra of intact molecular ions of lipopolysaccharides comprehensive of the heterogeneity inferred by the lipid A presence, showing high sensitivity also at relatively high molecular mass. The usage of high energy laser source allows to cleave the labile linkage between the Kdo and the glucosamine backbone lipid A, in a similar way to the acetate buffer treatment (see paragraph 2.2.1). In case of LOS, in the deriving spectra there are three regions of signals originated by the lipid A, the core oligosaccharide and the intact LOS. In LPS, due to the dispersion of molecular weight of the O-polysaccharide, information on the size of the repeating unit can be deduced.

2.3 Structural determination of the lipid A moiety

The lipid fraction obtained by precipitation, after mild acid treatment of LPS (or LOS) consists of a mixture of intrinsically heterogeneous lipid A molecules. The structural approach makes an extensive use of mass spectrometry analysis by MALDI-TOF and ESI MS techniques, as well as NMR spectroscopy and chemical analyses both on the native and selectively degraded lipid A fractions. The lipid A structure characterisation requires the determination of:

- the saccharide backbone
- the amide and the ester linked fatty acids
- the distribution of the acyl chains on the sugar backbone
- the phosphorylation sites

- the sites of heterogeneity relative to the acylation pattern that is number, type and distribution of the acyl chains or relative to the non-stoichiometric presence of phosphate substituents.

The determination of the nature, the ring size, the attachment point and the absolute configuration of the sugar components of the lipid A is performed has already described (see paragraph 2.2.1).

2.3.1 Chemical analyses of the lipid A moiety

Fatty acids determination is usually achieved through GC-MS analysis of their methyl ester derivatives. Lipid A is first treated with HCl and then neutralised with NaOH and acyl chains are then extracted in $CHCl_3$, methylated with diazomethane and analysed by GC-MS. O-linked acyl chain can be extracted from the entire molecule through an alkaline treatment that consists with NaOH, followed by methylation with diazomethane and analysis by GC-MS. The choice of cleavage conditions allows the selective detection of the linkage type of the fatty acids (Rietschel, 1976).

2.3.2 Mass Spectrometry Analysis of the Lipid A moiety

Mass Spectrometry is the most common approach used in lipid A structural determination. MALDI-TOF and ESI-MS data allow gaining insights into the number of lipid A species present in the fraction, the presence of polar heads and the distribution of acyl residues on each GlcN units of the disaccharide backbone (Que et al., 2000). Novel general approaches gaining structural insights on the native and selectively degraded lipid A fractions have been developed. In particular, combining MALDI-MS or ESI-MS and selective chemical degradations it is possible to understand the acylation profile of the molecule. Firstly, the amide linked fatty acids are identified by MS analysis of completely de-*O*-acylated lipid A with anhydrous hydrazine (Holst, 2000). An enormous advantage in lipid A structural analysis is the treatment with

NH_4OH (Silipo *et al*., 2002). This procedure selectively cleaves the ester linked acyloxyacyl groups, leaving untouched the amide-linked acyloxyacil groups. Thus, MS analysis of the ammonium treated lipid A allows the detection of the secondary fatty acid distribution, which is one of most demanding issues in the structural determination of the LPS lipidic moiety (Sforza *et al*., 2004; Sturiale *et al*., 2005). These approaches must be supported by the classical chemical analyses of the lipid A, which imply the removal of ester-linked fatty acid moiety by mild alkaline treatment, or complete removal by strong alkaline treatment and GC-MS analyses of fatty acids as methyl ester derivatives (Hase and Rietschel, 1976). MALDI spectra can be executed in positive and negative mode. The use of the former mode is expedient to differentiate the fatty acid allocation between the two GlcN of lipid A in case of asymmetric distribution; this is possible since during the execution of positive ion MS spectra a selective ionisation after fragmentation of the GlcN backbone occurs, and the only oxonium ion that is visible is relative to the non-reducing GlcN (Domon and Costello, 1988). On the other hand, both negative and positive mass spectra furnish indication of the presence of non-stoichiometric phoshorylation sites. The intact or the fully *O*-deacylated lipid A are also used to study the location of the phoshorylation sites.

References

Brecker L., Nuclear magnetic resonance of lipid A--the influence of solvents on spin relaxation and spectral quality. **2003**, *Chem. Phys. Lipids*, 125, 27-39.

Domon B., Costello C.E., Structure elucidation of glycosphingolipids and gangliosides using high-performance tandem mass spectrometry. **1988**, *Biochemistry*, 27(5), 1534-43.

Galanos C., Luderitz O., Westphal O., A new method for the extraction of R lipopolysaccharides. **1969**, *Eur. J. Biochem*., 9, 245-249.

Hakomori S., A rapid permethylation of glycolipid, and polysaccharide catalyzed by methylsulfinyl carbanion in dimethyl sulfoxide. **1964**, *J. Biochem.*, 55, 205-208.

Hase S., Rietschel E.T., Isolation and analysis of the lipid A backbone. Lipid A structure of lipopolysaccharides from various bacterial groups. **1976**, *Eur. J. Biochem*., 63, 101-107.

Holst O., Deacylation of lipopolysaccharides and isolation of oligosaccharide phosphates. **2000**, *Methods Mol. Biol.*, 145, 345 –353.

Kittelberger R., Hilbink F., Sensitive silver-staining detection of bacterial lipopolysaccharides in polyacrylamide gels. **1993**, *J. Biochem. Biophys. Methods*, 26 (1), 81-86.

Leontein K., Lönngren J., Determination of the absolute configuration of sugars by Gas-Liquid Chromatography of their acetylated 2-octyl glycosides. **1978**, *Methods Carbohydr. Chem.*, 62, 359-362.

Que N.L.S., Lin S.H., Cotter R.J., Raetz C.R., Purification and mass spectrometry of six lipid A species from the bacterial endosymbiont *Rhizobium etli*. Demonstration of a conserved distal unit and a variable proximal portion. **2000**, *J. Biol. Chem*., 275, 28006-28016.

Rietschel E.T. Absolute configuration of 3-hydroxy fatty acids present in lipopolysaccharides from various bacterial groups. **1976**, *Eur. J. Biochem.*, 64, 423-428.

S. Sforza, A. Silipo, A. Molinaro, R. Marchelli, M. Parrilli and R. Lanzetta, Determination of fatty acid positions in native lipid A by positive and negative electrospray ionization mass spectrometry. **2004**, *J. Mass Spectrom.,* 39, 378-83.

Silipo A., De Castro C., Lanzetta R., Molinaro A., Parrilli M., Full structural characterization of the lipid A components from the *Agrobacterium tumefaciens* strain C58 lipopolysaccharide fraction. **2004**, *Glycobiology*, 14, 805-815.

Silipo A., Lanzetta R., Amoresano A., Parrilli M., Molinaro A., Ammonium hydroxide hydrolysis: a valuable support in the MALDI-TOF mass spectrometry analysis of Lipid A fatty acid distribution. **2002**, *J. Lipid Res.*, 43, 2188 – 2195.

Sturiale L., Garozzo D., Silipo A., Lanzetta R., Parrilli M., Molinaro A., New conditions for matrix-assisted laser desorption/ionization mass spectrometry of native bacterial R-type lipopolysaccharides. **2005**, *Rapid Communications in Mass Spectrometry*, 19, 1829–1834.

Westphal O., Jann K., Bacterial lipopolysaccharides: extraction with phenol-water and further applications of the procedure. **1965**, *Methods Carbohydr. Chem*., 5, 83–91.

SECTION II

Chemistry and Immunity of Endotoxins isolated from Cystic Fibrosis Pathogens

Chapter 3

Structural and biological activity elucidation of the potent endotoxin isolated from *Burkholderia dolosa*

Premise

Here is reported the first study on the chemical and biological properties of the lipooligosaccharide (LOS) endotoxin isolated from *Burkholderia dolosa* strain IST4208, an isolate recovered from a cystic fibrosis (CF) patient in the major Portuguese CF center (Di Lorenzo *et al*., 2013). *Burkholderia dolosa* is a member of the *Burkholderia cepacia* complex (BCC) (see Section I, paragraph 1.5.2) and was the first BCC species to be identified involved in patient-to-patient transmission: the same isolate was found in 36 patients characterised by accelerated decline in lung function and, compared with patients colonised with *B. multivorans*, reduced survival (Kalish *et al*., 2006). Furthermore, five of the patients colonised by *B. dolosa* died from *cepacia syndrome*, a rapid decline in pulmonary function, within four months, differently to other BCC infections. These findings provide additional evidence that *B. cepacia* complex species differ to each others in their virulence and clinical implications and emphasize the importance of examining, at chemical level, the virulence factors of BCC strains (Caraher *et al*., 2007). Understanding how these divergent clinical outcomes arise by studying differences in the biology between important Bcc strains like *B. dolosa*, *B. cenocepacia* and *B. multivorans* might allow new therapeutic strategies to emerge, to help improve transplant outcome and to extend the life expectancy of CF patients. Thus, it has been carried out a complete study of structural and immunological properties of *B. dolosa* endotoxin by means of chemical analyses, MALDI mass spectrometry, and NMR spectroscopy the .

3.1 Isolation and SDS-PAGE analysis of *B. dolosa* LOS

LOS was obtained from cells of *Burkholderia dolosa* strain IST 4208 through the hot phenol-water extraction protocol (Westphal and Jann, 1965), then purified with DNase, RNase, and proteinase K, followed by extensive dialysis, and gel-permeation chromatography. Purity was examined by SDS-PAGE. The *B. dolosa* LPS fraction revealed that the extracted lipopolysaccharide was a *rough*-type LPS (LOS) due to the presence of a single dark band at the bottom of the gel diagnostic of a low molecular weight molecule.

3.2 Chemical analyses of LOS from *B. dolosa*

Monosaccharide analysis (see Section V) of the LOS from *B. dolosa* revealed the presence of 2,6-dideoxy-2-amino-D-glucose (D-quinovosamine, D-QuiN), 4-amino-4-deoxy-L-arabinose (L-Ara4N), D-Glc, D-Gal, D-GlcN, L-*glycero*-D-*manno*-heptose (L,D-Hep), 3-deoxy-D-*manno*-oct-2-ulopyranosonic acid (D-Kdo), and D-*glycero*-D-*talo*-oct-2-ulopyranosonic acid (D-Ko).
Methylation analysis revealed the occurrence of terminal QuiN, terminal Glc, terminal Gal, terminal Hep, 3-substituted Glc, 7-substituted Hep, 2,6-disubstituted Gal, 3,4-disubstituted Hep, 3,7-disubstituted Hep, 2,3,7-trisubstituted Hep, 4,5-disubstituted Kdo, and terminal Ko all in pyranose rings.Fatty acids analysis (see Section V) showed the presence of (R)-3-hydroxyhexadecanoic acid (C16:0 (3-OH)) with an amide linkage, and of (R)-3-hydroxytetradecanoic (C14:0 (3-OH)) and tetradecanoic acid (C14:0) with an ester linkage (Hughes *et al*., 1997).

3.3 Structural characterisation of LOS oligosaccharide moiety by NMR spectroscopy

In order to determine the primary structure of the oligosaccharide portion of *B. dolosa* LOS, the lipid A part was cleaved by mild hydrolysis with acetate buffer (see Section V), and the oligosaccharide fraction purified by gel permeation chromatography and characterised by NMR spectroscopy. In order to assign all the spin systems and to establish the monosaccharide sequence, a plethora of homo- and heteronuclear 2D NMR experiments (DQF-COSY, TOCSY, ROESY, NOESY, $^{1}H,^{13}C$ HSQC, $^{1}H,^{13}C$ HSQC-TOCSY, and $^{1}H,^{13}C$ HMBC) was performed. In particular, starting from anomeric proton signals, TOCSY and DQF-COSY spectra allowed the correct identification and attribution of all ring protons and the subsequent assignment of each carbon atom from analysis of the $^{1}H,^{13}C$ HSQC spectrum. The anomeric configuration of each monosaccharide was attributed on the basis of the $^{3}J_{H\text{-}1,H\text{-}2}$ coupling constant values obtained by DQF-COSY, whereas the relative configuration of sugar residues was assigned on the basis of the $^{3}J_{H,H}$ ring coupling constants; finally, the *intra*-residue pattern of dipolar correlations gave further confirmation of the anomeric configurations.

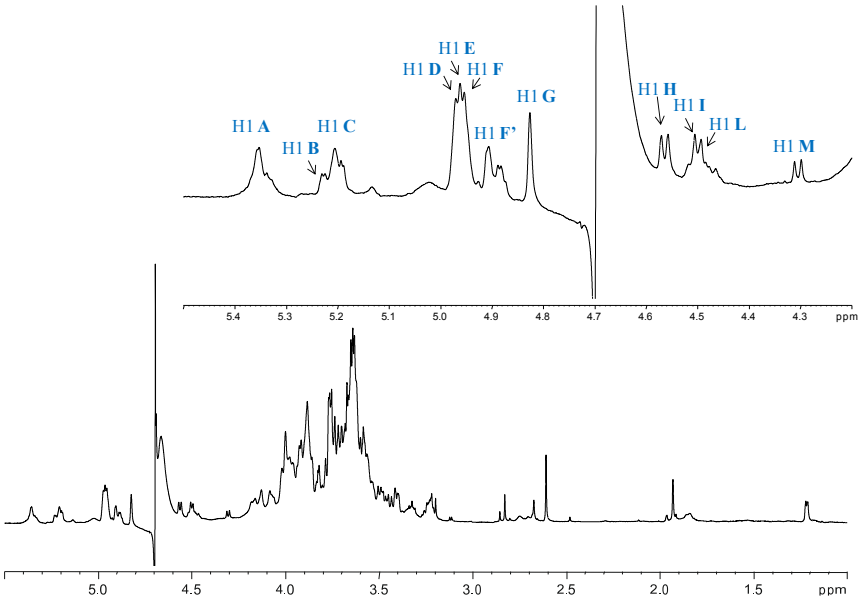

Figure 3.1 ^{1}H NMR spectrum of product core oligosaccharide with zoom of anomeric region.

In the anomeric region of the ^{1}H NMR spectrum (Figure 3.1), eleven anomeric signals were identified (**A**-**M**, Table 3.1); furthermore, the signals at 1.85/ 2.05 ppm were attributed to the H-3 methylene protons of the Kdo residue. The relative intensities and the shifts of anomeric signals suggested marked heterogeneity, typical of non-stoichiometric carbohydrate substitutions. In accordance with chemical analyses, spin systems **B**, **C**, **D**, **E**, **G** were all identified as Hep residues, as indicated by their $^{3}J_{\text{H-1,H-2}}$ and $^{2}J_{\text{H-2,H-3}}$ coupling constants (below 3 Hz), and by the *intra*-residue NOE of H-1 with H-2. Moreover, the ^{13}C chemical shift value of C-6 of these heptose residues (all below 72 ppm) allowed to identify them as L,D-Hep residues. Residues **A** and **H** (Table 3.1) were identified as *galacto*-configured monosaccharides because of

their low $^{3}J_{H-3,H-4}$ and $^{3}J_{H-4,H-5}$ values (~3 Hz and 1 Hz respectively). In particular, residue **A** was identified as α-Gal, based on the H-1 and C1 chemical shifts (5.35 and 97.3 ppm, Figure 3.1, Table 3.1), the $^{3}J_{H-1,H-2}$ value, and the *intra*-residual NOE contact of H-1 with H- 2 (all in agreement with an α-anomeric configuration and a $^{4}C_{1}$ ring conformation). The anomeric $^{1}J_{C-1,H-1}$ $^{3}J_{H-1,H-2}$ values (164 and 8.0 Hz, respectively) of residue **H** (H-1 at 4.56 ppm) indicated a β-anomeric configuration; this was further corroborated by *intra*-residue NOE connectivity between H-1 and H-3/H-5 signals in the NOESY spectrum. Spin systems **F**, **F'**, **L**, and **M** (Table 3.1) were identified as Glc residues by their characteristically large $^{3}J_{H,H}$ ring coupling constants (~9 Hz). The strong *intra*-residue NOE contacts of H-1 **L** and **M** with H-3 and H-5 of both residues **L** and **M**, together with the $^{3}J_{H-1,H-2}$ coupling constants (7 Hz) were diagnostic of a β-configuration, whereas the *intra*-residue NOE contact of H-1 with H-2, and the $^{3}J_{H-1,H-2}$ coupling constants (3 Hz) were indicative of a α-anomeric configuration for residues **F** and **F'**. Residue **I** was recognised as a β-QuiN: the *gluco* configuration was indicated by the $^{3}J_{H,H}$ ring coupling constants (~9 Hz). The *intra*-residue NOE contacts of H-1 with H-3 and H-5, and the $^{3}J_{H-1,H-2}$ coupling constant were indicative of a β-anomeric configuration. The $^{1}H,^{13}C$ HSQC spectrum showed the presence of a correlation of H-2 **I**, at 3.69 ppm, with a nitrogen-bearing carbon signal at 54.1 ppm. The downfield shift of the H-2 **I** proton resonance was diagnostic of *N*-acetylation at this position; this was confirmed by the dipolar correlation of H-2 **I** with the methyl protons of the acetyl group at 1.96 ppm. The spin system of Kdo **K** was assigned starting from the diastereotopic H-3 methylene proton signals, resonating in a shielded region at 1.85 and 2.28 ppm ($H\text{-}3_{ax}$ and $H\text{-}3_{eq}$, respectively). The Kdo residue was present in multiple forms, because of its free reducing end; nevertheless, the signals from the

α-reducing unit were clearly assignable, and the α-anomeric orientation at C-2 was assigned by the chemical shift values of H-3 and by the values of the $^{3}J_{H\text{-}7,H\text{-}8a}$ and $^{3}J_{H\text{-}7,H\text{-}8b}$ coupling constants (Birnbaum *et al*., 1987; Holst *et al*., 1994). Ko residue (**J**) was detected by the presence of the characteristic *inter*-residue NOE contact in 2D NOESY spectra between H-3_{eq} of Kdo (**K**) and H-6 of Ko (**J**); this is also diagnostic for a α-D-Ko-(2→4)-α-D-Kdo linkage (Birnbaum *et al*., 1987; Bock *et al*., 1994).

The downfield shift of the carbon resonances identified the glycosilated positions: O-2 and O-6 of residue **A**; O-2, O-3, and O-7 of **B**; O-3 and O-4 of **C**; O-3 and O-7 of **D**; O-3 of **F'**; and O-4 of Kdo (**K**). Residues **E**, **F**, **G**, **H**, **I**, **L**, **M**, and **J** were non-reducing terminal sugars, in agreement with the methylation data (see paragraph 3.2). The oligosaccharide sequence was established on the basis of the *intra*-residue NOE contacts identified in the ROESY and NOESY spectra (Figure 3.2), and in the long-range scalar correlations in the HMBC spectrum. The linkage of the heptose **C** (H-1 at 5.19 ppm) to O-5 of Kdo **K** was proven by the NOE connectivity between H-1 of the Hep **C** and H-5 of **K** (4.16 ppm). Given the L,D relative configuration of Hep **C**, the presence of further NOE contacts between H-1 of Hep **C** and H-6 and H-7 of **K** ultimately proved the D-configuration for the Kdo residue (Bock *et al*., 1994). Residue **C** was in turn substituted at O-3 and O-4; the NOE contacts (Figure 3.3) of H-4 **C** (3.97 ppm) and H-3 C (3.93 ppm) with H-1 of residue **L** (4.46 ppm) evidenced that the O-4 of α-Hep **C** was glycosilated by residue **L**, the β-Glc. Moreover, residue **C** was also substituted at O-3 by residue **B** of α-Hep, according to the NOE of H-3 and H-2 **C** with H-1 **B**. Residue **B** was identified as a 2,3,7-trisubstituted α-Hep. The NOE contacts of H-1 **M** (4.30 ppm) with H-1 and H-2 **B** (5.20 and 4.08 ppm, respectively) evidenced that the O-2 of residue **B** was glycosilated

by the β-Glc residue **M**. Furthermore, the NOE correlation of H-3 **B** (3.91 ppm) with H-1 **A** (5.35 ppm) proved the substitution of residue **B** at O-3 with the α-Gal residue **A**. Residue **B** was also glycosilated at O-7 by the terminal α-Hep **G**, as attested by the NOE contact between H-1 **G** (4.82 ppm) and H-7 **B** (3.63/3.55 ppm). Residue **A** was substituted at O-2 and O-6; thus, the NOE correlation of H-6 **A** (4.00/3.57 ppm) with H-1 **F** (4.95 ppm) of α-Glc gave evidence of the substitution of residue **A** at O-6 by the α-Glc **F**. An alternative spin system was identified for residue **F**, namely residue **F'**; this was recognised as a 3-α-substituted Glc that was, in turn, non-stoichiometrically substituted at position 3 by β-Gal **H**, as shown by the NOE contact of H-3 **F'** (3.85 ppm) with H-1 of residue **H** (4.56 ppm). Residue **A** was, in turn, also substituted at position O-2 by the α-Hep residue **D** (4.97 ppm), as showed by the NOE correlation of H-2 of **A** (3.56 ppm) with H-1 of **D**. Unit **D** was, in turn, glycosilated at O-3 by residue **E** as attested by the NOE contact of H-3 **D** (4.03 ppm) with H-1 **E** (4.95 ppm). Finally, residue **D** was shown to be glycosilated, in a non-stoichiometrical fashion, at O-7 (3.63/3.55 ppm) by residue **I**, as evidenced by the NOE correlation between H-1 **I** (4.50 ppm) and H-7 (3.63/3.55 ppm) of residue **D**. The HMBC spectrum confirmed the assigned structure, as it contained all the required long-range correlations to demonstrate the proximity of the residues.

Thus, in summary, all of the data allowed to establish the overall oligosaccharide structure that is reported below:

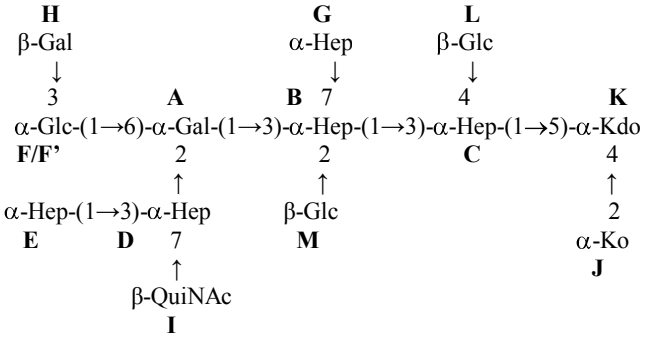

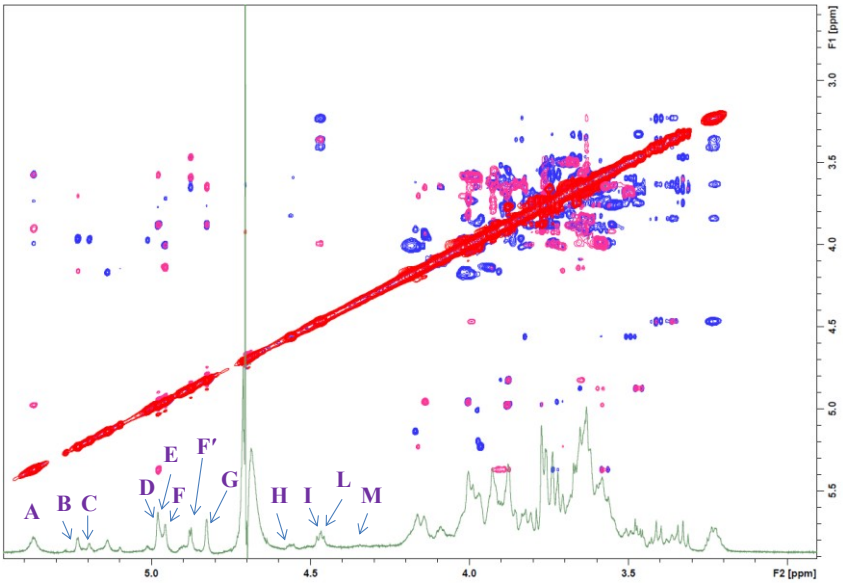

Figure 3.2 Overlapped TOCSY (**blue**) and NOESY (**pink**) spectra of product core oligosaccharide

Chemical shift δ ($^{1}H/^{13}C$)								
Unit	**1**	**2**	**3**	**4**	**5**	**6**	**7**	**8**
A	5.35	3.56	3.73	3.99	3.64	4.00/3.57		
2,6-α-Gal	97.3	74.4	71.3	70.3	71.2	64.6		
B	5.20	4.08	3.91	3.55	3.70	3.64	3.63/3.55	
2,3,7-α-Hep	99.1	77.2	79.9	68.9	70.7	71.9	70.1	
C	5.19	3.95	3.93	3.97	3.81	3.91	3.92/3.49	
3,4-α-Hep	99.1	65.7	71.6	71.6	72.1	68.7	63.0	
D	4.97	3.88	4.03	3.70	3.53	3.95	3.63/3.55	
3,7-α-Hep	97.4	70.7	76.5	71.5	72.2	70.4	70.1	
E	4.95	4.00	4.11	3.64	3.53	4.07	3.63	
t-α-Hep	102.3	69.8	69.3	71.1	71.1	67.9	62.9	
F	4.95	3.71	3.70	3.43	3.58	3.74		
t-α-Glc	97.4	68.5	70.6	71.5	71.2	60.3		
F'	4.90	3.67	3.85	3.44	3.44	3.76		
3-α-Glc	97.6	71.1	82.5	72.9	68.0	60.3		
G	4.82	3.88	3.76	3.64	3.53	3.91	3.62	
t-α-Hep	100.6	69.9	70.4	71.1	71.1	68.7	62.9	
H	4.56	3.49	3.60	3.82	3.64	3.67		
t-β-Gal	103.3	71.1	72.0	68.5	75.2	60.5		
I	4.50	3.69	3.73	3.24	3.40	1.21		
t-β-QuiNAc	100.6	54.1	74.7	75.6	75.4	16.2		
L	4.46	3.22	3.58	3.56	3.35	3.64		
t-β-Glc	102.0	73.4	75.7	68.9	76.3	60.8		
M	4.30	3.26	3.58	3.40	3.35	3.64		
t-β-Glc	101.3	72.2	75.8	71.6	76.4	60.8		
K	-	-	1.85/2.28	4.02	4.16	3.71	3.78	3.87/3.58
4,5-α-Kdo	174.1	n.d.	33.4	71.9	69.1	71.6	69.3	62.7
J	-	-	3.70	3.93	n.d	3.56	3.99	3.86/3.59
t-α-Ko	n.d.	n.d.	70.8	71.6	n.d	71.8	71.9	62.8

Table 3.1 ^{1}H and ^{13}C NMR chemical shifts of the oligosaccharide derived from mild hydrolysis of the LOS from *Burkholderia dolosa*. N.d. is not determined.

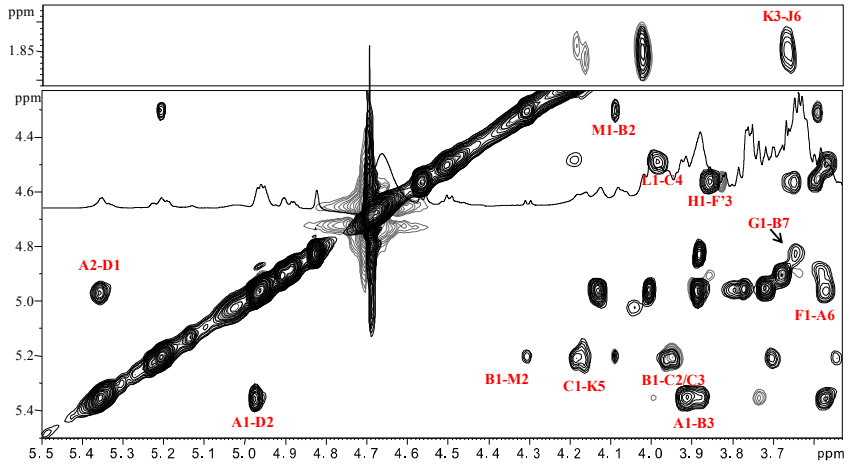

Figure 3.3 Zoomed region of overlapped TOCSY (**grey**) and NOESY (**black**) spectra of product core oligosaccharide in which the relevant *inter*-residual NOE contacts are reported.

3.4 Structural characterisation by MALDI mass spectrometry of the intact LOS and lipid A

Intact LOS was analysed by MALDI-MS to gain further information on both lipid A and the core region. This approach is very useful as it allows the study of integral LOS molecules (Sturiale *et al.*, 2005; Sturiale *et al.*, 2011) without any chemical manipulation, thus preventing the loss (either by alkaline or acid treatment) of labile groups (e.g., phosphate, acetyl), typically present on LPSs (see also Section I, paragraph 2.2.3). LOS was analysed by using a sample preparation procedure specifically optimised for these amphiphilic molecules (Sturiale *et al.*, 2005; Sturiale *et al.*, 2011). The negative-ion MALDI mass spectrum of intact LOS showed, in addition to the molecular ions related to the native LOS mixture (*m/z* 3400-4000), fragments between *m/z* 1400 and 2300 (Figure 3.4). These originated from the β-elimination

cleavage of the labile glycoside bond between Kdo and the lipid A moiety, which yielded either oligosaccharide (OS) ions (B-type ions) or lipid A ions. This low-mass region (Figure 3.4) presented a very heterogeneous OS mixture, including the peak at *m/z* 2225.6 (OS1), which matched a dodecasaccharide of five Hep residues, five Hex residues, one Kdo residue, and one Ko residue—the core oligosaccharide structure determined (above) by NMR spectroscopy. Minor species were also present: *m/z* 2063.9 (OS2), 2033.5 (OS3), 1871.6 (OS4), and 2164.0 (OS5); these differed from OS1 by the lack of one terminal Hex and/or Hep and one Ara4N residues (Figure 3.4). Each OS peak possessed a minor but confirmed twin-ion peak (Δ*m/z* 44), which matches neutral loss of a CO_2 molecule from the reducing terminal Kdo. It is worth noting that the oligosaccharide ion with the terminal QuiNAc residue was not detected in the MALDI analysis. The same mass region (*m/z* 1400-2300) also included ion peaks derived from a mixture of tetra-acylated lipid A, distinguishable by the absence or presence of one/two Ara4N residues, (Figure 3.4). Species L_1 (*m/z* 1444.8) matched a tetra-acylated bis-phosphorylated disaccharide backbone carrying one 14:0 (3-OH) acyl chain in the ester linkage and two 16:0 (3:OH) acyl chains in amide linkage; one of these, on GlcN II, was further substituted by a secondary 14:0 fatty acid. Species L_2 at *m/z* 1575.6 (Δ*m/z* 131 from L_1) and L_3 at *m/z* 1706.1 (Δ*m/z* 131 from L_2) were tetra-acylated lipid A, and carried one and two Ara4N residues, respectively.

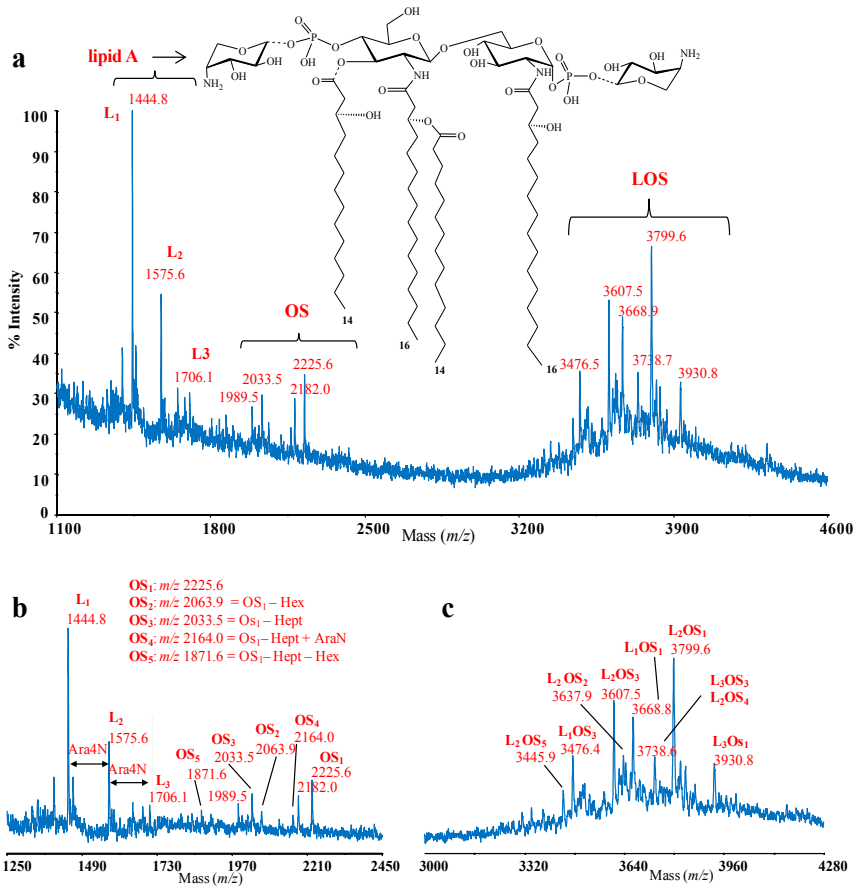

Figure 3.4 MALDI TOF MS analysis of the intact LOS from *Burkholderia dolosa*; (**A**) Negative-ion mass spectrum showing both LOS molecular ions and their ion fragments, attributable to the core oligosaccharides and to the reported lipid A structure(s). (**B**) Detail of the lower mass region (*m/z* 1250 – 2450) including lipid A and core oligosaccharide (OS) ion fragments and their assignments. (**C**) Detail of the higher mass region (*m/z* 3000 – 4280) reporting the composition of each LOS species as emerges from the heterogeneity of the core fraction and lipid A components, mainly due to non-stoichiometrically linked terminal sugar moieties.

The identity of either a primary ester-linked 14:0 (3-OH) or a secondary amide-linked 14:0 fatty acid on the GlcN II was established by the MS/MS analysis of the lipid A moiety after

acetate buffer hydrolysis. This treatment left the lipid A fraction partially dephosphorylated. In particular, the positive-ion MS/MS spectrum of the pseudomolecular ion $[M+Na]^+$ at *m/z* 1387.89 (corresponding to the tetra-acylated monophosphorylated lipid A) presented a very interesting fragmentation pattern, with a significant fragmentation due to the rupture of the glycosidic linkage between the two GlcN units (Figure 3.5). It gave rise to a tri-acylated B-type ion at *m/z* 954.6 carrying one 14:0 (3-OH), one 14:0, and one 16:0 (3-OH) residue at the non-reducing GlcN unit, and a very intense diacylated B-type ion (base-peak) at *m/z* 726.4 that arose from further loss of the 14:0 moiety (Figure 3.5).

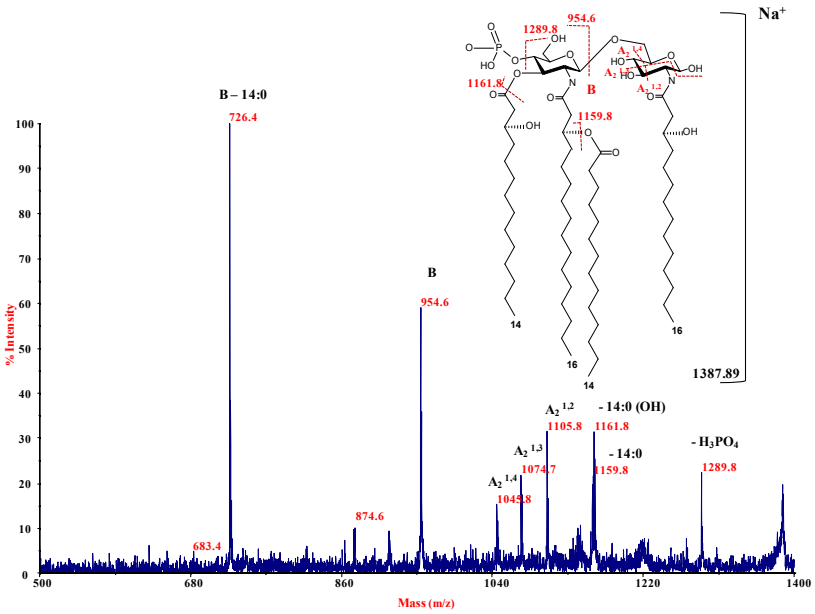

Figure 3.5 MALDI MS/MS spectrum (positive ionisation) and fragmentation pattern of the monophosphorylated, tetra-acylated lipid A moiety obtained by acetate buffer hydrolysis

The assignment of the main LOS molecular ions (Figure 3.4) resulted from the combination of the lipid A moieties and the core oligosaccharide species. LOS composed of tetra-acylated lipid A and OS species were found at *m/z* 3668.8 (L_1+ OS1), 3799.6 (L_2+OS1), 3930.8 (L_3+OS1), 3637.9 (L_2+OS2), 3476.4 (L_1+OS3), 3607.5 (L_2+ OS3), 3738.6 (L_3+OS3 and L_2+ OS4) and 3445.9 (L_2+OS5). In summary, MS analysis of the intact LOS completed and confirmed the previous structural hypotheses and allowed the full assignment of the LOS structure from the cystic fibrosis pathogen *B. dolosa* (Figure 3.8).

3.5 Assessment of the Biological Activity of *B. dolosa* LOS

To establish the biological activity of pure LOS from *Burkholderia dolosa*, commercially available HEK293 cells, stably transfected with LPS-recognising molecular complex CD14, MD-2 and TLR4 (Invivogen) have been stimulated with different concentrations of *B. dolosa* LOS (1, 10, and 100 ng/mL). *E. coli* serotype OIII:B4 is well known to possess a fully hexa-acylated lipid A that acts as an agonist on TLR4/MD-2 receptors (see Section III), thus was used at the same concentrations as a positive control. Activation of NF-kB (nuclear factor kappa B) and IL-8 release were the read-outs of this experiment. The results showed that the intact LOS from *B. dolosa* had a potent immunostimulatory activity as it was able to trigger activation of NF-kB at the same level as for *E. coli* LPS at all concentrations tested (Figure 3.6A); IL-8 release matched the *E. coli* behavior (Figure 3.6A).
It has been assessed also whether, and to what extent, *B. dolosa* LOS could interfere with TLR4-mediated signaling induced by lipid A of *E. coli*. Several natural and synthetic lipid A structures have been reported to exhibit high potential as antagonists against

endotoxically active LPS (see Section III). For this purpose, HEK hTLR4/MD2/CD14 cells (HEK293 hTLR4) were pre-incubated with different amounts (1, 10, and 100 ng) of *B. dolosa* LOS for 1 h and then re-stimulated with 10 ng of *E. coli* LPS for 4 h. NF-kB activation and IL-8 production were evaluated as above. It was found that cell priming (pre-incubation) with *B. dolosa* LOS at the lowest concentration (1 ng/mL) was able to change both NF-kB activation (Figure 21B) and IL-8 production (Figure 3.6B), relative to *E. coli* LPS stimulation alone. At the higher concentrations (10 and 100 ng/mL), no significant differences were observed in IL-8 release and NF-kB activation by either of the two LPS forms following pre-incubation (Figure 3.6B).

Then, it was tested the release of inflammatory cytokines by bone marrow-derived macrophages (BMDMs), collected and differentiated from wild-type C57BL/6 female mice. BMDMs expressing the entire TLR repertoire were stimulated with different concentrations (1, 10, or 100 ng/mL) of either *B. dolosa* LOS or *E. coli* OIII:B4 LPS. After 12 h of stimulation, secretion of TNF-α (tumor necrosis factor alpha), IL-6 and IL-10 was measured by an ELISA assay. It was found that 100 ng/mL *B. dolosa* LOS elicited significantly higher amounts of inflammatory cytokines (e.g., TNF-α and IL-6) than *E. coli* LPS (Figure 3.6A). Even at 10 ng/mL, the amount of produced IL-10 with *B. dolosa* LOS was statistically significantly higher ($p<0.05$; Figure 3.6A).

Finally, a competition assay in BMDMs to assess whether *B. dolosa* LOS could interfere with TLR4-mediated signaling induced by LPS of *E. coli* was executed. BMDMs were pre-incubated for 1 hour with different amounts (1, 10, or 100 ng/mL) of *B. dolosa* LOS for 1 h and then re-stimulated with 10 ng/mL *E. coli* LPS for 12 h. Cytokine secretion was measured with an ELISA assay. Results showed that cell priming with *B. dolosa* LOS did not antagonize the endotoxic activity of *E. coli* LPS at all

concentrations tested (Figure 3.7B). Indeed, the release of IL-6, IL-10, and TNF-α was significantly higher ($p<0.05$) when BMDMs were pre-exposed to *B. dolosa* LOS, relative to *E. coli* LPS stimulation alone (Figure 3.7). The above immunology data confirm that the LOS from *B. dolosa* is a powerful pro-inflammatory agent and a major virulence factor.

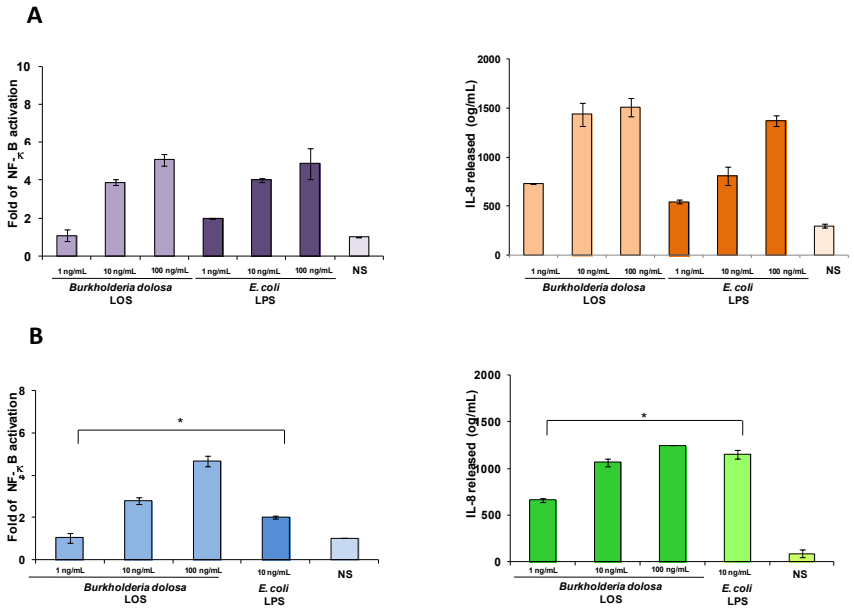

Figure 3.6 NF-κB activity and IL-8 production of HEK293 hTLR4 stimulated with *Burkholderia dolosa* LOS and *E. coli* LPS. (**A**) Fold of NF-κB activation (left panel) upon stimulation of HEK293 hTLR4 after 4 h with either 1, 10 and 100 ng/mL of *B. dolosa* LOS or commercial hexa-acylated *E. coli* LPS; (right panel) IL-8 secretion after stimulation for 4 h as above. (**B**) TLR4-dependent antagonistic activity of *B. dolosa* LOS on hexa-acylated *E. coli* LPS. Fold of NF-κB activation (left panel) and IL-8 release (right panel) upon stimulation of HEK293 hTLR4 after 1 h with 1, 10 and 100 ng/mL of *B. dolosa* LOS and then exposed to 10 ng/ml of *E. coli* LPS (4 h). $p< 0,05$ after Student t-Test

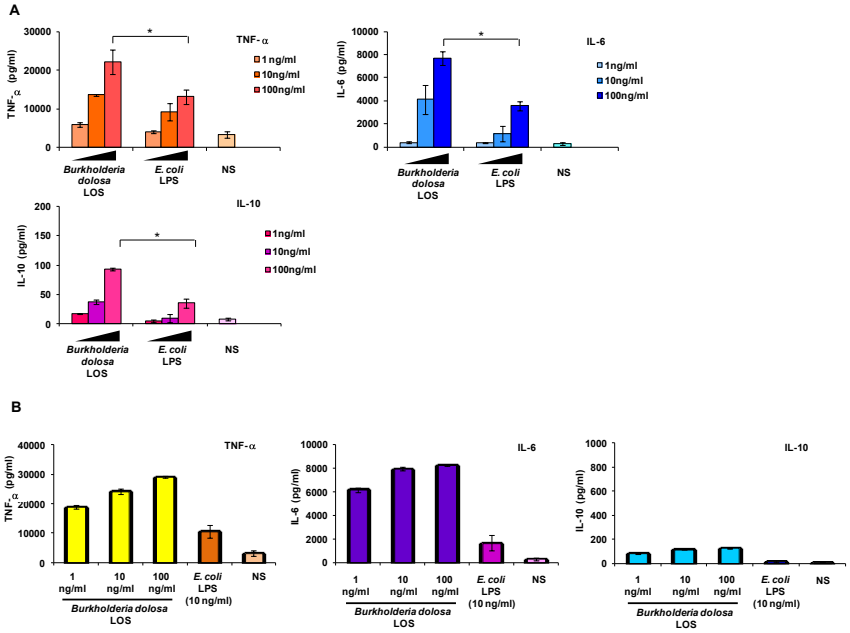

Figure 3.7 Cytokines release in BMDMs stimulated with *B. dolosa* LOS and *E. coli* LPS. (**A**) TNF-α, IL-6 and IL-10 released by BMDMs after stimulation with either 1, 10 and 100 ng/mL of *Burkholderia dolosa* LOS or *Escherichia coli* LPS measured by ELISA at 12 h. (**B**) TLR4-dependent antagonistic activity of *B. dolosa* LOS on hexa-acylated E. coli LPS in BMDMs. TNF-α, IL-6 and IL-8 release upon stimulation of BMDMs for 1 h with 1, 10 and 100 ng/mL of *B. dolosa* LOS and then re-exposed to 10 ng/ml of *E. coli* LPS (12 h). Cytokine secretion was measured through ELISA assay. $p<0,05$ after Student t-Test

3.6 Discussion

The complete structure and biological activity of LOS from a *B. dolosa* clinical isolate retrieved from a CF patient showed interesting features peculiar for this bacterium. Composition of the *B. dolosa* lipid A species displayed a relatively homogeneous tetra-acylated lipid A bearing Ara4N residue(s) (De Soyza *et al.*, 2008). The substitution of Ara4N in LPS molecules is essential for bacterial survival, as it prevents the interactions with antibiotic

compounds and host antimicrobial peptides (Hamad *et al*., 2012). These residues are positively charged under physiological conditions and so they reduce the net charge on the bacterial membrane surface. By preventing ionic attraction, these residues prevent membrane permeability by positively charged antimicrobial peptides.

The core oligosaccharide from *B. dolosa* showed to have a novel structure. From the chemical point of view, the *B. dolosa* LOS also has no negative charge at the outer core, which contains neither phosphate groups nor uronic acids. This confers on the LPS an overall neutral characteristic that renders it resistant to cationic antimicrobial peptides. The *Burkholderia* genus has a highly conserved LPS inner core structure, with several characteristics replicated in the current study. The main feature is the presence of the [3,4-α-L,D- Hep-(1→5)-α-D-Kdo-(4→2)-α-D-Ko] trisaccharide in the inner core. Notably, within this genus, the Ko residue is frequently not at the terminal, but rather bears an Ara4N residue. The presence of Ko monosaccharide is limited to a few bacterial LPS molecules, such as those of *Acinetobacter* (Vinogradov *et al*., 1997), *Yersinia* (Vinogradov et al., 2002) and *Serratia* (Vinogradov et al., 2006).

Usually, as in the present case, the α-L,D-Hep of the above-mentioned trisaccharide bears another Hep residue linked at O-3 and glycosilated at O-4 by a β-D-Glc residue. In this *B. dolosa* strain, the latter Hep residue of inner core is glycosilated at O-2, O-3, and O-7, as previously noted for *B. multivorans* (Hughes *et al*., 1997); however, the heptose carries an additional heptose at O-7, as found in *B. cenocepacia* ET-12 LOS (Silipo *et al*., 2007), and at O-2 there is a β-D-Glc, and at O-3 there is a α-D-Gal. This latter monosaccharide was, in turn, substituted at position O-2 by an α-Hep residue and at O-6 by a α-D-Glc which can be, in turn, non-stoichiometrically glycosilated by a β-D-Gal residue.

Finally, the latter Hep was glycosilated at position O-3 by another Hep. Interestingly, this α-Hep-(1→3)-α-Hep disaccharide is infrequently found as a component of the outer core of LOSs (Holst, 1999), and its presence might involve the existence of an additional different heptosyl transferase. Moreover, in the outer core region, we found the presence of a non-stoichiometric residue, the β-D-QuiNAc linked to the α-Hep-(1→3)-α-Hep disaccharide.
In summary, *B. dolosa* LOS possesses a peculiar structure, the biosynthesis of which requires further study. From a biological point of view, it was observed that *B. dolosa* LOS acts as potent inflammatory agent through the TLR-4, MD- 2, CD-14 pathway, thereby inducing high levels of NF-kB and IL-8 release from HEK293 cells stably transfected for LPS complex recognition (HEK293 hTLR4). These data were corroborated by the results obtained from analysis of inflammatory cytokines released in BMDMs after stimulation with intact LOS from *B. dolosa*. The high levels of TNF-α, IL-10, and IL-6 secretion confirm the virulence and support the concerns about this cystic fibrosis pathogen. Lipid A contributes to the majority of the endotoxic activity of LPS. A number of factors influence the lipid A biological activity, including the number and the distribution of acyl chains, the phosphorylation pattern, and the presence of charged groups on the polar heads. The correlation between increasing acylation of lipid A and elevated cytokine induction has previously been reported in *Pseudomonas* (Ernst *et al*., 1999) and *Burkholderia* (Ernst *et al*., 1999). Interestingly, lipid A from *B. dolosa* did not show high levels of acylation, but the entire LOS still remains a potent immunostimulator with HEK293 cells.

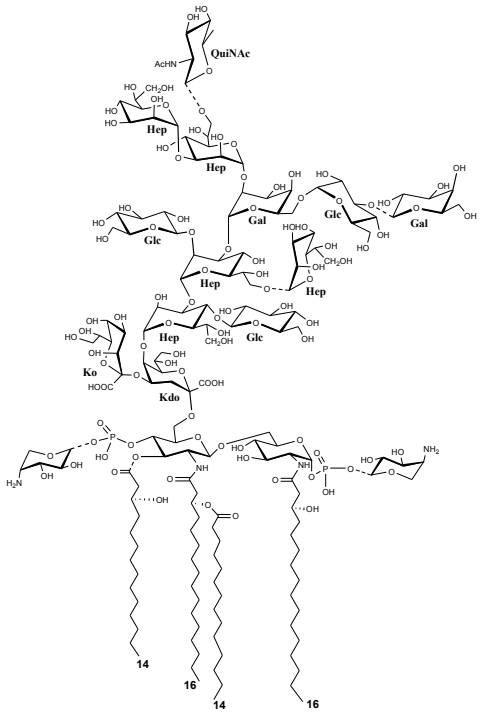

Figure 3.8 Structure of the LOS from *Burkholderia dolosa*. The dotted lines indicate non-stoichiometric substitution. The anomeric configuration of lipid A residues is assigned in analogy to all *Burkholderia* LPS lipid A elucidated so far.

Taking into account these findings, it might be speculated that the novel and heterogeneous structure of the core oligosaccharide portion plays a key function in the molecular mechanism of the interaction with the TLR-4/MD-2 receptors, thus demonstrating a notable role in the pathogenicity of *B. dolosa*. Further studies will be performed to test this hypothesis.

In conclusion, this study improves the understanding of the endotoxin structure-function relationship, which is of pivotal

importance in the comprehension of the overall process of pathogenesis of such important microorganisms.

References

Birnbaum G.I., Roy R., Brisson J.R., Jennings H., **1987**, *J. Carbohydr. Chem*., 6, 17-39.

Bock K., Vinogradov E., Holst O., Brade H., Isolation and structural analysis of oligosaccharide phosphates containing the complete carbohydrate chain of the lipopolysaccharide from *Vibrio cholerae* strain H11 (non-O1). **1994**, *Eur. J. Biochem*., 225, 1029-1039.

Caraher E., Duff C., Mullen T., McKeon S., Murphy P., Callaghan M., McClean S., Invasion and biofilm formation of Burkholderia dolosa is comparable with *Burkholderia cenocepacia* and *Burkholderia multivorans*. **2007**, *J. Cystic Fibrosis*, 6, 49-56.

De Soyza A., Silipo A., Lanzetta R., Govan J.R., Molinaro A., Chemical and biological features of *Burkholderia cepacia* complex lipopolysaccharides. **2008**, *Innate Immun*., 14, 127-144.

Di Lorenzo F., Sturiale L., Palmigiano A., Fazio L.L., Paciello I., Coutinho C.P., Sá-Correia I., Bernardini M.L., Lanzetta R., Garozzo D., Silipo A., Molinaro A., Chemistry and biology of the potent endotoxin from a *Burkholderia dolosa* clinical isolate from a cystic fibrosis patient. **2013**, *ChemBioChem*., 14, 1105-1115.

Ernst R.K., Yi E.C., Guo L., Lim K.B., Burns J.L., Hackett M., Miller S.I., Specific lipopolysaccharide found in cystic fibrosis airway *Pseudomonas aeruginosa*. **1999**, *Science*, 286, 1561-1565.

Hamad M.A., Di Lorenzo F., Molinaro A., Valvano M.A., Aminoarabinose is essential for lipopolysaccharide export and intrinsic antimicrobial peptide resistance in *Burkholderia cenocepacia*. **2012**, *Molecular Microbiology*, 85, 5, 962–974.

Holst O. in Endotoxin in Health and Disease (Eds.: Brade H., Opal S.M., Vogel S.N., Morrison D.C.), Dekker, New York, pp. 115-154, **1999**.

Holst O, Thomas-Oates J.E., Brade H., Preparation and structural analysis of oligosaccharide monophosphates obtained from the lipopolysaccharide of recombinant strains of *Salmonella minnesota* and *Escherichia coli* expressing the genus-specific epitope of *Chlamydia* lipopolysaccharide. **1994**, *Eur. J. Biochem*. 222, 183-194.

Hughes J.E., Stewart J., Barclay G.R., Govan J.R.W., Priming of neutrophil respiratory burst activity by lipopolysaccharide from *Burkholderia cepacia*. **1997**, *Infect. Immunol*., 65, 4281-4287

Kalish L.A., Waltz D.A., Dovey M., Potter-Bynoe G., McAdam A.J., LiPuma J.J., Gerard C., Goldman D., Impact of *Burkholderia dolosa* on lung function and survival in cystic fibrosis. **2006**, *Am. J. Respir. Crit. Care Med*., 173, 421-425.

Silipo A., Molinaro A., Ieranò T., De Soyza A., Sturiale L., Garozzo D., Aldridge C., Corris P.A., Khan C.M., Lanzetta R., Parrilli M., The complete structure and pro-inflammatory activity of the lipooligosaccharide of the highly epidemic and virulent gram-negative bacterium *Burkholderia cenocepacia* ET-12 (strain J2315). **2007**, *Chemistry*., 13, 3501-11.

Sturiale L., Garozzo D., Silipo A., Lanzetta R., Parrilli M., Molinaro A., New conditions for matrix-assisted laser desorption/ionization mass spectrometry of native bacterial R-type lipopolysaccharides. **2005**, *Rapid Communications in Mass Spectrometry*, 19, 1829–1834.

Sturiale L., Palmigiano A., Silipo A., Knirel Y.A., Anisimov A.P., Lanzetta R., Parrilli M., Molinaro A., Garozzo D., Reflectron MALDI TOF and MALDI TOF/TOF mass spectrometry reveal novel structural details of native lipooligosaccharides. **2011**, *J. Mass Spectrom*. 46, 1135-1142.

Vinogradov E.V., Bock K., Petersen B.O., Holst O., Brade H., The structure of the carbohydrate backbone of the lipopolysaccharide from *Acinetobacter* strain ATCC 17905. **1997**, *Eur. J. Biochem*., 243(1-2):122-7.

Vinogradov E.V., Lindner B., Kocharova N.A., Senchenkova S.N., Shashkov A.S., Knirel Y.A., Holst O., Gremyakova T.A., Shaikhutdinova R.Z., Anisimov A.P., The core structure of the lipopolysaccharide from the causative agent of plague, *Yersinia pestis*. **2002**, *Carbohydr. Res*. 337, 775-777.

Vinogradov E.V., Lindner B., Seltmann G., Radziejewska-Lebrecht J., Holst O., Lipopolysaccharides from *Serratia marcescens* possess one or two 4-amino-4-deoxy-L-arabinopyranose 1-phosphate residues in the lipid A and D-*glycero*-D-*talo*-oct-2-ulopyranosonic acid in the inner core region. **2006**, *Chem. Eur. J.*, 12, 6692-6700.

Westphal O., Jann K., Bacterial lipopolysaccharides: extraction with phenol-water and further applications of the procedure. **1965**, *Methods Carbohydr. Chem*., 5, 83–91.

Chapter 4

Structural Characterisation of the LPS O-antigen moiety isolated from *Pandoraea pulmonicola*

Premise

Environment is a never-ending source of microorganisms, and new bacteria are currently associated with pulmonary exacerbations in cystic fibrosis (Atkinson *et al*., 2006). Among these newly identified organisms are bacteria belonging to the genus *Pandoraea* (Coenye *et al*., 2000). *Pandoraea* is a novel genus composed of aerobic Gram-negative rod-shaped microbes with polar flagella (Stryjewski et al., 2003). These microorganisms have been isolated from the lung tissue, blood, sputum, and urine of cystic fibrosis (CF) patients and other primary chronic lung diseases (Stryjewski *et al*., 2003; Daneshvar *et al*., 2001). Chronic lung inflammation, the major contributor to morbidity and mortality in CF patients, is exacerbated by the upregulation of the pro-inflammatory cytokines IL-8 and IL-6, which have been shown to lead to increased neutrophil recruitment and further enhancement of lung inflammation (Tabary *et al*., 2000; Yu *et al*., 2002). Recent *in vitro* data demonstrated that 19 *Pandorea* strains from five species examined elicited a pro-inflammatory response with a remarkable production of cytokines, such as IL-8 and IL-6 in lung epithelial cells, and that *P. pulmonicola* strains showed the most potent pro-inflammatory response. This might be an important mechanism of virulence for this genus, which likely contributes to the pathogenesis of colonised CF patients (Caraher *et al*., 2008). However, the role of the genus *Pandoraea* in the course and prognosis of CF lung disease merits further study at molecular level due to its demonstrated invasive potential and reports of decline in lung function. Since the O-chain is the antigenic determinant of the LPS, rendering this latter highly immunogenic, the present work reports for the first time the structure of the O-chain from the LPS extracted from the *Pandoraea pulmonicola* strain LMG 18108, a clinical isolate from a US CF patient (Coenye *et al*., 2000), which

represents one of the most virulent and predominant species within the *Pandoraea* genus that has emerged recently in the Irish CF population (Costello *et al*., 2011).

4.1 Purification and Chemical Analyses of the LPS

Large-scale isolation of the LPS for structural analysis was achieved by the hot phenol/water extraction method (Westphal and Jann, 1965) and checked by SDS-PAGE (see Section V) (Kittelberger and Hilbink, 1993). The sample showed a polydisperse banding fashion, giving rise to the ladder-like pattern typical of S-LPS due to the occurrence of molecules with a different number of repeating units in the O-chain. Compositional analyses of the *P. pulmonicola* LPS revealed the presence of L-Rha, 3,6-dideoxy-3-amino-D-glucose (D-quinovosamine, D-Qui3N), D -GlcN, D -GalN, and a minor amount of 4-amino-4-deoxy-L-arabinose (L-Ara4N), D-Man, D-Glc, D-Gal, L-*glycero*-D-*manno*-heptose (L,D -Hep), and 3-deoxy-D-*manno*-oct-2-ulopyranosonic acid (Kdo). To determine the structure of the O-chain portion, a mild hydrolysis with acetate buffer was performed to cleave the labile ketosidic linkage between the GlcN of lipid A and Kdo. The water-soluble polysaccharide was purified by gel-permeation chromatography and characterised by NMR spectroscopy.

4.2 NMR analysis of the LPS O-chain from *P. pulmonicola*

Spin systems and saccharide sequence of the O-chain were assigned through a combination of homo- and heteronuclear NMR experiments .

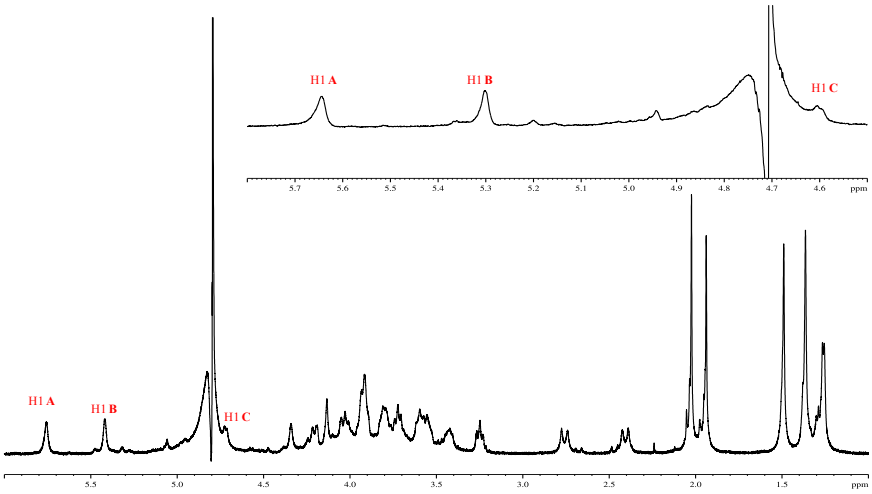

Figure 4.1 ^{1}H NMR spectrum of the O-chain portion. In the inset the expanded anomeric region is shown.

In the anomeric region of the ^{1}H NMR spectrum (Figure 4.1), three anomeric signals were identified related to three different spin systems referred to as **A**, **B**, and **C** (Table 4.1). Residues **A** and **B** possess an α-configuration, whereas **C** was identified as a β-configured monose. In the aliphatic region of the ^{1}H NMR spectrum, three singlets at δ = 1.34, 1.21, and 1.11 ppm were attributed to methyl groups, whereas the two doublets resonating at δ = 2.60 and 2.25 ppm are diagnostic of a diastereotopic methylene group. These latter signals suggested the presence of an unusual non-glycidic substituent linked to a monosaccharide of the O-chain. Furthermore, the large value of the geminal coupling of the methylene group (Table 4.1, $^{2}J_{H,H}$ = 17.7 Hz) is indicative of a five-membered cyclic structure (Zatonsky *et al*., 2002; Molinaro *et al*., 2003).

Spin system **A** (H-1, δ = 5.61 ppm; Figure 4.1, Table 4.1) was identified as *gluco*-configured by its characteristic large $^{3}J_{H,H}$ ring coupling constants (~9 Hz). The H-1 and C-1 chemical shifts, the

$^{3}J_{H-1,2-H}$ value, and the *intra*-residual NOE contact of H-1with H-2 are all in agreement with an α-anomeric configuration. Furthermore, H-2 of **A** is correlated with a nitrogen-bearing carbon atom in the HSQC spectrum (δ = 53.0 ppm), and the downfield shift of the proton resonance of H-2 of **A** at δ = 3.78 ppm is diagnostic of *N*-acetylation at this position, which was also confirmed by the dipolar correlation with the methyl protons of the acetyl group resonating at δ = 1.78 ppm in the NOESY spectrum. These data allowed us to identify residue **A** as an α-2-acetamido-2-deoxyglucose (α-D-Glc*p*NAc).

Residue **B** (H-1 at δ = 5.27 ppm) was recognised as a *galacto*-configured monosaccharide owing to its small $^{3}J_{H-3,H-4}$ and $3J_{H-4,H-5}$ values (~3 and 1 Hz, respectively). In fact, the H-5 resonance of **B** was definitely identified by a NOE effect with H-4 of **B**. The correlation between H-2 (δ = 4.06 ppm) and a nitrogen-bearing carbon atom (δ = 51.1 ppm) and the NOE contact of the same resonance with the methyl protons of the acetyl group resonating at δ = 1.87 ppm allowed its identification as an α-2-acetamido-2-deoxygalactose (α-D-Gal*p*NAc).

The spin system **C** (H-1 at δ = 4 ppm) was identified as a β-3,6 dideoxy-3-amino-D-glucose (β-D-Quip3N). The *gluco* configuration was inferred from the ring $^{3}J_{H,H}$ coupling constants (~10 Hz), whereas the *intra*-residual NOE contact of H-1 with H-3 and H-5 and the $^{3}J_{H-1,H-2}$ coupling constants are diagnostic of a β-anomeric configuration. Moreover, the signal from H-3 of **C** is correlated with a signal of a nitrogen-bearing carbon atom (δ = 57.4 ppm).

	Chemical shift δ ($^{1}H/^{13}C$)					
Unit	**1**	**2**	**3**	**4**	**5**	**6**
A	5.76	3.93	3.57	3.74	3.80	3.76/3.92
3-α-GlcNAc	*95.6*	*53.0*	*79.2*	*72.0*	*71.8*	*62.6*
B	5.42	4.21	3.90	4.35	4.14	3.92
4-α-GalNAc	*99.8*	*51.1*	*68.2*	*79.4*	*72.6*	*62.6*
C	4.71	3.61	4.04	3.25	3.43	1.26
2-β-QuiN	*105.7*	*72.7*	*57.4*	*74.4*	*74.6*	*18.1*

Chemical shifts for the 3-hydroxy-2,3-dimethyl-5-oxoprolyl group: C1 to C5 at 176.1, 72.8, 79.7, 46.2 (δ_H 2.40, 2.75) and 180.0 ppm respectively. Two methyl groups at δ_C/δ_H 19.5/1.49 (CH_3-2) and 23.5/1.36 (CH_3-3). Two acetyl groups at δ_C/δ_H 23.8/2.02 and 23.4/1.93.

Table 4.1 ^{1}H and ^{13}C NMR chemical shifts of sugar residues of the O-chain moiety.

The sequence and linkage positions of the monosaccharides within the repeating unit of the O-polysaccharide were established by observation of the *inter*-residual dipolar correlations in the 2D NOESY spectra (Figure 4.2) and from the scalar long-range correlations present in the $^{1}H,^{13}C$ HMBC spectrum. Furthermore, the downfield shifts of the carbon resonances are diagnostic of the positions of glycosilation: O-3 of **A**, O-4 of **B**, and O-2 of **C** (Table 4.1). The strong NOE contact between H-1 of **C** and H-4 of **B** (δ = 4.20 ppm) and the weak NOE contacts between H-3 of **B** and H-5 of **B** (Figure 4.2) are an indication of the (1→4) linkage between the residues **C** and **B**. Moreover, the strong NOE correlation between H-1 of **B** and H-3 of **A** (δ = 5.27 and 3.42 ppm, respectively) suggests the substitution at O-3 of residue **A** by the α-D-Gal*p*NAc unit of **B**. The linkage of residue **A** to O-2 of β-Qui*p*3N of **C** was proven by the NOE connectivity between H-1 of **A** and H-2 of **C** (δ = 3.46 ppm). The sequence of the carbohydrate repeating unit was confirmed by the long-range correlations present in the HMBC spectrum, because it contained all of the required contacts to demonstrate the proximity of the residues.

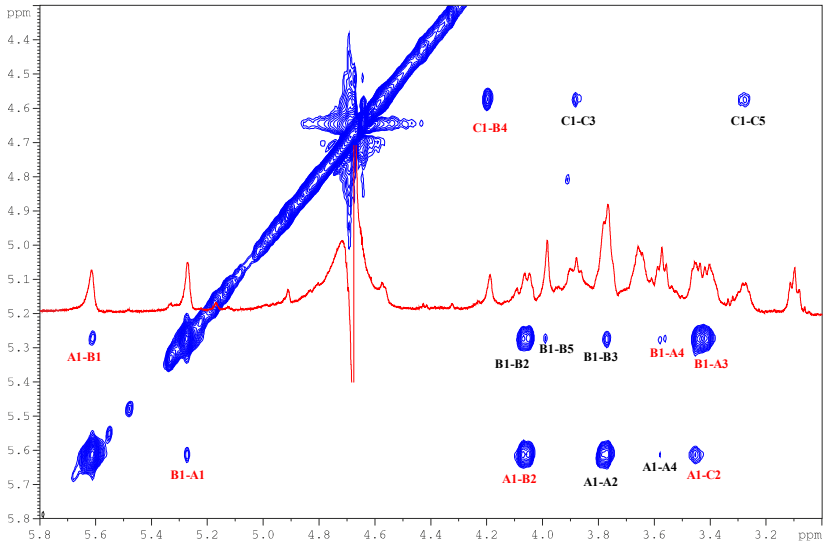

Figure 4.2 Section of the NOESY spectrum of the O-chain. In **red** *inter*-residual NOE connectivities are shown, while *intra*-residual are indicated in **black**.

In the HMBC spectrum, the methylene signals show a long-range correlation with the signals of three unsubstituted carbon atoms: a quaternary carbon atom (C-2, δ = 72.8 ppm), a carbonyl group (C-5, 180.0 ppm), and another oxygen-bearing carbon (C-3, δ = 79.7 ppm). Both the signals of C-2 and C-3 correlate with two of the methyl signals (δ = 1.34 and 1.21 ppm, respectively) present in the ^{1}H NMR spectrum. The methyl groups are located at tetrasubstituted carbon atoms C-2 and C-3 (Figure 4.3). In agreement, the NOESY spectrum shows a cross-peak of only the CH_3 (C-3) signal and the methylene protons of C-4, whereas in the HMBC spectrum only CH_3 of C-2 shows a long-range scalar correlation with another carbonyl signal (δ = 176.1 ppm, Figure 4.3), which is, in turn, correlated with the H-3 of residue **C**. Furthermore, the NOESY spectrum displays a cross-peak between the two methyl groups CH_3, which indicates they are in a *syn*-(pseudo) axial orientation.

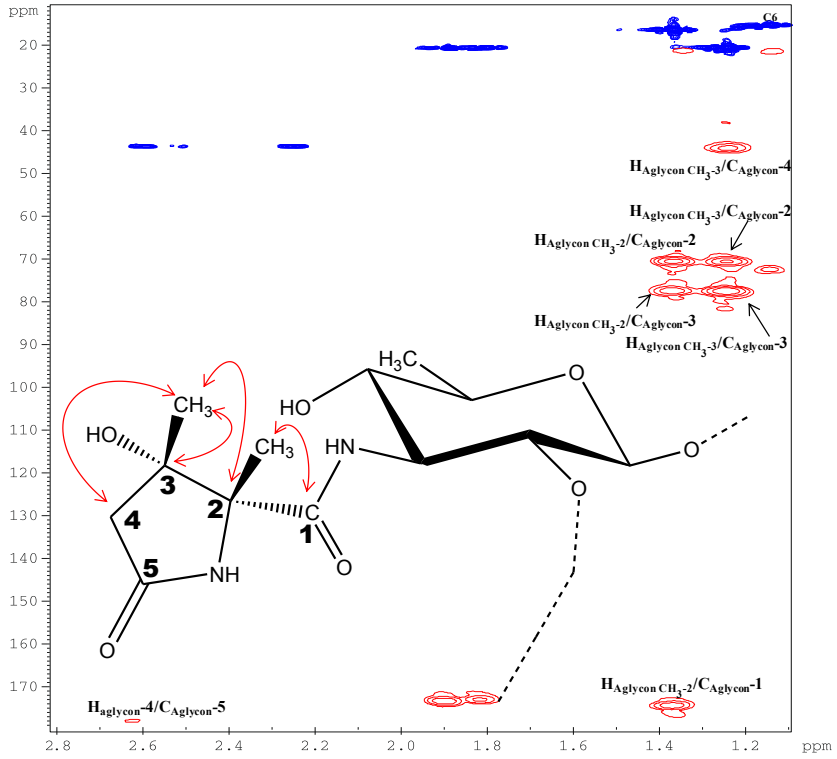

Figure 4.3 Section of the HMBC (**red**) and HSQC (**blue**) spectrum of the O-chain. The relevant long-range connectivities which allowed the identification of the aglycon are indicated.

Taking together all the above data and all the literature data (Zatonsky *et al.*, 2002; Molinaro *et al.*, 2003) a non-sugar five-membered ring with an exocyclic carbonyl group, named 3-hydroxy-2,3-dimethyl-5-oxoprolyl, was identified as the unusual acyl group at N-3 of Qui3N. The absolute configuration of this acyl group was not determined. This conclusion was confirmed by GC–MS analysis of the methylation data; the mass spectrum shows an ion peak for a carbohydrate derivative with a rather high

retention time, and the fragmentation pattern (Figure 4.4) reveals a partially methylated derivative of Qui3N with retention of the *N*-acyl group.

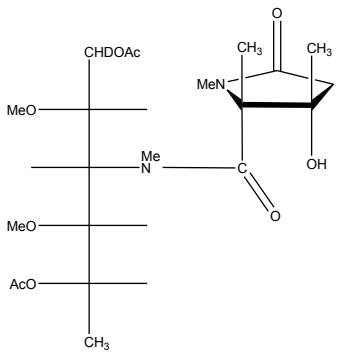

Figure 4.4 The permethylated and acetylated derivative of Qui3N bearing the 3-hydroxy-2,3-dimethyl-5-oxoprolyl group as found in GC-MS.

Thus, all the data are in agreement with the structure formulated as

[→2-β-D-Qui*p*3NAcyl-(1→4)-α-D-Gal*p*NAc-(1→3)-α-D-GlcpNAc-1→]*n*

and shown in Figure 4.6.

This structure was further confirmed by MS. Actually, MALDI-TOF MS analysis of the intact LPS chains from *P. pulmonicola* (Figure 4.5) allowed the identification of a main series of peaks differing by 724 Da, the incremental mass of the trisaccharide repeating unit, further substantiating the above findings.

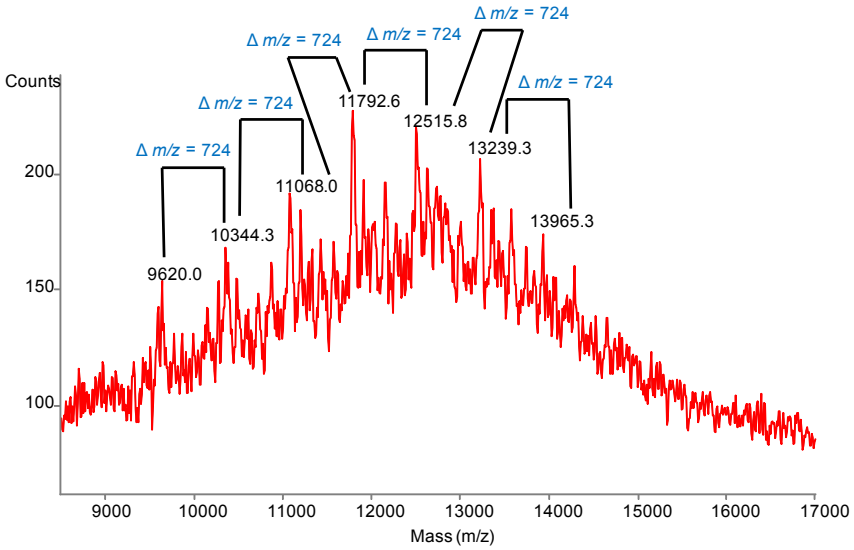

Figure 4.5 MALDI mass spectrum of the native *P. pulmonicola* LPS (high mass-region). Main peak differences are due to the O-chain repeating unit accounting for 724.3 Da. Minor molecular mass distributions arise from the structural heterogeneity of lipid A and core oligosaccharide domains.

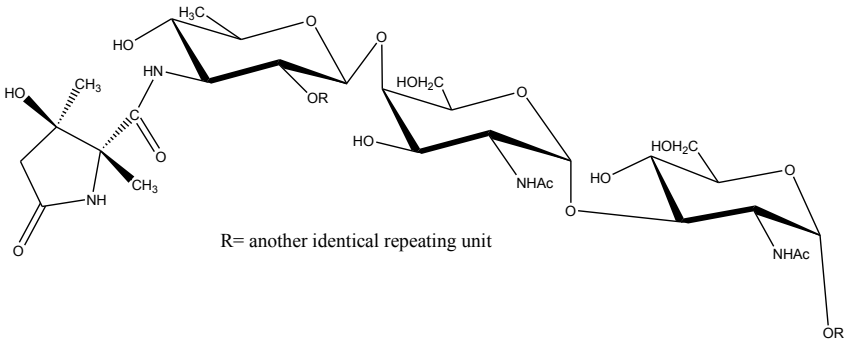

Figure 4.6 The O-chain moiety of LPS from *Pandoraea pulmonicola*

4.3 Discussion

This is the first work on the structure of the O-polysaccharide chain derived from the lipopolysaccharide isolated from *P. pulmonicola* strain LMG 18108, the most virulent and predominant *Pandoraea* species among Irish CF patients. Case reports have demonstrated that many CF patients experience a decline in lung infection after chronic *P. pulmonicola* colonisation. This may be due to the ability of the *P. pulmonicola* LPS to increase IL-6 and IL-8 production in lung epithelial cells (Caraher *et al*., 2008). Because the LPS is one of the most important bacterial virulence factors and it is known to activate host inflammation by multiple mechanisms, it is crucial to elucidate the primary structure of this macromolecule as well as its antigenic determinant portion, the O-antigen, to understand its biological activity and its role in bacterial pathogenicity. Different strains among the same species and genus can produce highly different O-polysaccharides, specifically recognized by the host's acquired immune system that produces specific antibodies. The structure of the O-chain from *P. pulmonicola* strain LMG 18108 has been elucidated by chemical analyses and 2D NMR spectroscopy. The data revealed that *P. pulmonicola* produces a *smooth*-type LPS characterised by a trisaccharide O-chain repeating unit: [→2-β-D-Qui*p*3N-(1→4)-α-D-Gal*p*NAc-(1→3)-α-D-Glc*p*NAc-1→]$_n$. A five-membered ring aglycon residue has been found covalently attached through its exocyclic carbonyl group to the amine group of Qui3N. This cyclic structure has been identified as a 3-hydroxy-2,3-dimethyl-5-oxoproline. Taking into account the fact that the antigenic portion of the LPS characterises the external cellular surface of Gram-negative bacteria, conferring on it the uniqueness indispensable for antibody recognition, it might be speculated that the non-sugar substituent found in the O-chain moiety might play a role in the

molecular mechanism of pathogenicity of *P. pulmonicola*. Moreover, being one of the major targets of the host's adaptive immune response, the determination of the O-antigen sequence is an important prerequisite for vaccination studies incorporating either conjugates of synthetic carbohydrate antigen or protein conjugates of synthetic oligosaccharides or peptides that mimic complex bacterial polysaccharide antigens (Fernandez Santana *et al.*, 2006).

References

Atkinson R.M., Lipuma J.J., Rosenbluth D.B., Dunne W.M., Chronic colonization with *Pandoraea apista* in cystic fibrosis patients determined by repetitive-element-sequence PCR. **2006**, *J. Clin. Microbiol.,* 44, 833-836.

Caraher E., Collins J., Herbert G., Murphy P.G., Gallagher C.G., Crowe M.J., Callaghan M., McClean S., Evaluation of in vitro virulence characteristics of the genus Pandoraea in lung epithelial cells. **2008**, *J. Med. Microbiol.,* 57, 15-20.

Coenye T., Falsen E., Hoste B., Ohlen M., Goris J., Govan J.R., Gillis M., Vandamme P., Description of *Pandoraea* gen. nov. with *Pandoraea apista* sp. nov., *Pandoraea pulmonicola* sp. nov., *Pandoraea pnomenusa* sp. nov., *Pandoraea sputorum* sp. nov. and *Pandoraea norimbergensis* comb. nov., **2000**, *Int. J. Syst. Evol. Microbiol.*, 50, 887-899.

Costello A., Herbert G., Fabunmi L., Schaffer K., Kavanagh K.A., Caraher E.M., Callaghan M., McClean S., Virulence of an emerging respiratory pathogen, genus *Pandoraea*, in vivo and its interactions with lung epithelial cells. **2011**, *J. Med. Microbiol.,* 60, 289-99.

Daneshvar M.I., Hollis D.G., Steigerwalt A.G., Whitney A.M., Spangler L., Douglas M.P., Jordan J.G., MacGregor J.P., Hill B.C., Tenover F.C., Brenner D.J., Weyant R.S., Assignment of CDC weak oxidizer group 2 (WO-2) to the genus *Pandoraea* and characterization of three new *Pandoraea* genomospecies. **2001**, *J. Clin. Microbiol.,* 39, 1819-1826.

Fernandez Santana V., Peña Icart L., Beurret M., Costa L., Verez Bencomo V., Glycoconjugate vaccines against *Haemophilus influenzae* type b. **2006**, *Glycobiology*,415, 153-63.

Kittelberger R., Hilbink F., Sensitive silver-staining detection of bacterial lipopolysaccharides in polyacrylamide gels. **1993**, *J. Biochem. Biophys. Methods*, 26 (1), 81-86

Molinaro A., De Castro C., Lanzetta R., Parrilli M., Raio A., Zoina A., Structural elucidation of a novel core oligosaccharide backbone of the lipopolysaccharide from the new bacterial species *Agrobacterium larrymoorei*. *Carbohydr. Res.*, **2003**, 338, 2721-2730.

Stryjewski M.E., LiPuma J.J., Messier R.H. Jr., Reller L.B., Alexander B.D., Sepsis, multiple organ failure, and death due to *Pandoraea pnomenusa* infection after lung transplantation.**2003**, *J. Clin. Microbiol*., 41, 2255-2257.

Tabary O., Escotte S., Couetil J.P., Hubert D., Dusser D., Puchelle E., Jacquot J., High susceptibility for cystic fibrosis human airway gland cells to produce IL-8 through the I kappa B kinase alpha pathway in response to extracellular NaCl content. **2000**, *J. Immunol.,*164, 3377-3384.

Westphal O., Jann K., Bacterial lipopolysaccharides: extraction with phenol-water and further applications of the procedure. **1965**, *Methods Carbohydr. Chem*., 5, 83–91.

Yu M., Zheng X., Witschi H., Pinkerton K.E., The role of interleukin-6 in pulmonary inflammation and injury induced by exposure to environmental air pollutants. **2002**, *Toxicol. Sci.,* 68, 488-497.

Zatonsky G.V., Kocharova N.A., Veremeychenko S.N., Zdorovenko E.L., Shapovalova V.Y., Shashkov A.S., Zdorovenko G.M., Knirel Y.A., Somatic antigens of pseudomonads: structure of the O-specific polysaccharide of *Pseudomonas fluorescens* IMV 2366 (biovar C). **2002**, *Carbohydr. Res.*, 337, 2365-2370.

Chapter 5

Structural and Biological Study of the LOS isolated from the chronic strain *Pseudomonas aeruginosa* RP73

Premise

Pseudomonas aeruginosa, the major pathogen involved in lethal infections in cystic fibrosis (CF) population, is able to cause permanent chronic infections that can persist over the years (see also Section I, paragraph 1.5.2). This ability to chronic colonise CF airways is related to a series of adaptive bacterial changes involving also the immunostimulant lipopolysaccharide (LPS) molecule. The structure of LPSs isolated from several *P. aeruginosa* strains showed conserved features that can undergo chemical changes during the establishment of the chronic infection. Commonly it is observed loss of the O-chain polysaccharide, that results in a non-typable strain sensitive to the serum complement (Smith *et al*., 2006), differences in lipid A structure such as the addition of amino-arabinose and palmitate, that causes an increase of the bacterial resistance to the host innate immune response or to the most common used antibiotics (mainly to β-lactam antibiotics), as well as an increment of the pro-inflammatory response (Ernst *et al*., 1999; Bragonzi *et al*., 2009). Although genetic evidences in the O-chain polysaccharide biosynthetic locus have been described, very little is known about the mechanisms involved in the other chemical changes that occur in the LPS of CF chronic strains.

Infection seriousness, high versatility and antibiotic resistance and its ability to acquire further resistance, are hallmark of chronic lung infections caused by *P. aeruginosa* in CF population. Given these premises, understanding the molecular mechanism of infection that eventually leads to pulmonary failure is an essential step in order to pursue an effective treatment.

In the present work, it is reported the elucidation of the structure and the biological activity of the R-LPS (LOS) isolated from the persistent CF isolate *P. aeruginosa* strain RP73, in order to give further insights in the adaptation mechanism of the pathogen in the

CF environment. The complete structural analysis of *P. aeruginosa* RP73 LOS was achieved by chemical analyses, NMR spectroscopy and MALDI MS spectrometry, while the assessment of the biological activity was attained testing the *in vivo* pro-inflammatory capacity of the isolated LOS molecule, using LPS from PAO1, the most widely used *P. aeruginosa* laboratory strain, as benchmark.

5.1 Isolation and Compositional Analysis of LOS from *Pseudomonas aeruginosa* RP73

LOS was extracted from dry cells by the phenol/chloroform/light petroleum procedure and analysed by SDS PAGE by using *E. coli* O55 LPS as benchmark (Galanos *et al*., 1969; Kittelberger and Hilbink, 1993). The silver staining revealed a migration pattern to the bottom of the gel typical of a low-molecular weight lipopolysaccharide. The isolated LOS was further purified by enzymatic hydrolysis with DNAse, RNAse and protease, followed by dialysis. Compositional analyses, carried out by GC/MS indicated the presence of L-Rha, D-Glc, D-GlcN, D-GalN, L-*glycero*-D-*manno*-heptose (L,D-Hep), 3-deoxy-*manno*-oct-2-ulopyranosonic acid (Kdo) and, in low amount, 2,6-dideoxy-2-amino-D-glucose (D-quinovosamine, D-QuiN), according to previously published data about *P. aeruginosa* core oligosaccharide (Rowe and Meadow, 1983; Sadovskaya *et al*., 1998)). Methylation analysis revealed the occurrence of terminal-L-Rha, terminal-D-Glc, 3-substituted-L,D-Hep, 6-substituted-D-GlcN, 3,6-disubstituted-D-Glc, 3,4-disubstituted-D-GalN, terminal-Kdo, 4,5-disubstituted-Kdo and, in trace, terminal-D-QuiN and 3-substituted-L-Rha. Fatty acids composition, obtained by GC/MS analysis of their methyl ester derivatives, showed the presence of 3-hydroxydodecanoic acid [C12:0(3OH)], 3-hydroxydecanoic

[C10:0(3-OH)] and dodecanoic acid (C12:0) in agreement with lipid As isolated from other *Pseudomonas*.

5.2 Structural Characterisation of OS Product by NMR spectroscopy

LOS from *P. aeruginosa* RP73 was completely de-acylated by mild hydrazinolysis and strong alkaline hydrolysis with hot KOH (see Section V). After desalting on a Sephadex G-10 column and lyophilisation, the core oligosaccharide comprehensive of the lipid A glucosamine-backbone was obtained. To elucidate the full structure of core oligosaccharide (**OS**) of *P.aeruginosa* RP73 LOS, a complete 1D and 2D NMR analysis (DQF-COSY, TOCSY, NOESY, ROESY, $^{13}C,^{1}H$ -HSQC, $^{13}C,^{1}H$ HMBC and $^{31}P,^{1}H$ HSQC) was performed.

The ^{1}H NMR spectrum of **OS** (Figure 5.1), together with the $^{1}H,^{13}C$ HSQC spectrum, showed the occurrence of 11 anomeric signals (**A-L**, Table 5.1, Figure 5.1), while signals resonating at 1.88/2.11 ppm and 1.96/1.67 were identified as the H-3 methylene proton signals of Kdo residues **K** and **J** (Table 5.1, Figure 5.1). Anomeric configurations were assigned on the basis of the $^{3}J_{H1,H2}$ coupling constants and the *intra*-residual NOE contacts; the relative configuration of each residue was assigned based on vicinal $^{3}J_{H,H}$ coupling constants. The α-configuration of both Kdo residues was attributed on the basis of the chemical shift values of H-3 and of the $^{3}J_{H7,H8a}$ and $^{3}J_{H7,H8b}$ coupling constants (Birnbaum *et al*., 1987; Holst *et al*., 1994).

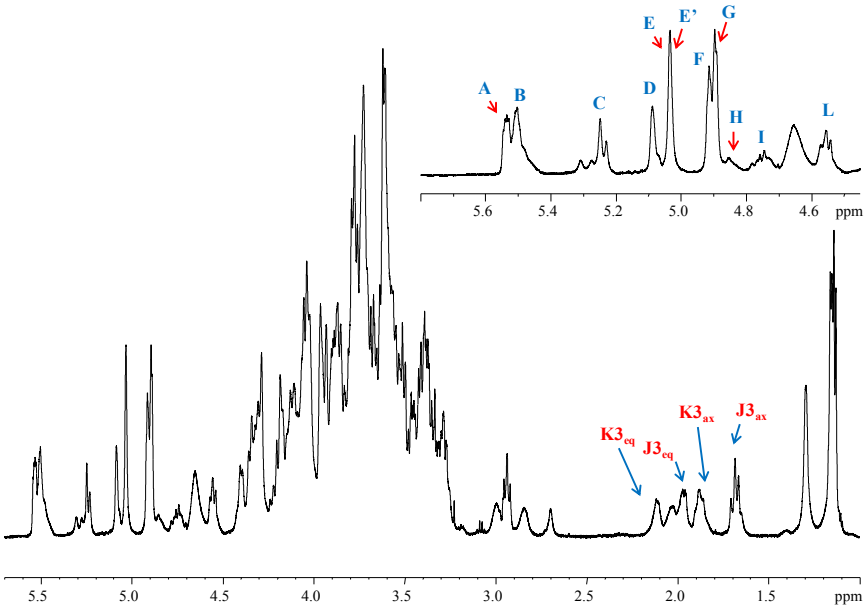

Figure 5.1 ^{1}H NMR spectrum of core oligosaccharide (OS) with zoom of anomeric region (top-right).

All sugar residues were present as pyranose rings, according to either ^{13}C chemical shift values and the presence of long range correlations between C-1/H-1 and H-5/C-5 in the ^{1}H, ^{13}C HMBC spectrum (for Kdo residues between C-2 and H-6) (Silipo *et al.*, 2004). The ^{31}P NMR spectrum gave evidence for the presence of six different monophosphate ester groups in the range of chemical shift between 1.30 and 5.10 ppm. The disaccharide backbone of the lipid A moiety was represented by residues **A** (δ = 5.53 ppm, Table 5.1) and **I** (δ = 4.75 ppm, Table 5.1) that are the α-GlcN*1P* and β-GlcN*4P*, respectively; the *gluco* configuration was indicated by high $^{3}J_{H,H}$ ring proton values (8–10 Hz). In details, the H-2 of both residues **A** and **I** correlated with two nitrogen-bearing carbon atoms at δ = 54.4 and δ = 55.4 ppm. Moreover, the H-1 of residue **A** showed to possess the typical multiplicity of a phosphorylated α-

anomeric proton signal ($^{3}J_{H-1,H-2}$= 3.2 Hz, $^{3}J_{H-1,P}$= 8.1 Hz), as reported in the $^{31}P,^{1}H$ HSQC (Figure 5.4). Phosphorylation of residue **I** at position O-4 was assigned by the observation of the H-4 and C-4 downfield shifts (3,61 ppm and 73.8 ppm respectively, Table 5.1) and by the presence of correlation in the $^{1}H,^{31}P$ HSQC spectrum with a signal at 3.97 ppm (Figure 5.4); the chemical shift values of H-1/C-1 **I**, the $^{3}J_{H1,H2}$ coupling constant (8.7 Hz) and the *intra*-residual NOE correlation of H-1 with H-3 and H-5 were indicative of its β-anomeric configuration. A minor spin system was also identifiable for GlcNII residue in which phosphate at position O-4 was missing, based on the chemical shift of H-4 and C-4; this allowed to establish that phosphate at position 4 of GlcNII is not stoichiometrically present. The spin systems **C** and **D** were identified as α-*manno* configured residues due to the low coupling constant values $^{3}J_{H1,H2}$ and $^{3}J_{H2,H3}$ (below 3 Hz), diagnostic of H-2 equatorial orientation, moreover in the TOCSY spectrum it was possible to assign from H-2 all the other resonances of the ring protons allowing to identify it as a heptose monosaccharide. The chemical shift value of C-6 of residues **C** and **D** shown in the HSQC spectrum (below 70 ppm) led to the final identification as L-*glycero*-D-*manno*-heptoses (Hep^{I} and Hep^{II}, respectively), in accordance with the compositional analysis. Finally, the observation of chemical shift values at δ = 4.40, δ = 4.22 for H-2 **C** and H-4 **C**, as well as the presence of cross peaks in the $^{1}H,^{31}P$ HSQC spectrum with signals at 1.48 and 4.21 ppm respectively were indicative of *O*-phosphorylation at these positions (Figure 5.4). Likewise, for residue **D** chemical shifts at δ = 4.08 ppm, δ = 4.31 ppm for H-4 **D** and H-6 **D** and the presence of cross peaks in the $^{1}H,^{31}P$ HSQC spectrum with signals at 5.04 and 4.26 ppm (Figure 5.4) were diagnostic of phosphorylated positions. Residue **B** (δ= 5.49 ppm, Table 5.1), identified as a *galacto*-configured monosaccharide owing to the small $J_{H,H}$ values for H-3/H-4 and H-

4/H-5 (3 and 1Hz, respectively), possessed a signal for C-2 at 50.4 ppm indicating that C-2 was a nitrogen-bearing carbon atom; these characteristics allowed the identification of spin system **B** as a α-GalN. The spin systems **F**, **G** and **L** were attributed to glucose residues due to the large ring $^{3}J_{H,H}$ coupling constants; in details, both residues **F** and **G** were identified as α-anomeric configured glucoses whereas **L** was identified as a β-anomeric configured glucose. Residues **E** and **E'** were recognised as two α-rhamnose residues being characterised by low $^{3}J_{H\text{-}1,H\text{-}2}$ and $^{3}J_{H\text{-}2,H\text{-}3}$ values, indicative, as previously mentioned, of α-*manno*-configuration, and in addition, by the occurrence in the TOCSY spectrum of correlations to methyl signals in the shielded region at 1.14-1.15 ppm, respectively. Finally, a further spin system (H-1 **H** at 4.84 ppm, Table 5.1), present in non-stoichiometric ratio, was identified as β-QuiN owing to the $^{3}J_{H,H}$ ring coupling constants (~9 Hz), the *intra*-residual NOE contact of H-1 with H-3 and H-5, and the $^{3}J_{H1,H2}$ coupling constant. Moreover, the ^{1}H-^{13}C HSQC spectrum showed the presence of a correlation of H-2 **H**, at 2.99 ppm, with a nitrogen-bearing carbon signal at 56.6 ppm.

Unit	1	2	3	4	5	6	7	8
A	5.53	3.30	3.78	3.49	4.04	4.18/3.65		
6-α-GlcN1*P*	*90.5*	*54.4*	*69.4*	*69.6*	*72.4*	*69.3*		
B	5.49	3.71	4.34	4.38	4.34	3.66		
3,4-α-GalN	*96.5*	*50.4*	*76.5*	*75.4*	*71.8*	*61.7*		
C	5.24	4.40	4.05	4.22	4.29	3.95	3.78/3.52	
3-α-Hep2,4*P*	*97.3*	*74.3*	*73.7*	*72.3*	*74.2*	*71.2*	*63.5*	
D	5.08	4.30	4.13	4.08	4.02	4.31	3.78/3.52	
3-α-Hep4,6*P*	*101.9*	*69.3*	*76.5*	*72.5*	*68.8*	*70.0*	*63.5*	
E	5.03	3.37	3.89	3.63	4.02	1.14		
3-α-Rha	*100.5*	*73.0*	*80.1*	*72.4*	*71.0*	*16.4*		
E'	5.03	4.18	3.67	3.33	3.89	1.15		
t-α-Rha	*102.2*	*69.9*	*70.1*	*71.8*	*71.8*	*16.4*		
F	4.91	3.38	3.72	3.64	3.95	3.78		
t-α-Glc	*99.1*	*71.7*	*72.3*	*N.D.*	*71.2*	*59.8*		
G	4.89	3.45	3.72	3.36	3.67	3.61		
t-α-Glc	*97.9*	*73.0*	*73.5*	*69.6*	*72.1*	*60.7*		
H	4.84	2.99	3.53	3.18	3.38	1.30		
t-β-QuiN	*100.9*	*56.6*	*74.2*	*73.2*	*75.2*	*16.9*		
I	4.75	2.93	3.72	3.61	N.D.	3.34		
6-β-GlcN4*P*	*99.3*	*55.4*	*72.3*	*73.8*	*N.D.*	62.5		
L	4.55	3.33	3.54	3.57	3.57	3.77/3.71		
3,6-β-Glc	*104.3*	*73.5*	*82.0*	*68.2*	*74.3*	*66.3*		
K	-	-	1.88/2.11	4.00	4.16	3.72	N.D.	3.67
4,5-α-Kdo	*174.4*	*101.7*	*34.3*	*71.0*	*68.2*	*69.5*	N.D.	*63.0*
J	-	-	1.96/1.67	4.05	3.96	3.66	N.D.	3.58
t-α-Kdo	*174.4*	*101.7*	*34.9*	*65.6*	*66.6*	*70.1*	N.D.	*62.7*

Table 5.1 Chemical shift δ ($^{1}H/^{13}C$) of the de-acylated LOS.

Low-field shifted carbon signals were useful to identify substitution at O-3 of residues **C**, **D** and **E**, O-6 of **A** and **I**, whereas residues **B** and **L** were di-substituted at O-3 and O-4 for the first monosaccharide and at O-3 and O-6 for the second residue. Sugar residues **E'**, **F**, **G** and **H** were recognised as terminal residues; finally, residue **K** was identified to be Kdo substituted at positions O-4 and O-5 whereas residue **J** resulted to be a terminal Kdo. Abovementioned results were in full accordance with the methylation analysis.

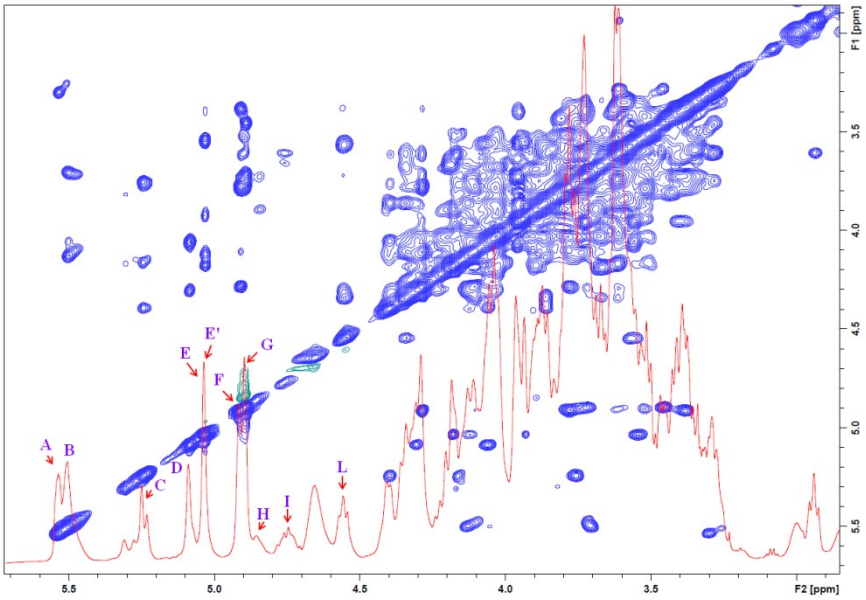

Figure 5.2 NOESY spectrum of the oligosaccharide product.

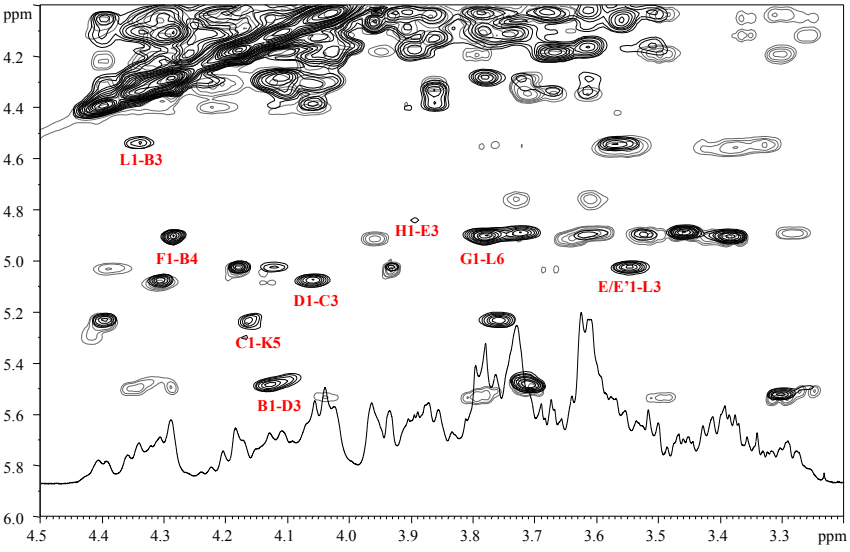

Figure 5.3 Section of the NOESY (**black**) and TOCSY (**grey**) spectra of oligosaccharide from *P. aeruginosa* RP73. The most relevant *inter*-residue NOE cross-peaks are indicated.

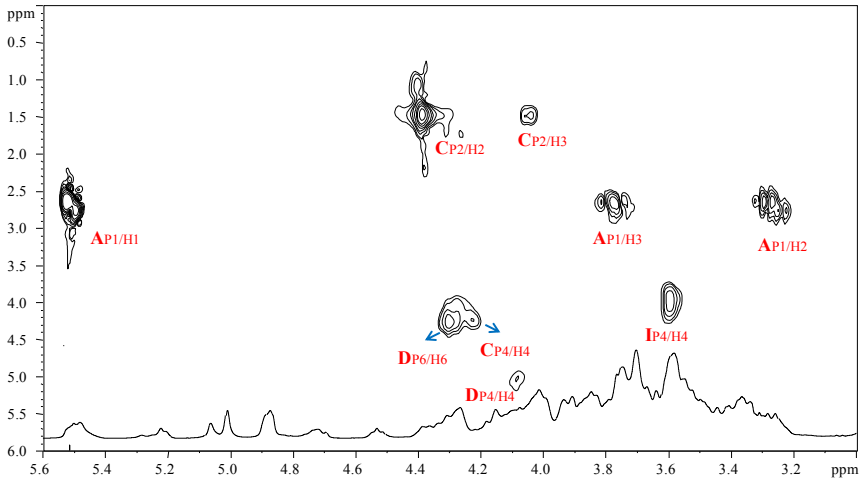

Figure 5.4 Section of the ^{1}H NMR and ^{1}H, ^{31}P HSQC spectra of fully de-acylated LOS from *Pseudomonas aeruginosa* RP73. The localization of the phosphate groups is indicated.

The sequence of the monosaccharide residues was inferred by using NOE correlations of the ROESY and NOESY spectra (Figures 5.2 and 5.3) and by long-range scalar correlations of ^{1}H,^{13}C-HMBC. The typical lipid A backbone, composed by residues **A** and **I**, was validated by the *inter*-residual NOE contact of H-1 **I** with H-6 **A** and by the corresponding long-range correlation. NOE cross peaks between H-5 **K**/H-6 **I**, H-3$_{eq}$ **K**/H-6 **J**, and H-1 **C**/H-5 **K** (Figure 5.3) confirmed the typical *Pseudomonas* inner core backbone composed of [α-L,D-Hep(1→5)-[α-Kdo-(2→4)]-α-Kdo (Bystrova *et al.*, 2002; Bock *et al.*, 1994). Moreover, heptose **C** was in turn substituted in position O-3 by heptose residue **D** owing to the NOE contact between H-1 **D**/H-3 **C** (Figure 5.3) and to the relative long range correlation. This latter heptose monosaccharide was, in turn, substituted by GalN residue (**B**). The two glucose residues **F** and **L**, were linked to residue **B** to O-4 and O-3, respectively, as shown by NOE correlations H-1 **F**/H-

4 **B** (Figure 5.3) and H-1**L**/H-3 **B**. Residue **L** was in turn substituted at O-6 and O-3 positions by residues **G** and **E**/**E'**, respectively. Finally residue **H** was found to be linked, in a non stoichiometrical fashion, to the residue **E** at position O-3 (δ = 3.89 ppm, Table 5.1) as shown by the NOE correlation H-1 **H**/H-3 **E** (Figure 5.3). The full oligosaccharide skeleton from *P. aeruginosa* RP73 LOS is depicted below:

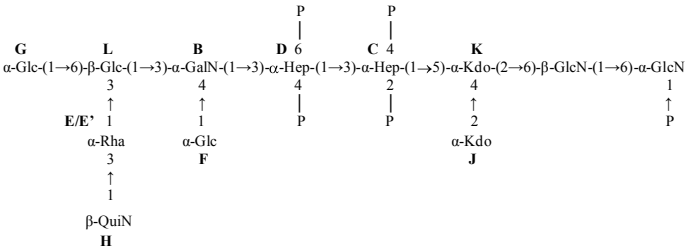

Eventually, by chemical analyses and MALDI MS on the intact LOS (not shown) it was possible to ascertain the presence of a further L-alanine residue which must be occurring on GalN residue and the absence of the typical carbamoyl group sitting at position O-7 of Hep^{II} (Sadovskaya *et al*., 1998; Sánchez Carballo *et al*., 1999).

Overall, the above data revealed that core OS from *P. aeruginosa* RP73 LPS is a heterogeneous structure very similar to those previously proposed ones (Knirel *et al*., 2001; Kooistra *et al*., 2003), including another cystic fibrosis clinical isolate (Knirel *et al*., 2001) and some other strains containing O-antigen (Dean *et al*., 2002; Bystrova *et al*., 2002). So, resuming the NMR data there was no substantial difference between this LPS and other CF LPSs; what substantially differed was the lipid A part of the LOS (see below).

5.3 Structural Characterisation by MALDI Mass Spectrometry of the Lipid A moiety

The lipid A carbohydrate backbone was already established by NMR spectroscopy as above described. In order to analyse the fatty acid number, location and distribution on lipid A moiety MALDI mass spectrometry was used directly on lipid A itself obtained by a mild hydrolysis with acetate buffer; this is typically performed to cleave the labile glycosidic linkage between Kdo residue and the GlcNII of lipid A. The negative-ion MALDI mass spectrum of native lipid A from *P. aeruginosa* RP73 is reported in Figure 5.5 where it was immediately apparent the very profound chemical difference of this lipid A blend compared with canonical CF *P. aeruginosa* lipid A. It was in fact a pattern of molecular ion peaks, in the mass range 800-2000 amu, representative of a complex mixture essentially consisting of *bis*- and *mono*-phosphorylated penta-acylated, tetra-acylated and tri-acylated species; where in *mono*-phosphorylated species phosphate is lacking from GlcNII (see above).

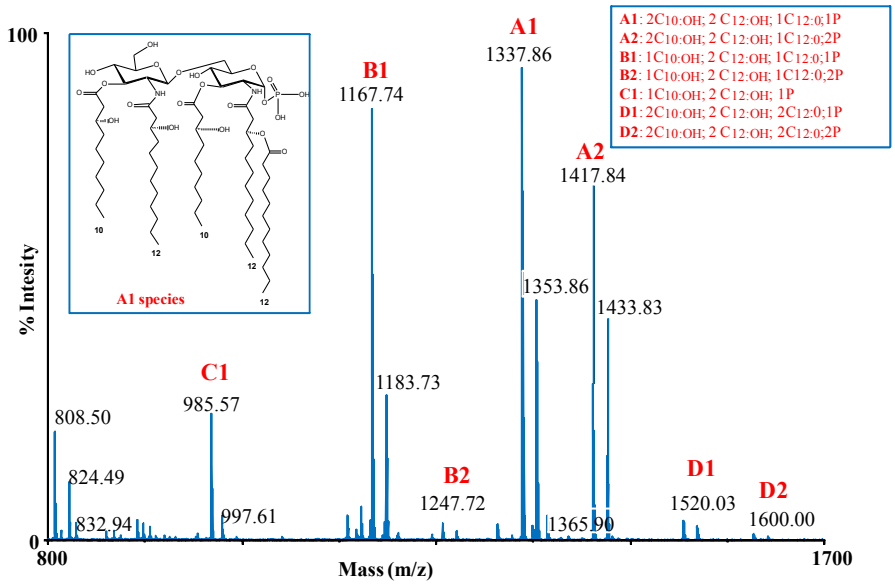

Figure 5.5 Negative ion MALDI-TOF spectrum of the lipid A from *Pseudomonas aeruginosa* RP73. Assignment of the ion peaks is shown in the top-right panel. The main lipid A specie structure is reported in the top-left panel.

The hexa-acylated lipid A was present in a very minor amount, no traces of hepta-acylated species were found. The location of either the primary ester-linked C10:0 (3-OH) or the secondary amide-linked C12:0 (3-OH) fatty acid on the GlcNII was established by ammonium hydroxide hydrolysis protocol and/or the MS/MS analysis of the lipid A moiety (Silipo *et al.*, 2002; Sturiale *et al.*, 2011). In details, the intense peak at *m/z* 1417.84 (Figure 5.5) was attributable to a *bis*-phosphorylated disaccharide backbone characterised by a C10:0 (3-OH) and a C12:0 (3-OH) in ester linkage and in amide linkage respectively on GlcNII, and by a further C10:0 (3-OH) in ester linkage and a C12:0 (3-OH) in amide linkage on GlcNI; this latter C12:0 (3-OH), in turn, was substituted by a C12:0 residue. These assignments were supported by the MS/MS spectrum (not shown): the Y ion at *m/z* 626.4 confirms that

GlcNI is di-acylated, peak at *m/z* 1229.5 originates from the C10:0 (3OH) loss, while peak at *m/z* 1217.5 corresponds to the C12:0 loss. Absence of a peak corresponding to a C12:0 (3OH) loss (216 amu) confirms that these fatty acids are linked in amide linkages. Specie at *m/z* 1337.86 (Figure 5.5) was consistent with the same above mentioned penta-acylated lipid A lacking the phosphate group on the GlcNII. Peaks at *m/z* 1353.86 and 1433.83 (+16 amu) corresponded to structures bearing a C12:0 (3-OH) instead of the C12:0 residue. At lower mass range was also present an ion peak at *m/z* 1167.74 (Figure 5.5) representative of a *mono*-phosphorylated tetra-acylated lipid A that lacks in the C10:0 (3-OH) carried by GlcNI at position O-3; the relative *bis*-phosphorylated specie was also found in a minor peak at *m/z* 1247.72 (Figure 5.5). The *mono*-phosphorylated tri-acylated specie was represented by the minor ion peak at *m/z* 985.57 (Figure 5.5) characterised by the absence of both C10:0 (3-OH) in ester linkage on GlcNI and the secondary fatty acid C12:0; the relative *bis*-phosphorylated specie was not detected in this analysis. Minor peaks at *m/z* 1520.03, 1536.02, 1600.00 and 1615.99 are related to hexa-acylated species with a further C12:0 (*m/z* 1520.03 and 1600.00) or a C12:0 (3-OH) (*m/z* 1536.02 and 1615.99) linked to the C12:0 (3OH) of the GlcNII. No traces of addition of amino-arabinose or palmitate to lipid A species, typical of CF-associated *P.aeruginosa* lipid A phenotypes, was observed. Interestingly, the elucidated structure of lipid A from *P.aeruginosa* RP73 was found to possess the same fatty acids location and distribution of a non-mucoid non-cystic fibrosis blood isolate grown in LB medium already described as very low inflammatory molecule (Ernst *et al*., 1999). This prompted to verify the *in vivo* pro-inflammatory capacity.

5.4 *In vivo* pro-inflammatory effect of the LOS from *P. aeruginosa* RP73

Since it was established that lipid A is the LPS moiety able to elicit the host innate immune system and that this capability strictly depends on its general architecture, it was tested the *in vivo* pro-inflammatory capacity of the particular LOS structure of *P. aeruginosa* RP73 strain. It was analysed leukocytes recruitment in the bronchoalveolar lavage fluid (BALF) of C57Bl/6NCrlBR mice exposed for 16 h to LOS and LPS of strains RP73 and PAO1 respectively, by intranasal instillation. When cellular recruitment in BALF in mice treated with LOS from RP73 clinical isolate was compared to those treated with LPS from PAO1 reference strain, there was no significant difference in the two groups in recruited total cells and macrophages number (data not shown), however significant lower recruitment of neutrophils was observed in mice exposed to LOS from RP73 clinical isolate when compared to those treated with LPS from PAO1 reference strain (LOS RP73 vs LPS PAO1 $p<0.05$) (Figure 5.6), accordingly to the MPO activity measured in BALF (Figure 5.6). Thus, it is possible to conclude that LOS from the chronic strain of *P. aeruginosa* RP73 possesses a low inflammatory activity that is consistent with the elucidated hypo-acylated structure of its lipid A moiety (Hajjar *et al.*, 2002).

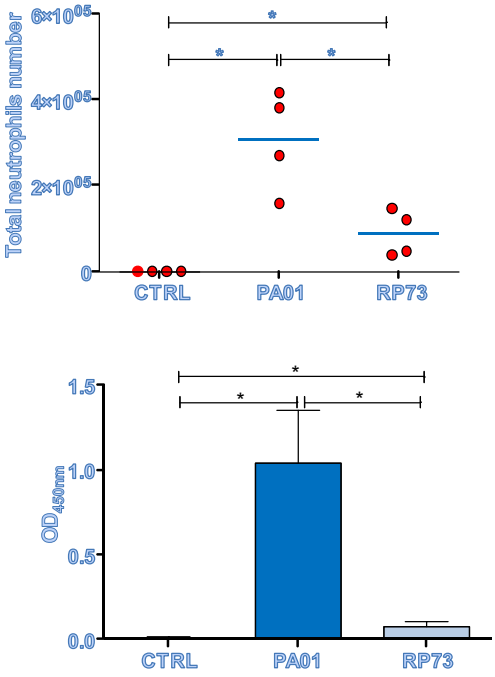

Figure 5.6 Neutrophils recruitment and MPO release in murine lungs after 16 h treatment with LOS derived from *P. aeruginosa* RP73 CF isolate and LPS from PAO1 reference strain.

5.5 Discussion

The lipopolysaccharide molecule isolated from strains of *P. aeruginosa* belonging to environment, CF and non-CF isolates, has been extensively investigated due to its essential role in the bacterial virulence and resistance to the common used antibiotics in the treatment of infection. Clearly, in order to develop therapeutic intervention strategies in *P. aeruginosa* infections, the assessment of its structure is a pivotal first step to enhance our insights into the

microbial capability to cause infection and to modify their genotypic and phenotypic characteristics. In the present work it is reported the structure and immunological activity of the LPS isolated from the cystic fibrosis chronic strain *P.aeruginosa* RP73. As expected, as first chemical modification of the chronicisation this LPS lacked the O-antigen (Smith *et al*., 2006), it was indeed a LOS. As mentioned above, all *P. aeruginosa* LPSs, investigated so far, possess a conserved inner core region composed by two residues of 3-deoxy-D-*manno*-octulosonic acid (Kdo), two residues of L-*glycero*-D-*manno*-heptose (Hep) and a 2-amino-2-deoxy galactose residue (GalN), which is the branching point of the core oligosaccharide (Bystrova *et al*., 2002; Bock *et al*., 1994). Likewise, *P. aeruginosa* RP73 LPS inner core showed the presence of the aforesaid typical monosaccharide residues and the GalN residue was substituted by an *N*-alanyl group (Sadovskaya *et al*., 1998; Sánchez Carballo *et al*., 1999), and the two Hep residues possessed a total of four phosphate groups as found in a *P. aeruginosa* cystic fibrosis *rough*-LPS isolates (Knirel *et al*., 2001). *P. aeruginosa* outer core region is more variable but it is still possible to find a common architecture composed by two glucose moieties and a rhamnose residue, the first monosaccharide composing the O-polysaccharide region (Bystrova *et al*., 2002; Pier, 2003). Overall, there was no consistent difference in LPS core oligosaccharide of this strain and the other CF strains of *P. aeruginosa*.

Very interesting chemical characteristics were found in the lipid A structure of the LPS under study. Indeed, in stark contrast with previous reports about lipid A isolated from cystic fibrosis strains, *P. aeruginosa* RP73 showed to possess mainly a penta-acylated lipid A with no amino-arabinose and/or palmitate residues; the presence in very low amount of the hexacyl- or the total absence of

the heptacyl- type lipid A found in other cystic fibrosis isolates (Ernst *et al*., 1999), as well as the total absence of amino-arabinose residues, render RP73 lipid A unique in its case. Given these results, it was tested in a murine model of intranasal instillation the pro-inflammatory capacity of this particular LOS. In the lung of mice treated with the purified LOS of *P.aeruginosa* RP73, neutrophils recruitment was eloquently lower with respect to LPS from reference strain PAO1. It has been extensively described in several papers that on the canonical *P.aeruginosa* lipid A skeleton the glycosilation by amino-arabinose and/or acylation by palmitate residues strongly increase the production of pro-inflammatory molecules by eukaryotic cell and that this chemical modifications are the hallmark of the CF *P. aeruginosa* lipid A (Ernst *et al*., 1999; Hajjar *et al*., 2002). On the basis of previous notions (Hajjar *et al*., 2002; Alexander and Rietschel, 2001) about the connection between the acylation state of lipid A and the capability to elicit the inflammatory response, the observed low inflammatory power, fulfilled by LOS from *P. aeruginosa* RP73, is not surprising since its under-acylated structure is identical to a non-cystic fibrosis *P. aeruginosa* lipid A previously described (Ernst *et al*., 1999).

Altogether these results corroborate what has been previously shown concerning the reduction of the immunopotential of LPS extracted from late *P. aeruginosa* isolates from CF patients respect to their clonal early isolate (Ciganà *et al*., 2009), that is consistent with the phenotypic changes that characterise *P. aeruginosa* strains during the establishment of chronic infections (Smithe *et al*., 2006).

References

Alexander C., Rietschel E.T., Bacterial lipopolysaccharides and innate immunity. **2001**, *J. Endotoxin Res.*, 7: 167-202.

Birnbaum G.I., Roy R., Brisson J.R., Jennings H., **1987**, *J. Carbohydr. Chem.*, 6, 17-39.

Bock K., Vinogradov E., Holst O., Brade H., Isolation and structural analysis of oligosaccharide phosphates containing the complete carbohydrate chain of the lipopolysaccharide from *Vibrio cholerae* strain H11 (non-O1). **1994**, *Eur. J. Biochem.*, 225, 1029-1039.

Bragonzi A., Paroni M., Nonis A., Cramer N., Montanari S., Rejman J., Di Serio C., Döring G., Tümmler B., *Pseudomonas aeruginosa* microevolution during cystic fibrosis lung infection establishes clones with adapted virulence. **2009**, *AJRCCM*, 180, 138-145.

Bystrova O.V., Shashkov A.S., Kocharova N.A., Knirel Y.A., Lindner B., Zähringer U., Pier G.B., Structural studies on the core and the O-polysaccharide repeating unit of *Pseudomonas aeruginosa* immunotype 1 lipopolysaccharide. **2002**, *Eur. J. Biochem.*, 269, 2194-2203.

Ciganà C., Curcurù L., Leone M.R., Ieranò T., Lorè N.I., Bianconi I., Silipo A., Cozzolino F., Lanzetta R., Molinaro A., Bernardini M.L., Bragonzi A., *Pseudomonas aeruginosa* exploits lipid A and muropeptides modification as a strategy to lower innate immunity during cystic fibrosis lung infection. **2009**, *PLoS One*, 4 (12), e8439.

Dean C.R., Datta A., Carlson R.W., Goldberg J.B., WbjA adds glucose to complete the O-antigen trisaccharide repeating unit of the lipopolysaccharide of *Pseudomonas aeruginosa* serogroup O11. **2002**, *J. Bacteriol.* , 184 (1), 323-6.

Ernst R.K., Yi E.C., Guo L., Lim K.B., Burns J.L., Hackett M., Miller S.I., Specific lipopolysaccharide found in cystic fibrosis airway *Pseudomonas aeruginosa*. **1999**, *Science*, 286(5444), 1561-5.

Galanos C., Luderitz O., Westphal O., A new method for the extraction of R lipopolysaccharides. **1969**, *Eur. J. Biochem.*, 9, 245-249.

Hajjar A.M., Ernst R.K., Tsai J.H., Wilson C.B., Miller S.I., Human Toll-like receptor 4 recognizes host-specific LPS modifications. **2002**, *Nat. Immunol.*, 3, 354-359.

Holst O, Thomas-Oates J.E., Brade H., Preparation and structural analysis of oligosaccharide monophosphates obtained from the lipopolysaccharide of recombinant

strains of *Salmonella minnesota* and *Escherichia coli* expressing the genus-specific epitope of *Chlamydia* lipopolysaccharide. **1994**, *Eur. J. Biochem*. 222, 183-194.

Kittelberger R., Hilbink F., Sensitive silver-staining detection of bacterial lipopolysaccharides in polyacrylamide gels. **1993**, *J. Biochem. Biophys. Methods*, 26 (1), 81-86.

Knirel Y.A., Bystrova O.V., Shashkov A.S., Lindner B., Kocharova N.A., Senchenkova S.N., Moll H., Zähringer U., Hatano K., Pier G.B., Structural analysis of the lipopolysaccharide core of a rough, cystic fibrosis isolate of *Pseudomonas aeruginosa*. **2001**, *Eur. J. Biochem*., 268 (17), 4708-19.

Kooistra O., Bedoux G., Brecker L., Lindner B., Sánchez Carballo P., Haras D., Zähringer U., Structure of a highly phosphorylated lipopolysaccharide core in the Delta algC mutants derived from *Pseudomonas aeruginosa* wild-type strains PAO1 (serogroup O5) and PAC1R (serogroup O3). **2003**, *Carbohydr Res*., 338 (23), 2667-77.

Pier, G.B., Promises and pitfalls of *Pseudomonas aeruginosa* lipopolysaccharide as a vaccine antigen. **2003**., *Carbohydr. Res*., 338, 2549-2556.

Rowe P.S., Meadow P.M., Structure of the core oligosaccharide from the lipopolysaccharide of *Pseudomonas aeruginosa* PAC1R and its defective mutants. **1983**, *Eur. J. Biochem*., 132 (2), 329-37.

Sadovskaya I., Brisson J.R., Lam J.S., Richards J.C., Altman E., Structural elucidation of the lipopolysaccharide core regions of the wild-type strain PAO1 and O-chain-deficient mutant strains AK1401 and AK1012 from *Pseudomonas aeruginosa* serotype O5. **1998**, *Eur. J. Biochem*., 255 (3), 673-84.

Sánchez Carballo P.M., Rietschel E.T., Kosma P., Zähringer Ü., Elucidation of the structure of an alanine-lacking core tetrasaccharidetrisphosphate from the lipopolysaccharide of *Pseudomonas aeruginosa* mutant H4. **1999**, *Eur. J. Biochem.*, 261 (2), 500-8.

Silipo A., Lanzetta R., Amoresano A., Parrilli M., Molinaro A., Ammonium hydroxide hydrolysis: a valuable support in the MALDI-TOF mass spectrometry analysis of Lipid A fatty acid distribution. **2002**, *J. Lipid Res.* 43, 2188-2195.

Silipo A., Leone S., Molinaro A., Lanzetta R., Parrilli M., The structure of the phosphorylated carbohydrate backbone of the lipopolysaccharide of the phytopathogen bacterium *Pseudomonas tolaasii*. **2004**, *Carbohydr. Res*., 339, 2241-2248.

Smith E.E., Buckley D.G., Wu Z., Saenphimmachak C., Hoffman L.R., D'Argenio D.A., Miller S.I., Ramsey B.W., Speert D.P., Moskowitz S.M., Burns J.L., Kaul R., Olson M.V., Genetic adaptation by *Pseudomonas aeruginosa* to the airways ofcystic fibrosis patients. **2006**, Proc. Natl. Acad. Sci. USA, 103(22), 8487-92.

Sturiale L., Palmigiano A., Silipo A., Knirel Y.A., Anisimov A.P., Lanzetta R., Parrilli

M., Molinaro A., Garozzo D., Reflectron MALDI TOF and MALDI TOF/TOF mass spectrometry reveal novel structural details of native lipooligosaccharides. **2011**, *J. Mass Spectrom.*, 46, 1135-1142.

Chapter 6

Structural Determination of endotoxins from clinical isolates of *Burkholderia cenocepacia* retrieved at different stages of colonisation

Premise

Burkholderia cenocepacia represents one of the most prevalent clinical cystic fibrosis (CF) isolates in which there were recognised a number of different strains, e.g. the *B. cenocepacia* epidemic strain ET-12 clonal strains J2315 and K56-2 strains (Mahenthiralingam *et al*., 2005) that showed to behave differently when used *in vitro* and *in vivo* models (De Soyza *et al*., 2003). Furthermore, pulmonary infections caused by *B. cenocepacia* strains are viewed as so detrimental that lung transplantation, to date the only treatment that offers improved quantity and quality of life in CF patients, is frequently excluded for infected patients (De Soyza *et al*., 2003; Hadjiliadis *et al*., 2007).

During the infection process, bacteria within the CF airways are exposed to stressing selection pressures, such as antibiotic treatments, oxygen limitations and host immune defenses (Harrison, 2007; Hogardt and Heesemann, 2013), that lead to the emergence of clonal variants exhibiting different phenotypic characteristics also inherent to the bacterial pathogenesis, such as production of different size of biofilm and different antimicrobial sensitivity patterns (Mahenthiralingam *et al*., 2002). Comparing to *Pseudomonas aeruginosa*, the major CF pathogen about which many studies have been performed in the past years (see also Chapter 5), very little is known about the molecular mechanisms involved in the adaptation of *B. cenocepacia* to the CF lung environment. A contribution to this field of research was given by a number of published papers (Leitão *et al*., 2008; Coutinho *et al*., 2011) focused on the phenotypic and genome-wide expression analyses of serial BCC clonal variants isolated during different stages of infection in CF patients, where authors demonstrated that the adaptation process mainly affects metabolic pathways leading to alteration of the bacterial cell wall structure (Coutinho *et al*.,

2011). Being one of the major component of the outer membrane of Gram-negative bacteria, the lipopolysaccharide (LPS) is considered one of the cell wall component that should be affected by the most consistent changes in its structure during the adaptation of *B. cenocepacia* in the course of chronic infection. To elucidate this matter, the present work reports the characterisation of the complete structure of the LPS isolated from a CF patient (patient J) (Coutinho *et al*., 2011) who was chronically colonised by *B. cenocepacia* for three and half years until death with the "cepacia syndrome" (Coutinho *et al*., 2011). In details, it is showed the structure of LPS isolated from IST439, the first *B. cenocepacia* isolate recovered, which presumably initiated the infection; IST4113 (Figure 6.1), obtained almost 3 years later after a period of exacerbated infection and intravenous therapy (Figure 6.1); and IST4134, the last isolate retrieved from the patient immediately before death with cepacia syndrome (Figure 6.1). Recently, IST4129, a less virulent isolate recovered from the same patient 32 months after the beginning of the infection, has also been included in this research (Coutinho *et al*., 2011).

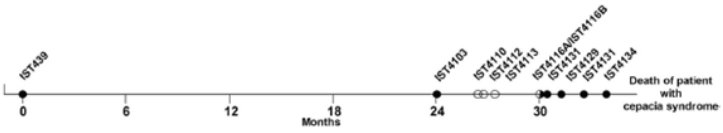

Figure 6.1 Clinical isolates from patient J.

6.1 Isolation and Chemical Analyses of LPSs isolated from *B. cenocepacia* strains IST439, IST4113 IST4129, IST4134

The lipopolysaccharide from *B. cenocepacia* IST439, IST4113, IST4129 and IST4134 was extracted by the hot phenol/water method (Westphal and Jann, 1965). Extracted material was purified with nucleases and proteases followed by dialysis, gel permeation chromatography and eventually examined by SDS electrophoresis (Kittelberger and Hilbink, 1993). *B. cenocepacia* IST439 revealed that the extracted lipopolysaccharide was a *smooth*-type LPS, while strains IST4113, IST4129 and IST4134 showed the presence of a *rough*-type LPS. Monosaccharide analysis of LOSs from IST4113, IST4129 and IST4134 resulted identical in all the three strains and showed the presence of D-GlcN, 4-amino-4-deoxy-L-arabinose (L-Ara4N), D-Glc, D-Gal, L-*glycero*-D-*manno* -heptose (L,D-Hep), 3-deoxy-D-*manno*-oct-2-ulopyranosonic acid (D-Kdo) and D-*glycero*-D-*talo*-oct-2-ulopyranosonicacid (D-Ko). The above composition was already reported for *B. cenocepacia* ET-12 clone LMG 16656 (also known as J2315) (Silipo *et al*., 2007). The strain IST439 revealed the same composition of the other three strains but showed also the presence of a further D-ribose residue. Methylation studies were consistent to previously found data (Silipo *et al*., 2007) for all strains and showed the subsequent composition: 3,4-disubstituted Hep, 3,7-disubstituted Hep, 7-substituted Hep, terminal Hep, 2,6-disubstituted Gal, 6-substituted Glc, terminal Glc, terminal Ara4N, 6-substituted GlcN, 4,5-disubstituted Kdo, and, in particular, only strain IST439 revealed the presence of a 2-substituted ribofuranose (Rib*f*) and 4-substituted GalN. Fatty acids analysis showed the presence of (*R*)-3-hydroxyhexadecanoic acid (C16:0 (3-OH)) in amide linkage and of (*R*)-3-hydroxytetradecanoic (C14:0 (3-OH))

and tetradecanoic acid (C14:0) in ester linkage. The overall chemical composition matched with the archetypal *Burkholderia* LPSs/LOSs (Silipo *et al.*, 2007).

6.2 Structural Determination of oligo-/polysaccharide moieties of LOSs/LPS from strains *B. cenocepacia* strains IST439, IST4113 IST4129, IST4134 by NMR spectroscopy

The primary structure of the LPS/LOSs isolated from the four strains was achieved by chemical analyses, mass spectrometry and NMR spectroscopy on intact and partially degraded LPS/LOSs. In order to characterise the monosaccharide sequence, both LPS and LOSs were hydrolysed using typical mild acidic conditions followed by centrifugation that gave a lipid A as sediment and a water soluble carbohydrate fraction (see Section V). The carbohydrate fractions were purified by gel-permeation chromatography and analysed by NMR spectroscopy. The overlapping of ^{1}H-NMR spectra is reported in Figure 6.2. The ^{1}H-NMR spectrum relative to strain IST439 showed two main signals in the anomeric region at δ = 5.09 and 4.99 ppm (Figure 6.2, Table 6.1) belonging to the O-chain polysaccharide moiety, while the ^{1}H-NMR spectra relative to the other three strains exhibited eight anomeric signals relative to the core oligosaccharide (Figure 6.2). Furthermore, the presence of the spin system of Kdo **K** was demonstrated by the detection of the diastereotopic H-3 methylene protons signals, which resonate in a shielded region at δ = 1.87 and 2.03 ppm (H-3_{ax} and H-3_{eq} respectively) for all the oligosaccharide fractions obtained from strains IST4113, IST4129 and IST4134. The assignment of the ^{1}H and ^{13}C resonances for the four carbohydrate fractions was performed by the analysis of the 2D NMR spectra. In particular, the proton resonances were assigned

from DQF-COSY, TOCSY, NOESY and ROESY spectra, while the ^{13}C resonances were attributed by $^{1}H,^{13}C$-HSQC and $^{1}H,^{13}C$-HMBC spectra.

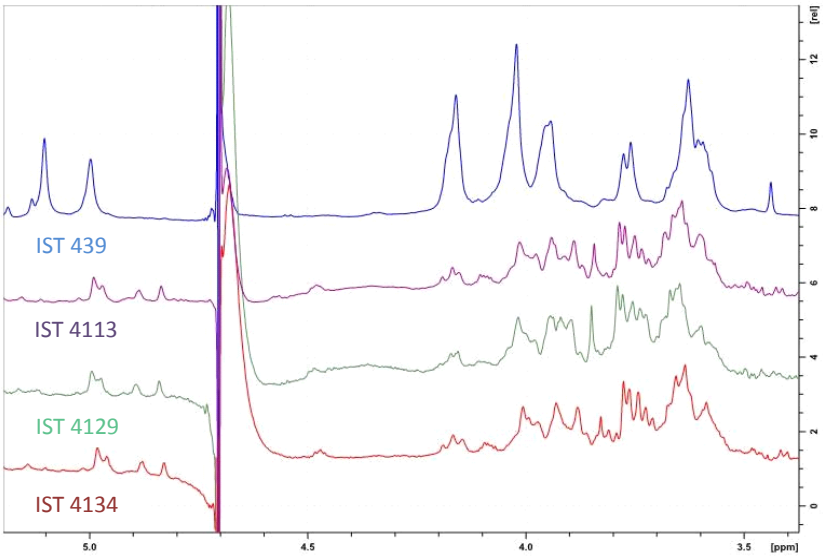

Figure 6.2 ^{1}H NMR spectra of products after mild acid hydrolysis.

Here we describe the structural assignment, by NMR analysis, of the O-polysaccharide (OPS) from strain IST439. The delineation of the structural characterisation by NMR spectroscopy of the core oligosaccharides from strains IST4113, IST4129 and IST4134 is not reported since the LOSs showed to be identical to each other and to the previously described core oligosaccharide from *B. cenocepacia* ET-12 strain J2315 (Silipo *et al*., 2007).

Chemical shift δ ($^{1}H/^{13}C$)						
Unit	**1**	**2**	**3**	**4**	**5**	**6**
A	5.09	4.15	4.03	3.95	3.77-3.59	---
2-β-Rib	106.6	78.7	67.2	82.3	62.5	----
B	4.99	4.02	3.93	3.61	3.63	4.03
4-α-GalNac	95.5	50.0	76.2	78.9	60.5	70.8

Table 6.1 Chemical shift δ ($^{1}H/^{13}C$) of the O-chain moiety from strain IST439.

The two spin systems identified in the ^{1}H-NMR spectrum of IST439 were designed as **A** (H-1 at δ = 5.09 ppm) and **B** (δ = 4.99 ppm). Spin system **A** was identified as a ribofuranose residue due to the correlations observed in the DQF-COSY and TOCSY spectra from the H-1 **A** signal up to a diastereotopic methylene signal at position C-5. The anomeric configuration was attributed by the low $^{3}J_{H\text{-}1,H\text{-}2}$ value obtained from the DQF-COSY spectrum, indicative of β-configuration in aldofuranose rings (less than 2 Hz), and by the chemical shift of C-4 (around 83.0 ppm in case of β-configuration) (Ahrazem *et al*., 2002). The downfield displacement of C-2 signal in the $^{1}H,^{13}C$-HSQC spectrum (Figure 6.3) indicated glycosilation at this position. Spin system **B** (H-1 at δ = 4.99 ppm) was identified as an α-galactose as attested by the low $^{3}J_{H3,H4}$ and $^{3}J_{H4,H5}$ values (3 Hz and 1 Hz, respectively) as well as the TOCSY scalar correlations between the anomeric signal and the other ring protons until the H-4 resonance; moreover, the *intra*-residual NOE correlation of H-1 **B** with H-2 **B**, the anomeric proton and carbon chemical shifts (δ = 4.99 ppm and 95.5 ppm) and the $^{3}J_{H1,H2}$ were

all in agreement with an α-anomeric configuration and a $^{4}C_{1}$ ring conformation.

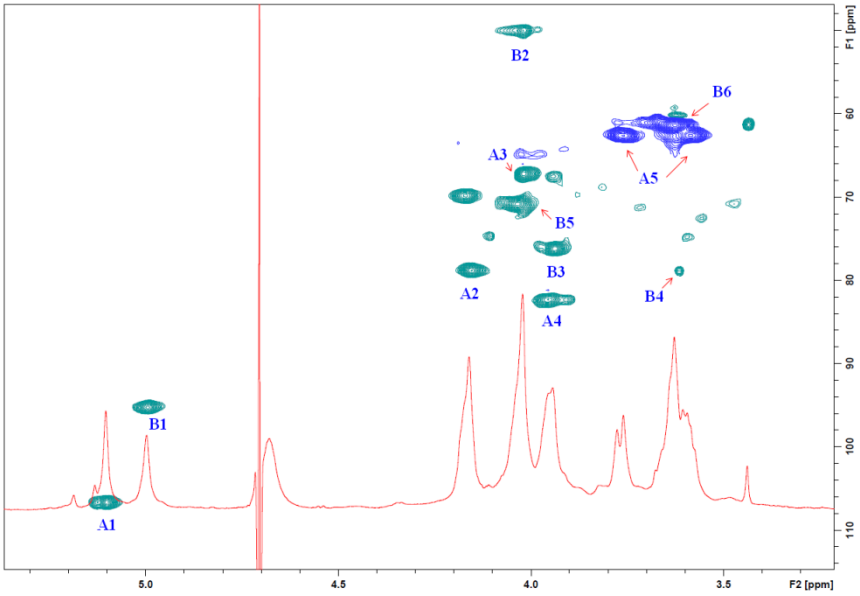

Figure 6.3 $^{1}H,^{13}C$-HSQC spectrum of the O-chain moiety from IST439 strain.

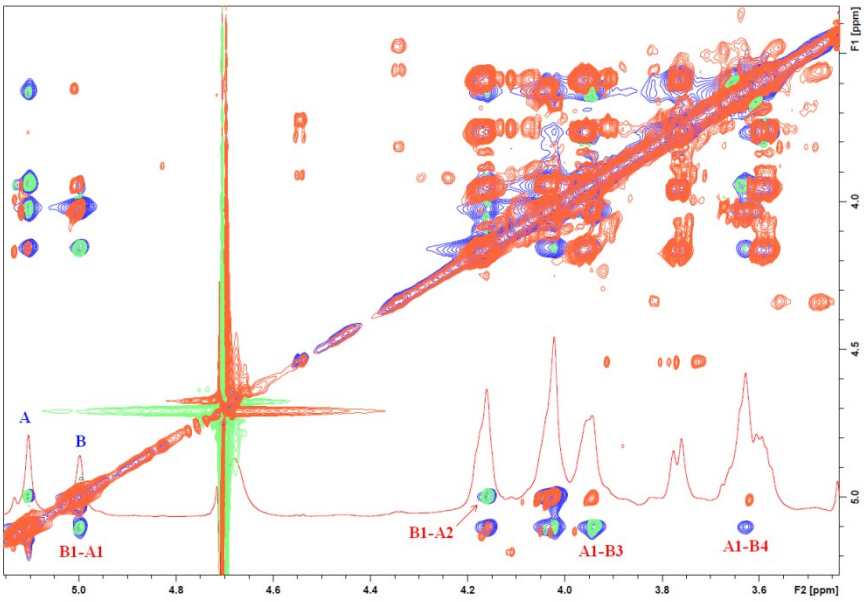

Figure 6.4 Section of the NOESY (**blue** and **green**) and TOCSY (**orange**) spectra of polysaccharide from IST439 strain. The most relevant *inter*-residue NOE cross-peaks are indicated.

The detection of a signal for C-2 at 50.0 ppm indicated that it was a nitrogen-bearing carbon atom; furthermore, the downfield shift of proton resonance of H-2 **B** was diagnostic of *N*-acetylation at this position, which was also corroborated by the NOE contact of H-2 **B** with the methyl protons of the acetyl group resonating at δ = 1.92 ppm. Thus residue **B** was identified as a α-GalNAc. The downfield shift of its C-4 (δ = 78.9 ppm) was indicative of glycosilation at this position. ROESY and NOESY spectra (Figure 6.4) gave possibility to elucidate the linkage between the two residues, and thus of the repeating unit of the O-polysaccharide from *B. cenocepacia* strain IST439. In details, the anomeric proton of GalNAc **B** gave a NOE correlation with H-2 and H-1 proton signals of ribose **A**, whose anomeric signal showed a NOE

correlation with the H-4 of residue **B**. These data were confirmed by the long scalar range connectivities obtained by the $^{1}H,^{13}C$-HMBC spectrum.

In summary, the OPS structure from *B. cenocepacia* strain IST439 was found to have the following repeating unit, previously identified in another *Burkholderia* strain (Cox and Wilkinson, 1989):

[→2)-β-D-Rib*f*-(1→4)-α-D-Gal*p*NAc-(1→]

6.3 MALDI-MS Analysis on intact LOSs/LPS from strains *B. cenocepacia* strains IST439, IST4113 IST4129, IST4134

MALDI mass spectrometry analysis on the intact LPS of strain IST439 completely confirmed the structural hypotheses (Figure 6.5). In details, in the mass range 1400-2400 Da of the negative-ion MALDI mass spectrum (Figure 6.5) ion peaks relative to lipid A species and to core oligosaccharide species were present, derived from the rupture of the labile glycosidic linkage between Kdo and lipid A. Ion peaks relative to lipid A species were as previously described (Silipo *et al*., 2007).
The ion peak **A** (*m/z* = 2033.3) was indicative of an oligosaccharide composed by five heptoses, three hexoses, one Kdo, one Ko and one Ara4N, while ion peaks **B** (*m/z* = 2166.2) carried an additional amino-arabinose residue (Figure 6.5). The species derived from the core oligosaccharide were in accordance with the structure already elucidated elsewhere (Silipo *et al*., 2007). The mass range 3000-4000 Da, (Figure 6.5) containing peaks relative to either oligosaccharide and lipid A, also confirmed previously analysis

(Silipo *et al.*, 2007). Furthermore, the mass range 7280-15400 Da showed ion peaks relative to the OPS confirming the abovementioned disaccharide repeating unit structure (not shown).

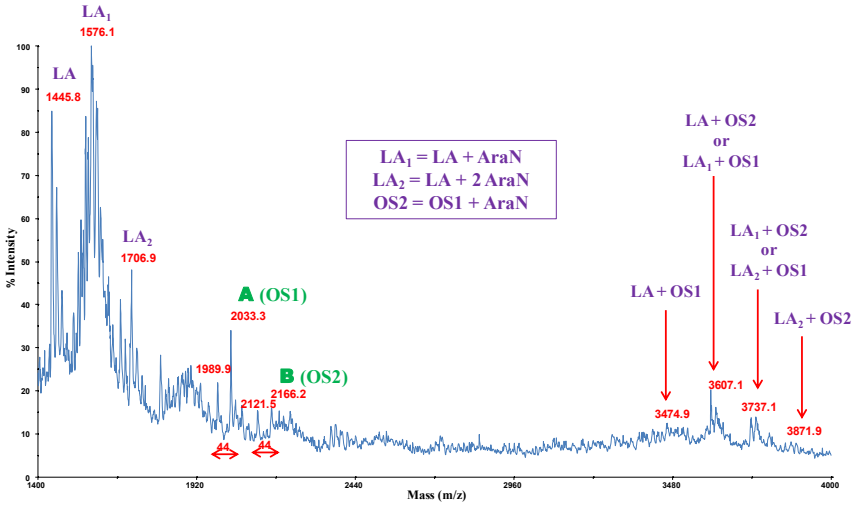

Figure 6.5 MALDI mass spectrum of of intact LPS from strain IST439.

Negative-ion MALDI mass spectra executed on the intact LOSs isolated from the three strains IST4113, IST4129 and IST4134 are identical each other and very similar to previously described mass spectra performed on intact LOS of *B. cenocepacia* ET-12 strain J2315 (Silipo *et al.*, 2007), confirming NMR analysis. For illustrative purpose, the MALDI mass spectrum on the intact LOS of strain IST4113 showed at mass range 1300-2500 Da a plethora of OS species (Figure 6.6), presenting from four to six heptoses and from three to five hexoses, one Kdo, one Kdo and showing or not one amino-arabinose residue. In particular, the ion peak termed **OS3** (*m/z* = 2032.5) was indicative of the core oligosaccharide elucidated by NMR analysis. The LOS molecular ions in the mass

range 3000-4200 Da (Figure 6.7), given by the combination of the peaks of lipid A species and the OS species, confirmed the NMR analysis. Interestingly, as mentioned above, species carrying additional heptoses and/or hexoses were present in the MALDI mass spectra but they were not detected by NMR spectroscopy.

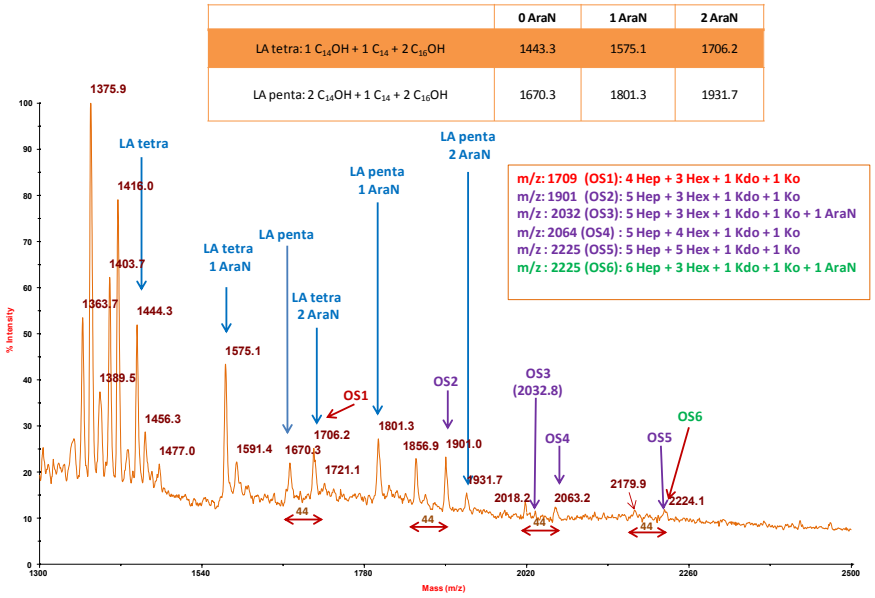

Figure 6.6 MALDI mass spectrum of the intact LOS from strain IST4113 (mass range 1300-2500).

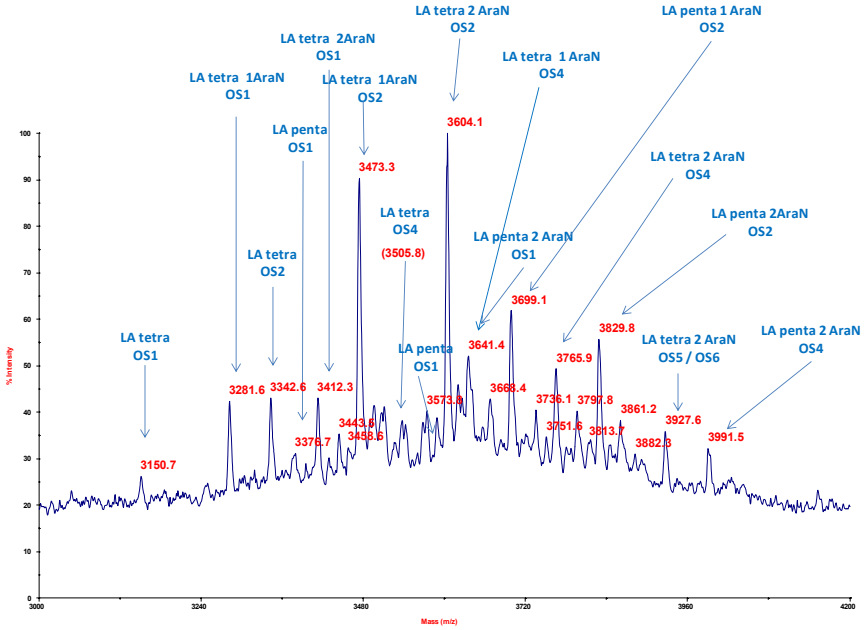

Figure 6.7 MALDI mass spectrum of the intact LOS from strain IST4113 (mass range 3000-4200).

By merging information deriving from chemical, NMR spectroscopy and MALDI mass spectrometry analyses, it was possible to define the complete structure of the LPS/LOSs isolated from the four clinical strains of *Burkholderia cenocepacia* which can be reassumed in the following monosaccharide sequences:

α-L,D-Hep-(1→7)- α-L,D-Hep-(1→7)-α-L,D-Hep-(1→3)-α-L,D-Hep-(1→5)-α-D-Kdo
3 4 4
↑ ↑ ↑
1 1 2
α-L,D-Hep-(1→2)-α-D-Gal β-D-Glc α-D-Ko
3
↑
α-D-Glc

6.4 Discussion

During chronic infection, *Burkholderia cenocepacia* is subjected to *in vivo* selection processes, resulting in less virulent variants showing different phenotypic features from the original colonising strain. In the present study, it has been demonstrated that *Burkholderia cenocepacia* chronic strains are characterised by the loss of the O-chain polysaccharide moiety on their LPS molecules compared to the initial colonizing strain that possesses a *smooth*-type LPS. Results wer obtained from a combination of chemical analyses, NMR spectroscopy and MALDI mass spectrometry experiments, performed on four clinical isolates retrieved during the patient care period at the HSM CF Treatment Center Hospital in Lisbon (Coutinho *et al*., 2011). These results, together with data belonging to the extensive phenotypic and genotypic approaches performed by Coutinho et al., provide essential contribution to the understanding of the adaptive and evolutionary mechanisms employed by *Burkholderia cenocepacia* to chronic colonise CF lungs, with the ultimate goal to improve therapeutic outcomes of chronic infections in cystic fibrosis patients. From the chemical viewpoint, the elucidated structures are in agreement with the LPS/LOS structures from the *Burkholderia* genus so far characterised. In details, the lipid A moiety showed the typical *Burkholderia* disaccharide backbone possessing a [P→4-β-D-Glc*p*N-(1→6)-α-D-Glc*p*N1→P] sequence that possesses two Ara4N residues linked to the phosphate groups. The inner core is composed by the characteristic Ara4N-Ko-Kdo trisaccharide, previously elucidated in other *Burkholderia* species (Isshiki *et al*., 1998; Gronow *et al*., 2003), carrying a high heptosylated sequence from which starts the outer core region. This latter normally shows the presence of a non-stoichiometric Rha-QuiNAc disaccharide, linked to the α-Hep-(1→2)-α-Gal disaccharide of the outer core,

not found in the present analysis, that plays as a cap for the linkage of the O-chain polysaccharide to the core region. The abovementioned structure is identical for the three examined *Burkholderia* chronic strains IST4113, IST4129 and IST4134 showing a *rough*-type LPS. The original colonising strain IST439, presenting a *smooth*-type LPS, showed the presence of a disaccharide repeating unit, linked to the outer core, composed by the [→2)-β-D-Rib*f*-(1→4)-α-D-Gal*p*NAc-(1→] sequence, already described elsewhere (Cox and Wilkinson, 1989).

The investigation of mechanisms and dynamics of microbial evolution within a host environment, and how it relates to pathogenicity and virulence, is currently a topic of paramount importance in health sciences.

References

Ahrazem O., Prieto A., Leal J.A., Jiménez-Barbero J., Bernabé M., Fungal cell wall polysaccharides isolated from Discula destructiva spp. **2002**, *Carbohydr. Res*., 337, 1503-1506.

Coutinho C.P., de Carvalho C.C., Madeira A., Pinto-de-Oliveira A., Sá-Correia I., *Burkholderia cenocepacia* phenotypic clonal variation during a 3.5-year colonization in the lungs of a cystic fibrosis patient. **2011**, *Infection and Immunity*, 2950-2960.

Coutinho C.P., Dos Santos S.C., Madeira A., Mira N.P., Moreira A.S., Sá-Correia I., Long-term colonization of the cystic fibrosis lung by *Burkholderia cepacia* complex bacteria: epidemiology, clonal variation, and genome-wide expression alterations. **2011**, *Front. Cell Infect. Microbiol*.,1, 12.

Cox A.D., Wilkinson S.G., Structures of the O-specific polymers from the lipopolysaccharides of the reference strains for *Pseudomonas cepacia* serogroups O3 and O5. **1989**, *Carbohydr. Res*., 195, 123-129.

De Soyza A., Corris P.A., Lung transplantation and the *Burkholderia cepacia* complex. **2003**, *J Heart Lung Transplant.*, 22:954-958.

Gronow S., Noah C., Blumenthal A., Lindner B., Brade H., Construction of a deep-rough mutant of *Burkholderia cepacia* ATCC 25416 and characterization of its chemical and biological properties.**2003**, *J. Biol. Chem*., 278(3), 1647-55.

Hadjiliadis D., Steele M.P., Chaparro C., Singer L.G., Waddell T.K., Hutcheon M.A., Davis R.D., Tullis D.E., Palmer S.M., Keshavjee S., Survival of lung transplant patients with cystic fibrosis harboring panresistant bacteria other than *Burkholderia cepacia*, compared with patients harboring sensitive bacteria. **2007**, *J. Heart Lung Transplant*., 26, 834-8.

Harrison F., Microbial ecology of the cystic fibrosis lung. **2007**, *Microbiology*, 4, 917-23.

Hogardt M., Heesemann J., Microevolution of *Pseudomonas aeruginosa* to a chronic pathogen of the cystic fibrosis lung. **2013**, *Curr. Top Microbiol. Immunol*., 358, 91-118.

Isshiki Y., Kawahara K., Zähringer U., Isolation and characterisation of disodium (4-amino-4-deoxy-β-L-arabinopyranosyl)-(1→8)-(D-glycero-α-D-talo-oct-2 ulopyranosylonate)-(2→4)-(methyl 3-deoxy-D-manno-oct-2-ulopyranosid)onate from the lipopolysaccharide of *Burkholderia cepacia*. **1998**, *Carbohydr. Res*., 313(1), 21-7.

Kittelberger R., Hilbink F., Sensitive silver-staining detection of bacterial lipopolysaccharides in polyacrylamide gels. **1993**, *J. Biochem. Biophys. Methods*, 26 (1), 81-86.

Leitão J.H., Sousa S.A., Cunha M.V., Salgado M.J., Melo-Cristino J., Barreto M.C., Sá-Correia I., Variation of the antimicrobial susceptibility profiles of *Burkholderia cepacia* complex clonal isolates obtained from chronically infected cystic fibrosis patients: a five-year survey in the major Portuguese treatment center. **2008**, *Eur. J. Clin. Microbiol. Infect. Dis*., 27(11),1101-11.

Mahenthiralingam E., Baldwin A., Vandamme P., Burkholderia cepacia complex infection in patients with cystic fibrosis. **2002**, *J. Med. Microbiol*., 51(7), 533-8.

Mahenthiralingam E., Urban T.A., Goldberg J.B., The multifarious, multireplicon *Burkholderia cepacia* complex. **2005**, *Nat. Rev. Microbiol.,* 3, 144-56.

Silipo A., Molinaro A., Ieranò T., De Soyza A., Sturiale L., Garozzo D., Aldridge C., Corris P.A., Anjam Khan C.M., Lanzetta R., Parrilli M., The complete structure and pro-inflammatory activity of the lipooligosaccharide of the highly epidemic and virulent gram-negative bacterium *Burkholderia cenocepacia* ET-12 (strain J2315). **2007**, *Chem. Eur. J*., 13, 3501-3511.

Westphal O., Jann K., Bacterial lipopolysaccharides: extraction with phenol-water and further applications of the procedure. **1965**, *Methods Carbohydr. Chem*., 5, 83–91.

Chapter 7

Assessment of the biological role of amino-arabinose residues on *Burkholderia cenocepacia* LPS structure

Premise

One common mechanism of resistance against antimicrobial peptides in Gram-negative bacteria is the addition of 4-amino-4-deoxy-L-arabinose (L-Ara4N) to the lipopolysaccharide (LPS) molecule. *Burkholderia cenocepacia* exhibits extraordinary intrinsic resistance to antimicrobial peptides and other antibiotics. It was previously discovered that, unlike other bacteria, *B. cenocepacia* requires L-Ara4N for viability. Conditionally lethal *B. cenocepacia* mutants impaired in L-Ara4N synthesis and transport revealed accumulations of membranous material in the bacterial cells, which were reminiscent of the phenotype found in bacteria with defects in LPS export to the outer membrane (Ortega *et al*., 2009). Therefore, it is possible to hypothesize that L-Ara4N modification of the LPS in *B. cenocepacia* is critical for the proper export of the LPS molecule to the outer membrane and that the lethality of L-Ara4N depleted cells is due to the inability to properly assemble the outer membrane. Genetic manipulations of bacteria by gene deletion are a valuable method to unravel gene function. However, this approach becomes limited when the gene of interest is essential for bacterial viability. The essentiality of L-Ara4N production and L-Ara4N transfer to lipid A-core OS preclude from directly assessing the role of the L-Ara4N modification in mediating the resistance of *B. cenocepacia* to polymyxin B (Ortega *et al*., 2009). In the present work, with a combination of structural analyses and *ad hoc* molecular biology experiments it is assessed the biological role of amino-arabinoses on *Burkholderia cenocepacia* LPS structural architecture by using *B. cenocepacia* suppressor mutants that remain viable despite the deletion of genes required for L-Ara4N synthesis and transfer to the LPS.

7.1 Isolation of suppressor *B. cenocepacia* strains

To isolate suppressor mutants in a strain with an inactivated L-Ara4N biosynthesis gene cluster (*arn*), it was first constructed the conditional strain *Prha-arn* by placing the *arn* gene cluster under the control of the rhamnose inducible promoter (*Prha*). This straincan only form colonies when *arn* gene expression is turned on by the addition of rhamnose. These colonies were then examined for polymyxin B sensitivity. Three polymyxin B-sensitive colonies were isolated, which resulted in polymyxin B-sensitive *B. cenocepacia* mutants lacking *arnBC* (Δ*arnBC*). The deletion of the *arnBC* genes in the three mutants was confirmed by polymerase chain reaction (PCR) amplification. To distinguish between L-Ara4N synthesis and L-Ara4N transfer onto the lipid A-core OS, it was constructed a mutant that can synthesize L-Ara4N but lacks the L-Ara4N transferase ArnT, resulting in the strain Δ*arnT-arnBC*$^{+}$.
Both Δ*arnBC* and Δ*arnT-arnBC*+ strains harbouring suppressor mutation(s) were viable irrespective of rhamnose in the medium indicating that the suppressor mutation(s) can rescue growth of *B. cenocepacia* in the absence of L-Ara4N synthesis or L-Ara4N transfer to the lipid A-core OS. In contrast to the parental or conditional *Prha-arn* strains grown with rhamnose, the suppressor strains Δ*arnBC* and Δ*arnT-arnBC*+ failed to grow in the presence of polymyxin B regardless of rhamnose addition, demonstrating that production and transfer of L-Ara4N to the lipid A-core OS are critical for polymyxin B resistance in *B. cenocepacia*.

Introduction of a replicative plasmid expressing *arnT* into D*arnT-arnBC*$^{+}$ restored polymyxin B resistance, confirming that the polymyxin B sensitive phenotype was due to the loss of *arnT*.
Similarly, genomic complementation of the L-Ara4N synthesis defect in Δ*arnBC* by reintroducing the parental genes restored

polymyxin B resistance in the presence of rhamnose. The complemented Δ*arnBC-araBC* $^{+}$ strain retained viability with or without rhamnose in the growth medium, indicating that the suppressor mutation(s) was stable. These results demonstrate that suppressor mutation(s) allow for viability of *B. cenocepacia* in the absence of L-Ara4N synthesis and transfer to lipid A-core OS, and that transfer of L-Ara4N to lipid A-core OS is required for polymyxin B resistance in *B. cenocepacia*.

It was also determined the minimal inhibitory concentration (MIC) of the *arn* mutants to more precisely assess their level of sensitivity to polymyxin B. MIC values for parental *B. cenocepacia* to polymyxin B are unknown since the bacterium can grow at concentration of up to 4000 mg/mL of polymyxin B (Loutet *et al*., 2011). In contrast, Δ*arnBC* (lacking the ability to synthesize L-Ara4N) and Δ*arnT-arnBC*$^{+}$ (lacking the L-Ara4N transferase) had MIC values of 0.25 mg/mL each. Therefore, L-Ara4N production and L-Ara4N transfer to LPS are critical for bacterial viability and for the extreme resistance to APs.

7.2 Isolation and SDS-PAGE analysis of LPS from suppressor *B. cenocepacia* strains

Extraction of the LPS for structural elucidation was achieved by the hot phenol/water protocol (Westphal and Jann, 1965) and checked by SDS-PAGE (Kittelberger and Hilbink, 1993) (see Section V). Samples isolated from suppressor mutants showed the ladder-like pattern typical of S-LPS due to the occurrence of the O-chain. No difference in the migration pattern or modality of O-antigen repeats was observed for any of the strains examined when compared with the parental isolate (Figure 7.1). However, LPS extracted from Δ*arnBC* and Δ*arnT-arnBC*$^{+}$ displayed more

intensely stained bands relative to those of the parental strain. The staining pattern was consistent and reproducible, and could not be attributed to chemical differences with the LPS other than the absence of L-Ara4N (see below). This suggested that loss of L-Ara4N in the lipid A-core OS may cause an effect on silver staining, as indicated by the observed loss of the intense staining and reversion to the parental staining pattern in the complemented strain Δ*arnBC-arnBC*$^{+}$ (Figure 7.1).

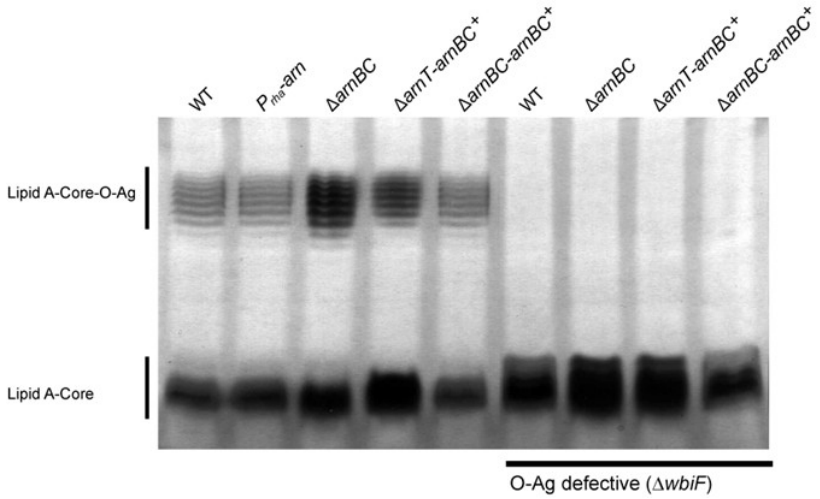

Figure 7.1. LPS profile of *B. cenocepacia* strains on Tricine-SDS-polyacrylamide gel.

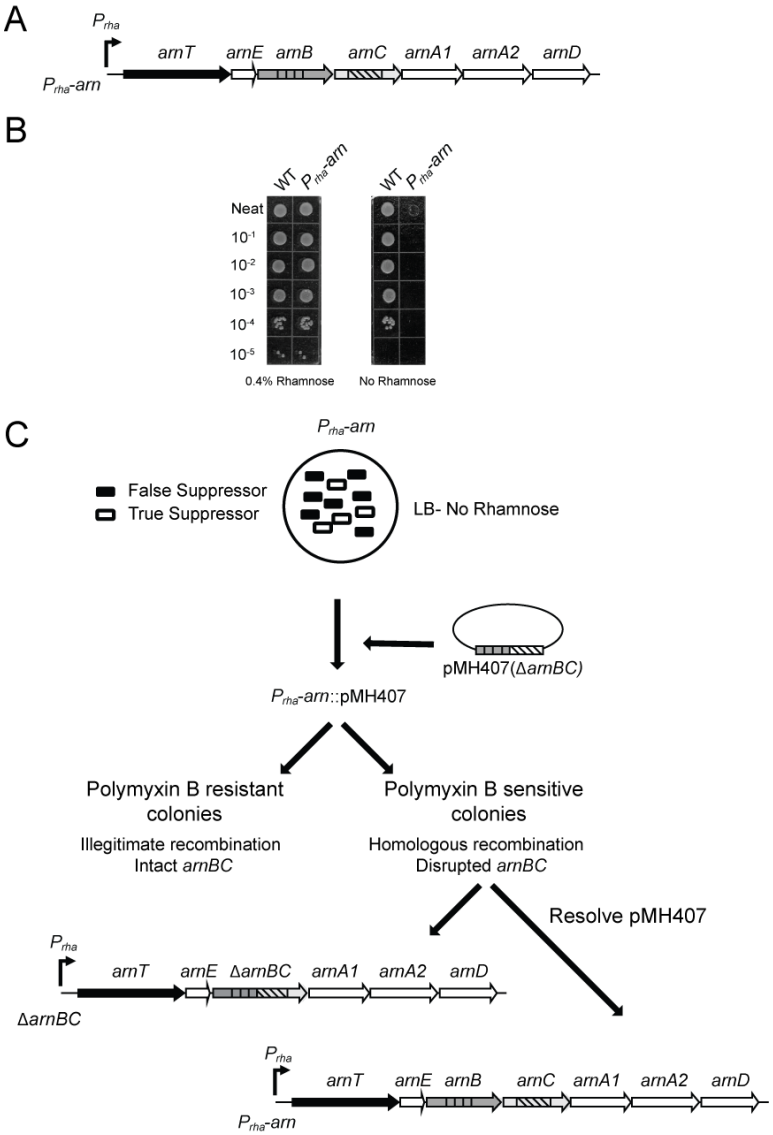

Figure 7.2 Genetic strategy used to isolate a suppressor *B. cenocepacia* strain that remains viable in absence of L-Ara4N synthesis. **A)** Genetic organisation of the *arn* operon in *B. cenocepacia* and construction of conditional P_{rha}-*arn* strain. **B)** Wild type and conditional P_{rha}-*arn B. cenocepacia* strains grown on LB agar with or without 0.4% rhamnose. **C)** Suppressor enrichment by growing conditional P_{rha}-*arn* under non-inducing conditions.

7.3 Structural analyses of LPS isolated from suppressor *B. cenocepacia* strains

A detailed analysis was performed to determine the composition and structure of the LPS produced by the mutants, but since the presence of O-polysaccharide in parental and mutant strains complicates the structural analysis of the lipid A-core OS moiety, it was first introduced a *wbiF* (*BCAL3122*) gene deletion in the parental strain and the Δ*arnBC*, Δ*arnT-arnBC*$^{+}$ and Δ*arnBC-arnBC*$^{+}$ mutants. Deletion of *wbiF* results in the loss of a rhamnosyltransferase that is required for O-chain synthesis and, therefore, the mutant lacks surface O-chain. Carbohydrate and fatty acid analyses performed by gas-liquid chromatography/mass spectrometry (GLC-MS) on purified LPS samples from O-chain defective Δ*arnBC* and Δ*arnT-arnBC*$^{+}$ mutants confirmed the absence of L-Ara4N both in the lipid A and inner core OS, and detected no other modifications. Mass spectrometry analyses of lipid A and core OS using matrix-assisted laser desorption/ionisation time of flight mass spectrometry (MALDI-TOF) were performed to further confirm their structures (Figure 7.3). The negative-ion MALDI-TOF mass spectrum showed ion peaks related to lipid A and core OS fragments, as well as molecular ions of intact LOS molecules. The fragmentation is characteristic for the cleavage of labile bond between Kdo and lipid A (Sturiale *et al*., 2005). The MALDI-TOF mass spectrum obtained from the LPS sample of the O-chain defective Δ*arnBC-arnBC*$^{+}$ strain showed ion peaks corresponding to core oligosaccharide (at *m/z* 1547; Figure 7.3) containing four heptoses, two hexoses, one Kdo, and one Ko residue and a mixture of tetra- and penta-acylated lipid A species (Figure 7.3). The ion peak **A** at *m/z* 1444.7 corresponded to tetra-acylated di-glucosamine backbone carrying one 14:0 (3-OH), one 14:0 and two 16:0 (3-OH) fatty acids. Peak **B**

at *m/z* 1575.5 and peak **C** at *m/z* 1706.3 corresponded to the tetra-acylated species in peak **I** with one and two additional L-Ara4N residues respectively (Figure 7.3). Peak **D** at *m/z* 1801.5 corresponded to penta-acylated lipid A species carrying additional 14:0 (3-OH) residues and one L-Ara4N. Peaks corresponding to lipid A-core OS quasi-molecular ions were present in the mass range between *m/z* 2500 and 4000 (Figure 7.3). The MALDI-TOF mass spectrometry data obtained from LPS samples of O-chain defective strains Δ*arnT-arnBC*$^{+}$ (Figure 7.3B) and Δ*arnBC* (Figure 7.3C) showed essentially the same pattern of molecular ions as described above for tetra- and penta-acylated lipid A species, but without detecting the presence of any species carrying L-Ara4N (Figures 7.3B,C). Moreover, the absence of L-Ara4N in lipid A-core OS species at higher masses demonstrated that not only the lipid A but also the core OS lacked L-Ara4N (Figures 7.3B,C). These results were further confirmed by NMR analysis (Figure 7.4). Therefore, it is possible to conclude that the only change observed in LPS molecules prepared from the O-polysaccharide defective mutants Δ*arnT-arnBC*$^{+}$ and Δ*arnBC* is the absence of L-Ara4N in the lipid A-core OS, while the lipid A-core OS structure in the O-chain defective mutant Δ*arnBC-arnBC*$^{+}$ is identical to that of parental LPS. These results also suggested that ArnT is required for the modification of both lipid A and core OS with L-Ara4N.

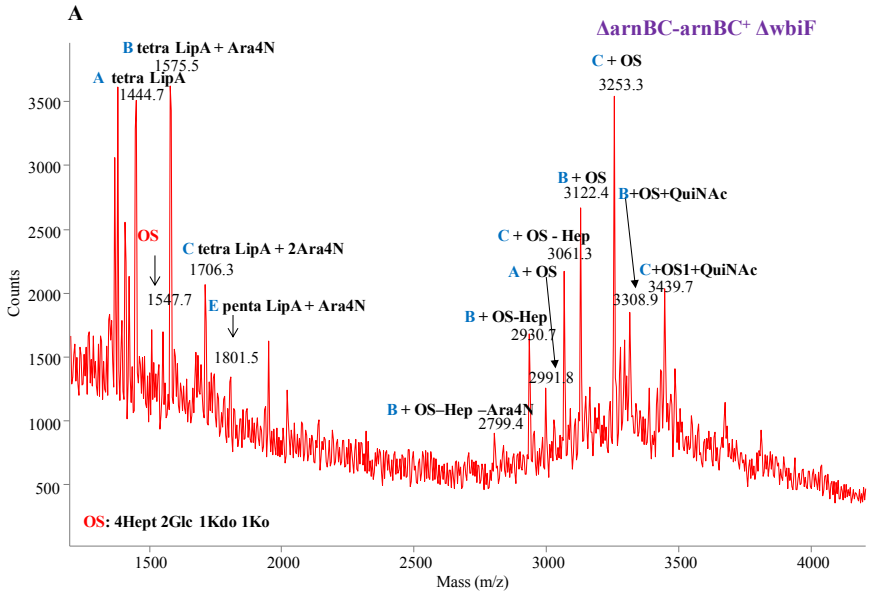
A
ΔarnBC-arnBC⁺ ΔwbiF
B tetra LipA + Ara4N
1575.5
A tetra LipA
1444.7
C + OS
3253.3
B + OS
3122.4
B+OS+QuiNAc
OS
1547.7
C tetra LipA + 2Ara4N
1706.3
C + OS - Hep
3061.3
A + OS
C+OS1+QuiNAc
3439.7
3308.9
E penta LipA + Ara4N
1801.5
B + OS-Hep
2930.7
2991.8
B + OS–Hep –Ara4N
2799.4
OS: 4Hept 2Glc 1Kdo 1Ko
Counts
Mass (m/z)

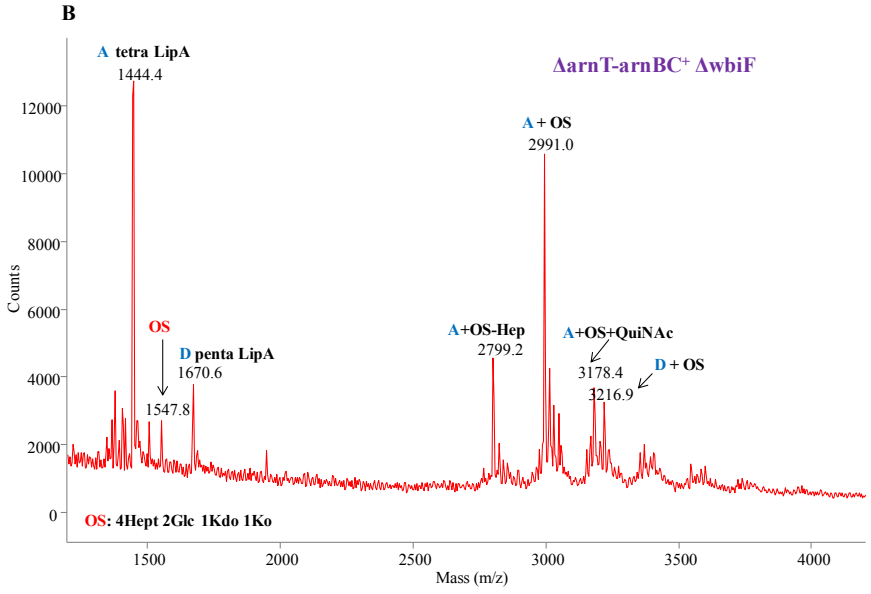
B
A tetra LipA
1444.4
ΔarnT-arnBC⁺ ΔwbiF
A + OS
2991.0
OS
D penta LipA
1670.6
1547.8
A+OS-Hep
2799.2
A+OS+QuiNAc
3178.4
D + OS
3216.9
OS: 4Hept 2Glc 1Kdo 1Ko
Counts
Mass (m/z)

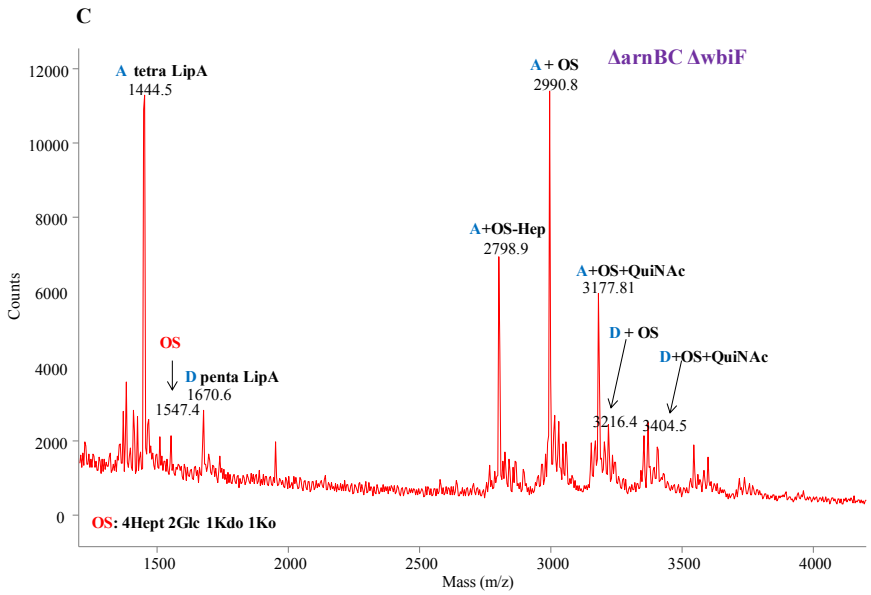

Figure 7.3 MALDI-MS spectra from purified core OS produced by O-chain defective mutants. Purified core OS fractions from the Δ*arnT-arnBC*$^{+}$ Δ*wbiF* (**A**), Δ*arnBC-arnBC*$^{+}$ Δ*wbiF* (**B**), and Δ*arnBC* Δ*wbiF* (**C**) strains were investigated using MALDI-TOF mass spectrometry.

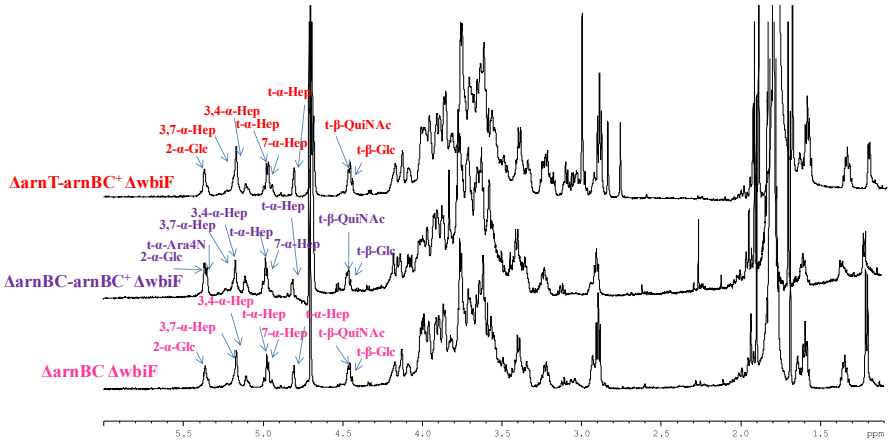

Figure 7.4 ^{1}H-NMR spectra of core OSs from O-chain defective derivatives of Δ*arnT-arnBC*$^{+}$, Δ*arnBC-arnBC*$^{+}$, and Δ*arnBC strains*.

7.4 Assessment of the role of amino-arabinoses on *B. cenocepacia* LPS structure

It was previously hypothesized that addition of L-Ara4N to the LPS of *B. cenocepacia* is essential for export of LPS to the outer membrane by the Lpt pathway (Ortega *et al*., 2007). Therefore, it was investigated whether Δ*arnBC* has one or more mutations in *lpt* genes that suppress a putative LPS export defect, allowing growth in the absence of L-Ara4N synthesis and/or transfer to the LPS.

B. cenocepacia lpt genes, identified by bioinformatic analyses, were PCR-amplified from the Δ*arnBC* suppressor mutant and cloned into a multicopy plasmid. Recombinant plasmids expressing these genes were introduced into the conditional strain *Prha-arn* and the resulting colonies were examined for viability in the absence of rhamnose. Only a plasmid expressing *lptFG* could rescue the growth of the conditional strain *Prha-arn* in the absence of rhamnose. This indicates that the suppressor effect is due to a specific mutation in *lptFG*. DNA sequencing of the suppressor *lptFG* plasmid revealed a G→C point mutation in codon 31 of *lptG*, which resulted in the substitution of an aspartic acid (D) by a histidine (H). The same mutation was also found in the *lptG* gene of the two other Δ*arnBC* suppressor mutants recovered, suggesting that the $LptG_{D31H}$ protein supports viability in strains lacking functional *arnBC* genes.

To confirm that $lptG_{D31H}$ is sufficient to rescue growth of *B. cenocepacia* in the absence of L-Ara4N synthesis, *lptG* was PCR-amplified from parental *B. cenocepacia* DNA, cloned into a plasmid, and the D31H replacement was introduced by site directed mutagenesis. This recombinant plasmid was then used to replace the native *lptG* with $lptG_{D31H}$ in the conditional strain *Prha-arn*.

The resulting strain *Prha-arn-lptG*$_{D31H}$ was viable in the absence of rhamnose and L-Ara4N synthesis, confirming that LptG$_{D31H}$ is sufficient to fully suppress loss of viability in *B. cenocepacia*. Together, these results demonstrate that the D31H substitution in LptG can bypass the requirement of L-Ara4N synthesis for the viability of *B. cenocepacia*.

7.5 Trasmission electron microscopy analysis on *B. cenocepacia* suppressor mutant cells

In a previous study it was reported that conditional mutants in the synthesis of L-Ara4N or its transfer to LPS have dramatic morphological defects that were attributed to the absence of L-Ara4N in the LPS molecule (Ortega *et al*., 2007). Transmission electron microscopy was performed on bacteria depleted for L-Ara4N to determine whether the suppressor strains Δ*arnBC* and *Prha-arn-lptG*$_{D31H}$ depleted for L-Ara4N displayed normal cell morphology. The results demonstrated that cells from both suppressor strains have a membrane structure similar to that of the parental strain K56-2. In contrast, the conditional strain *Prha-arn* grown in the absence of rhamnose showed cells with cell division defects, abnormal membranous subcellular structures and cells representing empty sacculi. The abnormal ultrastructure of these cells is consistent with a defect in LPS export, which is overcome in the presence of the *lptG*$_{D31H}$ suppressor mutation.

7.6 Discussion

In this work, by using a strategy to delete the L-Ara4N biosynthesis genes resulting in stable viable suppressor mutants lacking amino-arabinoses in their LPS, it was showed a more than 16000-fold reduction in resistance to polymyxin B. Based on these results demonstrating for the first time that loss of L-Ara4N from

the LPS molecule abolishes the extreme resistance of *B. cenocepacia* to APs, it was proposed that the L-Ara4N modification of the *B. cenocepacia* LPS is the key determinant of the extreme intrinsic resistance of these bacteria to antimicrobial peptides.

In *B. cenocepacia* and *Burkholderia* species, L-Ara4N may be found attached to the phosphate groups of lipid A and the branched Ko sugar of the core OS (Isshiki *et al*., 1998; Molinaro *et al*., 2003). Whereas the presence of L-Ara4N in the lipid A is common to many bacteria, only those with L-Ara4N in the core OS residue, such as *Burkholderia*, *Proteus*, and *Serratia* species demonstrate very high levels of resistance to polymyxin B (Boll *et al*., 1994; Silipo and Molinaro, 2010). The addition of L-Ara4N to the core OS might therefore provide a higher level of protection to bacteria against APs. Moreover, all *Burkholderia* LPS structurally identified to date lack negatively charged sugar residues in any region of the LPS besides the Kdo–Ko disaccharide and do not possess any other negatively charged molecules besides the two phosphate groups of the lipid A. This suggests that the modification of *Burkholderia* LPS with L-Ara4N heavily influences its overall charge transforming it in a net positive or neutral molecule, which prevents interactions with APs and accounts for the extreme resistance by *Burkholderia* to these molecules (De Soyza *et al*., 2008).

The detailed chemical and structural analyses of the lipid A-core OS of the LPS produced by the mutant strains demonstrates a role for ArnT, the L-Ara4N transferase, in the transfer of L-Ara4N to lipid A and core OS acceptor sites. Prior to this work, there was no evidence in the literature that ArnT from other species can catalyse the addition of L-Ara4N to a sugar residue in the core OS. ArnT in other Gram-negative bacteria, such as *Salmonella* and *Escherichia coli* only transfers L-Ara4N to the phosphate groups of the lipid A (Trent *et al*., 2001).

In a previous study, it was speculated that the L-Ara4N LPS modification was required for the export of nascent LPS molecules from the periplasmic side of the inner membrane to the outer membrane (Ortega *et al*., 2007). LPS export is achieved by the Lpt pathway, which consists of inner membrane, periplasmic, and outer membrane proteins working in concert to transport the LPS molecule from the periplasmic face of the inner membrane to the outer leaflet of the outer membrane (Ruiz *et al*., 2009; Sperandeo *et al*., 2009). The identification of a point mutation in the LPS transporter gene *lptG* in the current work provides genetic evidence to support this hypothesis. LptG is a highly conserved inner membrane protein in Gram-negative bacteria and is required for the export of LPS to the outer membrane a process that is essential for the viability of most Gram-negative bacteria (Ruiz *et al*., 2009).
In this study it was discovered here that a single point mutation in LptG changing aspartic acid to histidine at position 31 results in a protein that bypasses the need of L-Ara4N synthesis for *B. cenocepacia* viability and allows for the proper assembly of outer membrane. Strains containing parental LptG (with histidine at position 31) are nonviable in absence of L-Ara4N synthesis and show membranous invaginations and other morphological abnormalities indicative of the inability of to properly assemble the outer membrane (Ortega *et al*., 2007). This suggested that the parental LptG is unable to export LPS lacking L-Ara4N modification, resulting in a lethal phenotype likely due to the failure to organize the outer membrane in the absence of LPS export, while $LptG_{D31H}$ can export unmodified LPS which allows for proper assembly outer membrane and bacterial viability. Previous observations of membranous invaginations and other morphological abnormalities observed in *B. cenocepacia* strains depleted in L-Ara4N synthesis support this conclusio(Ortega *et al*., 2007).

Nevertheless, the molecular mechanism involving LptG in the export of L-Ara4N-modified LPS remains to be elucidated. One could speculate that the D31H substitution in LptG allows export of unmodified LPS. However, $LptG_{D31H}$ can also export L-Ara4N-modified LPS, as indicated by the polymyxin B-resistant phenotypes of the Δ*arnBC-arnBC*$^{+}$ and *Prha-arn* $lptG_{D31H}$ strains, and is confirmed by the chemical analysis of LPS extracted from the O-polysaccharide deficient derivative of Δ*arnBC-arnBC*$^{+}$ strain, which contains the spontaneous $lptG_{D31H}$ allele. Interestingly, D31 is a highly conserved residue in LptG proteins of *Burkholderia* and related species, such as *Ralstonia* and *Cupriavidus* but not in *Enterobacteriaceae*, *Vibrio cholera*, or *Pseudomonas aeruginosa*. Interestingly, the bacterial species that show no conservation at D31 in LptG do not require L-Ara4N for viability suggesting that the native LptG of these bacteria does not display any specificity toward L-Ara4N-LPS or unmodified LPS for proper export (Kabir, 1982; Moskowitz *et al*., 2004). The conservation of D31 in LptG, together with the observation that L-Ara4N is present in the lipid A and core OS LPS of different *Burkholderia* species, and the experimental data in this study lead us to hypothesize that L-Ara4N not only plays a critical role as a determinant of resistance to APs but also provides a molecular signature required for LPS export thus playing an essential role in determining the architecture of the outer membrane in *B. cenocepacia* and related species. Additionally, by linking the AP-resistance mediated through L-Ara4N to LPS export and viability, *B. cenocepacia* employs an elegant mechanism to select for a progeny that retains high levels of intrinsic resistance to APs.

References

Boll M., Radziejewska-Lebrecht J., Warth C., Krajewska-Pietrasik D., Mayer H., 4-amino-4-deoxy-L-arabinose in LPS of enterobacterial R-mutants and its possible role for their polymyxin reactivity. **1994**, *FEMS Immunol. Med. Microbiol.*, 8, 329-341.

De Soyza A., Silipo A., Lanzetta R., Govan J.R., Molinaro A., Chemical and biological features of *Burkholderia cepacia* complex lipopolysaccharides.**2008**, *Innate Immun.*, 14, 127-144.

Isshiki Y., Kawahara K., Zähringer U., Isolation and characterisation of disodium (4-amino-4-deoxy-β-L-arabinopyranosyl)-(1→8)-(D-*glycero*-alpha-D-*talo*-oct-2-ulopyranosylona te)- (2→4)-(methyl 3-deoxy-D-*manno*-oct- 2-ulopyranosid)onate from the lipopolysaccharide of *Burkholderia cepacia*. **1998**, *Carbohydr. Res*., 313(1), 21-7.

Kabir S., Characterization of the lipopolysaccharide from *Vibrio cholerae* 395 (Ogawa). **1982**, *Infect. Immun.,* 38, 1263-1272.

Kittelberger R., Hilbink F., Sensitive silver-staining detection of bacterial lipopolysaccharides in polyacrylamide gels. **1993**, *J. Biochem. Biophys. Methods*, 26 (1), 81-86.

Loutet S.A., Di Lorenzo F., Clarke C., Molinaro A., Valvano M.A., Transcriptional responses of *Burkholderia cenocepacia* to polymyxin B in isogenic strains with diverse polymyxin B resistance phenotypes. **2011**, *BMC Genomics*, 12, 472.

Molinaro A., Lindner B., De Castro C., Nolting B., Silipo A., Lanzetta R., Parrilli M., Holst O., The structure of lipid A of the lipopolysaccharide from *Burkholderia caryophylli* with a 4-amino-4-deoxy-L-arabinopyranose 1-phosphate residue exclusively in glycosidic linkage. **2003**, *Chemistry*, 9, 1542-1548.

Moskowitz S.M., Ernst R.K., Miller S.I., PmrAB, a two-component regulatory system of *Pseudomonas aeruginosa* that modulates resistance to cationic antimicrobial peptides and addition of aminoarabinose to lipid A.**2004**, *J. Bacteriol.*, 186, 575-579.

Ortega X.P., Cardona S.T., Brown A.R., Loutet S.A., Flannagan R.S., Campopiano D.J., Govan J.R., Valvano M.A., A putative gene cluster for aminoarabinose biosynthesis is essential for *Burkholderia cenocepacia* viability. **2007**, *J. Bacteriol.*, 189**,** 3639-3644.

Ortega X., Silipo A., Saldias M.S., Bates C.C., Molinaro A., Valvano M.A., Biosynthesis and structure of the *Burkholderia cenocepacia* K56-2 lipopolysaccharide core oligosaccharide: truncation of the core oligosaccharide leads to increased binding and sensitivity to polymyxin B. **2009**, *J. Biol. Chem.,* 284, 21738-21751.

Ruiz N., Kahne D., Silhavy T.J., Transport of lipopolysaccharide across the cell envelope: the long road of discovery. **2009**, *Nat. Rev. Microbiol.*, 7, 677-683.

Silipo A., Molinaro A., The diversity of the core oligosaccharide in lipopolysaccharides. **2010**, *Subcell* Biochem., 53, 69-99.

Sperandeo P., Deho G., Polissi A., The lipopolysaccharide transport system of Gram negative bacteria. **2009**, *Biochim Biophys Acta*, 1791, 594-602.

Sturiale L., Garozzo D., Silipo A., Lanzetta R., Parrilli M., Molinaro A., New conditions for matrix-assisted laser desorption/ionization mass spectrometry of native bacterial R-type lipopolysaccharides. *Rapid Commun. Mass Spectrom.,* **2005**, 19, 1829-1834.

Trent M.S., Ribeiro A.A., Lin S., Cotter R.J., Raetz, C.R., An inner membrane enzyme in *Salmonella* and *Escherichia coli* that transfers 4-amino-4-deoxy-L-arabinose to lipid A: induction on polymyxin-resistant mutants and role of a novel lipid-linked donor. **2001**, *J. Biol. Chem.*, 276, 43122-43131.

Westphal O, Jann K. Bacterial lipopolysaccharides: extraction with phenol-water and further applications of the procedure. **1965**, *Methods Carbohydr. Chem*., 5, 83-91.

SECTION III

Molecular mechanism of TLR4/MD-2/LPS interaction

Chapter 8

The activation of TLR4/MD-2 by LPS from *Burkholderia cenocepacia*

8.1 TLR4/MD-2/LPS interaction: state-of-art

Lipopolysaccharide (LPS, endotoxin) elicits a potent innate immune response through the interaction with TLR4 (Toll-like receptor 4) and MD-2 (myeloid differentiation factor 2) receptor complex (Nagai *et al*., 2002). This recognition is crucial since tiny amounts of LPS, released from invading microorganisms, prepare the immune system to protect the host against further infection. In contrast, excessive exposure (or excessive responses) to LPS can lead to uncontrolled inflammatory responses manifested by the sepsis-systemic inflammatory response syndrome (SIRS), which is associated with high mortality, especially in intensive care units (Angus *et al*., 2001; Rangel-Fausto, 2005). The TLR4/MD-2/LPS heterodimer can activate two parallel signaling pathways both resulting in production of inflammatory cytokines. The lipid A represents the LPS portion recognised by the TLR4/MD-2 receptor complex and its bioactivity is strongly influenced by its primary structure; of main importance is certainly the grade of acylation and the fatty acid (FA) distribution, which determines the three-dimensional structure of the lipid A moiety (Schromm *et al*., 2000; Seydel *et al*., 2000) and its agonistic and antagonistic activity (Brandenburg *et al*., 1993; Rietschel *et al*., 1994).

Hexa-acylated bisphosphorylated lipid A with an asymmetric 4:2 lipid chain distribution, found in the majority of enterobacteria (e.g. *E. coli*), is considered to have the highest cytokine-inducing capacity in mammals. In contrast, the hypoacylated synthetic precursor of *E. coli* lipid A, the tetra-acylated lipid IV_A, has weak agonistic effects for some species of mammals and is well known to possess a strong antagonistic activity on human cells (Golenbock *et al*., 1991). The crystal structure of the TLR4/MD-2/LPS complex showed that the receptors act as a heterodimer composed of two copies of the TLR4/MD-2/LPS system, where lipid A, which is

accommodated in a hydrophobic pocket formed by two anti-parallel β-sheets of MD-2, mediates dimerization and activation of the (TLR4/MD-2)2 complex (Park *et al*., 2009). The MD-2 hydrophobic pocket can accommodate up to five acyl chains; in the case of *E. coli* lipid A, five acyl chains are buried inside the pocket while the sixth one is exposed and lies on the surface of MD-2 and interacts with TLR4, mediating hydrophobic interactions bridging the TLR4/MD-2/LPS multimer, and promoting the activation of the immune response (Mend *et al*., 2010). On the other hand, antagonist lipid IV_A binds to the human MD-2 (hMD-2) with all four acyl chains completely buried inside the hydrophobic pocket and in this way it is not able to trigger any dimerization. In contrast, lipid IV_A can activate the murine TLR4/MD-2 complex, demonstrating a species-specific difference in the recognition of lipid IV_A by MD-2 (Hajjar *et al*., 2002). MD-2 binds to TLR4 primarily through hydrophilic interactions such as hydrogen bonds and charge interactions, and a few hydrophobic residues were found in the binding interface (Park and Lee, 2013; Park *et al*., 2009). The TLR4 binding surface can be divided into two sections, the A and B patches. The A patch, negatively charged, interacts with the positively charged surface of MD-2, and the positively charged B patch with the negatively charged surface of MD-2. Mutation of amino acid residues involved in this interaction blocks TLR4 and MD-2 binding, and LPS signaling. Given this premise, several studies, comprising site-directed mutagenesis, molecular modeling experiments and comparative analysis with other agonist and antagonist molecules (such as eritoran for the latter case and *E. coli* lipid A for the first one), have been dedicated to clarify lipid IV_A species-specificity identifying residues that are exclusively involved in the binding and, in case of murine cells, TLR4 activation (Gay and Gangloff, 2007; Janeway, 1989). The ability of murine MD-2 to bind lipid IV_A and activate TLR4 was explained with a shift of the lipid A glucosamine backbone that relocates the

negative phosphate groups so that they can interact with specific positively charged residues on TLR4 allowing the dimerization of the complex (Broz and Monack, 2013). Other experiments strongly suggested that the main force for receptor dimerization is represented by hydrophobic interactions at the dimerization interface (Janeway, 1989); however, it was also shown that these interactions by themselves are not sufficient to mediate complex dimerization (Janeway, 1989). Similarly to lipid IV_A, a penta-acylated lipid A was seen to act as antagonist or also to be poorly recognised (as example, the lipid A from environmental strains of *Pseudomonas aeruginosa*) (Hajjar *et al*., 2002) by the hTLR4/hMD-2 complex.

Despite the large number of investigations, mechanisms underlying the TLR4 dimerization and activation merit further studies in order to extend the knowledge on lipid A-induced activation and its species-specificity. Furthermore, it is of great interest studying the binding mode possessed by lipid A moieties that have structural features different from the highly studied *E. coli* lipid A in order to better understand the role of each singular component of the lipidic portion into the TLR4 activation process.
In this scenario, the present study reports, for the first time, a combination of theoretical and experimental experiments using LOS and isolated lipid A (LA) from the well-known cystic fibrosis (CF) pathogen *Burkholderia cenocepacia* (BC-LOS). The present work has a notable importance also if it is contextualised into CF disease problem; indeed since LPS and, in particular, lipid A moiety are involved in the above described host–bacterial interaction inducing host innate immune response, the investigation of the molecular mechanisms of interaction between *B. cenocepacia* LPS and host immune system components is mandatory to understand the virulence of the CF pathogen. The full structure of the *B. cenocepacia* LOS (BC-LOS) has been

previously described (Hamad *et al*., 2012) and is sketched in Figure 8.1. The LA showed the typical *Burkholderia* disaccharide backbone, possessing a [P→4-β-D-Glc*p*N-(1→6)-α-D-Glc*p*N1→P] sequence that also bears two additional Ara4N residues linked to the phosphate groups. Moreover, fatty acids composition analysis showed the presence of (*R*)-3-hydroxyhexadecanoic acid (C16:0 (3-OH)) in the amide linkage and of (*R*)-3-hydroxytetradecanoic (C14:0 (3-OH)) and tetradecanoic acid (C14:0) in the ester linkage, matching with the archetypal *Burkholderia* LPSs/LOSs bearing a total of five acyl chains (Hamad *et al*., 2012). The presence of the two Ara4N residues and the peculiar acylation pattern renders *Burkholderia cenocepacia* (BCLA) completely different from the *E. coli* analogue and from all enterobacterial LA. Hence, the archetypal mechanism of binding/activation of TLR4/MD2 complex cannot apply in this case.

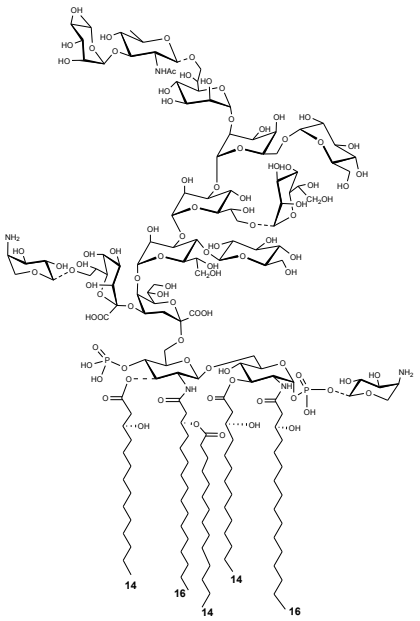

Figure 8.1 LOS structure from *Burkholderia cenocepacia*.

In this study, it was investigated the molecular basis of the mechanisms of LA recognition by employing a multidisciplinary approach comprising molecular microbiology, cellular biology, organic chemistry, and molecular modeling.

8.2 Assessment of the agonist activity of *B. cenocepacia* lipid A on TLR4/MD-2 complex

In order to test TLR4/MD-2 activation by BC-LOS and its LA (BCLA), all experiments were executed by measuring activation of transient transfected HEK293 and HEK293T cells coexpressing murine or human MD-2 (mMD-2, hMD-2) and murine or human TLR4 (mTLR4, hTLR4). Moreover, it was used site-directed mutagenesis to swap different amino acid residues of the mouse and human MD-2 proteins to determine the critical residues involved in the binding to BCLA. Measurement of the activation of NF-κB, tested with luciferase assays, was the read-out of all performed experiments in which *E. coli* LPS, its lipid A (the synthetic compound **506**) (Kotani *et al*., 1985) (Figure 1.5) or the biosynthetic precursor lipid IV_A were used as control.

Preliminary results showed that BC-LOS and BCLA act as agonists both for human and mouse TLR4/MD-2 complexes (data not shown). In order to further study the structure-activity relationship of BCLA, by *ad hoc* molecular biology, it was conceived and constructed a BCLA mutant (LAMUT) lacking the Ara4N residues (see also chapter 7) and observed the activation of HEK293 cells expressing human or mouse MD-2. Figures 8.2 show dose-response curves for human and murine TLR4/MD-2 to BC-LOS and LOS bearing the LAMUT (MUT-LOS) (Figure 8.2Top), and to BCLA and LAMUT (Figure 8.2Bottom), respectively. These studies corroborated preliminary results showing that also at a minimal concentration (1 ng/mL, Figure 8.2Top) both *B. cenocepacia* LOSs are able to induce activation of TLR4/MD-2. As

stated above, these evidences also suggest that a different binding mode indeed occurs. Similar experiments were performed by using isolated BCLA and LAMUT (Figure 8.2Bottom) and the results showed consistent agonistic activity, also for the lowest concentration employed (5 ng/mL; Figure 8.2Bottom). However, it is important to note a significant difference in NF-κB activation induced by BCLA species with or without Ara4N. In the latter, LAMUT had a slightly reduced immunostimulatory activity (Figure 8.2Bottom).

Furthermore, it was also checked to what extent could BC-LOS interfere with the TLR4 signaling process elicited by the LPS of *E. coli*. In order to answer to this question, it was performed a competition assay in which HEK293 cells transfected with either hTLR4/hMD-2 or mTLR4/mMD-2 were pre-incubated with BC-LOS for 1 h and then re-stimulated with *E. coli* LPS for 4 h (Figure 8.3). It was observed that the lowest tested concentration (1 ng/mL, Figure 8.3) of BC-LOS was not able to change the NF-κB activation elicited by 1 ng/mL of *E. coli* LPS (Figure 8.3). Interestingly, when pre-incubation was performed using 10ng/mL of BC-LOS, followed by stimulation by 1 ng/mL of *E. coli* LPS, the *E.coli* LPS-induced NF-kB activation was lower than with *E. coli* LPS alone (Figure 8.3). In particular, a 2-fold reduction of *E. coli* LPS-NF-κB activation was observed when pre-incubation with *B. cenocepacia* MUT-LOS was performed (10 ng/mL; Figure 8.3). These results suggest that BC-LOS lacking Ara4N partially antagonizes the activity of the archetypical TLR4/MD-2 agonist *E. coli* LPS (Figure 8.3). Hence, summarising the above results, it can be assessed that BC-LOS and its lipid A moiety activate HEK293 cells expressing human or mouse MD-2 and that Ara4N plays a significant role in the effective activation of NF-κB by binding to the TLR4/MD-2 complex.

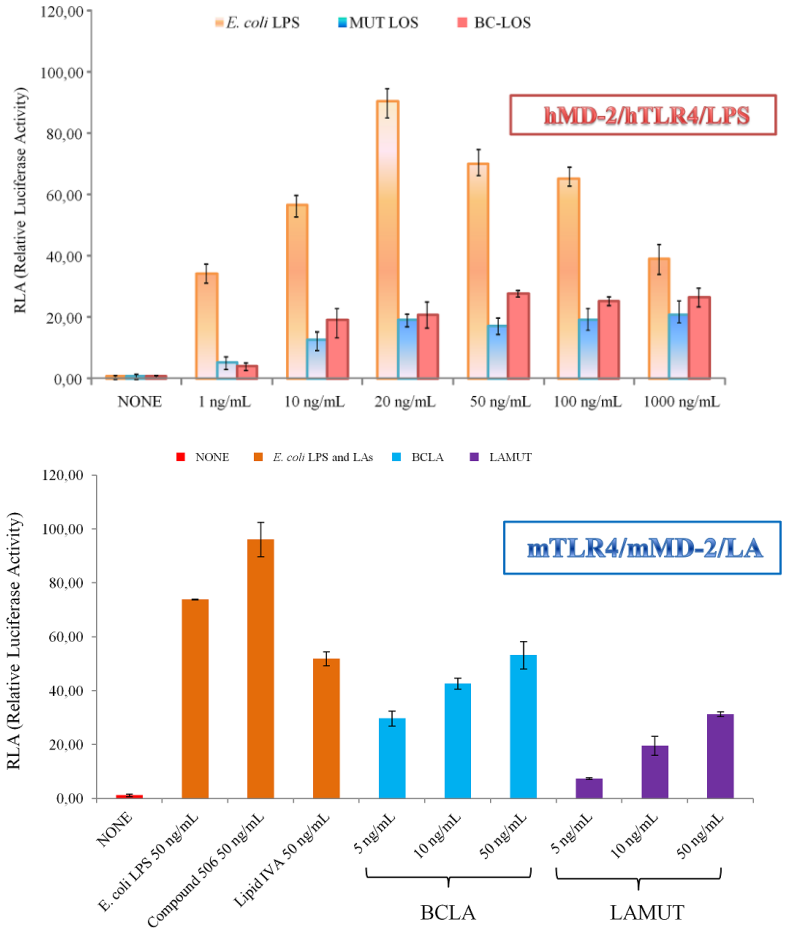

Figure 8.2 Top) NF-κB activation upon stimulation of HEK293 hTLR4/hMD-2 with BC-LOS, MUT-LOS and *E. coli* LPS. **Bottom)** NF-κB activation upon stimulation of HEK293 mTLR4/mMD-2 with BCLA and LAmut. Stimulations with *E. coli* LPS, compound **506** and lipid IV_A were used as benchmark.

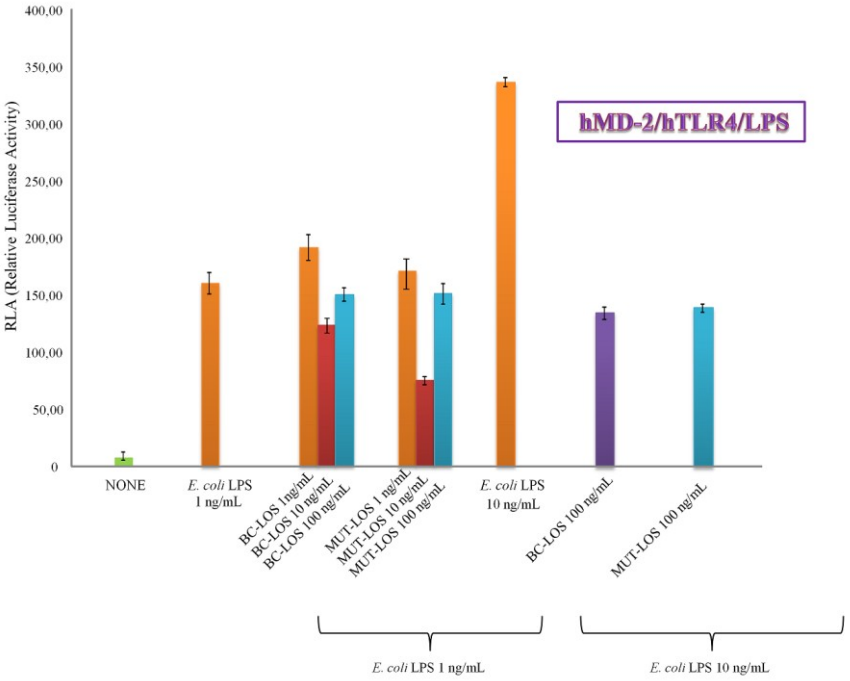

Figure 8.3 Assay on the potential antagonist activity of BC-LOS and MUT-LOS on hexa-acylated *E. coli* LPS.

8.3 Identification of amino acid residues of MD-2 involved in the interaction with LPS

8.3.1 The hydrophobic pocket

In order to further investigate the molecular recognition events between *B. cenocepacia* LA and TLR4/MD-2, were generated several human and mouse MD-2 mutants that were employed to transfect HEK293 cells coexpressing human or mouse TLR4. The attention was focused on several residues that reside at the dimerization interface of the MD-2 protein, whose importance in lipid IV_A- and *E. coli* LPS-induced activation has previously been

tested (Meng *et al*., 2010; Resman *et al*., 2009). First analyses were focused on Val-82 that resides in the proximity to the pocket entrance, at a loop between β-strands 5 and 6, which is comprised of several conserved solvent-exposed hydrophobic residues, thus contributing to the establishment of crucial hydrophobic interactions in the activated receptor complex (Resman *et al*., 2009). To introduce a change at this position that could affect LPS binding without disturbing the hydrophobic nature of the interactions, aliphatic Val82 was substituted by the aromatic phenylalanine residue (V82F), with a bulkier hydrophobic side chain. Mutation resulted in increased activation of the HEK293 cells transfected with the hTLR4/hMD-2V82F when stimulated with BC-LOS, compared to the control (Figure 8.4). No relevant differences were detected between the stimulation with BC-LOS and the MUT-form (Figure 8.4). Thus, V82F mutation of the hMD-2 protein affected the binding of LA to MD-2, inducing a greater activation of NF-κB levels. Computational models (see below) suggest that the change of van der Waals interactions into CH-π interactions could account for a higher affinity. The experiment was executed only on HEK293 cells transfected with the human receptors since virtually all the hydrophobic residues involved in the abovementioned MD-2 hairpin loop are conserved between the two species (Meng *et al*., 2010). Therefore, it is expected that these hydrophobic interactions between mTLR4/mMD-2 and LA are fairly similar to those concerning the hTLR4/hMD-2 complex (Meng *et al*., 2010).

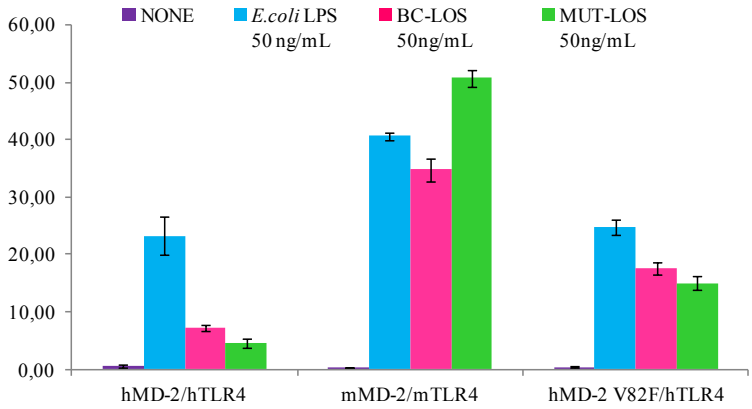

Figure 8.4 NF-κB release upon stimulation of HEK293 hTLR4/hMD-2 and HEK293 mTLR4/mMD-2 with BC-LOS and MUT-LOS. Stimulation with *E. coli* LPS was used as benchmark.

8.3.2 The surface charged residues

While the hydrophobic residues of both TLR4 and MD-2 involved in hydrophobic interactions are conserved among different species, the electrostatic interactions that have been shown to contribute to receptor activation are mediated by amino acid residues that markedly differ between mouse and human MD-2. In particular, the hMD-2 protein has a positively charged lysine residue at position 122 (Lys-122) near the pocket entrance, whereas mMD-2 has a negatively charged glutamic acid (Glu-122) moiety (Meng *et al.*, 2010). Moreover, hMD-2 has a positively charged lysine at position 125 (Lys-125), while murine MD-2 has a neutral hydrophobic leucine (Leu-125) (Meng *et al.*, 2010). In the complex, both residues are close to the disaccharide backbone of LA (Kim *et al.*, 2007) and have been shown to be important for species-specific differences in the recognition of lipid IV_A between human and mouse MD-2. Therefore these two positions, 122 and

125, were mutated on both MD-2 homologues, assuming that these substitutions could affect LA binding and consequently influence TLR4 activation (Meng *et al*., 2010). While the single E122K mutation on mMD-2 (E122 of murine MD-2 was replaced by the corresponding human residue) had little or no effect on the activation induced by the BC-LOS or the *E.coli* LPS, a remarkable decrease of the NF-κB activation after stimulation with lipid IV_A was observed (Figure 8.5Top). As previously demonstrated (Muroi and Tanamoto, 2006), the charge alteration from glutamic acid to lysine substantially decreases the agonistic activity of lipid IV_A, likely due to the removal of the repulsive forces versus the *bis*-phosphorylated disaccharide backbone. These interactions are essential for lipid IV_A to tilt towards the Cys-95/Cys-105 loop, responsible for the binding of MD-2 to TLR4 (Meng *et al*., 2010). Thus, the unchanged *B. cenocepacia* LA responsiveness suggested that replacement of the amino acid in position 122 was not enough to alter the TLR4/MD-2 activity. This fact strongly suggests that the single 122 residue of the MD-2 protein is not pivotal for BC-LOS signaling. Additionally, in the docking calculations (see below), no major role was observed for this residue in terms of predicted binding. These results were partly corroborated by luciferase assays performed on HEK293 cells transfected with the human MD-2 K122E mutant and with mTLR4. Indeed, replacement of Lys122 in human MD-2 by glutamic acid (present in murine MD-2) did not affect the BC-LOS signaling, while a substantial increase of the NF-kB activation by the *B. cenocepacia* MUT-LOS was observed (Figure 8.5Bottom). This behavior is now probably due to the presence of repulsive forces towards the phosphate groups of the lipid A, which might facilitate the orientation toward the Cys-95/Cys-105 loop. Thus, the different BC-LOS responsiveness might be related to the presence of the Ara4N residues that mask the negatively charged phosphate

groups, and could reduce the repulsive forces introduced with the K122E mutation.

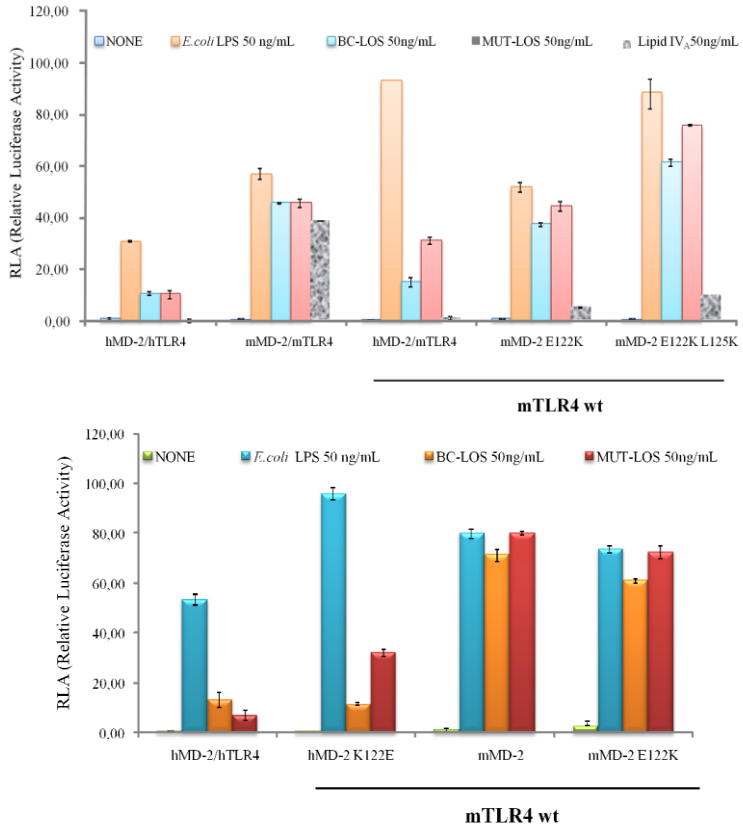

Figure 8.5 (**Top**) NF-κB-luciferase reporter assay executed stimulating HEK293 hTLR4/hMD-2, HEK293 mTLR4/mMD-2, HEK293 mTLR4/mMD-2 E1222K and HEK293 mTLR4/mMD-2 E122K L125K cells with BC- LOS and MUT-LOS, *E. coli* LPS and lipid IV_A. (**Bottom**) NF-κB activation by stimulation of: HEK293 hTLR4/hMD-2, HEK293 mTLR4/mMD-2, HEK293 mTLR4/hMD-2 K122E and HEK293 mTLR4/mMD-2 E122K with BC-LOS and MUT-LOS. Stimulation with *E. coli* LPS was used as benchmark.

On the contrary, the absence of Ara4N residues in the MUT-lipid A backbone might explain the augmentation of its agonistic activity when tested on HEK293 cells transfected with hMD-2 K122E/mTLR4. On the other hand, when stimulation occurred on cells expressing the double E122K/L125K murine MD-2 mutant (Figure 8.5Top), a substantially increased activity of the mutant MD-2 was detected, when compared to the wild type MD-2 or other tested mutants (Figure 8.5Top). In particular, it was observed an appreciable difference between the NF-κB activation induced by BC-LOS and the MUT-form (Figure 8.5Top), where the latter seemed to have acquired a greater agonistic activity compared to the WT BC-LOS. Interestingly, simultaneous mutations of K122E, K125L, together with Y41F, and R69G, on human MD-2, have been reported to be required to promote an immune response by lipid IV_A, which is known to be an antagonist of human TLR4/MD-2 (Meng *et al*., 2010).

8.3.3 Conclusions on biological assays results

Taken together, experiments on human and mouse MD-2 mutants allowed to confirm initial hypothesis about the "non-archetypal" BCLA binding mechanism to the TLR4/MD-2 receptor. Indeed, results provided direct evidence that the peculiar architecture of *B. cenocepacia* LA plays a key role in the interaction with MD-2 as well as in the dimerization process. In particular, summarising the results regarding modification experiments on charged residues (see above), it is possible to suggest that the presence of the amino-arabinose residues on the BCLA glucosamine backbone affects the binding to the TLR4/MD-2 complex, although their absence (MUT-LOS and LAMUT) seems to be not sufficient by itself to impair the BCLA signaling. This conclusion was drawn on the basis of an increased agonistic activity acquired by LAMUT when tested on human mutant MD-2 K122E (Figure 8.5); this singular

behavior might be explained assuming that the Ara4N residues, besides acting as additional anchorage points to the receptor complex, act also as a mask of the negatively charged phosphate groups on LA backbone. In case of the human MD-2 protein, which is characterised by several positively charged residues near the pocket entrance, as described above, this "charge-masking mechanism" may be essential to explain the high levels of HEK293 cells activation observed in the biological assays. Furthermore, it is worth to emphasise again that, even in absence of Ara4N, *B. cenocepacia* LA showed a significant agonist activity that could be explained by its peculiar acylation pattern. To pursue this hypothesis and to validate speculations derived from luciferase assays results, molecular modeling experiments were performed by Dr. Sonsoles M.S. and collaborators.

8.4 Molecular modelling of docking of BC-LOS to the MD-2 and TLR4 activation

The biological results seem to suggest different MD-2 binding affinities driving the agonist activity. In order to propose a binding mode of MUT- and BC-LOSs, docking calculations were undertaken and the two ligands were docked into both MD-2 proteins, human and murine. Two different docking methodologies were used, by means of AutoDock and AutoDock Vina programs; while AutoDock is a widely used semi-empirical docking method (Goodsell *et al.*, 1996), the recently released AutoDock Vina combines empirical and knowledge-based scoring functions, with good performance and reduced computing time (Trott and Olson, 2010). Firstly, the validation of the docking protocols was performed with both AutoDock and AutoDock Vina, by docking *E. coli* lipid A from crystallographic structures (PDB codes 3fxi –human- and 3vq2 –murine-) into the MD-2 protein from their corresponding PDB files. Values of root-mean-square deviation

and predicted free energy of binding values indicated an excellent performance of both programs in predicting the crystallographic binding pose for both human and murine MD-2 proteins (Table 8.1).

	human MD-2	murine MD-2
BCLA	-20.02/**-25.30**	-17.73/**-23.60**
LAmut	-18.22/**-18.60**	-13.09/**-17.20**
E. coli lipid A	-24.41**/-28.3** (RMSD = 0.282/**0.599**)	-24.73/**-27.9** (RMSD = 0.647/**0.394**)

Table 8.1 Theoretical free energy of binding for the docking calculations with AutoDock 4.2 and AutoDock Vina (in bold). Energy values are in kcal/mol. Root-mean-square deviation (RMSD) values are in Å.

8.4.1 Model for the binding of LAMUT and BCLA

Once both docking programs and docking protocols were shown to be efficient and reliable for predicting the binding conformation of these type of ligands, and calculations conditions were set up, calculations with LAMUT and BCLA were undertaken. First, the docking of LAMUT and BCLA structures was carried out. Regarding predicted binding energies, results were consistent in both AutoDock and AutoDock Vina programs, both predicting better values for *E. coli* lipid A, followed by wild type BCLA and then LAMUT, in agreement with the biological data. General results are shown in Table 8.1. Both lipid A, BCLA and LAMUT, were predicted to bind both human and murine MD-2, with binding poses in agreement with the crystallographic binding poses for *E. coli* lipid A (superimposition with *E. coli* lipid A in Figures 8.6 and 8.7). Docking poses consisted on four fatty acid chains deeply immersed into the hydrophobic pocket of MD-2, making van der Waals and CH-π interactions with the side chains of most of the lipophilic residues of the MD-2 pocket, mainly consisting of

aliphatic Leu, Ile and Val residues, aromatic Phe (numbering 76, 104, 119, 121, 126, 147, and 151), and Tyr (numbering 102, and 131) residues. With most of these residues, all the docked poses were found to participate in hydrophobic interactions. Given the longer length of these four fatty acid chains, higher efficiency in the establishment of lipophilic interactions can be deduced. The fifth chain is placed into the groove or channel defined by Phe126, Leu87, Val82 and Arg90. This channel has been identified in the X-ray structures of the complex of TLR4/MD-2 with *E. coli* lipid A (Park *et al*., 2009) as the allocation site for one lipid chain, allowing to complete the hydrophobic interface required for dimerization with the second TLR4/MD-2/ligand partner (referred to here as TLR4*/MD-2*). This precludes formation of the activated TLR4/MD-2/ligand multimer. Also Phe126 has been proposed as a switch controlling the agonist/antagonist conformation of MD-2, since Phe126 mutation prevents dimerization and abolishes downstream signaling (Park *et al*., 2009; Kobayashi *et al*., 2006).

In summary, the major length of the five fatty acids is able to trigger the dimerization excluding from MD-2 pocket the fifth one, which builds the dimerization interface in the Phe126, Leu87, Val82 and Arg90 groove, analogously to the sixth FA of *E. coli* lipid A.

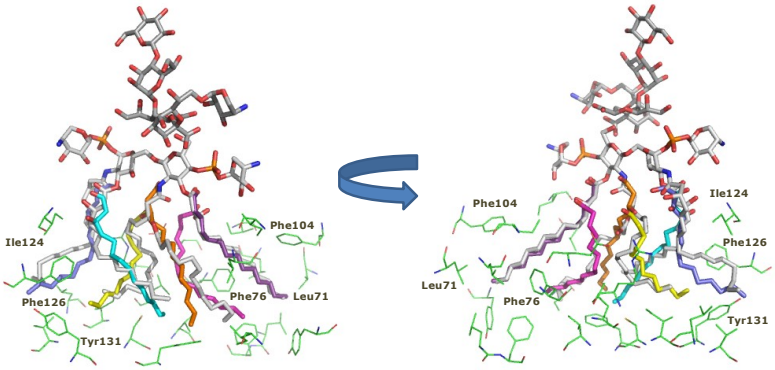

Figure 8.6 *B. cenocepacia* WT LOS (CPK colours) docked to MD-2. Superimposed fatty acids chains from *E. coli* lipid A are shown in different colours.

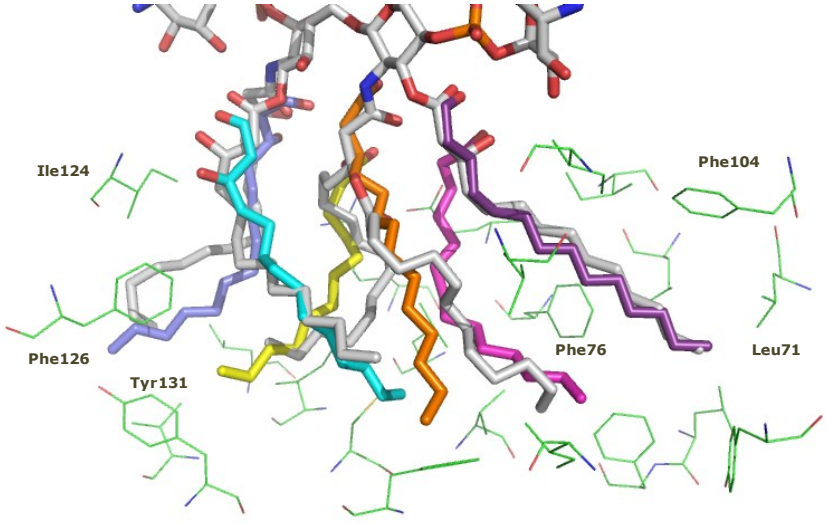

Figure 8.7 Detail *B. cenocepacia* WT LOS (CPK colours) docked to MD-2. Superimposed fatty acids chains from *E. coli* lipid A are shown in different colours.

Additionally, the disaccharide scaffold of BCLA and LAMUT, together with the phosphate groups, are located in the outer region,

establishing electrostatic interactions with the polar residues defining this external part of the MD-2 pocket (Figure 8.8). The higher predicted affinity for BC-LOS can be explained in terms of additional anchorage points arising from the amino-arabinose residues. In particular, these Ara4N moieties are able to establish additional interactions with MD-2. The hydroxyl (OH) group from Tyr102 establishes bridged H-bonding with the OH at position 2 of Ara4N and the OH from the FA chain (Figure 8.9), while OH at position 3 from the same amino-arabinose establishes a hydrogen bond with Ser118 OH group. In the case of amino-arabinose 2, the OH group from one of the FA chains establishes a hydrogen bond with Lys122 CO group, whereas OH-3 and ammonium groups, although out of the H-bond distance range (4.5 Å), are well oriented towards carbonyl groups from Lys122 and Gly123, maybe enabling a putative H-bond networking at this site. These interactions could also be identified in the complex with the murine MD-2. This putative binding mode of BCLA could thus explain the high level of activation in the biological assays. The lack of some lipophilic interactions arising from the absent sixth fatty acid chain, in comparison to *E. coli* lipid A, could also be compensated by these extra polar interactions from the amino-arabinoses. It is worth noting that the Ara4N moieties are playing also a major role in the full complex architecture (see below), justifying biological activation responses.

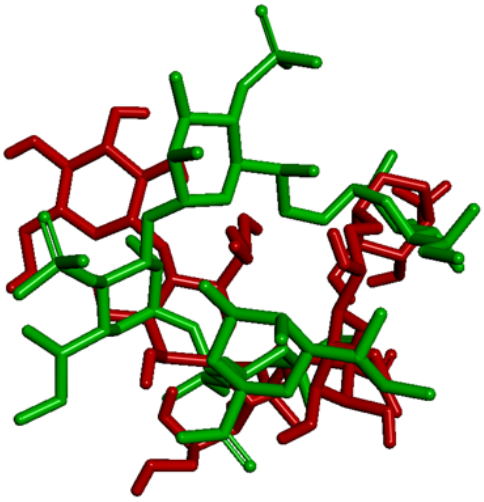

Figure 8.8 Superimposition of best docked results of *B. cenocepacia* LOS core. The docking was obtained using AutoDock Vina (depicted in **red**) and *E. coli* LPS core from PDB 3fxi (depicted in green). TLR4 is not shown for the sake of clarity.

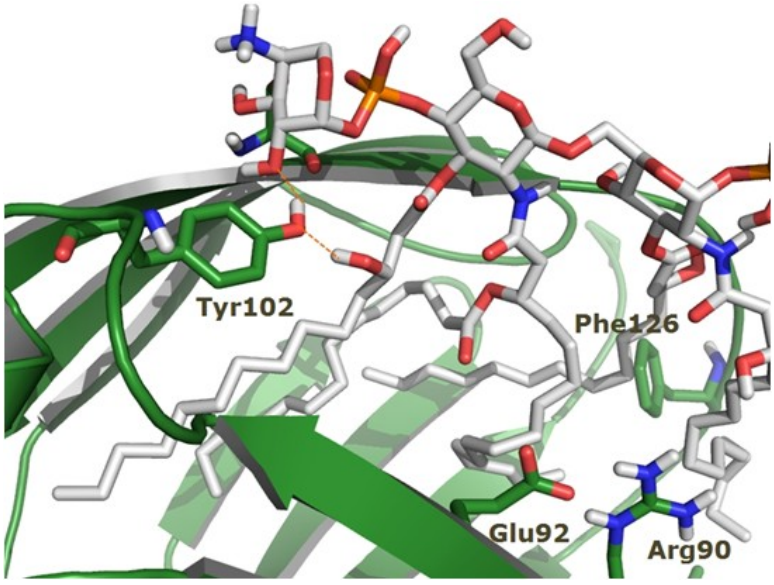

Figure 8.9 Detail of Tyr102. Docked pose of *B. cenocepacia* WT LOS in MD-2. Detail of some H-bond interactions involving Tyr102.

8.4.2 3D model for the human TLR4/MD-2 dimer in complex with *B. cenocepacia* LPS

First, docking of the core oligosaccharide moiety was performed on human TLR4, focusing on the region where *E. coli* LPS core binds. The best binding pose was selected (theoretical binding free energy of -2.8 kcal/mol, by AutoDock Vina), taking also into account a proper orientation for the building of the full complex. Docked pose, superimposed with *E. coli* LPS core from PDB 3fxi, is shown in Figure 8.8. The human TLR4/core complex was then assembled to the MD-2/BCLA complex (best result from AutoDock Vina calculations), leading to a full hTLR4/MD-2/BC-LOS complex, which was submitted to molecular dynamics (MD) simulations. Receptor dimer building was performed by using PDB 3fxi as template. The full 3D structure of the dimer complex was submitted to MD simulations and is shown in Figure 8.9. MD simulations did not show meaningful differences with the docked complexes (data not shown).

Building of a 3D model of the full complex may allow the identification of key interactions for the molecular recognition mediated by BCLA. Apart from the already mentioned participation in MD-2 anchoring, BCLA amino-arabinoses are playing a fundamental role in complex formation as they participate in H-bond networking in the dimerization interfaces as follows: both ammonium groups from Ara4Ns 2 and 3, are establishing hydrogen bonds with residues belonging to TLR4: with the Arg264 CO group, and with Asp294 carboxylate groups respectively; ammonium group of arabinose 1 is close to Asp395 carboxylate and Ser416 OH group, both residues belonging to the opposite TLR4* and OH-3 from amino-arabinose 1 is establishing a H bond with Ser 415 CO group (TLR4*) (Figure 8.10). The 3D models from docking could suggest higher activation for BC-LOS

vs MUT-LOS, arising from the extra anchorage points from arabinoses, in agreement with the biological results, which showed weaker activation for both LOSs, BC-LOS and MUT-LOS.

8.4.3 Conclusions on molecular modeling experiments

The structural peculiarities of *B. cenocepacia* core and the presence of two amino-arabinoses in the lipid A region provide relevant hints at an atomic level for the binding to and activation ability of TLR4/MD-2 receptor complex. Actually, the network of hydrogen bonds and polar interactions contributing to the anchorage of the lipid A into the TLR4/MD-2 involves not only the sugars from the core oligosaccharide (for example, hydrogen bonds involving with Arg322 (Figure 8.10), but also the three amino-arabinoses. Reported mutagenesis studies demonstrate that several Lys residues involved in LPS binding play indispensable roles through the polar interactions with the phosphate groups (Griber *et al*., 2004; Re and Strominger, 2003). In the present dimer model, Lys122 is involved in binding the BCLA through polar interactions with the core; as for Val82Phe, it has been already mentioned its role in building the groove that accommodates the acyl chain from lipid A, completing the interaction surface required for dimerization. The replacement of Val82 by Phe involves changes of van der Waals interactions into CH-π interactions, which may favor the binding of this chain, longer than the corresponding one on *E. coli* LPS. Thus, the biological results on mutants support our 3D models and open new insights into the molecular recognition of LPS by TLR4/MD-2.

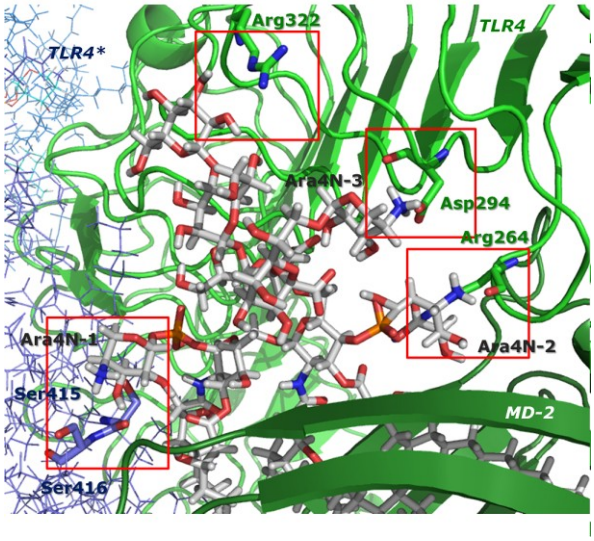

Figure 8.10 Details of some interactions between the *B. cenocepacia* LOS and TLR4/MD-2 from the 3D model.

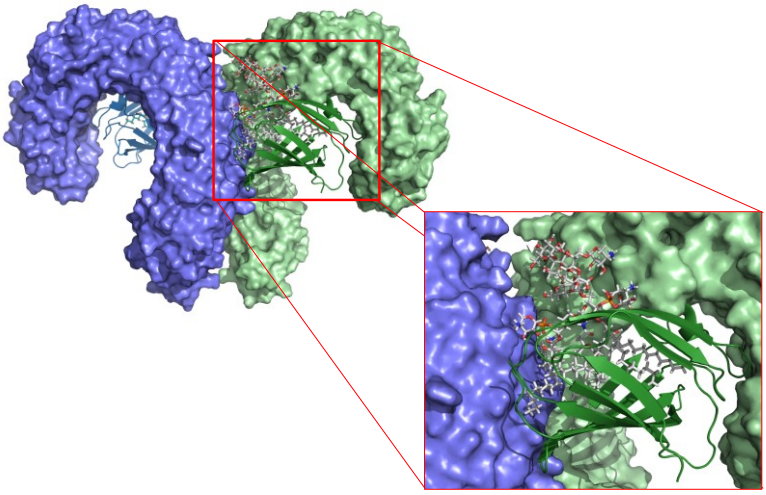

Figure 8.11 Left panel) 3D Model of the dimer of *B. cenocepacia* LOS in complex with TLR4/MD-2. **Right panel)** Detail of the dimer of *B. cenocepacia* LOS in complex with TLR4/MD-2.

8.5 Discussion

Opportunistic bacterial infections normally rapidly cleared from the airway of healthy individuals, cause persistent inflammation in individuals with impaired immune defences such as patients affected by cystic fibrosis (CF). Indeed, beyond the genetic defect, CF may be considered as an inflammatory disorder with neutrophilic airway wall inflammation, bronchiectasis and mucus retention (De Soyza *et al*., 2012); this latter provides a niche for bacteria that would normally try to evade immune system recognition. In this scenario, *Burkholderia cenocepacia* has been recognised as one of the CF pathogens with the greatest proinflammatory potential (and capacity for harm), particularly in patients undergoing lung transplantation (De Soyza *et al*., 2001; Aris *et al*., 2001). The pro-inflammatory capability is mainly attributed to the lipopolysaccharide, able to stimulate a nine-fold higher release of cytokines compared with that of *P. aeruginosa* (Shaw *et al*., 1995), the most common CF opportunistic pathogen. Several experiments (Rallabhandi *et al*., 2008) demonstrate that the highest immunostimulatory activity correlates with the higher degrees of lipid A acylation and to the asymmetrical distribution of the acyl chains with respect to the glucosamine disaccharide backbone (De soyza *et al*., 2012). Indeed, whether the synthetic tetra-acylated lipid IV_A antagonizes the elicitation of the inflammatory response, on the contrary, the hexa-acylated lipid A of *E. coli* has been shown to exhibit the highest agonistic activity on human cells. Likewise, it has previously been shown that *P. aeruginosa*, synthesizes hexa-acylated LPS during the adaptation step of the chronic infections seen in CF. On the other hand penta-acylated LPS from *P.aeruginosa* does not activate human TLR4/MD-2 complex (Hajjar *et al*., 2002). Therefore the current dogma of LPS detection considers the hexa-acylated lipid A as the typical agonist for the TLR4/MD-2 complex whereas

underacylated LPSs have been shown to be less or not sensed by the PRR complex. Interestingly, as shown herein through a plethora of biological assays, *B. cenocepacia* penta-acylated lipid A can elicit a significant inflammatory response activating the human MD-2/TLR4 complex despite the relative underacylated structure as compared to *P. aeruginosa*, suggesting a different model of TLR4/MD-2 activation.

In this frame, the present work highlights the ability of penta-acylated LPS to strongly activate TLR4 . Furthermore, the role of amino-arabinose has been investigated using Ara4N modified chemotype. Results, using point mutants of MD-2 and molecular modeling, indicate that the increased length of acyl chains of the lipid A moiety and the presence of the amino-arabinose residues are synergistically working for the activation and dimerization of LPS receptors. Modeling experiments show that both amino-arabinoses contribute to the dense network of interactions involving sugars of core region providing additional anchorage points of the lipid A moiety into the receptor complex; indeed the absence of amino-arabinoses in LAMUT is responsible for its lower immunostimulatory activity with respect to BCLA, as observed in Figure 8.2, Bottom. Interestingly, the observation of the increased agonistic activity of LAMUT when tested on human mutant MD-2 K122E (Figure 8.5, Bottom) suggests a further potential role for amino-arabinoses consisting in masking the negative charges of phosphate groups of lipid A backbone; this hypothesis could be explained considering the repulsive charges between the LA phosphate groups and the Glu122 on MD-2 surface that might be responsible to relocate the disaccharide backbone so that it is able to expose the acyl chain required for activation/dimerization of the receptorial complex. Although LAMUT lacks the additional "points of anchorage" to the MD-2 represented by amino-arabinoses, in any case exerts a consistent agonist activity on

human cells. In this work it is showed that this behavior is due to the increased length of the acyl chains of the BCLA with respect to *E.coli* lipid A, in particular due to the one of the 16:0 (3-OH) fatty acids not present in the *E.coli* lipid A acylation pattern. Therefore, the presence of longer acyl chains is responsible for the fulfillment of the MD-2 binding pocket by the hypo-acylated lipid A from *B. cenocepacia* thus allowing the exposition of the acyl chain responsible for the TLR4 activation, as it could be assumed by observing our computational models and experimental results from luciferase assays executed on human mutant MD-2 V82F (Figure 8.4). Indeed, computational analyses suggest that the higher immunostimulatory activity observed for BCLA and LAMUT when tested on hMD-2 V82F is due to the capacity of the longer acyl chains to establish lipophilic interactions with higher efficiency arising from the change of van der Waals interactions (valine) into CH-π interactions (phenylalanine).

In summary, it can be stated that the "uncommon" model of TLR4/MD-2 activation by BCLA is due to a combination of two pivotal features: i) the amino-arabinoses that provide extra polar interactions facilitating the BCLA binding to the TLR4/MD-2 multimer, and ii) the length of the two primary 16:0 (3-OH) acyl chains compared to those possessed by the prototype *E.coli* lipid A, that compensates the minor number of fatty acids filling the hydrophobic binding pocket of MD-2 protein, allowing the exposition of the acyl chain responsible for the TLR4 dimerization. Taking into account the role of the BCLA structure in promoting the inflammatory response of human innate immunity and the high social impact of inflammation-related pathogenicity of *B. cenocepacia* in cystic fibrosis, the present work results of great interest since it opens new insights into the molecular recognition of *B. cenocepacia* LPS by the TLR4/MD-2 complex, a key events

of the pathophysiology of the inflammatory responses in cystic fibrosis.

References

Angus D.C., Linde-Zwirble W.T., Lidicker J., Clermont G., Carcillo J., Pinsky M.R., Epidemiology of severe sepsis in the United States: analysis of incidence, outcome, and associated costs of care. **2001**, *Crit. Care Med*., 29, 1303-1310.

Aris R.M., Routh J.C., LiPuma J.J., Heath D.G., Gilligan P.H., Lung transplantation for cystic fibrosis patients with *Burkholderia cepacia* complex: survival linked to genomovar type. **2001**, *Am. J. Respir. Crit. Care. Med*.,164:2102-2106.

Brandenburg K., Mayer H., Koch M.H., Weckesser J., Rietschel E.T., Seydel U, Influence of the supramolecular structure of free lipid A on its biological activity. **1993**, *Eur. J. Biochem*., 218, 555-563.

Broz P., Monack D.M.,Newly described pattern recognition receptors team up against intracellular pathogens. **2013**, *Nat. Rev. Immunol*., 13, 551-65.

De Soyza A., Di Lorenzo F., Silipo A., Lanzetta R., Molinaro A., Lung transplantation for cystic fibrosis patients with *Burkholderia cepacia* complex: survival linked to genomovar type. **2012**, *Carbohydrate Chemistry*, RSC Publishing, 38. 13-39.

De Soyza A., McDowell A., Archer L., Dark J.H., Elborn S.J., Mahenthiralingam E., Gould K., Corris P.A., *Burkholderia cepacia* complex genomovars and pulmonary transplantation outcomes in patients with cystic fibrosis. **2001**, *Lancet*, 358, 1780-1781.

Gay N.J., Gangloff M., Structure and function of Toll receptors and their ligands. **2007**, *Annu. Rev. Biochem.*, 76,141-165.

Golenbock D.T., Hampton R.Y., Qureshi N., Takayama K., Raetz C.R., Lipid A-like molecules that antagonize the effects of endotoxins on human monocytes. **1991**, *J. Biol. Chem*., 266, 19490-19498.

Goodsell D.S., Morris G.M. Olson A.J., Automated docking of flexible ligands: applications of AutoDock. **1996**, *J. Mol. Recognit*., 9, 1-5.

Gruber A., Mancek M., Wagner H., Kirschning C.J., Jerala R., Structural model of MD-2 and functional role of its basic amino acid clusters involved in cellular lipopolysaccharide recognition **2004**, *J. Biol. Chem*., 279, 28475-28482.

Hajjar A.M., Ernst R.K., Tsai J.H., Wilson C.B., Miller S.I., Human Toll-like receptor 4 recognizes host-specific LPS modifications, **2002**, *Nat. Immunol*., 3, 354-359.

Hamad M.A., Di Lorenzo F., Molinaro A., Valvano M.A., Aminoarabinose is essential for lipopolysaccharide export and intrinsic antimicrobial peptide resistance in *Burkholderia cenocepacia*. **2012**, *Molecular Microbiology*, 85, 5, 962-974.

Janeway C.A. Jr., Approaching the asymptote? Evolution and revolution in immunology. **1989**, *Cold Spring Harb. Symp. Quant. Biol.*, 54, 1-13.

Kim H.M., Park B.S., Kim J.I., Kim S.E., Lee J., Oh S. C., Enkhbayar P., Matsushima N., Lee H., Yoo O.J., and Lee, J.O., Crystal structure of the TLR4-MD-2 complex with bound endotoxin antagonist Eritoran. **2007**, *Cell*, 130, 906-917.

Kobayashi M., Saitoh S., Tanimura N., Takahashi K., Kawasaki K., Nishijima M., Fujimoto Y., Fukase K., Akashi-Takamura S., Miyake K., Regulatory roles for MD-2 and TLR4 in ligand-induced receptor clustering. **2006**, *J. Immunol*., 176, 6211-6518.

Kotani S., Takada H., Tsujimoto M., Ogawa T., Takahashi I., Ikeda T., Otsuka K., Shimauchi H., Kasai N., Mashimo J., Synthetic lipid A with endotoxic and related biological activities comparable to those of a natural lipid A from an Escherichia coli re mutant. **1985**, *Infect. Immun*., 49, 225-237.

Meng J., Drolet J.R., Monks B.G., Golenbock D.T., MD-2 residues tyrosine 42, arginine 69, aspartic acid 122, and leucine 125 provide species specificity for lipid IVA. **2010**, *The Journal of Biological Chemistry*, 285, 27935-27943.

Meng J., Lien E., Golenbock D.T., MD-2-mediated ionic interactions between lipid A and TLR4 are essential for receptor activation. **2010**, *The Journal of Biological Chemistry*, 285, 8695-8702.

Muroi M., Tanamoto K., Structural regions of MD-2 that determine the agonist-antagonist activity of lipid IVa. **2006**, *J. Biol. Chem.*, 281:5484-5491.

Nagai Y., Akashi S., Nagafuku M., Ogata M., Iwakura Y., Akira S., Kitamura T., Kosugi A., Kimoto M., Miyake K., Essential role of MD-2 in LPS responsiveness and TLR4 distribution **2002**, *Nat. Immunol.*, 3, 667-672.

Park B.S., Lee J.O., Recognition of lipopolysaccharide pattern by TLR4 complexes. **2013**, *Experimental & Molecular Medicine*, 45, e66.

Park B.S., Song D.H., Kim H.M., Choi B.S., Lee H., Lee, J.O., The structural basis of lipopolysaccharide recognition by the TLR4-MD-2 complex. **2009**, *Nature*, 458, 1191-1195.

Rallabhandi P., Awomoyi A., Thomas K.E., Phalipon A., Fujimoto Y., Fukase K., Kusumoto S., Qureshi N., Sztein M.B., Vogel S.N. , Differential activation of human TLR4 by Escherichia coli and Shigella flexneri 2a lipopolysaccharide: combined effects of lipid A acylation state and TLR4 polymorphisms on signaling **2008**, *J. Immunol*., 180**,** 1139-1147.

Rangel-Frausto M.S., Sepsis: Still going strong **, 2005**, *Arch. Med. Res*., 36, 672-681.

Re F., Strominger J.L., Separate functional domains of human MD-2 mediate Toll-like receptor 4-binding and lipopolysaccharide responsiveness. **2003**, *J. Immunol*., 171, 5272-5276.

Resman N., Vašl J., Oblak A., Pristovšek P., Gioannini T.L., Weiss J.P., Jerala R., Essential roles of hydrophobic residues in both MD-2 and toll-like receptor 4 in activation by endotoxin. **2009**, *The Journal of Biological Chemistry*, 284, 15052-15060.

Rietschel E.T., Kirikae T., Schade F.U., Mamat U., Schmidt G., Loppnow H., Ulmer A.J., Zähringer U., Seydel U., Di Padova F., Schreier,M., Brade H., Bacterial endotoxin: molecular relationships of structure to activity and function. **1994**, *FASEB J*., 8, 217-225.

Seydel U., Oikawa M., Fukase K., Kusumoto S., Brandenburg K., Intrinsic conformation of lipid A is responsible for agonistic and antagonistic activity. **2000**, *Eur. J. Biochem*., 267, 3032-3039.

Schromm A.B., Brandenburg K., Loppnow H., Moran A.P., Koch M.H., Rietschel E.T., Seydel U., **2000**, Biological activities of lipopolysaccharides are determined by the shape of their lipid A portion. *Eur. J. Biochem*., 267(7):2008-13.

Shaw D., Poxton I.R.,Govan J.R.. Biological activity of *Burkholderia* (*Pseudomonas*) *cepacia* lipopolysaccharide.**1995**, *FEMS Immunol. Med. Microbiol*.,11, 99-106.

Trott O., Olson A.J., AutoDock Vina: improving the speed and accuracy of docking with a new scoring function, efficient optimization and multithreading. **2010**, *J. Comput. Chem*., 31, 455-461.

SECTION IV

Study of LPS isolated from Extremophilic bacteria

Chapter 9

Elucidation of the Structure and Biological Activity of endotoxins isolated from the thermophilic bacteria *Thermomonas hydrothermalis*

9.1 Extremophiles: an overview

Belonging to both two Dominia of *Archaea* and *Bacteria*, and to either Gram-positive and Gram-negative family, extremophiles are life-forms capable to live and thrive in inhospitable, from a human viewpoint, environments such as alkaline and acidic waters, boiling hot springs, high pressure waters, ultra saline brines, without excluding a combination of aforesaid chemical and physical extremes which is typical of polyestremophilic microbes (Mesbah and Wiegel, 2008). On the basis of the physical or chemical parameters these microrganisms can be distinguished in: ***acidophiles*** and ***alkalophiles*** that live at extreme pH values; ***thermophiles*** that are able to live in extremely high temperatures, ranging from 40°C up to 100°C; ***psycrophiles*** able to survive in frozen habitats, i.e. glaciers or polar seas; ***halophiles*** that live in extreme salt concentrations from 3 M to saturation of NaCl; ***barophiles*** that require elevated pressure for proliferation and ***xerophiles*** that can be isolated from extremely anhydrous environments (Figure 9.2). Several studies of extremophiles have helped redraw the three-domain system of life. Indeed, the typical dogma held that living organisms could be grouped into two domains: *Bacteria*, with a simple structural architecture, and *Eukarya*, whose cells are more complex (see also Section I). The discovery of microorganisms in environments that were assumed to be sterile supported to the once heretical proposal that yet a third group, the *Archaea*, exists (Figure 9.1). Many microbiologists believe that ancestors of today's archeal species might represent a type of organism that first inhabited Earth when it was a young and hot planet. These unique features led the American microbiologist Carl Woese to propose these microorganisms be lumped together and called *Archeabacteria*, as already described in Section I, Chapter 1. Anatomically, archaeans differ from bacteria since their

cell membrane is composed by isoprenoid and isoprenyl glycerol ether-linked lipids, with fully saturated acyl chains (Gulik *et al*., 1985). The presence of these lipids and the production of exopolysaccharides allowing the formation of biofilms, are responsible for the extraordinary stability shown by extremophiles. The notable resistance offered by these components to hydrolysis at acidic and alkaline pHs and at high temperature, have been proposed as the feature that allowed the development of archaeal extremophile strains. Noticeable, recently researchers have focused on DNA and have completely sequenced a number of bacterial and archaeal genomes; these studies have demonstrated that some genes of archaea are similar to bacterial genes and others to eukaryotic genes. On the other hand, a large fraction of archaeal genes appear to be unique. These unshared genes establish archaea's separate identity.

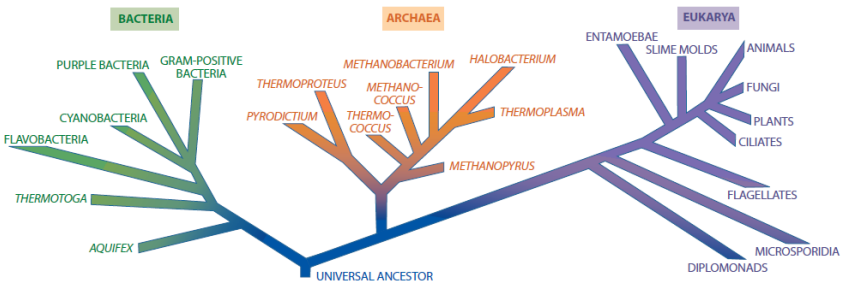

Figure 9.1. Evolutionary tree of the three domains system.

Owing to their unique features, estremophiles have attracted much interest since they showed to possess a high biotechnological potential with a number of important industrial applications comprising bioremediation and biomining processes (Taylor et al., 2012). Of particular interest are the enzymes that help

extremophiles to function in hostile circumstances such as synthetic catalysts that speed up chemical reactions without being altered themselves. The common used enzymes degrade or stop working when exposed to heat or other extreme conditions, and so manufacturers that rely on them must take specific steps to protect the molecules during reactions or storage. Since enzymes from extremophiles – termed "extremozymes" – remain active when other enzymes would fail, they can potentially remove the need for those steps, thereby increasing efficiency and reducing costs (Madigan and Marrs, 1997). Furthermore, they can form the basis of entirely new enzyme-based processes (Madigan and Marrs, 1997).

Environmental parameter	Type	Definition	Examples
Temperature	Hyperthermophile	Growth >80 °C	*Pyrolobus fumarii*, 113 °C
	Thermophile	Growth 60–80 °C	*Synechococcus lividis*
	Mesophile	15–60 °C	*Homo sapiens*
	Psychrophile	<15 °C	*Psychrobacter*, some insects
Radiation			*Deinococcus radiodurans*
Pressure	Barophile	Weight-loving	Unknown
	Piezophile	Pressure-loving	For microbe, 130 MPa
Gravity	Hypergravity	>1*g*	None known
	Hypogravity	<1*g*	None known
Vacuum		Tolerates vacuum (space devoid of matter)	Tardigrades, insects, microbes, seeds
Desiccation	Xerophiles	Anhydrobiotic	*Artemia salina*; nematodes, microbes, fungi, lichens
Salinity	Halophile	Salt-loving (2–5 M NaCl)	Halobacteriaceae, *Dunaliella salina*
pH	Alkaliphile	pH > 9	*Natronobacterium, Bacillus firmus* OF4, *Spirulina* spp. (all pH 10.5)
	Acidophile	low pH-loving	*Cyanidium caldarium*, *Ferroplasma* sp. (both pH 0)
Oxygen tension	Anaerobe	Cannot tolerate O_2	*Methanococcus jannaschii*
	Microaerophile	Tolerates some O_2	*Clostridium*
	Aerobe	Requires O_2	*H. sapiens*
Chemical extremes	Gases		*C. caldarium* (pure CO_2)
	Metals	Can tolerate high concentrations of metal (metalotolerant)	*Ferroplasma acidarmanus* (Cu, As, Cd, Zn); *Ralstonia* sp. CH34 (Zn, Co, Cd, Hg, Pb)

Figure 9.2 Classification and examples of extremophiles.

9.2 Thermophiles: an overview

Among all environmental factors, temperature is considered one of the most important variable controlling the viability and activities of microorganisms as well as the parameter that can be easily measured (Brock, 1970). In this context, thermophiles represent a class of microorganisms, including *Archaea*, *Bacteria* and *Eukarya*, that can live and reproduce at relatively high temperatures, between 50° and 60°C (Stetter, 1999), but also microbes living at temperatures above 80°C, termed hyperthermophiles, were found (Stetter, 1999). Some hyperthermophiles even thrive in environments hotter than 100°C (Madigan and Marrs, 1997). Hot habitats are encountered in correspondence of volcanic areas above and below the sea level, where mineralised water comes to the surface, and in the deep rock formations heated by the Earth's interior. All thermophiles require hot water but differ in other habitat needs. Some thrive in only acidic water, others require calcium or sulphur carbonate, still others live in alkaline springs. Depending on these other features, thermophiles are described more specifically with terms such as thermoacidophile that live in heat and acid environments or halophilic alkalithermophiles that grow optimally at or above Na^+ concentrations of 1.7 M, pH greater than or equal to 8.5, and temperatures greater than or equal to 50°C (Bowers and Wiegel, 2011). The first extremophile capable of growth at temperatures greater than 70°C was *Thermus aquaticus,* that has become famous as the source of the heat-resistant enzyme Taq DNA polymerase, one of the most used enzymes in the molecular biology field (Brock, 1986). approximately at same time the first hyperthermophile in an extremely hot and acidic spring was isolated. This organism, the archaean *Sulfolobus acidocaldarius,* grows at temperatures as high as 85°C. Thermophiles grow in communities composed of billions

of individuals and often dozens of species. Some communities form long, flexible structures called *streamers* in fast-flowing water of runoff channels (Figure 9.3). The thermophilic species in these streamers are direct descendants of early bacteria. Many other bacteria communities grow in columns or pedestals termed *mats* (Figure 9.3). The thermophilic mat community can be compared to a forest community. Its superficial species either need or can withstand abundant light, while its understory species live with less or no light and may metabolize chemicals such as hydrogen and iron.

Figure 9.3 Thermophilic streamers (left) and mats (right).

In case of mesophilic organisms, exposure to heat shock conditions induces the transiently synthesis of the Heat Shock Proteins (HSPs). The synthesis of HSPs is triggered by the accumulation, within the cell, of misfolded proteins, as a consequence of the stress condition as in case of drastical changes in pH, UV irradiation, osmolarity and the presence of variously toxic substances such as antibiotics, ethanol, aromatic compounds or heavy metals (Ramos *et al.*, 2001). These proteins act like chaperones for the other biomolecules, assuring their correct folding and translocating them into the right cell compartments, even in case of altered functionality of the cell itself.

Changes in temperature result in alterations of the cell membrane lipid composition, in order to retain the fluidity of the membrane. In *Bacteria*, this can be obtained by increasing the length of the acyl chains, the ratio of *iso to ante-iso* branching and/or the degree of saturation (Prado *et al*., 1988). The growth temperature-dependent alterations in fatty acids composition seem to be aimed to maintaining the proton permeability of the plasmatic membrane at a rather constant level (van de Vossenberg *et al*., 1998).

In *Archaea*, the acyl chains undergo cyclisation or transition from the diether to tetraether. These latter show lowered proton permeability due to the hindrance brought to the lipid layer of the membrane. Moreover, ether linkages are far more resistant to oxidation and to high temperature than ester linkages, as well as to enzymatic degradation by phospholipases (Choquet *et al*., 1994). Consequently, membranes composed by tetraether lipids result more termostable.

Premise

Thermomonas hydrothermalis is a newly identified, rod-shaped, non-motile, strictly aerobic Gram-negative bacterium with the optimum temperature for growth of about 50°C (Alves *et al*., 2003). It was isolated for the first time from the hot spring at São Gemil in Central Portugal and, on the basis of the phylogenetic analysis of the 16S rRNA gene sequence, it was considered to be closely related to another slightly thermophilic bacterium named *Thermomonas haemolytica* that, nevertheless, has a lower growth temperature range than *T. hydrothermalis* (Alves *et al*., 2003). The knowledge that these microorganisms have developed peculiar chemical modifications in their cell wall components to survive at high temperatures, makes *Thermomonas hydrothermalis* a fascinating group of bacteria to be studied in order to verify which alterations can occur in their membrane constituents that can be

associated to their extreme lifestyle. Owing to their location, lipopolysaccharides are permanently exposed to environmental stresses that likely affect their general structure; indeed LPSs isolated from extremophilic bacteria frequently show unusual chemical characteristics that influence their biological effects on the innate immune system. Interestingly, previous studies demonstrated that LPSs or LOSs belonging to non-pathogenic bacteria exert an antagonist or partial antagonist activity towards toxic LPSs both *in vivo* and *in vitro* experiments (Rose *et al*., 1995). Nevertheless, despite their key role in viability of Gram-negative bacteria and their potential "beneficial effects" on innate immune system, very little is known about structure and biological activity of lipopolysaccharides isolated from extremophilic bacteria. Given these premises, the elucidation of the structure together with the study of the biological activity of the lipopolysaccharide molecule isolated from the slightly thermophilic bacteria *Thermomonas hydrothermalis* become a fascinating target to pursue. The present paper is consistent with this objective and, therefore, it reports the complete structure of the lipooligosaccharide extracted from *T. hydrothermalis*, that is the first LOS that has been characterised among the genus *Thermomonas*. The overall structure was obtained by a combination of chemical, NMR spectroscopic and mass spectrometric analyses executed on the entire molecule and on its partially deacylated and fully deacylated forms. Moreover, a meticulous study on *T. hydrothermalis* LOS bioactivity was performed by testing it on important innate immune system components.

9.3 Extraction, Purification and Compositional Analyses of LOS from *Thermomonas hydrothermalis*

Crude LOS (R-LPS) was isolated from lyophilised cells of *T. hydrothermalis* strain SGM-6^{T}using the phenol/chloroform/light petroleum extraction protocol (Galanos *et al*., 1969). The presence of a *rough*-type LPS was confirmed by the SDS-PAGE (Kittelberger and Hilbink, 1993) after silver nitrate gel staining (Kittelberger and Hilbink, 1993) that showed a run to the bottom of the gel due to the low molecular mass of the LOS form; the material was purified from other cell contaminants by enzymatic digestion with RNase, DNase, and proteases followed by dialysis and Sephacryl HR-300 chromatography.

Structural analyses (Leontein and Lönngren, 1978; De Castro *et al*., 1964) on pure LOS revealed the following monosaccaride composition: D-GalA, D-Man, D-Gal, D-GlcN (2-amino-2-deoxy-D-glucose) and 3-deoxy-D-*manno*-oct-2-ulopyranosonic acid (D-Kdo). Methylation analysis (Hakomori, 1964) of the intact LOS indicated the presence of 6-substituted galactofuranose, terminal galactopyranose, terminal galactopyranuronic acid, 3-substituted galactopyranose, 6-substituted aminoglucopyranose, 4,6-disubstituted mannopyranose and 4,5-disubstituted Kdo. Fatty acids composition, obtained by using GC-MS, showed the occurrence of (R)-3-hydroxyundecanoic acid [C11:0 (3-OH)] in amide and in ester linkages and undecanoic acid (C11:0) exclusively in ester linkage.

9.4 Isolation and structural characterisation of core oligosaccharide by NMR spectroscopy

The complete structure of the core oligosaccharide moiety was achieved by NMR spectroscopy and MALDI MS analyses executed both on the de-O-acylated LOS and on its fully deacylated form. Combination of data belonging to these products was pivotal to obtain clear information regarding the peculiar structure of *Thermomonas hydrothermalis* LOS. The de-O-acylation was executed using anhydrous hydrazine (Holst, 2000). The ^{1}H NMR spectrum of the de-O-acylated product, showed in Figure 9.4, highlighted the presence of nine anomeric signals (**A-I**) between δ = 5.80 and 4.40 ppm (Table 9.1) relative to nine distinct spin systems. It is worth to note that NMR analysis performed on partially deacylated LOS did not show the presence of the signals typically assigned to the H-3 methylene protons of the Kdo residue.

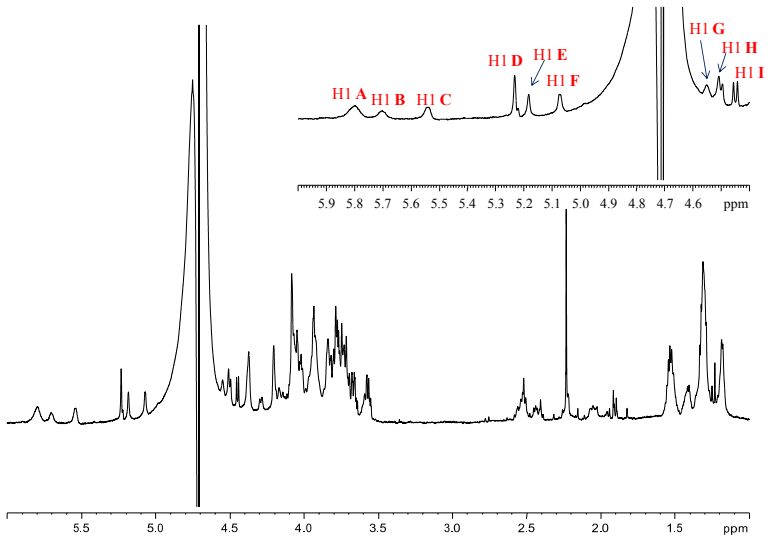

Figure 9.4 ^{1}H NMR spectrum of de-O-acylation product with zoom of anomeric region (top-right).

All residues, except residue **D**, were present as pyranose rings as proven by the ^{13}C chemical shift values and by the *intra*-residual long-range correlations between C-1/H-1 and H-5/C-5 observed in the $^{1}H,^{13}C$-HMBC spectrum, whereas the observation of correlations between protons of residue **D** and down-field shifted carbon signals, around 83.0 ppm suggested the occurrence of a furanose ring, as confirmed by the *intra*-residual H-1/C-4 and C-1/H-4 correlations in the $^{1}H,^{13}C$-HMBC spectrum. Residue **C** (H-1/C-1 signals at δ = 5.54/94.3 ppm, Table 9.1) and **G** (H-1/C-1 signals at δ = 4.63/101.3 ppm, Table 9.1) were assigned to the lipid A GlcN*p*1*P* and GlcN*p*4*P* on the basis of their H-2 protons that showed a correlation with two nitrogen-bearing carbon atoms at δ=53.7 and δ=55.3 ppm respectively. Moreover, the multiplicity of the anomeric proton signal ($^{3}J_{H\text{-}1,P}$ = 8.0 Hz) of residue **C** and the downfield shifts of H-4 and C-4 (3.95 ppm and 76.5 ppm respectively) of residue **G** were diagnostic of the presence of a phosphate group linked at position O-1 **C** and O-4 **G**. The occurrence of an *inter*-residue connectivity between H-1 of **G** and H-$6_{a,b}$ of **C**, identified in the NOESY and HMBC spectra, corroborated the assignment of residues **C** and **G** to the lipid A backbone. Spin systems **A** (H-1/C-1 at δ=5.79/95.4 ppm, Table 9.1) and **B** (H-1/C-1 at δ=5.70/95.0 ppm, Table 9.1) were identified as α-GalA residues due to the presence of a correlation of H-5 **A** and H-5 **B** (4.54 ppm and 4.51 ppm respectively) with two carboxyl groups (175.8 ppm and 176.2 ppm respectively), that allowed us to recognise spin systems **A** and **B** as uronic acid residues. The α-anomeric configuration was attributed on the basis of the *intra*-residual NOE contact of H-1 with H-2 and the $^{1}J_{C1,H1}$ and $^{3}J_{H1,H2}$ values (172.3 and 3.4 Hz, respectively) whereas the $^{3}J_{H3,H4}$ and $^{3}J_{H4,H5}$ values (3 and 1 Hz, respectively) were diagnostic of a *galacto* configuration. Furthermore, spin systems **A** and **B**, as residue **C**, showed the typical multiplicity of a phosphorylated α-

anomeric proton signal ($^3J_{H\text{-}1,H\text{-}2}$= 3.2 Hz, $^3J_{H\text{-}1,P}$= 7.6 Hz); both residues were terminal galacturonic acids since none of their carbon atoms was shifted by glycosilation. Residue **E** (H-1/C-1 at δ=5.18/100.7 ppm, Table 9.1) was recognised as a β-mannose, as shown by its $^3J_{H1,H2}$ and $^3J_{H2,H3}$ low values (3 Hz) and by the *intra*-residual NOE correlation of H-1 only with H-2 (diagnostic of a *manno*-configured residue); the β-anomeric configuration was assigned on the basis of the strong *intra*-residue NOE contacts of H-1 with H-3 and H-5, together with the $^3J_{H1,H2}$ coupling constant (7.8 Hz). Substitution was observed at position O-6, as testified by the glycosylation shift for C-6 (66.7 ppm, Table 9.1).

Chemical shift δ (^{1}H/^{13}C) of the de-O-acylated LOS								
Unit	**1**	**2**	**3**	**4**	**5**	**6**	**7**	**8**
A	5.79	3.92	3.99	4.37	4.54			
t-α-GalA*p*	*95.4*	*67.5*	*69.1*	*70.3*	*73.3*	*175.8*		
B	5.70	3.90	4.01	4.29	4.51			
t-α-GalA*p*	*95.0*	*67.5*	*69.2*	*70.3*	*73.2*	*176.2*		
C	5.54	3.97	3.72	3.57	4.01	4.16/3.82		
6-α-GlcN*p*1P	*94.3*	*53.7*	*70.2*	*69.5*	*71.5*	*68.2*		
D	5.23	4.21	4.08	4.07	3.73	4.06/3.77		
6-α-Gal*f*	*109.2*	*81.5*	*76.7*	*83.0*	*73.4*	*71.0*		
E	5.18	4.20	3.84	4.13	3.80	4.18/3.90		
6-β-Man*p*4P	*100.7*	*69.6*	*72.1*	*75.9*	*73.5*	*66.7*		
F	5.07	3.84	3.93	4.04	3.76	3.81/3.65		
t-α-Gal*p*	*99.6*	*69.2*	*69.0*	*69.0*	*70.3*	*62.5*		
G	4.63	3.86	3.78	3.95	3.71	3.76/3.59		
6-β-GlcN*p*4P	*101.3*	*55.3*	*72.1*	*76.5*	*75.2*	*63.5*		
H	4.50	3.68	3.72	4.08	3.73	*3.64*		
3-β-Gal*p*	*102.9*	*70.2*	*80.0*	*68.7*	*75.1*	*61.2*		
I	4.44	3.56	3.66	3.92	3.56	3.78/3.71		
t-β-Gal*p*	*103.8*	*70.9*	*72.8*	*70.1*	*75.2*	*60.9*		
Chemical shift δ (^{1}H/^{13}C) of the fully de-acylated LOS								
L	5.46	3.68	3.86	4.20	4.42			
t-α-GalA*p*	*93.4*	*68.4*	*69.4*	*70.5*	*72.3*	*175.8*		
K	-	-	1.97/1.72	4.02	4.17	3.67	N.D	3.81
4,5-α-Kdo*p*			*34.8*	*70.0*	*73.0*	*73.1*	*N.D.*	*63.2*

Table 9.1 ^{1}H and ^{13}C NMR chemical shifts of the product oligosaccharide derived from the de-O-acylated (top) and the fully de-acylated (bottom) LOS from *Thermomonas hydrothermalis*. N.d. is not determined.

Spin systems **D**, **F**, **H** and **I** were all attributed to galactose residues. In details, residue **D** (H-1/C-1 at δ=5.23/109.2 ppm, Table 9.1), as described above, showed to be a α-galactofuranose (α-Gal*f*) due to the $^{1}J_{C,H}$ coupling constant value of 174.0 Hz together with the ^{13}C chemical shift of the anomeric carbon signal and the *intra*-residual NOE connectivities; furthermore, residue **D** was found to be substituted at position O-6 due to the downfield shift of its C-6 (71.0 ppm, Table 9.1). Spin system **F** (H-1/C-1 at δ=5.07/99.6 ppm, Table 9.1) was identified as a terminal α-galactose residue about which the α-anomeric configuration and the *galacto* configuration were assigned as described above for residues **A** and **B**. Eventually, both residues **H** and **I** (H-1/C-1 at δ=4.50/102.9 ppm and 4.44/103.8 ppm, respectively, Table 9.1) were attributed to β-*galacto*-configured sugar residues, as proven by the chemical shift values of carbinolic protons and the $^{3}J_{H,H}$ ring coupling constants; moreover, as delineated for residue **E**, the large $^{3}J_{H-1,H-2}$ values and the NOE contacts of H-1 with H-3 and H-5, were diagnostic of the β-anomeric configurations. Residue **H** showed to be substituted at position O-3, whereas residue **I** was identified as a terminal glucose residue.

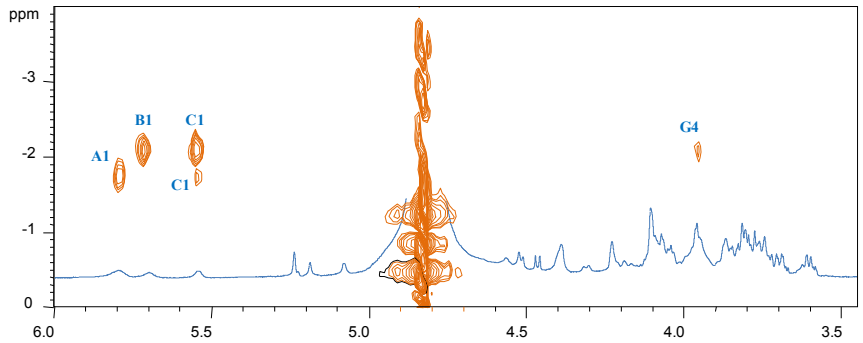

Figure 9.5 Section of ^{1}H NMR and ^{1}H, ^{31}P HSQC spectra of the de-O-acylated LOS from *T. hydrothermalis*. The localization of the phosphate groups is indicated.

The ^{31}P NMR spectrum of de-O-acylated product confirmed the presence of four phosphate signals that can be distinguished in three groups present in different regions of the spectrum, at –2.08 ppm, –2.11 ppm and –1.73 ppm. A ^{31}P, ^{1}H HSQC experiment (Figure 9.5) was executed in order to identify and localise abovementioned phosphate groups. The phosphorous signal at–2.08 ppm showed to be related to a double correlation with two different proton signals at 5.70 ppm (H-1 **B**) and 3.95 ppm (H-4 **G**). Above double correlation was attributed to H-1 **B** of the α-GalA residue attached to C-4 of β-GlcN II **G** of lipid A backbone via phosphodiester bond. Signal at –2,11 ppm in the ^{31}P-^{1}H HSQC spectrum (Figure 9.5) was connected to the proton signal at 5.54 ppm (H-1 **C**). Finally, signal at –1.73 ppm showed to have a double correlation with two anomeric proton signals at 5.79 ppm (H-1 **A**) and 5.54 ppm (H-1 **C**), underlining a further phosphodiester bond involving, in this case, the α-GlcN I **C** of lipid A backbone and the α-GalA residue **A**. Therefore, summarising all results belonging to the ^{31}P, ^{1}H HSQC experiment it was found that *T. hydrothermalis* LOS possess a peculiar lipid A carbohydrate backbone characterized by the presence of the disaccharide [P→4-β-D-Glc*p*N-(1→6)-α-D-Glc*p*N1→P] carrying one galacturonic acid on each phosphate group.

Owing to the absence of the signals relative to the Kdo residue, whose presence was detected in chemical analyses (see above), it was decided to perform 1D and 2D NMR experiments also on the fully deacylated lipooligosaccharide molecule. The complete deacylation was executed, after a mild hydrazinolysis, by a strong alkaline hydrolysis with KOH 4M; sample was desalted on a Sephadex G-10 column and then lyophilised to give the core oligosaccharide backbone. The ^{1}H NMR spectrum of the fully deacylated product (Figure 9.6) showed the presence of the diasterotopic methylene signals of the Kdo residue (H-3$_{ax}$/H-3$_{eq}$

1.97/1.72 ppm, Figure 9.6); moreover it showed the occurrence of an additional anomeric signal (H-1/C-1 at δ= 5.46/93.4 ppm, Table 9.1), not detected in the NMR analysis on the de-O-acylated LOS, whose presence, on the contrary, was evaluated in the mass spectrometric analysis on the de-O-acylated product (see below). The additional spin system, labeled as **L** (Table 9.1), was attributed to a phosphorylated α-GalA unit. The ^{31}P NMR and the ^{31}P, ^{1}H HSQC spectra of the totally deacylated LOS confirmed the peculiar structure of the lipid A backbone; furthermore both spectra highlighted the occurrence of another double correlation between the anomeric proton signal of residue **L** (H-1 at δ=5.46 ppm) and the H-4 of the core oligosaccharide mannose residue **E** (H-4/C-4 at δ=4.13/75.9 ppm, Table 9.1) allowing to identify a further phosphodiester linkage involving, in this case, two sugar residues of the core oligosaccharide moiety. All ^{31}P NMR spectroscopy experiments were confirmed through MALDI mass spectrometry performed on both de-O-acylated and fully deacylated LOS from *T. hydrothermalis* (see below).

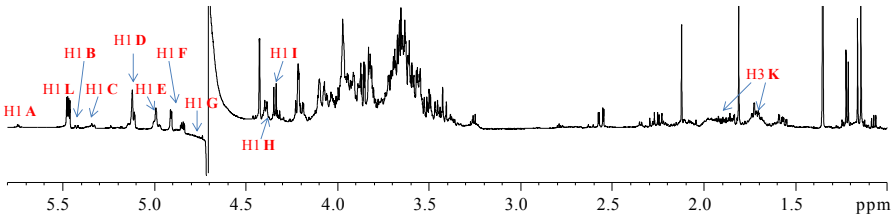

Figure 9.6 ^{1}H NMR spectrum of the fully deacylated product.

Rationalising all NMR results, NOESY and ROESY spectra and scalar long-range correlations observed in the ^{1}H,^{13}C-HMBC spectrum allowed to define the saccharide sequence. In details,

starting from the Kdo unit **K**, it was observed a substitution at its O-4 by mannose **E**, as suggested by the NOE correlation between H-1 **E** and H-4 **K** (Figure 9.8), and a substitution at O-5 by the β-galactose residue **H**, underlined by the occurrence of a NOE contact (Figure 9.8) and a long-range correlation between H-1 **H** and H-5 **K**. Mannose **E** was, in turn, substituted at position O-6 by residue **F**, the terminal α-galactose unit, as attested by the long-range correlation between H-1 **F** and H-$6_{a,b}$ **E** and the relative NOE connectivity (Figures 9.7 and 9.8); taking in account the double correlation between H-1 **L** and H-4 **E**, earned from the ^{31}P, ^{1}H HSQC spectrum of the fully deacylated LOS, mannose **E** is also

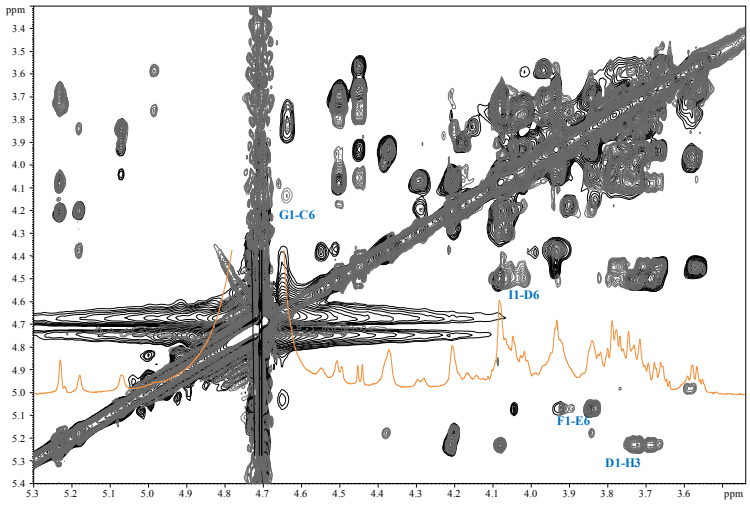

Figure 9.7 Section of the TOCSY (**black**) and NOESY (**gray**) spectra of the de-O-acylated LOS from *T. hydrothermalis*. The relevant *inter*-residue NOE cross-peaks are shown.

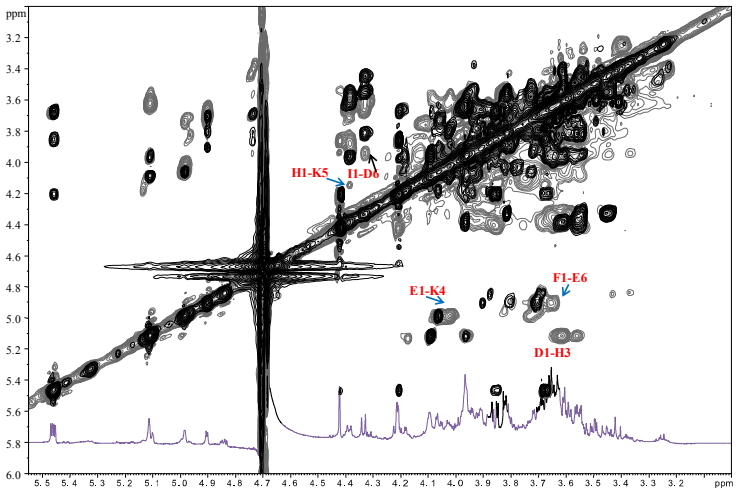

Figure 9.8 Section of the TOCSY (**black**) and NOESY (**gray**) spectra of the fully deacylated LOS from *T. hydrothermalis*. The relevant *inter*-residue NOE cross-peaks are shown.

substituted at position O-4 by galacturonic acid **L** via phosphodiester linkage. Furthermore, a strong NOE contact between H-1 **D** and H-3 **H** (Figures 9.7 and 9.8) attested that residue **H** was further substituted at position O-3 by galactofuranose **D**. This latter was, in turn, substituted at its O-6 by the terminal β-galactose unit **I**, highlighted by the NOE contact between H-1 **I** and H-$6_{a,b}$ **D** (Figures 9.7 and 9.8). In conclusion, the structure of core oligosaccharide moiety of LOS from *Thermomonas hydrothermalis* can be described as it follows:

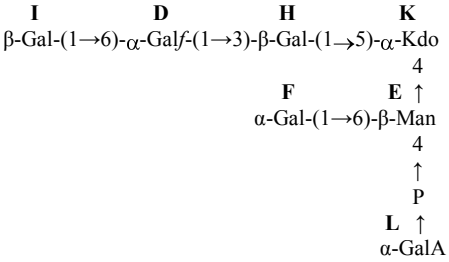

9.5 Structural analyses of lipid A and core oligosaccharide by MALDI mass spectrometry

In order to unveil the primary structure of lipid A from *Thermomonas hydrothermalis* LOS, an aliquot of intact LOS was analysed by MALDI MS spectrometry. The spectrum relative to the intact LOS (Figure 9.9) showed, at lower mass range, three ion peaks related to the lipid A moiety raising from the typical fragmentation between the lipid A portion and the Kdo-containing oligosaccharide domain (Sturiale *et al*., 2005). In particular, the main ion peak at *m/z* 1925.3 (Figure 9.9) was identified as a hexa-acylated bis-phosphorylated lipid A, carrying a galacturonic acid residue on both phosphate groups. The hexa-acylated lipid A was found to be characterized by the presence of two C11:0 (3-OH) in ester linkage and two C11:0 (3-OH) in amide linkage as primary fatty acids and two C11:0 as secondary fatty acids, in agreement with compositional analyses. The other two ion peaks related to the lipid A species were relative to lipid A species without one (*m/z* 1749.4) or two (*m/z* 1572.7) galacturonic acid residues (Figure 9.9). The nature and the positions of secondary acyl chains were also assessed analysing MALDI mass spectrum executed on the entire LOS after treatment with NH_4OH (Figure 9.10A), as previously described (Silipo *et al*., 2002). Thus, on the basis of mass spectrometry, chemical analyses and NMR spectroscopy data, the main lipid A species was depicted as reported in Figure 9.14.

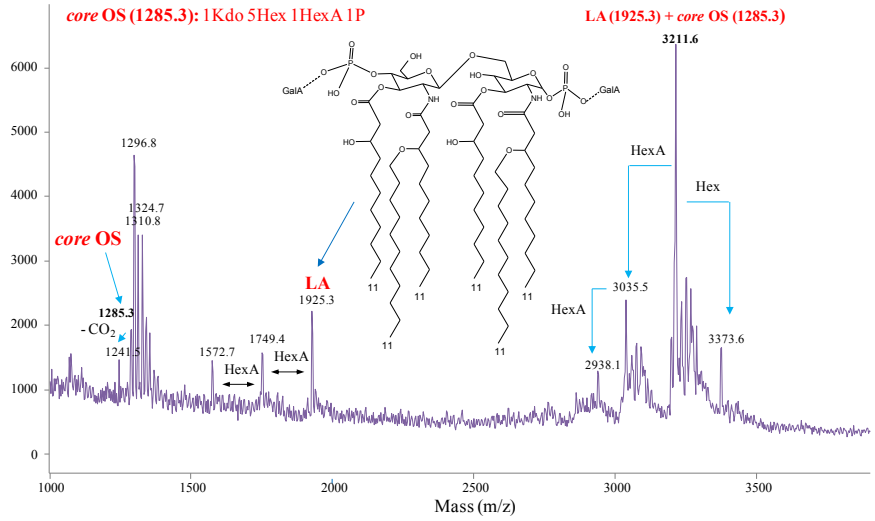

Figure 9.9 Negative-ion MALDI TOF mass spectrum of intact LOS of *Thermomonas hydrothermalis* recorded in linear mode. Assignment of the main ion peaks is shown. The main lipid A specie structure is sketched in the spectrum.

In Figure 9.9 it was also detectable the ion peak related to the core oligosaccharide moiety at *m/z* 1285.3 relative to a hexa-saccharide carrying an additional sugar residue, namely, the galacturonic acid linked to the core oligosaccharide via phosphodiester bridge, in agreement with the results by NMR analyses. At higher molecular masses (Figure 9.9), in the range 2800–3400Da, a cluster of ion peaks was detected corresponding to LOS species, given by the combination of core oligosaccharide and lipid A moieties. In particular main signal at *m/z* 3211.6 matched with a LOS characterized by a hexa-acylated bis-phosphorylated lipid A, carrying two galacturonic acids, covalently linked to a phosphorylated hepta-saccharide core moiety. Two minor peaks, at *m/z* 3035.5 and *m/z* 2938.1 (Figure 9.9) relative to LOS species without one or two galacturonic acid residues respectively, were also found. Further on, MALDI mass spectrometric analyses on the

de-O-acylated (Figure 9.10B) and fully deacylated LOS were undertaken. Spectrum inherent about the hydrazinolysis product (Figure 9.10B) showed the presence of an ion peak at *m/z* 1220.0 matching with a lipid A structure lacking in O-acyl chains, as expected, but lipid A species without one or two GalA residues were not present, in agreement with NMR data. Moreover, it was identified a cluster of peaks related to LOS species whose main signal (*m/z* 2505.5, Figure 9.10B) was consistent with the combination of the abovementioned lipid A (*m/z* 1220.0, Figure 9.10B) and the already described core oligosaccharide (*m/z* 1285.3, Figures 9.9 and 9.10A), further confirming NMR analyses. MALDI mass spectrum performed on fully deacylated LOS (not shown) corroborated all results about the core oligosaccharide structure reported above. In conclusion, all mentioned data allowed to define the complete structure of LOS from *Thermomonas hydrothermalis*, that is sketched in Figure 9.14.

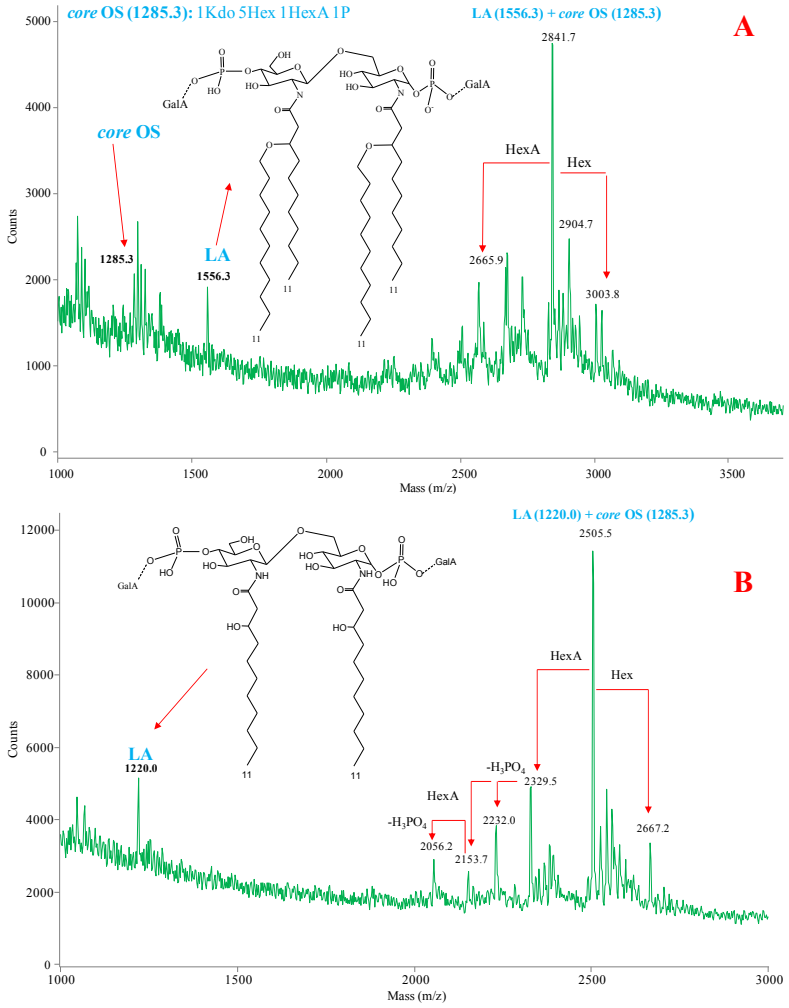

Figure 9.10 A) Negative-ion MALDI TOF mass spectrum of intact LOS of *Thermomonas hydrothermalis* after treatment with NH_4OH. Lipid A structure deprived of primary fatty acids in ester linkage to the diglucosamine backbone is shown. Assignment of the main ion peaks is indicated. **B)** Negative-ion MALDI TOF mass spectrum of purified LOS of *Thermomonas hydrothermalis* after de-O-acylation performed by using anhydrous hydrazine. Lipid A structure deprived of ester-linked acyl chains is sketched in figure. Assignment of the main ion peaks is shown.

9.6 Biological activity of isolated *T. hydrothermalis* LOS

To confirm the absence of contamination, the purified LOS of *T. hydrothermalis* was analysed for the presence of bacterial lipoproteins (BLPs) in HEK 293 cells expressing TLR2 (Nigro *et al.*, 2008), which is the PRR agonist of bacterial lipoprotein (BLP) (Figure 9.11A). NF-κB activation constituted the read out of this experiment. No activation of NF-κB was recorded, in agreement with the chemical data that confirm the absence of BLP in our sample (Figure 9.11A). Therefore, the biological activity of LOS was assessed in the model of HEK293 cells, which stably express human CD14, MD-2 and TLR4. HEK 293 hTLR4 were exposed to different LOS concentrations (1, 10 and 100 ng/ml). The *Escherichia coli* LPS, which possess a fully hexa-acylated lipid A structure, acts as a potent agonist for TLR4-MD2-CD14 receptors (see also Section III). This LPS was used as a positive control at the same concentrations as before. NF-κB activation was evaluated through the assessment of luciferase activity after 4 h stimulation. Likewise, IL-8 release was recorded via enzyme-linked immunosorbent assay (ELISA) after 4 h stimulation. The results showed that the *T. hydrothermalis* LOS induced a significantly lower NF-κB activation with respect to cells exposed to LPS of *E. coli* (LOS of *T. hydrothermalis vs* LPS of *E.coli* $p<0.01$ at 1 ng/ml, $p<0.001$ at 10 ng/ml and 100 ng/ml). In accordance with NF-κB activity, the level of IL-8 expression is lower after stimulation with *T. hydrothermalis* LOS with respect to LPS from *E. coli* LPS (LOS *T. hydrothermalis vs* LPS *E. coli* $p<0.001$ at 10 ng/ml and 100 ng/ml) (Figure 9.11B). It was then assessed whether *T. hydrothermalis* LOS could interfere with the TLR4-mediated signaling induced by hexa-acylated lipid A. HEK 293 hTLR4 cells were pre-incubated 1 h with different amounts (1, 10 and 100 ng/ml) of LOS and then exposed to 10 ng/ml of hexa-acyl *E. coli*

LPS for 4 h. *T. hydrothermalis* LOS significantly antagonized hexa-acyl LPS-dependent TLR4-mediated NF-κB activation and IL-8 release at the concentrations of 1 ng/ml (LOS *T. hydrothermalis vs* LPS *E.coli* P<0.05) (Figure 9.12).

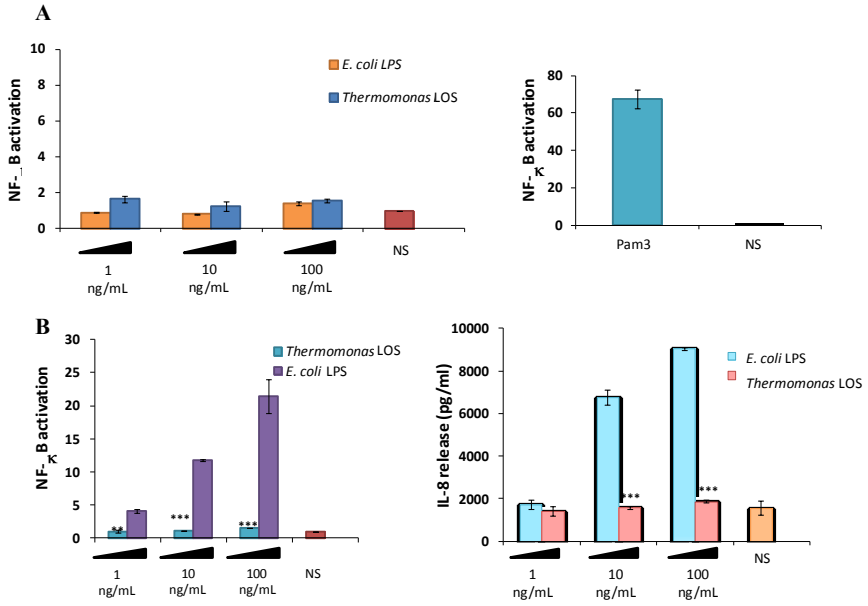

Figure 9.11 A) Assessment of contaminations in LOS. Fold of NF-κB activation upon stimulation of HEK 293 hTLR2 with 1,10 and 100 ng/ml of *T. hydrothermalis* LOS for 6h. Hexa-acylated *E. coli* LPS and Pam3CSK4 were used as controls. *p,0.05, **p,0.01, ***p,0.001 in the Student's t-test (*T. hydrothermalis* LOS vs *E. coli* LPS). **B)** Stimulation of HEK 293-hTLR4/MD2-CD14 with LOS derived from *T. hydrothermalis*. Fold of activation of NF-κB and IL-8 release after 4 h of stimulation with 1, 10 and 100 ng/ml of LOS; commercial LPS of *E. coli* was used as a control. Significant difference between *T. hydrothermalis* LOS generated values and the corresponding *E. coli* LPS values are indicated (*T. hydrothermalis* LOS vs E. coli LPS) (*P<0.05; **P <0.01; ***P <0.001).

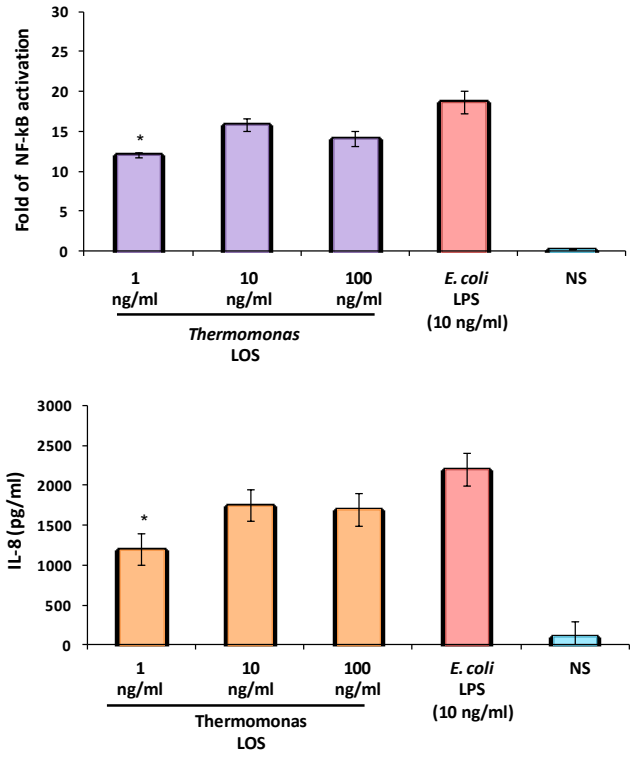

Figure 9.12 Competition assay. Fold of NF-κB activation and IL-8 release in HEK 293 hTLR4/MD2-CD14 stimulated with different concentrations (1, 10 and 100 ng/ml) of *T. hydrothermalis* LOS for 1 h and then re-stimulated with 10 ng/ml of *E. coli* LPS (LPS-EB ultrapure, InvivoGen) for 4 h. Significant difference between *T. hydrothermalis* LOS generated values and the corresponding *E. coli* LPS values are indicated (*T. hydrothermalis* LOS vs *E. coli* LPS) (*P<0.05; **P <0.01; ***P <0.001).

Furthermore it was compared the ability of the LOS of *T. hydrothermalis* to activate Bone Marrow-Derived Macrophages (BMDMs) for cytokine production (TNF-α, KC). BMDMs were treated with 1, 10 and 100 ng/ml of the *T. hydrothermalis* LOS, as above, and cytokine release was recorded after 18 h (Figure 9.13). Hexa-acylated *E. coli* LPS was used in parallel as a control. It was found that at all concentrations used *T. hydrothermalis* LOS

elicited significantly lower amounts of TNF-α release (LOS *T. hydrothermalis vs* LPS *E.coli* $p<0.05$ at 1 and 10 ng/ml, $p<0,01$ for 100ng/ml) and significantly lower amounts of KC release (LOS *T. hydrothermalis vs* LPS *E.coli* $p<0.05$ at 1 and 100 ng/ml, $p<0,01$ for 10 ng/ml) than *E. coli* LPS (Figure 9.13).

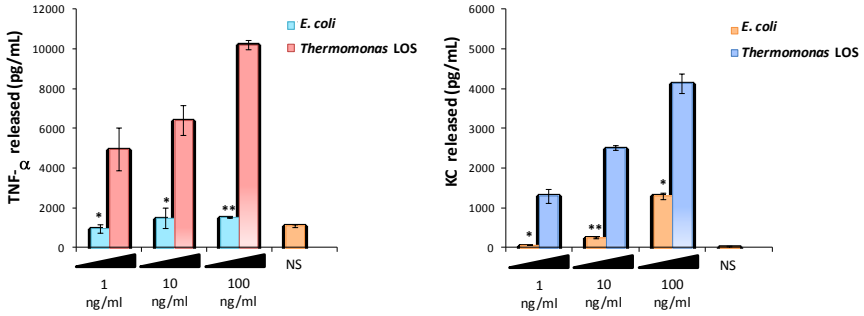

Figure 9.13 Cytokine release in BMDMs stimulated with *T. hydrothermalis* LOS. TNF-α and KC released by BMDMs after stimulation with 1, 10 and 100 ng/ml of LOS derived from *T. hydrothermalis* and *E. coli* LPS, measured by ELISA at 18 h. Significant difference between *T. hydrothermalis* LOS generated values and the corresponding *E. coli* LPS values are indicated (*T. hydrothermalis* LOS vs *E. coli* LPS) (*P<0.05; **P <0.01; ***P <0.001).

9.7 Discussion

Evolutionary bacterial adaptation to the extreme temperatures implies structural variations in outer and inner membranes of microbial cells. Since lipopolysaccharides are the main components of the outer leaflet of the external membrane of Gram-negative bacteria, it is reasonable to assume that some structural changes should also characterise LPSs isolated from thermophiles as *Thermomonas hydrothermalis*. Consequently, the elucidation of the full chemical structure of LPSs is a crucial point in order to dissect

the molecular mechanisms underlying their essential role in the adaptation of *T. hydrothermalis* to the peculiar external temperatures and also to define their activity on the components of the innate immunity system. In this context, it was determined the complete structure of *T. hydrothermalis* R-LPS enriching structural data with important results regarding the bioactivity of purified LOS tested on innate immune system cells. Structural elucidation of LOS was achieved by a multi-techniques approach comprising compositional analyses, 1D and 2D NMR spectroscopy and MALDI-MS spectrometry experiments. In details, the lipid A structure was carried out by mass spectrometric analysis executed on the intact LOS and all results were corroborated by fatty acids analysis and by further MALDI-MS experiments performed on partially deacylated lipooligosaccharide; whereas the elucidation of the core oligosaccharide skeleton was achieved by a combination of NMR experiments executed on the de-O-acylated and on the fully deacylated LOS but also by MALDI-MS experiments performed on the intact LOS and on its deacylated forms. *Thermomonas hydrothermalis* LOS was found to be characterised by a unique structure (Figure 9.14), lacking in heptose residues, composed of a hexa-saccharide skeleton in which the phosphorylated mannose residue (Figure 9.14) carries an additional sugar unit, a galacturonic acid, via phosphodiester linkage. Moreover, also lipid A turned out to have a peculiar backbone structure:[α-D-GalA*p*1→P→4-β-D-Glc*p*N-(1→6)-α-D-Glc*p*N1→P←1-α-D-GalA*p*] acylated by two C11:0 (3-OH) in ester linkage and two C11:0 (3-OH) in amide linkage as primary fatty acids and two C11:0 as secondary fatty acids (Figure 9.14). Thus, the overall structure of *T. hydrothermalis* LOS showed to be, at physiological pH, highly negatively charged since it possesses three phosphate groups and four sugar residues bearing carboxyl groups represented by Kdo unit and galacturonic acid residues.

This peculiarity confers to the entire macromolecule the ability to interact with divalent cations normally present on the surface of the outer membrane; these interactions between LOS-negative charges and aforesaid cations contribute to the rigidity and to the tightness of the outer membrane, resulting in bacterial high resistance to external stresses (Alexander and Rietschel, 2001). These findings concerning LOS structure might explain the *Thermomonas hydrothermalis* capability to survive in a hot spring at the uncommon temperature of 50°C, giving further confirmations to the key role of lipopoly/lipooligosaccharides on extremophilic bacterial outer membrane. Furthermore, since LPS/LOS is involved in immune system elicitation, it was mandatory to investigate the immunostimulatory activity of *T. hydrothermalis* LOS. This latter showed a lower ability to engage the TLR4-MD2-CD14 pathway with respect to the hexa-acylated LPS of *E.coli*. This is a fascinating result as the *T. hydrothermalis* lipid A is hexa-acylated like the *E. coli* lipid A, which is considered, as mentioned above, the prototype of the agonist of the TLR4 complex (Park *et al*., 2009) (see also Section III). However, several differences could underline the low immunopotential of this LOS: (i) the presence in *T. hydrothermalis* lipid A of acyl chains shorter than those of *E. coli* (11 carbon atoms *vs* 14 carbon and 12 carbon atoms); (ii) the symmetry of lipid A which is decorated by 3 acyl residues on each glucosamine molecule and, finally, (iii) the presence of galacturonic acid on both phosphate groups. Even if the addition of these residues should not influence the negative charge of the two phosphate groups, the change of the binding of the two decorated phosphates with the MD2-TLR4 complex is supposed to modulate the activation of the down-stream signaling. Interestingly, the *T. hydrothermalis* lipid A also displayed an antagonistic activity *vs* the hexa-acylated *E. coli* LPS at low dose; this property has been

extensively reported for tetra-acylated lipid A, such as eritoran and lipid IV_A (Kim *et al*., 2007; Ohto *et al*., 2007) (see also Section III).

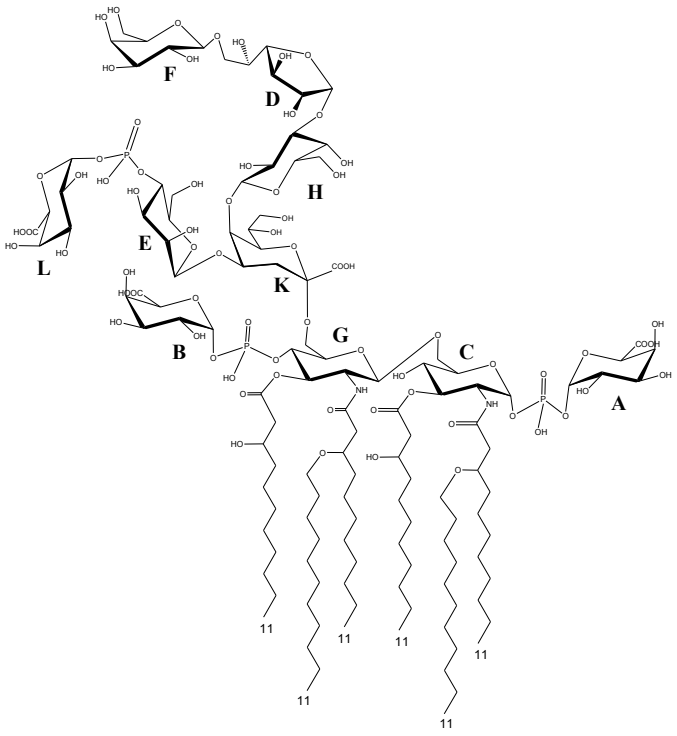

Figure 9.14 LOS from *Thermomonas hydrothermalis*.

Several models support the antagonistic activity of these molecules by disturbing the binding of the fully potent LPS and preventing the TLR4 dimerization (Saitoh *et al*., 2004). Nevertheless, the structures and activity of the molecular complexes, especially the intermediate forms, resulting upon LPS TLR4-MD2 binding are not fully understood. In this sense, it was not possible to identify the mechanism allowing the *T. hydrothermalis* lipid A to successfully compete with *E. coli* LPS in TLR4 binding.

Consistently with data of TLR4 activation, in BMDM the *T. hydrothermalis* LOS elicits a low amount of inflammatory cytokine, such as TNF-α and KC, thus confirming the low biological activity of this molecule.

References

Alexander C., Rietschel E.T., Bacterial lipopolysaccharides and innate immunity. **2001**, *J. Endotoxin Res.*, 7: 167-202.

Alves M.P., Rainey F.A., Nobre M.F., da Costa M.S., *Thermomonas hydrothermalis* sp. nov., a new slightly thermophilic gamma-proteobacterium isolated from a hot spring in central Portugal. **2003**, *System. Appl. Microbiol.*, 26, 70-75.

Brock T.D., High temperature systems. **1970**, *Annual Review of Ecology and Systematics*, 1, 191-220.

Brock T.D. in *Thermophiles: General, Molecular and Applied Microbiology* (Ed.: Brock T.D.), John Wiley & Sons, New York, 1-16, **1986**.

Bowers K.J., Wiegel J., Temperature and pH optima of extremely halophilic archaea: a mini-review. **2011**, *Extremophiles*, 15, 119-128.

Choquet C.G., Patel G.B., Beveridge T.J., Sprott G.D., Stability of pressure-extruded liposomes made from archaeobacterial ether lipids. **1994**, *Appl. Microbiol. Biotechnol.*, 42(2-3), 375-84.

De Castro C., Parrilli M., Holst O., Molinaro A., Microbe-associated molecular patterns in innate immunity: Extraction and chemical analysis of gram-negative bacterial lipopolysaccharides. **2010**, *Methods Enzymol.*, 480, 89-115.

Galanos C., Luderitz O., Westphal O., A new method for the extraction of R lipopolysaccharides. **1969**, *Eur. J. Biochem.*, 9, 245-249.

Gulik A., Luzzati V., De Rosa M., Gambacorta A., Structure and polymorphism of bipolar isopranyl ether lipids from archaebacteria. **1985**, *J. Mol. Biol.*, 182(1), 131-49.

Hakomori S., A rapid permethylation of glycolipid, and polysaccharide catalyzed by methylsulfinyl carbanion in dimethyl sulfoxide. **1964**, *J. Biochem.*, 55, 205-208.

Holst O., Deacylation of lipopolysaccharides and isolation of oligosaccharide phosphates. **2000**, *Methods Mol. Biol.*, 145, 345-353.

Kim H.M., Park B.S., Kim J.I., Kim S.E., Lee J., Oh S.C., Enkhbayar P., Matsushima N., Lee H., Yoo O.J., Lee J.O., Crystal structure of the TLR4-MD-2 complex with bound endotoxin antagonist Eritoran. **2007**, *Cell*, 130, 906-917.

Kittelberger R., Hilbink F., Sensitive silver-staining detection of bacterial lipopolysaccharides in polyacrylamide gels. **1993**, *J. Biochem. Biophys. Methods*, 26 (1), 81-86.

Leontein K., Lönngren J., Determination of the absolute configuration of sugars by Gas-Liquid Chromatography of their acetylated 2-octyl glycosides. **1978**, *Methods Carbohydr. Chem.*, 62, 359-362.

Madigan M.T., Marrs B.L., Extremophiles, *Scientific American*, **1997**.

Mesbah N.M., Wiegel J., Life at extreme limits: the anaerobic halophilic alkalithermophiles. **2008**, *Ann. NY Acad. Sci.*, 1125, 44-57.

Nigro G., Fazio L.L., Martino M.C., Rossi G., Tattoli I., Liparoti V., De Castro C., Molinaro A., Philpott D.J., Bernardini M.L., Muramylpeptide shedding modulates cell sensing of *Shigella flexneri*. **2008**, *Cell Microbiol*., 3, 682-695.

Ohto U., Fukase K., Miyake K., Satow Y., Crystal structures of human MD-2 and its complex with antiendotoxic lipid IV_A. **2007**, *Science*, 316(5831), 1632-1634.

Park B.S., Song D.H., Kim H.M., Choi B.S., Lee H., Lee J.O., The structural basis of lipopolysaccharide recognition by the TLR4-MD-2 complex. **2009**, *Nature*, 458 (7242), 1191-1195.

Prado A., da Costa M.S., Laynez J., Madeira V.M., Physical properties of membrane lipids isolated from a thermophilic eubacterium (*Thermus* sp.).**1988**, *Adv. Exp. Med. Biol*., 238,47-58.

Rose J.R., Christ W.J., Bristol J.R., Kawata T., Rossignol D.P., Agonistic and antagonistic activities of bacterially derived Rhodobacter sphaeroides lipid A: comparison with activities of synthetic material of the proposed structure and analogs. **1995**, *Infect. Immun.*, 63, 833-839.

Saitoh S., Akashi S., Yamada T., Tanimura N., Kobayashi M., Konno K., Matsumoto, F., Fukase K., Kusumoto S., Nagai Y., Kusumoto Y., Kosugi A., Miyake K., Lipid A antagonist, lipid IVa, is distinct from lipid A in interaction with Toll-like receptor 4 (TLR4)-MD-2 and ligand-induced TLR4 oligomerization. **2004**, *Int. Immunol.*, 16(7), 961-969.

Silipo A., Lanzetta R., Amoresano A., Parrilli M., Molinaro A., Ammonium hydroxide hydrolysis: a valuable support in the MALDI-TOF mass spectrometry analysis of Lipid A fatty acid distribution. **2002**, *J. Lipid Res.*, 43, 2188-2195.

Stetter K.O., Extremophiles and their adaptation to hot environments. **1999**, *FEBS Letters*, 452, 22-25.

Sturiale L., Garozzo D., Silipo A., Lanzetta R., Parrilli M., Molinaro A., New conditions for matrix-assisted laser desorption/ionization mass spectrometry of native bacterial R-type lipopolysaccharides. **2005**, *Rapid Commun. Mass Spectrom.*, 19, 1829-1834.

Taylor M.P., Van Zyl L., Tuffin M., Cowan D. in *Extremophiles: Microbiology and Biotechnology* (Ed.: R. P. Anitori), Caister Academic Press, Norfolk (UK), 1-24, **2012**.

van de Vossenberg J.L., Driessen A.J., Konings W.N., The essence of being extremophilic: the role of the unique archaeal membrane lipids. **1998**, *Extremophiles*, 2(3), 163-70.

SECTION V

Experimental Section

Chapter 10

Bacterial Growth and LPS Structural Analysis

10.1 Growth of *Burkholderia dolosa* cells for LOS extraction

Burkholderia dolosa IST4208 isolate was obtained from the respiratory secretions of a CF patient under surveillance at the Hospital de Santa Maria CF Center, in Lisbon. Isolate *B. dolosa* IST4208 was obtained in 2005 from a CF patient who passed away. Consent was obtained from the patient, and the isolate was provided by the hospital for this particular study; the patient's anonymity was preserved. This isolate was identified based on the polymorphisms of the recA gene (Vermis *et al*., 2004), followed by multilocus sequence typing (MLST) analysis. The MLST sequences of the allelic type of seven loci were assigned and submitted to the *B. cepacia* complex MLST database (http://pubmlst.org/bcc/) under the designation ST-668; the obtained profile confirmed the identification as *B. dolosa*.
Cells of *B. dolosa* IST4208 were grown overnight in lysogeny broth (LB; Difco, Sparks, MD), then inoculated into LB (initial OD_{640nm} 0.05) and grown in shake flasks with orbital agitation (250 rpm, 37°C) until mid-exponential phase. The cell culture was diluted (standardized OD_{640nm} 0.2±0.02), and a sample (100 mL) was plated onto LB agar (Difco) plates. These plates were incubated (37°C, 24 h) to allow cells to grow on the agar surface, to mimic bacterial growth in CF lungs. Cells were scraped, collected, autoclaved, and lyophilised.

10.2 Isolation of *Pseudomonas aeruginosa* strain RP73

The *P. aeruginosa* clinical isolate RP73 was isolated after 17 years of chronic lung infection in a CF patient (Jeukens *et al*., 2013). The strain was kindly provided by Prof. Burkhard Tummler (Klinische Forschergruppe, Medizinische Hochschule, Germany).

The strain was plated on trypticase soy agar (TSA) plates and cultured in trypticase soy broth (TSB) at 37°C.

10.3 Bacterial growth conditions for *Burkholderia cenocepacia* ΔarnBC and ΔarnT-arnBC^{+} strains

Bacterial strains were grown in LB medium at 37°C. Bacterial were grown in LB medium at 37°C. When required, antibiotics were added as follows: trimethoprim, 50 mg ml^{-1} for *E. coli* and 100 mg ml^{-1} for *B. cenocepacia*; tetracycline 20 mg ml^{-1} for *E. coli* and 100 mg ml^{-1} for *B. cenocepacia*; and kanamycin 40 mg ml^{-1} for *E. coli*. Gentamicin at 10 mg ml^{-1} and ampicillin at 100 mg ml^{-1} were used for triparental mating to select against donor and helper *E. coli* strains. Rhamnose was added to a final concentration of 0.4% as needed. Antibiotics and chemicals were purchased from Sigma Chemical (St Louis, MO, USA).

10.4 Growth of *Thermomonas hydrothermalis* cells

Strains SGM-6^{T} were isolated from the hot spring at São Gemil in Central Portugal. Water samples were transported at ambient temperature and filtered through membrane filters (Gelman type GN-6; pore size 0.45 μm, diameter 47 mm) within 12 hours, which were placed on the surface of *Thermus* agar plates. These preparations were wrapped in plastic bags and incubated at 50 °C for up 7 days. Cultures were purified by sub-culturing and were preserved at –80 °C in *Thermus* medium containing 15% glycerol (Alves *et al*., 2003). Growth of the organisms was examined in several media but was consistently better with *Thermus* medium, which was adopted to grow the organisms, unless otherwise stated. Cell morphology, dimensions and motility were examined by phasecontrast microscopy during exponential growth in liquid medium. The number and position of flagella were determined by

light microscopy after staining of the cells with the Ryu stain (Heimbrook *et al*., 1989; Alves *et al*., 2003).

10.5 Chemical Analyses

Determination of monosaccharides and of their absolute configuration through GC-MS analysis, were all carried out as described (Leontein and Lönngren, 1978). Sugar residues were identified as acetylated *O*-methyl glycosides derivatives. After methanolysis (1.25M HCl/MeOH, 85°C, 16 h) and acetylation with acetic anhydride in pyridine (85°C, 30 min) the sample was analysed by GC-MS. The absolute configuration of monosaccharides has been elucidated by GC-MS analysis of the acetylated *O*-(+)-Oct-2yl glycosides derivatives and comparison with standards. Linkage analysis was carried out by methylation of both complete core region and complete O-chain region as described (Hakomori, 1964): the sample was methylated with iodomethane, hydrolysed with 2 M trifluoroacetic acid (100°C, 2 h), carbonyl-reduced with $NaBD_4$, acetylated with acetic anhydride and pyridine, and analyzed by GC-MS. Total fatty acid content was determined by acid hydrolysis. LOS was first treated with HCl 4M (4h, 100°C) and then neutralised with NaOH 5M (30 min, 100°C). Fatty acids were then extracted in $CHCl_3$, methylated with diazomethane and analysed by GC-MS. The ester bound fatty acids were selectively released by base-catalysed hydrolysis with NaOH 0.5M/MeOH (1:1 v/v, 85°C, 2h), then the product was acidified, extracted in $CHCl_3$, methylated with diazomethane and analysed by GC-MS. The absolute configuration of fatty acids was determined as described (Rietschel, 1976)

10.6 Isolation of oligosaccharide (OS) from *B. dolosa*, *B. cenocepacia* IST and K56-2 strains

Isolation of OS was obtained by mild acid hydrolysis. Purified LOS (~10 mg) was dissolved in acetate buffer (1 mL, pH 4.4). SDS (1 mg/mL) was added, and hydrolysis proceeded (100°C, 3 h). After lipid A removal by centrifugation (10 000g, 30 min), the water-soluble product was purified by gel filtration chromatography on a Bio-Gel P-6 column (Bio-Rad, Hercules, CA).

10.7 Isolation of polysaccharide portion from *Padoraea pulmonicola*

The O-chain moiety was isolated by performing a mild acid hydrolysis. The purified LPS (~7 mg) was dissolved in acetate buffer (1 mL, pH = 4.4), SDS (1 mg/mL) was added, and the hydrolysis was carried out at 100°C for 3 h. After lipid A removal by centrifugation, the water-soluble product was then purified by gel filtration chromatography on a Sephacryl S-100 column.

10.8 Isolation of oligosaccharide moiety from *Pseudomonas aeruginosa* RP73 and *Thermomonas hydrothermalis*

LOS was treated with anhydrous hydrazine (1 mL), stirred at 37 °C for 90 min, cooled, poured into ice-cold acetone (20 mL) to allow its precipitation. Precipitated LOS was centrifuged (3000 g, 30 min), washed with ice-cold acetone, dried, dissolved in water, and lyophilized. The O-deacylated LOS product was *N*-deacylated with 4M hot KOH as described (Silipo *et al*., 2012). After removal of salts by gel permeation chromatography with Sephadex G-10

(Pharmacia) column, the resulting oligosaccharide OS was lyophilized.

10.9 Isolation lipid As from all bacterial strains analysed

Free lipid A was obtained by hydrolysis (100°C, 3 h) of LOS in sodium acetate buffer (100 mM, pH 4.4). The solution was extracted three times with $CHCl_3$/MeOH/H_2O (100:100:30, v/v/v) and centrifuged (10000g, 30 min). The obtained precipitate (free lipid A) was washed with water.

10.10 NMR Analyses

All the structural assignments of core oligosaccharides moieties characterised (chapters 3,5-7,9) and of O-chain portion isolated from *P. pulmonicola* (chapter 4) were carried as follows. 1D and 2D ^{1}H NMR spectra were recorded in D_2O (300 K, pD 7) with a 600 DRX spectrometer (Bruker) equipped with a cryoprobe. The spectrometer was internally calibrated with acetone (δ_H=2.225 ppm; δ_C=31.45 ppm). ^{31}P NMR experiments were carried out with a Bruker DRX-400 spectrometer; aqueous 85% phosphoric acid was used as external reference (δ = 0.00 ppm). Rotating frame Overhauser enhancement spectroscopy (ROESY) and nuclear Overhauser enhancement spectroscopy (NOESY) experiments were performed using data sets (t1×t2) of 4096×256 points with mixing times between 100 and 400 ms. Double quantum-filtered phase-sensitive COSY experiments were executed with sets of 4096×512 points. Total correlation spectroscopy (TOCSY) experiments were performed with spinlock times of 100 ms with data sets (t1×t2) of 4096×256 points. The data matrix in all the homonuclear experiments was zero-filled in both dimensions to give a matrix of 4 K×2 K points, and was resolution-enhanced in

both dimensions using a cosine-bell function before Fourier transformation. Coupling constants were determined by 2D phase-sensitive DQF-COSY (Piantini *et al*., 1982; Rance *et al*., 1983).

Heteronuclear single quantum coherence (HSQC) and heteronuclear multiple bond correlation (HMBC) experiments were performed in ^{1}H-detection mode by single-quantum coherence with proton decoupling in the ^{13}C domain using data sets of 2048×256 points. Experiments were carried out in the phase-sensitive mode. (States *et al*., 1982) A 60 ms delay was used for the evolution of long-range correlations in the HMBC experiment. The data matrix in all the heteronuclear experiments was extended to 2048×1024 points by using forward linear prediction extrapolation.

10.11 MALDI TOF mass spectrometry analysis

MALDI-TOF mass spectra were recorded in the negative and positive polarity in linear mode on a Perseptive (Framingham, MA, USA) Voyager STR equipped with delayed extraction technology. High resolution mass spectra were acquired in reflector mode on a 4800 Proteomics analyzer MALDI TOF/TOF mass spectrometer (Applied Biosystems, Framingham, MA, USA). In this case mass spectra, resulting from the sum of 1250 laser shots, were obtained with a resolution higher than 10000 (as the ratio between the mass of the peak and its full width at half maximum intensity) and with mass accuracy below 100 ppm.

Lipid A samples were dissolved in $CHCl_3/CH_3OH$ (50:50, v/v) at a concentration of about 25 pmol/μL. Matrix solution was prepared by dissolving 2,4,6-trihydroxyacetophenone (THAP) in CH_3OH/0.1% trifluoroacetic acid/CH_3CN (7:2:1, v/v) at a concentration of 75 mg/mL. A 1:1, v/v sample/matrix solution mixture (<1μl) was deposited onto a stainless-steel MALDI sample plate , and left to dry at room temperature.

LOS sample required a more laborious preparation as recently reported (Sturiale *et al*., 2005). Briefly, a small amount of the intact LOS was first suspended in a mixture of methanol/water (1:1) containing 5mM ethylenediaminetetraacetic acid (EDTA) and allowed to dissolve by a brief ultrasonication. A few microliters of the obtained mixture were then desalted on a small piece of ParafilmTM with some grains of cation-exchange beads (Dowex 50WX8-200, Sigma–Aldrich), previously converted into the ammonium form; 0.3 μL of this sample solution was finally deposited, together with the same volume of 20 mM dibasic ammonium citrate, in a thin layer of homogeneous matrix film obtained from a solution whose components were 2,4,6-trihydroxyacetophenone (THAP), 200 mg/mL in methanol, and nitrocellulose (Trans-blot membrane, BioRad), 15 mg/mL in acetone/propan-2-ol (1:1 v/v), mixed in a 4:1 v/v ratio. MS analysis of the oligosaccharide sample was performed utilising a matrix solution of dihydroxybenzoic acid (DHB) 50 mg/ml in TFA 0.1% ACN 80/20, by the classic dried drop method: 1 μl of a sample/matrix solution mixture (1:1, v/v) was deposited onto the MALDI sample plate and left to dry at room temperature.

10.12 HEK293 hTLR4/CD14/MD-2 cell culture, transfection, and stimulation of *B. dolosa*

Stably transfected HEK cell line 293-hTLR4-MD2-CD14 (Invivo-Gen, San Diego, CA) was cultured in DMEM (Lonza, Basel, Switzerland) with 10% FBS (Euroclone, Pero, Italy). Blasticidin-S (10 mg/mL; InvivoGen) and HygroGold (50 mg/mL; InvivoGen) were added to cell cultures according to the manufacturer's instructions. The cells were transiently transfected by using PolyFect Transfection Reagent (Qiagen) according to the manufacturer's instructions. For NF-kB studies, the cells were seeded into 96-well plates at a concentration of 3×10^5 cells per mL,

then transfected overnight with a reaction mixture of PolyFect transfection reagent (1 mL, Qiagen), and plasmids pGL3.ELAM.tk (150 ng; Promega), pRLTK (15 ng; Promega) (Silipo et al., 2004). pGL3.ELAM.tk encodes Firefly luciferase under control of the NF-kB promoter; pRLTK encodes Renilla luciferase, and was used as a control. HEK 293 hTLR4/MD2/CD14 cells were exposed to different concentrations of B. dolosa LOS or E. coli LPS (1, 10, or 100 ng/mL; Ultra-pure LPS-EB, InvivoGen), and stimulation was for 4 h.

10.13 Bone marrow-derived macrophages (BMDMs) culture and stimulation assay with *B. dolosa* LOS

Bone marrow-derived macrophages (BMDMs) were derived from bone marrow cells collected from five-week-old wildtype C57BL/6 female mice (Charles River Laboratories; all animals were maintained in a specific pathogen-free animal facility at the Sapienza University of Rome (Italy)). BMDMs were differentiated over 7 days in RPMI 1640 medium (Lonza), supplemented with heat-inactivated FBS (10%, Euroclone), L-glutamine (2 mM), sodium pyruvate (5 %), non-essential amino acids (NEAA 100×; 100 mm, Euroclone), β-mercaptoethanol (0.5%, Gibco), and macrophage colony-stimulating factor (30 ng/mL; Miltenyi Biotec, Calderara di Reno, Italy). At 7 days, BMDMs were characterized by immunostaining with FITC-F4/80 and Mac-1/CD11b (clone M1/70) monoclonal antibodies (Abcam, catalogue number ab105155 and BD Pharmingen, catalogue number 557397, respectively) by flow cytometric analysis in a FACSCalibur cytometer (BD Biosciences).

For stimulation assays, BMDMs were seeded in 24-well plates (5×105 cells per well), exposed to different concentrations of *B. dolosa* LOS or *E. coli* LPS (1, 10, or 100 ng/mL) and incubated for

12 h. Cell suspension supernatants were recovered and processed to measure TNF-α (R&D Systems, catalogue number DY410), IL-10 (R&D Systems, catalogue number DY417), and IL-6 (R&D Systems, catalogue number DY406) production by DuoSet ELISA assay according to manufacturer's instructions.

In the competition assays, BMDMs were primed with B. dolosa LOS (1, 10, or 100 ng/mL) for 1 h and then re-stimulated with of *E. coli* LPS (10 ng/mL). After 12 h of re-stimulation, TNF-α, IL-10, and IL-6 production was quantified by ELISA assay (DuoSet) according to manufacturer's instructions.

10.14 Mice treatment in *P. aeruginosa* LOS analysis

C57Bl/6NCrlBR mice (20–22 gr) were purchased by Charles River. Mice were housed in filtered cages under specific-pathogen free conditions and permitted unlimited access to food and water. Mice were exposed to intranasal injection of LOS (15 μg/mouse) derived from *P. aeruginosa* RP73 clinical isolate. Commercial LPS derived from PAO1 strain (Sigma-Aldrich) was used as reference. Control animals were exposed to phosphate buffered saline (PBS). Sixteen hours after exposure, mice were sacrificed and bronchoalveolar lavage fluid (BALF) was performed by washing the lungs three times with 1 ml of RPMI (Euroclone) with proteinase inhibitors. Lungs were removed and homogenised in 1 ml of PBS with ions containing proteinase inhibitors. Total cells present in the BALF were counted, and a differential cell count was performed on cytospins stained with Diff Quick (Dade, Biomap, Italy). Erythrocyte present in the BALF were lysed with ACK lysis solution (Sigma Aldrich), cells were then resuspended in cetyltrimethylammonium chloride 0.5% (Sigma Aldrich) and centrifuged. Supernatants were used to analyze the myeloperoxidase (MPO) activity by ELISA assay (Moalli *et al*., 2011).

10.15 HEK293 cell activation assay-luciferase reporter assay in chapter 8

HEK293 cells were seeded in 96-well plates at $3x10^4$ cells/well and incubated overnight in a humidified atmosphere (5% CO_2) at 37°C. The next day, when cells were 60-80 % confluent, they were co-transfected with the plasmids for MD-2 (10 ng), TLR4 (1 ng), NF-κB-dependent luciferase (50 ng) and constitutive Renilla (10 ng) expression using JetPEI transfection reagent (all amounts are in ng/well). Cells were stimulated 6 hours after transfection with endotoxin preparations. Cells were lysed after 16 hours of stimulation in 1x reporter assay lysis buffer (Promega, USA) and analysed for reporter gene activities using a dual-luciferase reporter assay system. Relative luciferase units (RLU) were calculated by normalizing each sample's luciferase activity for constitutive Renilla activity measured within the same sample.

10.16 HEK293 hTLR4/CD14/MD-2 cell culture, transfection, and stimulation in *T. hydrothermalis* analysis

HEK 293 hTLR4/MD2/CD14 were exposed to different concentrations of *T. hydrothermalis* LOS or *E. coli* LPS (LPS-EB ultrapure, InvivoGen) at different concentrations (1, 10, 100 ng/ml) and stimulation was prolonged for 4 h. For the competition assay, cells were primed with *T. hydrothermalis* LOS (1, 10 and 100 ng/ml) for 1 h and then re-stimulated with 10 ng/ml of *E. coli* LPS (LPS-EB ultrapure, InvivoGen) for 4 h. To assess the absence of contamination in LPS preparations HEK 293 hTLR2 were stimulated with LOS derived from *T. hydrothermalis* or *E. coli* LPS. Pam3CSK4 (invivoGen) was used with HEK 293 hTLR2. NF-κB-dependent luciferase activity was measured using the Dual-

Luciferase® Reporter Assay System (Promega, Milan, Italy), as reported (Nigro et al., 2008). Cell supernatants were recovered and IL-8 release in cell culture supernatants were measured using DuoSet R&D System.

10.17 BMDMs culture and stimulation assays in *T. hydrothermalis* analysis

Bone marrow-derived macrophages (BMDMs) were derived from bone marrow cells collected from five-week old wild-type C57BL/6 (Charles River Laboratories). For stimulation assays, BMDMs were seeded into 24-well plates ($5x10^5$ cells/ml) and were exposed to different concentrations of *T. hydrothermalis LOS* or *E. coli* LPS (1, 10, 100 ng/ml) for 18 h. Cell supernatants were recovered and cytokine levels in cell culture supernatants were measured through ELISA using DuoSet R&D System, following manufacturer suggestions.

10.18 Molecular modeling on *B. cenocepacia* LOS and lipid A

10.18.1 Docking studies of LAMUT-and BCLA on MD-2

Each ligand, LAMUT and BCLA, was docked into human and murine MD-2 protein using AutoDock 4.2, and separately using AutoDock Vina 1.1.2. For human MD-2 (from PDB 3fxi), the Autogrid grid point spacing was set at 0.375 Å, center coordinates of the grid box were 29.00, -7.00, 17.875(x, y, z), and number of grid points in xyz was 41, 53, 83. For murine MD-2 (from PDB 3vq2), the Autogrid grid point spacing was set at 0.375 Å, center coordinates of the grid box were -27.50, -15.50, 22.00 (x, y, z), leading to with 75 x 40 x 60 (x, y, z) grid points. Best result from each docking job with BCLA was used as starting geometry for

subsequent docking calculations. Different combinations of allowed rotatable bonds were also considered for the ligands.
Docking calculations with AutoDock were performed using Genetic Algorithm (number of individuals in population 150, maximum number of energy evaluations 2500000-5000000, maximum number of generations 27000, number of top individuals to survive to next generation 1, rate of gene mutation 0.02, rate of crossover 0.8, window size 10, Alpha parameter of Cauchy distribution 0.0, Beta parameter Cauchy distribution 1.0). When docking BC-LOS, flexible docking was also performed considering Asp101, Glu120 and Glu122 as flexible residues.
Docking calculations with AutoDock Vina were also performed. Coordinates and dimensions of grid boxes, starting geometries and general methodology were the same as for AutoDock. When docking BC-LOS, flexible docking was also performed considering Asp101 as flexible residue. 3D structures of the docked complexes were optimized by performing MD simulations with Impact (implicit water, and AMBER* force field).

10.18.2 Docking studies of BC-LOS core on TLR4

The core moiety of BC-LOS was docked into human TLR4 protein using AutoDock Vina 1.1.2. All torsional bonds from the ligand were allowed to rotate. Ammonium groups were considered as ionized. Grid box was built on TLR4 from PDB 3fxi with grid center at 26.00, -22.00, 11.50 (x, y, z), number of grid points of 41 x 41 x 43 (x, y, z), and spacing of 0.375 Å. Final optimization of the 3D structure of the docked complex was carried out by MD simulation with Impact (implicit water, and AMBER* force field).

10.18.3 Building of the full complex of human MD-2/TLR4 with BC-LOS

Docked MD-2/BC-LOS complex was merged to docked BC-LOS core/TLR4 using PDB 3fxi as template. The resulting structure was optimized by MD simulations with implicit water (AMBER* force field). Coupling of two TLR4/MD-2/BC-LOS complexes was finally performed also using PDB 3fxi as template. The full 3D structure of the dimer complex was submitted to MD simulations with implicit water and AMBER* force field (charges from: forcefield, cutoff: extended, method: PRCG, maximum iterations: 500, converge on: gradient, convergence threshold: 0.05).

10.19 Genetic manipulation on *B. cenocepacia* K56-2

PCR reactions were done with *Taq* DNA polymerase or HotStar HiFidelity DNA Polymerase (Qiagen, Mississauga, ON, Canada). Plasmid DNA was isolated using QiaPrep Spin kit (Qiagen). PCR products were purified using a QIAquick PCR purification kit or a QIAquick gel extraction kit (Qiagen). Plasmids were transformed into *E. coli* strains by the classical calcium chloride method or mobilized into *B. cenocepacia* by triparental mating as described (Flannagan *et al*., 2008). Gene deletions or insertions were performed by allelic exchange as described previously (Flannagan *et al*., 2008). This system relies on a suicide vector that contains an I-*Sce*I restriction site (pGPI-SceI) and the replicative vector encoding the I-*Sce*I endonuclease (pDAI-SceI-SacB). Two new derivatives of pGPI-SceI, pGPISceI-X and pGPI-SceI-2 were used. To create pGPI-SceI-X, the *xylE* gene was PCR-amplified from pMo130 using primers 3925 and 3929. This PCR product was digested with *Eco*RI and *Xba*I and ligated to pGPI-SceI digested with the same enzymes to create pGPI-SceI-X. pGPI-SceI-2 was created by cutting pGPI-SceI-X with *Eco*RV and *Sma*I, removal of the *xylE* gene, and self-ligation. pGPISceI-X and pGPI-SceI-2 were

created from pGPI-SceI in order to add new restriction sites at the multiple cloning sites.

10.19.1 Construction of an unmarked L-Ara4N conditional

B. cenocepacia strain *Prha-arn* was constructed by allelic exchange using pMH396, which was obtained by cloning two DNA fragments into pGPI-SceI-2. One DNA fragment, spanning about ~300 bp of the 5′-end of *arnT* coding region along with *Prha* and *rhaRS* genes, was PCR-amplified from pXO38 using primers 4993 and 2282. The second DNA fragment comprised a ~300 bp fragment upstream *arnT*, which was PCR-amplified from genomic *B. cenocepacia* DNA using primer number 4994 and 4486. The upstream fragment was digested with *Not*I and *Spe*I, the downstream fragment was digested with *Spe*I and *Xba*I and both fragments were ligated to pGPI-SceI-2 digested with *Not*I and *Xba*I to create pMH396. This plasmid was used to insert the *Prha* and rhamnose control elements by allelic exchange as previously described with the exception of including rhamnose at a concentration of 0.4% (w/v) in all media used throughout the allelic exchange process.

10.19.2 Construction of a suppressor strain that is viable in the absence of L-Ara4N synthesis

Strain Δ*arnBC* was derived from *Prha-arn* by deleting the L-Ara4N synthesis genes *arnB* (BCAL1931) and *arnC* (BCAL1932) using pMH407. To construct pMH407, an internal fragment of *arnC* was PCR amplified using genomic *B. cenocepacia* DNA and primers 5115 and 5116. The PCR product was digested with *Not*I and *Xba*I and ligated to pGP-SceI-2 to create pMH406. Next, an internal fragment of *arnB* was PCR-amplified using primer 5117 and 5118 and genomic *B. cenocepacia* DNA as a template. This fragment was digested with *Nhe*I and *Not*I and ligated into

pMH406 digested with the same enzymes to create pMH407. Next, an overnight culture of *Prha-arn* grown in LB broth and 0.4% rhamnose was washed twice with PBS to remove rhamnose and the plated onto 10 LB agar plates [~5×10^5 cfu (colony-forming units) per plate] to enrich for suppressor colonies. After 3 days incubation at 37°C, colonies were pooled and the suicide vector pMH407 was introduced into pooled cells by triparental mating. To isolate colonies where homologues recombination between pMH407 and *arnBC* genes took place, exconjugants were screened for polymyxin B sensitivity in the presence of rhamnose. Colonies that failed to grow on LB agar containing polymyxin B (100 mg/ml) and rhamnose (0.4%) were used to resolve pMH407 using I-*Sce*I endonuclease-encoding plasmid, and the deletion of *arnBC* was confirmed by PCR using the flanking primers 4778 and 4940.

10.19.3 Construction of a suppressor strain that can synthesize L-Ara4N but lacks arnT

The suppressor strain Δ*arnT-arnBC*$^+$ was constructed in two steps by first deleting *arnT* from the Δ*arnBC* strain and next, reintroducing *arnBC* into their native genomic loci. *arnT* was deleted by allelic exchange using the plasmid pMH414, which was created by cloning two DNA fragments flanking *arnT* into pGpSceI-2. The upstream fragment was PCRamplified from pXO38 using the primer 4867 and 4206. The downstream fragment was PCR-amplified using genomic *B. cenocepacia* DNA as template and primer 4840 and 4841. The upstream fragment was digested with *Not*I and *Bgl*II, while the downstream fragment was digested with *Bgl*II and *Xba*I and both fragments were ligated into pGpSceI-2 digested with *Not*I and *Xba*I to create pMH414. This plasmid was used to delete *arnT* resulting in strain Δ*arnBC* Δ*arnT*. pMH415 was subsequently used to reintroduce functional *arnBC* genes by allelic exchange into their genomic locus in Δ*arnBC* Δ*arnT* strain, resulting in the strain Δ*arnT*-a*rnBC*$^+$.

10.19.4 Single copy gene replacement of lpt genes into P*rha-arn*

Single copy, unmarked gene replacement was performed in *Prha-arn* by allelic exchange using the plasmid pMH447. pMH447 was created to replace the genes *amrAB* genes (BCAL1674–BCAL1675), which encodes aminoglycoside efflux pump, with any gene of interes. Successful replacement of the gene of interest with *amrAB* renders *B. cenocepacia* sensitive to gentamicin and allows for easy screen for single copy unmarked gene replacement. pMH447 was created by cloning two DNAfragments upstream and downstream BCAL1674–BCAL1675 into pGPI-SceI-2. The upstream fragment was PCR amplified using *B. cenocepacia* genomic DNA and primer 5386 and 5387. The downstream fragment was PCR amplified using *B. cenocepacia* genomic DNA and primer 5388 and 5389. PCR product of upstream fragment was digested with EcoRI and NdeI and the PCR product of downstream fragment was digested with NdeI and NheI, and both fragments ligated to pGPI-SceI-2 digested with XbaI and EcoRI. The ligation between the compatible cohesive ends of NheI and XbaI destroys both sites thus creating unique NdeI and XbaI sites suitable for cloning into pMH447. pMH447 was used to delete *amrAB* from *Prha-arn* creating the gentamicin sensitive strain *Prha-arn* Δ*amrAB*. *lptFG* (BCAL2677–BCAL2678) were PCR amplified using wild-type *B. cenocepacia* DNA and primers 5165 and 5166. PCR product was digested with NdeI and XbaI and cloned into pMH447 cut with the same enzymes to create pMH448. pMH448 was then used to replace *amrAB* with wild-type *lptFG* in *Prha-arn* background thus creating the strain *Prha-arn* Δ*amrAB::lptFGWT*. *lptFG* (BCAL2677–BCAL2678) genes were PCR amplified using genomic DNA from suppressor strain Δ*arnBC* and primers 5165 and 5166. PCR product was digested with NdeI and XbaI and cloned into pMH447 cut with the same enzymes to create pMH449. pMH449 was then used to replace *amrAB* with suppressor *lptFG* in

Prha-arn background thus creating the strain *Prha-arn* Δ*amrAB::lptFGS*. *lptG* was PCR amplified using genomic DNA from suppressor strain Δ*arnBC* and primers 5256 and 5166. PCR product was digested with NdeI and XbaI and cloned into pMH447 cut with the same enzymes to create pMH451. pMH451 was then used to replace *amrAB* with suppressor *lptFG* in *Prha-arn* background thus creating the strain *Prha-arn* D*amrAB::lptGS*. To test for the ability *lptGF* genes to suppress Ara4N lethality, overnight cultures of each strain, grown in LB broth plus rhamnose were washed twice with PBS to remove residual rhamnose, serially diluted, and 5 ml drops of each dilution were plated onto LB agar with or without 0.4% rhamnose.

10.19.5 Site direct mutagenesis and replacement of wild-type lptG with $lptG_{D31H}$

lptGF was PCR amplified using wild-type genomic *B. cenocepacia* DNA and primer 5449 and 5166. PCR product was then cut with NotI and XbaI and ligated to pGPI-SceI-2 cut with the same enzymes to create pMH461. Aspartic acid at position 31 was changed to histidine using pMH461 as template and primer 5436 and 5437 by site direct mutagenesis as previously described (Hamad and Nilles, 2007) pMH461 was then introduced into *Prha-arn* and then resolved which resulted in either reversion to wild-type *lptG* or $lptG_{D31H}$ replacement. To screen for successful $lptG_{D31H}$ replacement colonies where patched onto LB agar with or without rhamnose and colonies that grew in absence of rhamnose indicated replacement of wild-type *lptG* with $lptG_{D31H}$. The resulting strain was named *Prha-arn* $lptG_{D31H}$ and $lptG_{D31H}$ replacement was confirmed by DNA sequencing of the *lptG* gene.

10.19.6 Antimicrobial peptide sensitivity testing and MIC determination

The MIC values to polymyxin B were determined as previously described (Loutet *et al*., 2009) with a few modifications. Overnight cultures, grown in LB broth supplemented with 0.4% rhamnose, were adjusted to an optical density at 600 nm (OD600) of 0.002 in LB broth plus 0.4% rhamnose, and polymyxin B was added to samples at twofold dilutions. Samples were then aliquoted into 100-well plates and incubated at 37°C with constant shaking for 24 h in a Bioscreen C automated growth curve analyser (MTX Lab Systems, Vienna, VA, USA). The MIC values were determined as the lowest concentration of antibiotic that inhibited visible growth after 24 h of incubation.

10.19.7 Transmission electron microscopy

Cultures we depleted of L-Ara4N by growing bacteria in M9 minimal media supplemented with 5% yeast extract and 0.5% glucose for 8 h. Cells were fixed with 2.5% glutaraldehyde and stained with 2% uranyl acetate and lead citrate. Grids were visualized using a Philips 410 transmission electron microscope operating at 60 kV.

References

Alves M.P., Rainey F.A., Nobre M.F., da Costa M.S., *Thermomonas hydrothermalis* sp. nov., a new slightly thermophilic gamma-proteobacterium isolated from a hot spring in central Portugal. **2003**, *System. Appl. Microbiol.*, 26, 70-75.

Flannagan R.S., Linn T.,Valvano M.A., A system for the construction of targeted unmarked gene deletions in the genus *Burkholderia*.**2008**, *Environ Microbiol*, 10, 1652-1660.

Hakomori S. A rapid permethylation of glycolipid, and polysaccharide catalyzed by methylsulfinyl carbanion in dimethyl sulfoxide. **1964**, *J. Biochem.,* 55, 205-208.

Hamad M.A., Nilles M.L., Structure-function analysis of the C-terminal domain of LcrV from *Yersinia pestis*. **2007**, *J. Bacteriol.*, 189**,** 6734-6739.

Heimbrook M.E., Wang W.L.L., Campbell G., Staining bacterial flagella easily. **1989**, *J. Clin. Microbiol*., 27, 2612-2615.

Jeukens J., Boyle B., Bianconi I., Kukavica-Ibrulj I., Tümmler B., Bragonzi A., Levesque R.C., Complete Genome Sequence of Persistent Cystic Fibrosis Isolate *Pseudomonas aeruginosa* Strain RP73. **2013**, *Genome Announc*., 1(4).

Leontein K., Lönngren J., Determination of the absolute configuration of sugars by Gas-Liquid Chromatography of their acetylated 2-octyl glycosides.**1978**, *Methods Carbohydr. Chem.*, 62: 359-362.

Loutet S.A., Bartholdson S.J., Govan J.R., Contributions of two UDPglucose dehydrogenases to viability and polymyxin B resistance of *Burkholderia cenocepacia*. **2009**, *Microbiology*, 155, 2029-2039.

Moalli F., Paroni M., Véliz Rodriguez T., Riva F., Polentarutti N., Bottazzi B., Valentino S., Mantero S., Nebuloni M., Mantovani A., Bragonzi A., Garlanda C., The therapeutic potential of the humoral pattern recognition molecule PTX3 in chronic lung infection caused by *Pseudomonas aeruginosa.* **2011**, *J. Immunol*., 186, 5425-5434.

Nigro G., Fazio L.L., Martino M.C., Rossi G., Tattoli I., Liparoti V., De Castro C., Molinaro A., Philpott D.J., Bernardini M.L., Muramylpeptide shedding modulates cell sensing of *Shigella flexneri*. **2008**, *Cell Microbiol*., 10(3), 682-95.

Piantini U., Sorensen O.W., Ernst R.R., Multiple quantum filters for elucidating NMR coupling networks.**1982**, *J. Am. Chem. Soc*., 104, 6800-6801.

Rance M., Sørensen O.W., Bodenhausen G., Wagner G., Ernst R.R., Wüthrich K., Improved spectral resolution in COSY ^{1}H NMR spectra of proteins via double quantum filtering. **1983**, *Biochem. Biophys. Res. Commun*., 117, 479-485.

Rietschel E.T., Absolute configuration of 3-hydroxy fatty acids present in lipopolysaccharides from various bacterial groups.**1976**, *Eur. J. Biochem.*, 64, 423-428.

Silipo A., Sturiale L., De Castro C., Lanzetta R., Parrilli M., Garozzo D., Molinaro A., Structure of the lipopolysaccharide isolated from the novel species *Uruburuella suis*. **2012**, *Carbohydr. Res*., 357, 75-82.

Silipo A., Sturiale L., Garozzo D., De Castro C., Lanzetta R., Parrilli M., Grant W.D., Molinaro A., Structure elucidation of the highly heterogeneous lipid A from the lipopolysaccharide of the Gram-Negative extremophile bacterium *Halomonas Magadiensis* strain 21 M1. **2004**, *Eur. J. Org. Chem*., 2263-2271.

States D.J, Haberkorn R.A., Ruben D.J., A Two-Dimensional Nuclear Overhauser Experiment with Pure Absorption Phase in Four Quadrants.**1982**, *J. Magn. Reson*., 48, 286-292.

Sturiale L., Garozzo D., Silipo A., Lanzetta R., Parrilli M., Molinaro A., New conditions for matrix-assisted laser desorption/ionization mass spectrometry of native bacterial R-type lipopolysaccharides**.2005**, *Rapid. Commun. Mass Spectrom.,* 19, 1829-1834.

Vermis K., Coenye T., LiPuma J.J., Mahenthiralingam E., Nelis H.J., Vandamme P., Proposal to accommodate *Burkholderia cepacia* genomovar VI as *Burkholderia dolosa* sp. nov.. **2004**, *Int. J. Syst. Evol. Microbiol*., 54, 689-691.

Conclusions

The present PhD project has been entirely focused on the relationship between the structure and the biological activity of endotoxins isolated from cystic fibrosis opportunistic pathogens. The first chapters are dedicated to the structural characterisation of LOS and O-chain moiety from *Burkholderia dolosa* and *Pandoraea pulmonicola* respectively. Both elucidated structures have revealed peculiar features that can be correlated to the high virulence of these cystic fibrosis pathogen bacteria. In particular, *B. dolosa* was found to be characterised by a LOS possessing a novel core oligosaccharide structure with no negative charges at the outer core conferring on the LPS an overall neutral characteristic that renders it resistant to cationic antimicrobial peptides. Moreover, biological assays highlighted a notable pro-inflammatory activity exerted by isolated *B. dolosa* LOS thus confirming the important role of LOS in pathogenicity of this cystic fibrosis pathogen. Similarly, structural determination of the antigenic determinant of the LPS molecule from the newly identified *Pandoraea pulmonicola* revealed the occurrence of a trisaccharide repeating unit bearing an uncommon non-sugar substituent. Since the O-chain moiety is known to elicit the host adaptive immune response, it is possible to assume that its novel structure and, in particular, the aglycon substituent, might be involved in the high virulence of *P. pulmonicola* in CF patients which was observed to be related to a remarkable production of cytokines in lung epithelial cells leading to a potent inflammatory process responsible for patient's death.
Interesting insights were also obtained from data belonging to the structural analysis of endotoxins isolated from chronic strains of both *Pseudomonas aeruginosa* RP73 and *Burkholderia cenocepacia*. The former was isolated after 17 years of colonisation and its LOS structure was completely elucidated together with the assessment of the pro-inflammatory activity. The results have

demonstrated that *P. aeruginosa* can undergoes changes in its endotoxin structure, both the O-chain and lipid A moieties, to generate strains with a low immunostimulant activity in order to escape from host immune activity. Indeed, the absence of the antigenic determinant and the presence of an underacylated lipid A found in *P. aeruginosa* RP73, were related to an endotoxin with a very low inflammatory power as shown by the poor recruitment of neutrophils in bronchoalveolar lavage fluid of mice used in *in vivo* experiments. The analysis of the endotoxin structure isolated from *B. cenocepacia* strains isolated at different stages of chronic colonisation further confirmed that an important phenotypic change in CF pathogens is the loss of the LPS O-chain moiety to reduce their detectability by host immune defenses.

A second part of this thesis is dedicated to the role of amino-arabinoses in several biological activities exerted by *Burkholderia cenocepacia*. Through a plethora of genetic and biochemistry experiments it was possible to assign several fundamental roles to the amino-arabinoses: i) they were found to be involved in *B. cenocepacia* high resistance to the most common used antibiotics in treatment of CF; ii) their presence is required for viability of this opportunistic pathogen since they represent an important signal for the export of the LPS to the outer membrane. Furthermore, through a meticulous study of the binding mechanisms of the *B. cenocepacia* lipid A to its physiological receptor, the TLR4/MD-2 complex, two further roles were attributed to amino-arabinoses: i) they act as a mask of the negative charged phosphate groups of the lipid A leading to a fine orientation of this latter into the MD-2 binding pocket; ii) their presence gives additional polar interactions to the binding of *B. cenocepacia* lipid A to the receptorial complex thus providing additional points of anchorage that favor the interaction and the immunostimulant activity of the *B. cenocepacia* lipid A. The study of the interaction between *B. cenocepacia* lipid A and the TLR4/MD-2 complex demonstrated that the typical

paradigm that asserts that underacylated lipid As have no or low inflammatory power, can not be applied to the *B. cenocepacia* lipid A. Indeed, the analysis have showed that this latter exerts its immunostimulant activity through a sinergistical effect given by the presence of amino-arabinoses and by the presence of long fatty acid chains; in particular these latter are responsible for the complete fulfillment of the MD-2 binding pocket, leading to the exposition of one acyl chain that is required for the elicitation of the inflammatory process.

The last part of this PhD thesis has been focused on characterisation of endotoxins isolated from a thermophilic bacteria. The importance to insert this study in the present thesis is consistent with the discovery of LPSs from non-pathogenic bacteria exerting antagonist or partial antagonist activity towards toxic LPSs. Thus, by isolating and characterising the structure and biological activity of endotoxins from extremophilic bacteria it is possible to offer new perspectives for treatment of pathologies caused or exacerbated by bacterial LPS, such as in case of cystic fibrosis. In this context, the elucidated structure and biological activity of *Thermomonas hydrothermalis* LOS is of great interest since the determined novel structure was found to exert a very low immunostimulant activity and, more important, to antagonize the toxic activity of the high inflammatory *E. coli* lipid A.

The overall results obtained from the projects reported in this thesis work, further confirmed the importance of LPS in bacterial life and pathogenesis mechanisms. Furthermore, structural analyses and biological tests conducted showed which molecular components are mostly involved in LPS endotoxicity. The knowledge of molecular structures involved in elicitation of the inflammatory process or the comprehension of mechanisms adopted by bacteria to escape host immune defenses during its adaptation to host environment, as well as the isolation and study of

macromolecules from non-pathogenic bacteria, as microorganism living in extreme environments, can offer novel pharmacological targets for the development of new aimed biomedical therapies.